FRIEDEL-CRAFTS CHEMISTRY AT HALOGENATED SURFACES

Thesis Submitted To The University of Glasgow

In Fulfilment Of The Requirement Of The

Degree Of Doctor Of Philosophy

Christopher H. Barclay

Department Of Chemistry,

University Of Glasgow.

Glasgow.

August, 1999

ACKNOWLEDGEMENTS

I would like to express my appreciation to my supervisor, Prof. John Winfield, for the help and guidance he has given me throughout this work.

I appreciate the efforts of Liz Hughes and Sarah Swindle in the typing of this thesis.

I am grateful to I.C.I. Runcorn for their kind sponsorship of my final year.

I would also like to offer a special thanks to my learned colleagues Chris Kealey and Dr. Philip Landon, who under duress occasionally would sacrifice time in the lab to go for a light refreshment. The two gentlemen although not pretty! Were fairly reasonable company.

I am indebted to my mum and dad for the continual encouragement and support they have given me throughout my studies and for always impressing upon me the value of education. I would also like to thank my gran for 'jointly funding my research with the EPSRC'.

I owe a special thanks to my girlfriend, Fiona, for all her encouragement and support and for proof reading this thesis.

I would like to offer a special thanks to Dr. W.J. Cole for the GCMS analysis shown within this thesis. I would also like to thank Ron Spence for running BET surface area measurements.

TABLE OF CONTENTS **Page**

Acknowledgements

Table of Contents

Summary i

Chapter 1. Introduction

1.1 Friedel-Crafts Reactions 1.

1.1.1 History 1.

1.1.2 Friedel-Crafts Chemistry 2.

1.2 Chemistry of Aluminium Trihalides 8.

1.3 Problems Associated with Conventional Friedel-Crafts Catalysis 12.

1.4 Alternatives to $AlCl_3$ in Friedel-Crafts Catalysis 14.

1.5 The Aims of the Present Work 19.

1.6 Structure and Properties of γ-Alumina 22.

1.7 Chemistry of the Halogenating agents 25.

1.8 Halogenation of γ-Alumina 29.

1.9 Oxide Supported Organic Layer Catalysts as Potential Friedel-Crafts Catalysts 35.

1.10 Potential of β-AlF_3 as a Friedel-Crafts Catalyst 37.

Chapter 2. Experimental

2.1 Equipment 41.

2.1.1 The Vacuum Systems 41.

2.1.2 Pyrex Glass Vacuum Line 42.

2.1.3 Monel Metal Vacuum Line 42.

2.1.4 Inert Atmosphere Box 43.

2.1.5 Catalyst Microreactor 43.

2.2 Preparation and Purification of Reagents 44.

2.2.1 Sulfur Tetrafluoride 44.

2.2.2 Carbon Tetrachloride 44.

2.2.3 Purification of 1,1,1-Trichloroethane 44.

2.2.4 Purification of 1,1-Dichloroethene 45.

2.2.5 Preparation of Anhydrous Hydrogen Chloride 45.

2.2.6 [^{36}Cl]-Chlorine Radioisotope 46.

2.2.7 Preparation of [^{36}Cl]-Chlorine Labelled Hydrogen Chloride 47.

2.2.8 Preparation of [^{36}Cl]-Chlorine Labelled 2-Chloropropane 47.

2.2.9 Preparation of [^{36}Cl]-Chlorine Labelled *t*-Butyl Chloride 48.

2.2.10 Preparation of [^{36}Cl]-Chlorine Labelled Acetyl Chloride 48.

2.3 Preparation and Pretreatment of Catalysts 49.

2.3.1 Calcination of γ-Alumina 50.

2.3.2 Chlorination of γ-Alumina 50.

2.3.3 Fluorination of γ-Alumina 51.

2.3.4 Formation of Oxide Supported Organic Layer Catalysts 52.

2.3.5 Sublimation of $AlCl_3$ 52.

2.3.6 Preparation of β-AlF_3 53.

2.4 Friedel-Crafts Reactions 53.

2.4.1 Experimental Method 54.

2.5 Infrared Spectroscopy 55.

2.5.1 Infrared Spectroscopy in the Vapour Phase Over Surface Reactions 55.

2.5.2 Experimental Procedure 55.

2.5.3 Identification of Gaseous Samples 56.

2.6 Gas Chromatography (GC) 56.

2.7 Gas Chromatography Mass Spectrometry (GCMS) 57.

2.8 Radiochemical Counting 58.

2.8.1 Geiger Müller Counters 58.

2.8.2 Dead Time 59.

2.8.3 Plateau Region 60.

2.8.4 Background 60.

2.8.5 Self Absorption 61.

2.9 Direct Monitoring Geiger Müller Technique 61.

2.9.1 Equipment 62.

2.9.2 Experimental Method 63.

2.9.3 Statistical Errors 63.

Chapter 3. Preparation and Characterisation of [^{36}Cl]-Chlorine Labelled *t*-Butyl Chloride, 2-Chloropropane and Acetyl Chloride

3.1 Introduction 66.

3.2 Experimental Strategy 68.

3.3 Methods of Analysis 71.

3.4 Synthesis of [^{36}Cl]-Chlorine Labelled *t*-Butyl Chloride 72.

3.5 Synthesis of [^{36}Cl]-Chlorine Labelled 2-Chloropropane 75.

3.6 Synthesis of [^{36}Cl]-Chlorine Labelled Acetyl Chloride 78.

Chapter 4. Evaluation of Halogenated Surfaces as Catalysts in Model Friedel-Crafts Systems

4.1 Introduction 82.

4.2 Experimental Procedure 84.

4.3 Methods of Analysis 85.

4.4 Results 86.

4.4.1 Friedel-Crafts Reaction of *t*-Butyl Chloride with Toluene on Solid Surfaces 87.

4.4.2 Friedel-Crafts Reaction of *t*-Butyl Chloride with Benzene on Solid Surfaces 96.

4.4.3 Friedel-Crafts Reaction of *t*-Butyl Chloride with Benzene on CCl_4 Chlorinated γ-Alumina 102.

4.4.4 Friedel-Crafts Reaction of Benzoyl Chloride with Benzene on CCl_4 Chlorinated γ-Alumina 107.

Chapter 5. Infrared Spectroscopic Studies of the Vapour Phase in Solid/Vapour Systems

5.1 Introduction 110.

5.2 Experimental Procedure 112.

5.3 *t*-Butyl Chloride in the Vapour Phase Over Solid Surfaces 113.

5.4 2-Chloropropane in the Vapour Phase Over Solid Surfaces 119.

5.5 Acetyl Chloride in the Vapour Phase Over Solid Surfaces 123.

Chapter 6. Radiochemical Studies – Interactions of [^{36}Cl]–Chlorine Labelled *t*-Butyl Chloride, 2-Chloropropane and Acetyl Chloride with Halogenated Surfaces

6.1 Introduction 126.

6.2 Experimental 128.

6.2.1 Uptake of [^{36}Cl]–Chlorine on Solid Surfaces 128.

6.2.2 Lability of [^{36}Cl]–Chlorine on Solid Surfaces 130.

6.3 Results 131.

6.3.1 Uptake of [^{36}Cl]–Chlorine Labelled *t*-Butyl Chloride on $AlCl_3$ 131.

6.3.2 Uptake of [^{36}Cl]–Chlorine Labelled *t*-Butyl Chloride on Calcined γ-Alumina and CCl_4 Chlorinated γ-Alumina 134.

6.3.3 Uptake of [^{36}Cl]–Chlorine Labelled *t*-Butyl Chloride on Oxide Supported Organic Layer Catalyst Derived from CCl_4 Chlorinated γ-Alumina 139.

6.3.4 Uptake of [^{36}Cl]–Chlorine Labelled *t*-Butyl Chloride on SF_4 Fluorinated γ-Alumina and β-AlF_3 140.

6.3.5 Uptake of [^{36}Cl]–Chlorine Labelled *t*-Butyl Chloride on Oxide Supported Organic Layer Catalyst Derived from SF_4 Fluorinated γ-Alumina 145.

6.3.6 Uptake of [^{36}Cl]–Chlorine Labelled 2-Chloropropane on Solid Surfaces 147.

6.3.7 Uptake of [^{36}Cl]–Chlorine Labelled Acetyl Chloride on $AlCl_3$ and CCl_4 Chlorinated γ-Alumina 151.

6.3.8 Lability of [^{36}Cl]–Chlorine Labelled *t*-Butyl Chloride and 2-Chloropropane on $AlCl_3$ and CCl_4 Chlorinated γ-Alumina 155.

6.3.9 Lability of [^{36}Cl]–Chlorine Labelled Acetyl Chloride on $AlCl_3$ and CCl_4 Chlorinated γ-Alumina 161.

6.3.10 Behaviour of [^{36}Cl]–Chlorine Labelled *t*-Butyl Chloride and Benzene on Oxide Supported Organic Layer Catalyst 163.

Chapter 7. Discussion and Conclusions

7.1 Summary of Key Findings 168.

7.2 Behaviour of CCl_4 Chlorinated γ-Alumina in Model Friedel-Crafts Reactions 170.

7.3 Behaviour of Oxide Supported Organic Layer Catalysts Derived from CCl_4 Chlorinated γ-Alumina in Model Friedel-Crafts Reactions 183.

7.4 Behaviour of β-AlF_3 in Model Friedel-Craft Reactions 185.

7.5 Behaviour of SF_4 Fluorinated γ-Alumina in Model Friedel-Crafts Reactions 189.

7.6 Conclusions 197.

References

SUMMARY

Friedel-Crafts reactions play an important role in the synthesis of fine chemicals on an industrial scale. Aluminium trichloride has emerged as the catalyst of choice as it possesses strong Lewis acidity and is relatively inexpensive. Environmental considerations, in particular waste minimisation, dictate that aluminium trichloride be replaced as soon as possible. Strong interactions between the reagents and the $AlCl_3$ are problematic and result in complexation of the reagents to the Lewis acid catalyst, effectively deactivating the catalytic sites. The hydrolytic destruction of the spent catalyst thereafter and disposal of the associated waste poses a considerable burden on the environment.

A study has been made to identify materials to replace $AlCl_3$ which have comparable activity but are not prone to substrate deactivation. The Friedel-Crafts catalytic activity at room temperature of the solids: SF_4 fluorinated γ-alumina, CCl_4 chlorinated γ-alumina, β-AlF_3 and supported organic layer catalysts derived from treatment of chlorinated and fluorinated γ-alumina with CH_3CCl_3, were examined as they exhibit Lewis acidic properties in halogen exchange reactions. Catalytic performance of the solids was studied in the Friedel-Crafts alkylation of toluene and benzene with *t*-butyl chloride.

Chlorination of γ-alumina with CCl_4 results in a solid with catalytic activity comparable to the archetypal Lewis acid catalyst $AlCl_3$, in the model Friedel-Crafts

alkylation reactions. Interestingly, the SF_4 fluorinated γ-alumina was catalytically inactive in the model systems, instead interacting with the reactants to form a highly coloured deposit on the surface of the solid. *In-situ* infrared analysis showed that $(CH_3)_3CCl$ vapour was completely deposited on both the CCl_4 chlorinated γ-alumina and SF_4 fluorinated γ-alumina, notably with release of HCl(g) over CCl_4 chlorinated γ-alumina. Uptake and lability of [^{36}Cl]-chlorine labelled alkyl and acyl halides on the solid surfaces, were examined via the direct monitoring Geiger Müller counting technique. Interaction of [^{36}Cl]-chlorine labelled $(CH_3)_3CCl$ with CCl_4 chlorinated γ-alumina resulted in an appreciable [^{36}Cl]-chlorine surface count on the solid, 65-70% of which was displaced/exchanged on introduction of unlabelled HCl. Similar displacement/exchange of the [^{36}Cl]-chlorine associated with the solid surface was observed when the CCl_4 chlorinated γ-alumina was treated with [^{36}Cl]-chlorine labelled $CH_3CHClCH_3$ and CH_3COCl.

It has been shown previously that treatment of γ-alumina with CCl_4 results in two types of surface chlorine species, Al-Cl terminal chlorine species, associated with Brønsted acid sites and readily exchangeable, and Al-Cl-Al bridging chlorine species, associated with Lewis acid sites and inert to exchange. The Friedel-Crafts catalytic activity of the chlorinated solid is the result of activation of the alkyl halide species, to form a transient carbenium ion, via interaction of the alkyl halide with the surface of the solid. It is very difficult to determine the exact nature of the interaction between the Lewis basic reagent and solid surface; it may involve simple

adsorption of the alkyl halide at Brønsted acid sites on the solid or a more complex equilibrium involving dehydrochlorination of the alkyl halide at Lewis acid sites and protonation of the resultant alkene via surface Brønsted acidity.

Failure of the CCl_4 chlorinated γ-alumina to catalyse consecutive Friedel-Crafts alkylation reactions may be the result of inert chlorine species associated with Lewis acid sites, effectively deactivating the active sites on the solid, analogous to $AlCl_3$. In addition, the hygroscopic nature of γ-alumina makes it susceptible to moisture, resulting in deactivation of the catalytic activity via coordination of the water molecules to the surface sites on the solid. Efforts were made to eliminate moisture, by working in an inert atmosphere with dry reagents, but there was always the potential that residual moisture was present.

Interestingly, in preliminary studies, the CCl_4 chlorinated γ-alumina was not catalytic in a model Friedel-Crafts acylation reaction (i.e. benzoylation of benzene with benzoyl chloride). The formation of hydrolysis products may indicate that the lack of catalytic activity was due to deactivation of the solid via coordination of water molecules to the active sites on the solid surface, rather than an inherent lack of acidity of the solid.

Solid γ-alumina fluorinated with SF_4 was not an active Friedel-Crafts alkylation catalyst, due to preferential interaction of the alkyl halide starting material

with the solid, forming a highly coloured supported organic layer. Analysis of the supported organic layer by GCMS indicated it was based on a C_4 hydrocarbon unit, consistent with the $(CH_3)_3CCl$ dehydrochlorination product, $(CH_3)_2C{=}CH_2$. It is difficult to determine the exact mechanism of layer formation, it is possibly analogous to formation of the oxide supported organic layer catalysts, via dehydrochlorination and oligomerisation of $(CH_3)_3CCl$ on SF_4 fluorinated γ-alumina.

The character of the surface fluorine species is assumed to be analogous to the chlorinated γ-alumina, with the enhanced electronegativity of fluorine and the potential for the smaller fluorine atoms to fluorinate both the bulk and surface of the solid, resulting in high surface acidity. Interaction of [^{36}Cl]-chlorine species with the SF_4 fluorinated γ-alumina, did not result in an appreciable [^{36}Cl]-chlorine solid surface count due to absorption of the [^{36}Cl]-chlorine species within the supported organic layer, at the inorganic-organic interface. The [^{36}Cl]-chlorine radiotracer species within the supported organic layer were not detected due to self absorption of the weak [^{36}Cl]-chlorine β^- decay, within the layer.

It was concluded that failure of the CCl_4 chlorinated γ-alumina to form a supported organic layer when treated with *t*-butyl chloride, implies that the SF_4 fluorinated γ-alumina has stronger Lewis acid sites than the CCl_4 chlorinated γ-alumina.

Fluorination of γ-alumina with an SOF_2/SF_4 mixture resulted in a solid with greater catalytic activity in the model Friedel-Crafts alkylation reactions than SF_4 fluorinated γ-alumina, but not as active as CCl_4 chlorinated γ-alumina. The nature of the surface fluorine species are believed to be similar to the SF_4 fluorinated γ-alumina, however, SOF_2 is a weaker fluorinating agent and is therefore unlikely to fluorinate as effectively as SF_4. It is proposed that the reduced level of fluorination results in a solid of intermediate Lewis acidity, not capable of promoting formation of a supported organic layer on the solid, instead activating the alkyl halide starting material towards Friedel-Crafts reactions.

The catalytic performance of CCl_4 chlorinated and SF_4 fluorinated γ-alumina treated with 1,1,1-trichloroethane were examined in the model Friedel-Crafts alkylation reactions, to determine the effect of the supported organic layer. Deposition of the supported organic layer on CCl_4 chlorinated γ-alumina resulted in reduced catalytic activity vs the halogenated precursor. The surface sites on the solid are believed to be analogous to the chlorinated γ-alumina, however, absorption of the reactant molecules in the surface of the organic layer and within the layer, modifies the catalytic activity.

The reason for the reduction in catalytic activity is not completely understood, but it is possible that the 'quasi-liquid' supported organic layer traps reactants and products at the active sites on the solid surface, preventing further

catalysis. The supported organic layer on SF_4 fluorinated γ-alumina, like its halogenated precursor, was catalytically inactive in the Friedel-Crafts reactions studied. Absorption of the alkyl halide species within the supported organic layer, at the inorganic-organic interface, implies that the surface sites are analogous to the SF_4 fluorinated γ-alumina (i.e. strong Lewis acid sites capable of dehydrochlorination and oligomerisation of the alkyl halide starting material).

In addition to the fluorinated γ-aluminas, β-AlF_3 was examined in the model Friedel-Crafts alkylation reactions and showed moderate catalytic activity, comparable with SOF_2 fluorinated γ-alumina. The catalytic activity is the result of interaction of the alkyl halide starting material, *t*-butyl chloride, with the Lewis acid sites on the surface of the β–AlF_3. Rapid conversion of the alkyl halide starting material to Friedel-Crafts products, followed by no further conversion after approximately five minutes of reaction, implies that the Lewis acid sites on the solid surface were deactivated on contact with the Friedel-Crafts reagents. It was concluded that deactivation was due to coordination of the Lewis basic alkyl halide species to the Lewis acid sites on the surface of the solid, the reactant molecules being too large to enter the channels in the porous structure.

CHAPTER 1

INTRODUCTION

1.1 Friedel-Crafts Reactions

1.1.1 History

In 1877 Charles Friedel and James Mason Crafts synthesised the first classical Friedel-Crafts compounds, reacting organic chlorides with hydrocarbons, stating clearly the catalytic influence of aluminium trichloride (1). Prior to this discovery other workers had carried out Friedel-Crafts reactions without appreciating the catalytic role of the metal halide. Notably, Zincke in 1869, while attempting to synthesise β-phenyl propionic acid, observed the formation of diphenylmethane (2). Similarly in 1873, Grucarevic and Merc reported the reaction of benzene and benzoyl chloride in the presence of copper, silver or zinc, yielding benzophenone (3).

It is evident that Friedel and Crafts appreciated the technical importance of their discovery, immediately filing patents in France and Britain (i.e. French Patent 118 and British Patent 4769). In the period 1877 to 1888 they were responsible for over sixty publications on the action of aluminium(III) chloride in a variety of reaction systems including alkylation, acylation, oxidation, cracking and polymerisation reactions. They also established that the metal halides - iron chloride, zinc chloride and cobalt chloride, had similar catalytic activity in Friedel-Crafts reactions (4).

In the years since Friedel and Crafts discovery, the scope of what constitutes a Friedel-Crafts reaction has widened considerably. Olah defined Friedel-Crafts reactions in 1963:

> "We consider Friedel-Crafts reactions to be any substitution, isomerisation, elimination, cracking, polymerisation or addition reaction taking place under the catalytic effect of Lewis acid type acidic halides, with or without cocatalyst or proton acid" (5).

1.1.2 Friedel-Crafts Chemistry

Friedel-Crafts chemistry is best categorised into three main classes of reaction (i) alkylation, (ii) acylation and (iii) miscellaneous reactions. Key aspects of these will be discussed within this chapter.

Friedel-Crafts reactions involve the interaction of an electrophile with a π or σ-donor substrate, such as an aromatic compound. In alkylation or acylation reactions the polarity of the carbon-halogen bond is insufficient to produce an electrophile for reaction, hence a catalyst is required to induce polarisation in the bond. The interaction between a catalyst and an alkyl or acyl halide is a key stage in the Friedel-Crafts process.

The catalyst initiates this interaction by functioning as an electron acceptor (Lewis acid) towards species which possess unshared electrons (Lewis bases) i.e. O,

F, Cl, Br, etc. Metal halides are commonly used as Lewis acid catalysts as they have an electron deficient central metal atom, capable of accepting electrons and hence polarising the carbon to halogen bond (Eqn. 1.1 and 1.2). Aluminium trichloride has become the standard Friedel-Crafts catalyst, due to its ability to co-ordinate with the donor species via electron donation into the Al^{3+} vacant orbitals.

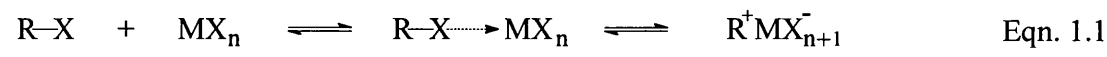

Eqn. 1.1

Eqn. 1.2

A number of miscellaneous reactions, involving reagents with no unshared electrons, have been reported under the influence of Lewis acid metal halides (i.e. alkylation or polymerisation of alkenes). These reactions require the presence of a cocatalyst, which produces a protonic acid or provides a cation which initiates reaction (i.e. Brønsted acid catalysts) (Eqn. 1.3).

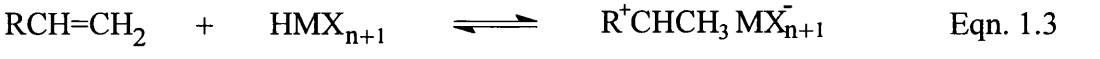

Eqn. 1.3

Alkylation and acylation reactions of aromatic compounds have been studied extensively over the years, but to date there is no one commonly accepted mechanistic pathway for these apparently simple reactions (Eqn. 1.4 and 1.5).

$$RX + ArH \longrightarrow ArR + HX \qquad \text{Eqn. 1.4}$$

$$RCOX + ArH \longrightarrow ArRCO + HX \qquad \text{Eqn. 1.5}$$

The uncertainty surrounds the nature of the interaction between the RX species and the metal halide catalyst. Whether the Lewis acid-base interaction results in the formation of the free carbocation (Eqn. 1.6) or a highly polarised donor-acceptor complex (Eqn. 1.7), is the subject of much discussion.

$$RX + AlCl_3 \longrightarrow R^+ + AlCl^-_4 \qquad \text{Eqn. 1.6}$$

$$RX + AlCl_3 \longrightarrow R^+\text{---}X^-\text{---}AlCl_3 \qquad \text{Eqn. 1.7}$$

The existence of a free carbocation as a result of a purely ionic mechanism is supported by the high reactivity of the alkyl fluorides (6,7). Further evidence for an ionic mechanism was shown in [^{82}Br]-Bromine labelled studies (8), in which alkyl bromide labelled with [^{82}Br]-Bromine was used in the presence of aluminium bromide ($Al^{80}Br_3$). The system yielded a mixture of hydrogen bromide ($H^{80}Br$) and labelled hydrogen bromide ($H^{82}Br$), consistent with halogen scrambling resulting from an ionic mechanism (Eqn. 1.8).

$$R^{82}Br + Al^{80}Br_3 \rightarrow R^+[Al^{80}Br_2{}^{82}Br]^- \qquad \text{Eqn. 1.8}$$

The first physical proof of the existence of an ionic mechanism was published in 1962 (9). Nuclear magnetic resonance (nmr) spectroscopy. N.M.R. spectroscopy of alkyl fluoride/antimony pentafluoride systems of isopropyl, *t*-butyl and *t*-amyl halides, yielded proton resonance peaks consistent with electron deficient carbenium ions - $[(CH_3)_2CH]^+$, $[(CH_3)_3C]^+$, etc. Notably, the alkyl chloride and bromide systems did not exhibit chemical shifts consistent with carbenium ion formation. They appear to exist as donor-acceptor complexes with the antimony pentafluoride. This study highlights the uncertainty surrounding the exact nature of the Friedel-Crafts mechanism.

The exact nature of the mechanism in Friedel-Crafts acylation reactions is also uncertain. Meerwin first reported the formation of an oxonium ion on reaction of acid chlorides with aluminium(III) chloride (10) [Figure 1.1(i)]. At around the same time Pfeiffer proposed a donor-acceptor complex, due to similarities between the addition reactions of ketones and acid halides with aluminium halide compounds (11) [Figure 1.1 (ii)].

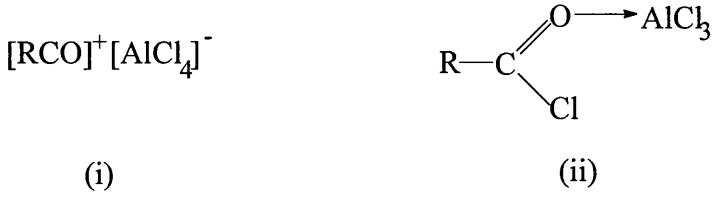

(i) (ii)

Figure 1.1

Susz and Wuhman (12) prepared the complex CH_3COCl-$AlCl_3$ and were able to assign an infrared band to the $[AlCl_4]^-$ species (~ 500 cm^{-1}), suggesting strongly the existence of an oxonium ion $[CH_3CO]^+$. Weak absorptions observed at 1639 and 1560 cm^{-1}, however, were possibly the result of donor-acceptor complex formation. More recent investigation has shown that both the oxonium ion and the donor acceptor complex exist, often as mixtures (13,14). Whether a distinct ion pair or a donor-acceptor complex is formed, the intermediate species is sufficiently electrophilic to react with π or σ-donor species. This enhanced reactivity of the alkyl or acyl halide as a result of interaction with the Lewis acid catalyst forms the basis of Friedel-Crafts reactions.

Dewar (15) proposed that the interaction of an electrophile with an aromatic substrate and its rate of substitution were dependent on the initial formation of a π complex (Scheme 1.1).

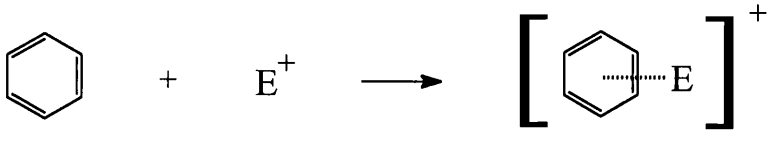

Scheme 1.1

In 1952 Brown while studying π complex formation of hydrogen chloride with *t*-butylbenzene and toluene respectively, observed an apparent contradiction between the stability of the so called π complex and the rate of substitution. This led

Brown to propose that the rate of substitution was determined, not by π-complexation, but σ-complexation (16) (Scheme 1.2).

Scheme 1.2

The formation of these previously unknown σ-complexes was confirmed when Olah and Kuhn (17,18) isolated the intermediates and characterised by spectroscopic data the systems (i) alkyl fluoride/benzene/boron trifluoride and (ii) alkyl (chloride and bromide)/benzene/silver tetrafluoroborate.

The classical Friedel-Crafts alkylation reaction of alkyl halide (RX), metal halide (MY_3) and aromatic substrate (C_6H_6), is commonly represented as in Scheme 1.3.

The product distribution from a Friedel-Crafts reaction depends upon a number of factors including the metal halide, the substrate and the presence of solvent. Olah studied the effect of the nature of the electrophile in the sulfonation (19) and acylation (20) reactions of aromatic substrates; concluding that the strength of the electrophile determined substrate and positional selectivity. Olah believed this

was the result of differences in what he termed the reaction coordinates of the π-transition states for weak or strong electrophiles (i.e. the starting position on the activation energy curve depended on the strength of the electrophile).

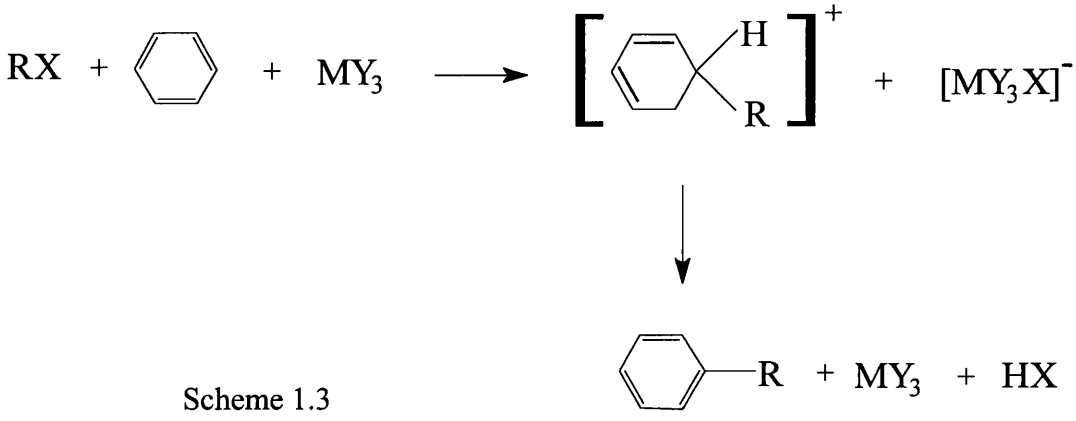

Scheme 1.3

1.2. Chemistry of Aluminium Trihalides

Aluminium is the most abundant metallic element in the earth's crust (8.8 mass %) and occurs widely in nature in alumina silicates as well as in the hydroxo-oxide bauxite and as cryolite (Na_3AlF_6) (21). Simple molecules such as aluminium halides or alkyls do not complete the metal's octet of electrons and result in the metal centre behaving as an electron acceptor. It is the electron deficient nature of the aluminium atom which accounts for the Lewis acidic properties of the aluminium halides.

The common oxidation state of +3 coupled with the small ionic radius of the tripositive ion tends to result in formation of largely covalent molecules. The

aluminium trichloride monomers, AlX_3, exist at high temperature and are believed to be planar molecules with sp^2 hybrid bonds in the plane and the electron pairs as far apart as possible. Proof of planarity was obtained for several matrix isolated species (22), with a pyramidal structure postulated for $AlCl_3$ in the presence of N_2, in which the N_2 forms a complex $N_2.AlCl_3$ (23,24). Formation of tetrahedral compounds of the type $[AlX_4]^-$ involves sp^3 hybridisation and reflects the tendency of the metal centre to complete its octet of electrons by accepting electrons from electron pair donors or Lewis bases.

Solid aluminium chloride is a colourless crystalline compound which sublimes at 456 K and is commonly represented by the general formula, $AlCl_3$. In the liquid and gas phases below 713 K it exists as the non planar dimer Al_2Cl_6 (25) (Figure 1.2).

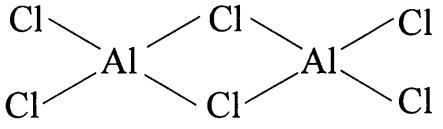

Figure 1.2

The configuration of halogen atoms around the metal atoms is approximately tetrahedral with the formation of the dimer attributed to the tendency of the metal to complete its octet of electrons. Between 713 K and 1073 K an equilibrium is established between the monomer ($AlCl_3$) and the dimer (Al_2Cl_6), with only the

monomer detected above 1073 K. At around 1273 K dissociation of the monomer, $AlCl_3$, takes place to some extent.

X-ray analysis of the solid aluminium chloride indicated a layer lattice structure with no D_{2h} symmetry, corresponding to the dimer structure detected (26). The covalent nature of the aluminium trichloride in the liquid phase is consistent with its extremely poor conduction of electricity at temperatures just above its melting point. Remarkably, the solid exhibits abnormally high expansion on heating and a large heat of fusion (27). Conductivity measurements (28,29) consistent with considerable ionic character (*ca.* $5x10^6\ \Omega^{-1}\ cm^{-1}$), led Blitz to propose that the solid exists as ions while the liquid phase is composed of molecules.

Aluminium chloride is widely used in Friedel-Crafts catalysis and is commonly accepted as the benchmark catalyst. The dipole moment of monomeric $AlCl_3$ (5.3D) is responsible for its strong polarising effect and accounts for the formation of addition compounds. Within such addition compounds the $AlCl_3$ exerts a strong influence on the binding forces within molecules, making reactions such as Friedel-Crafts possible via reactive intermediates.

Solid aluminium(III) fluoride is very different in nature to the chloride, bromide and iodide, as it exhibits ionic character in both the solid and liquid phases. X-ray analysis has shown that the solid consists of a continuous ionic network in

which each fluorine atom is shared between two AlF_6 octahedra. The ionic character is reflected in a high sublimation temperature of 1564 K and the lack of solubility in non-dissociating solvents. Previous studies of the vapour phase have indicated that some of the dimer component, Al_2F_6, was present (30).

Aluminium(III) fluoride is a considerably poorer Lewis acid than the other aluminium halides (6,31), as it has only a limited number of Lewis acid sites. The nature of the lattice results in fully saturated aluminium atoms within the lattice and electron deficient aluminium sites (Lewis acidic sites) on the surface. In recent years the interest in aluminium fluoride as a catalyst, is not due to its Lewis acidity, but its Brønsted acidity, associated with the hydrolysis product HF adsorbed on the surface.

Aluminium tribromide and triiodide have very similar properties and both exist predominantly as the halogen bridged dimers, as discussed for aluminium chloride. They are generally regarded as more reactive catalysts than aluminium chloride, partly due to the covalent nature of the dimeric molecules in the solid affording greater solubility in the majority of solvents (i.e. benzene, hydrocarbons and toluene nitro-benzene) (32,33). The enhanced catalytic activity is also attributed to the reduction in back donation from the halogen atoms, which increases the electronegativity of the aluminium metal centres. Aluminium tribromide and triiodide are therefore stronger Lewis acids than aluminium trichloride.

For many years the monomeric species, AlX_3 has been accepted as the catalytically active component. Walker proposed that the rate at which the monomeric species is produced determines the catalytic activity of any given metal halide and hence the overall reaction rate (34,35). Cocatalysts are particularly important as they are believed to function via complexation to the metal halide dimer, weakening the bonding in the dimer and liberating the active monomeric species, AlX_3. The cocatalyst CH_3Br is a good example, lowering the bonding strength in pure $AlBr_3$, from 26.5 to 20 $kJ\,mol^{-1}$, and increasing the catalytic activity.

1.3. Problems Associated with Conventional Friedel-Crafts Catalysis

Since the discovery of Friedel-Crafts chemistry last century, aluminium trichloride has remained the catalyst of choice as it gives good yields in alkylation reactions and is relatively cheap. It is however difficult to handle and store because of its toxic, corrosive and hygroscopic nature. Undesirable multiple alkylation of aromatic substrates is a feature of aluminium trichloride catalysis due to the (+I) inductive effect which the first alkyl substituent exerts on the ring system, activating the ring towards further electrophilic aromatic substitution.

The metal halide is very rarely truly catalytic, and stoichiometric quantities are often required, as complexation of substrates to the solid Lewis acid poisons the catalytically active sites. Acylations are particularly problematic with complexation

of the Lewis basic oxygen to the Lewis acid rendering the solid inactive. A good example is the synthesis of the analgesic ibuprofen (36). The intermediate, 4-isobutylacetophenone is prepared via an aluminium trichloride catalysed Friedel-Crafts acylation reaction, resulting in the formation of a complex with the Lewis acidic aluminium trichloride (Scheme 1.4).

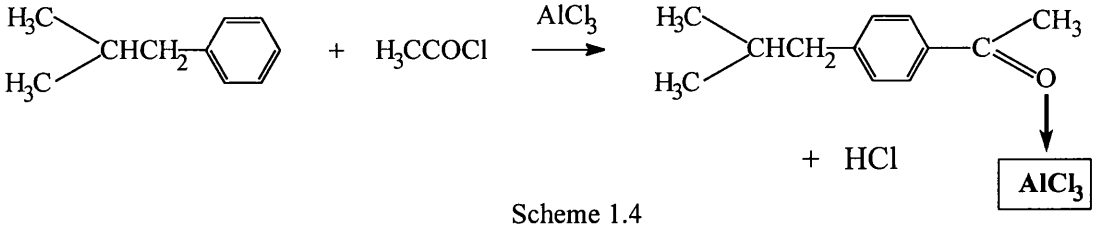

Scheme 1.4

The 4-isobutylacetophenone is recovered by destroying the complex by quenching with water. For each mole of the intermediate isolated, one mole of waste aluminium hydroxide and three moles of hydrochloric acid are produced (Scheme 1.5).

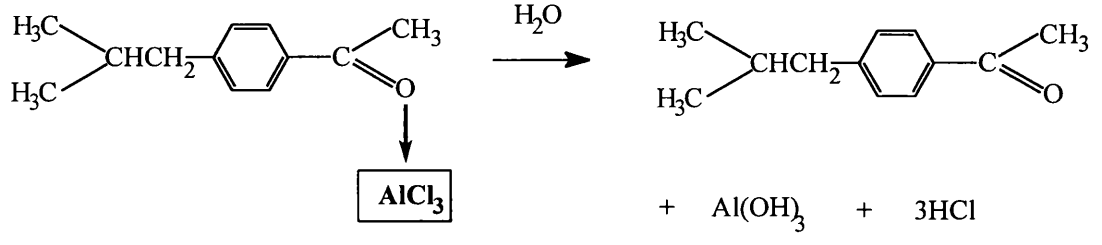

Scheme 1.5

The production of large quantities of solid and liquid waste from Friedel-Crafts catalysis is environmentally unacceptable and hence alternatives are being sought. With some 75000 tonnes of $AlCl_3$ used annually the benefits of cleaner processing techniques are self evident.

1.4. Alternatives to Solid $AlCl_3$ in Friedel-Crafts Catalysis

In recent years there has been considerable interest in the development of solid acid catalysts to replace solid $AlCl_3$. The soluble or 'pseudo homogeneous' nature of traditional $AlCl_3$ catalysis which results in environmentally unacceptable quantities of waste, was discussed in section 1.3. The heterogenisation of inorganic reagents and catalysts has become an important goal within the clean technology field because of the potential to offer highly reactive, low waste, environmentally friendly catalysts (36).

The most obvious solution to the problems associated with the solubility of $AlCl_3$ was to prepare insoluble or supported $AlCl_3$. Aluminium chloride was successfully immobilised on silica gel in both the vapour phase and by refluxing in carbon tetrachloride (37-39), producing the solid superacid denoted by $AlCl_2(SG)_n$ The acidity of $AlCl_2(SG)_n$ was evident in its ability as a cracking/isomerisation catalyst in the gas phase (38,40), however it displayed considerably less activity than unsupported $AlCl_3$, in liquid phase Friedel-Crafts alkylation reactions (41).

Clark developed a supported form of aluminium chloride which showed activity comparable with the parent compound, in alkene and chloroalkene alkylations in the liquid phase (42). Mesoporous silica, acid treated montmorillonite and acidic alumina prepared in benzene were effective supports, with the catalyst regeneration after use resulting in only minimal loss in activity.

The commercial importance of aluminium chloride catalysis within industry is reflected in the considerable active research in this area. The search to discover an acidic material which remains catalytic in the most demanding Friedel-Crafts systems, such as acetylations, has led to a variety of proposed replacements including montmorillonite clays, zeolites, sulfate promoted ZrO_2, heteropolyacids, metal triflates, nafion etc. The numerous publications on alternative Friedel-Crafts systems (e.g. 43-48) make it impossible to review completely this area, but it is appropriate to detail the key aspects of a selection of important systems.

A significant new range of Friedel-Crafts catalysts based on montmorillonite clays, has emerged within the last ten years (43,44). Montmorillonite clays are aluminum silicates. Evaluation of transition metal salts supported on acid treated montmorillonite clays indicated an enhanced acidity when $CuCl_2$, $NiCl_2$ and most notably $ZnCl_2$ was used. The relatively low acidity of the support prior to incorporation of the metal ions suggested that the acidity was a function of the metal ions. The combination of metal ions and the support resulted in a catalyst

capable of catalysing benzylation reactions within minutes at room temperature. The catalytic activity exhibited was attributed to the synergistic effect of the Zn^{2+} ions located within cavities or mesopores in the porous structure. Zinc chloride impregnated on K10 montmorillonite is known as 'Clayzic' and is marketed under the `Envirocat' tradename by Contract Chemicals (49,50). The ease of regeneration of the clay based catalysts considerably reduces waste compared to the $AlCl_3$ based processes, however they are not as active.

The use of zeolites in Friedel-Crafts reactions is well documented. Zeolites are crystalline hydrated aluminosilicates of alkali and alkali earth metal cations, with infinite 3-dimensional structures (51). The open regular structures are characterised by the ability to lose and gain water reversibly and exchange constituent cations without major change of structure. The earliest studies of rare earth modified zeolites, in the acylation of toluene using carboxylic acids in the gas phase, indicated a high selectivity towards the para-isomer (52,53). Zeolites active in the liquid phase were characterised by Corma in studies on the acylation of anisole by phenacetyl and phenyl propanoyl chlorides (54).

In more recent studies, different levels of transition metals and varying the Si/Al ratio, were examined in model Friedel-Crafts acylation reactions (55). The acylation of anisole by acetyl chloride and acetic anhydride was facilitated to the

greatest extent by lanthanum modified zeolites, and the greatest yield achieved from the most dealuminated zeolites. This was believed to be due to increased hydrophobicity of the zeolite structure.

The pore size of zeolites (3-13 Å) has limited their application to small molecules, with the reaction kinetics dependent on the ability of reactant molecules to enter the pores and product molecules to exit the pores. The advent of mesoporous molecular sieves (i.e. MCM-41), similar to zeolites but which possess mesopores of between 20-80 Å have been used in Friedel-Crafts reactions (56). Larger pores of this nature have extended catalysis to larger molecules such as the acetylation of 2-methoxynaphthalene (57).

Interest in the use of supported heteropolyacids, particularly dodecatungstophosphoric acid ($H_3PW_{12}O_{40}.25H_2O$), in Friedel-Crafts catalysis arose from their catalytic activity in proton catalysed organic reactions (58,59). The catalytic activity was limited to alkylation reactions and the problems encountered due to colloid formation of the heteropolyacids with polar solvents, made separation and recovery of products very difficult (60). Supporting heteropolyacids on silica (61,62) and carbon (63) offered considerable enhancements in activity as reflected by moderate activity in acylation reactions, and the materials were readily separated from polar solvents.

The most significant development in the application of supported heteropolyacids came from the preparation of Cs, Rb, K and ammonium salts (64,65). The Cs salt ($H_{.0.5}Cs_{2.5}PW_{12}O_{40}$) exhibited enhanced catalytic activity vs. the non-modified heteropolyacid and materials such as zeolites, Zn promoted montmorillonites and Nafion. Interestingly, uptake of water on the acidic heteropolyacid ($H_3PW_{12}O_{40}$), was not observed on the Cs salt ($H_{0.5}Cs_{2.5}PW_{12}O_{40}$). It was proposed that the hydrophobicity of the Cs salt resulted in strong adsorption of aromatic molecules, facilitating their activation. It was believed that the pseudo liquid phase formed on the surface of the salt, as a result of adsorption of the aromatic, promotes Friedel-Crafts catalysis.

The development of new Friedel-Crafts catalysts has primarily focussed on heterogeneous solid acid catalysts, readily recoverable after reaction without loss in activity. The development of metal triflate catalysts is particularly interesting as they appear to offer homogeneous catalysts, which are stable in aqueous conditions and readily recovered without loss in activity (66,67).

Lanthanum trifluoromethanesulfonate, commonly known as lanthanum triflate, catalysed acylations of anisole, mesitylene and xylene but was an ineffective catalyst on benzene and toluene. Previous studies had indicated the formation of a cationic species when lithium perchlorate ($LiClO_4$) was added to antimony and hafnium triflates (68,69). When lithium perchlorate was used in conjunction with

scandium triflate, the system was catalytically active in acylation reactions with moderate yields and complete recovery of the active catalyst (70). These novel homogeneous systems offer an interesting, moderately active, environmentally friendly low waste alternative to $AlCl_3$ catalysis.

It is important to realise that of the alternative catalysts discussed within this review, no one catalytic system exhibits the level of activity which $AlCl_3$ displays. The considerable potential reductions in process waste is indeed beneficial but the ultimate goal of obtaining a material with activity comparable to $AlCl_3$ in all systems and without the associated waste, has still not been achieved.

The considerable interest and ongoing development in the use of environment friendly reaction media, such as supercritical CO_2 and ionic liquids may have a key role to play in the future of Friedel-Crafts chemistry. These technologies appear to offer genuine solutions to the problems surrounding chemical processing (71-73).

1.5. The Aims of the Present Work

Friedel-Crafts reactions play an important role in the synthesis of fine chemicals on an industrial scale. Aluminium trichloride has emerged as the catalyst of choice as it possesses strong Lewis acidity and is relatively inexpensive. Environmental considerations, in particular waste minimisation, dictate that aluminium trichloride be replaced as soon as possible. Its use in acylation reactions

is particularly problematic, with complexation of the carbonyl oxygen to the Lewis acid catalyst effectively deactivating the catalytic sites. The hydrolytic destruction of the spent catalyst thereafter and disposal of the associated waste has serious effects on the environment.

It is desirable to replace $AlCl_3$ with materials of comparable activity and selectivity, which are not prone to substrate deactivation, allowing their use in continuous processing rather than batch preparations. Development of suitable alternatives will eradicate the considerable chemical waste produced annually in the use of $AlCl_3$ catalysis. Significant developments in this area to date include the work of Drago (39,41) and Clark (43,44) in which they employ supported reagent methodology successfully in heterogeneous catalytic systems. It is commonly accepted within the Friedel-Crafts research field, that heterogeneous catalytic systems will contribute to the replacement of $AlCl_3$.

Our proposed heterogeneous methodology originates from investigation of $AlCl_3$ surface chemistry (74) and the promotion of surface acidity of γ-alumina via halogenation (75). The deposition of oligomeric hydrocarbon layers derived from 1,1,1-trichloroethane, CH_3CCl_3, or $CH_2{=}CCl_2$ on fluorinated and chlorinated γ-alumina and the solid β-AlF_3 have strong Lewis acid sites and are active halogen exchange catalysts (76-78). The ability of these solids to promote exchange of halogen atoms made them of interest as potential Friedel-Crafts catalysts as they may

interact with halogen containing starting material to form reactive intermediates necessary for catalysis. The solids, chlorinated and fluorinated γ-alumina, β-AlF_3 and a range of supported organic layer catalysts derived from treatment of chlorinated and fluorinated γ-alumina with CH_3CCl_3 and $CHCl=CCl_2$ were proposed as replacement catalysts to $AlCl_3$.

The principal aim of this work was to study the activity of the Lewis acidic materials in model Friedel-Crafts reactions and develop a fundamental understanding of the nature of the substrate/solid interactions via radiochemistry and *in-situ* infrared spectroscopic studies.

Evaluation of the solids in liquid/solid phase Friedel-Crafts systems, followed by GC and GCMS analysis, affords activity and selectivity data, enabling comparisons to be made between the catalytic activity of the solid materials. Investigation of the catalytic performance for activated substrates (i.e. alkylation) in conjunction with more demanding catalytic systems (i.e. acylation), allows a true assessment of the potential scope of the acidic solids. Products from the reaction mixtures were analysed by GC as a function of time, to build up a dynamic picture of the catalytic processes.

The synthesis of [^{36}Cl]-chlorine labelled alkyl and acyl halides, relevant to the model Friedel-Crafts studies was necessary for use in the direct monitoring Geiger

Müller technique (79,80). This powerful radiochemical technique developed at Glasgow, allows the interaction between labelled substrates and solid materials to be monitored *in-situ.* Information on the presence of [^{36}Cl]-chlorine species on solid catalytic surfaces and the lability of such species can be obtained.

Infrared studies, of the vapour phase over solid acids, for systems analogous to those investigated in the direct monitoring technique were examined. The nature of the interaction between the substrates and the solids, may be indicated by the material released in the vapour phase. Observations from the radiochemical and spectroscopic studies will form the basis on which conclusions about the nature of the catalytic mechanisms in operation will be drawn.

The behaviour of the reactant molecules on the acidic solids in conjunction with the activity data from the Friedel-Crafts reactions is designed to enable characterisation of the catalytic properties of the solids and offer a fundamental understanding of the role which the solids play in Friedel-Crafts catalytic systems.

1.6. Structure and Properties of γ-Alumina

Only one stoichiometric form of aluminium oxide is known, namely alumina, Al_2O_3 (21). However, the existence of a number of polymorphic phases with the approximate stoichiometry Al_2O_3 and hydrated species is well documented (81-83). Classification of the polymorphs on the basis of the distribution of aluminium ions in

octahedral or tetrahedral interstices of close packed oxygen lattices, results in at least three distinct phases (α, β and γ):

- α-series consists of hexagonally close packed oxide lattices, schematically ABAB--
- β-series consists of alternating close packed oxide lattices, schematically ABAC-ABAC or ABAC-CABA
- γ-series consists of cubic close packed oxide lattices, schematically ABC ABC

α-Alumina is the only member of the α-series, occurring in nature as the mineral corundum or prepared by heating γ-Al_2O_3 or any hydrated oxides such as diaspore (AlO.OH) above 1273 K (84). The symmetrical distribution of the aluminium ions among the octahedral interstices of the hexagonal close packed array result in a phase which is metastable at low temperature. The β-series is represented by the alkaline or alkali earth oxides containing β-alumina. β-Alumina contains alkali metal ions and is ideally represented by $M_2O.Al_2O_3$ (85). The γ-series is prepared by dehydration of the hydrous oxides bayerite, norstrandite and boehmite and yields both low and high temperature phases (86).

In this work the low temperature phase of γ-alumina (87) was used as it is of particular interest in catalytic processes. γ-Alumina is used as a support in many industrial catalytic processes (88,89) due to its high surface area (>100 m^2g) and

thermal stability (90). It also plays a more active role in bifunctional catalysts, where the acidity of the alumina is essential for catalytic activity (91).

A key characteristic of the γ-alumina structure is the similarity between it and the cubic close packed oxide lattice of the classic spinel, $MgAl_2O_4$ (92). The unit cell of the spinel, AB_2O_4, consists of cubic close packing of 32 oxygen atoms with 16 trivalent atoms in half of the octahedral interstices and eight divalent atoms in tetrahedral holes. Lippens used powder X-ray diffraction studies to establish the defect spinel structure of γ-alumina (93), in which 32 oxygen atoms are arranged exactly as in the spinel but $21^1/_3$ aluminium ions are distributed over the 24 cation positions available. Electrical neutrality is achieved by the $2^2/_3$ vacant cation sites per unit cell and the presence of hydroxyl groups on the crystallite surface.

Investigation of the effects of surface hydration on catalytic activity (94,95), led Peri to propose a model structure for the surface of anhydrous γ-alumina (96). Experimental data from the infrared studies at 1073 K indicated the presence of five distinct types of hydroxyl group. The model [110] face of γ-alumina highlights the different environments that may exist for terminal hydroxyl groups (Figure 1.3 and 1.4).

The nature of the surface sites on γ-alumina were characterised by transmission spectroscopy (97,98) and FTIR photoacoustic spectroscopy (99). In

Figure 1.3 (i) : [110] Face of Spinel Structure

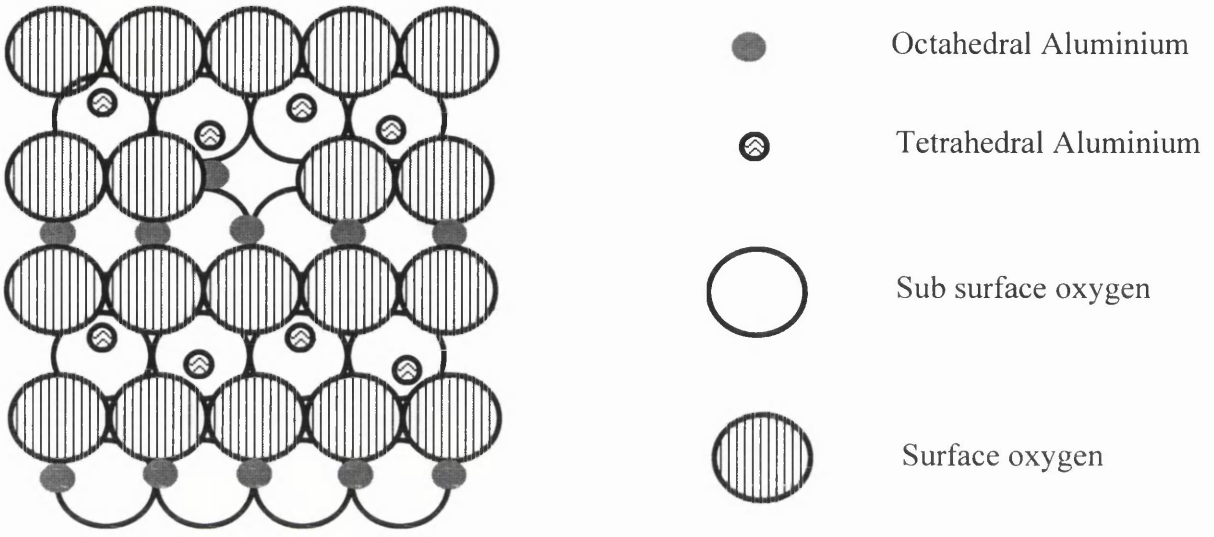

Figure 1.3 (ii) : Hydroxyl Environments of γ-Alumina

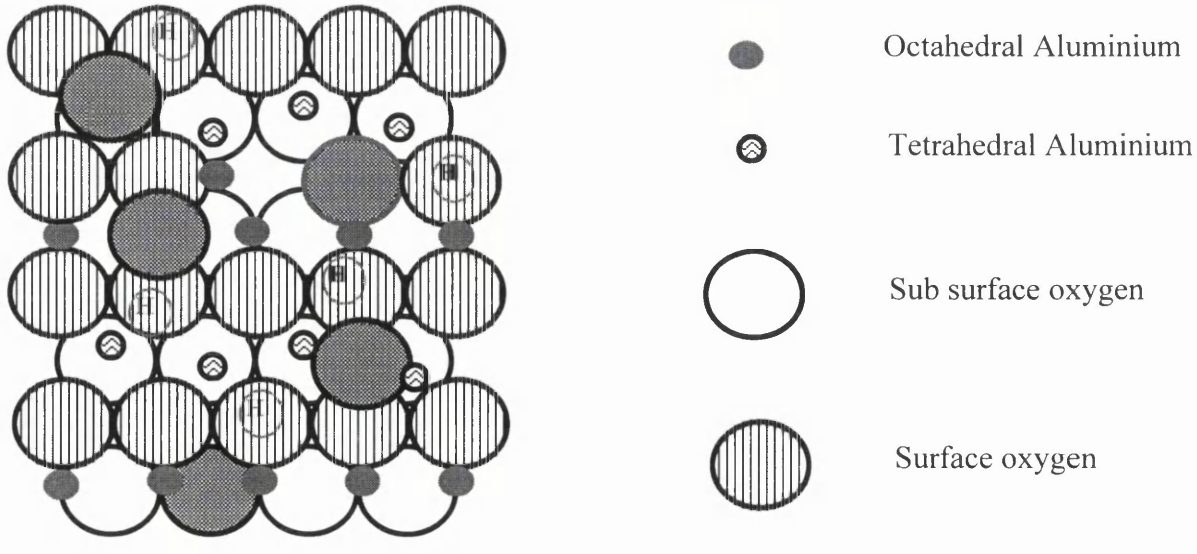

Figure 1.4 : Aluminium Environments for Terminal Hydroxyl Groups

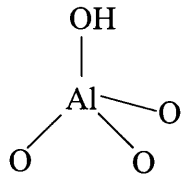

1. Tetrahedral

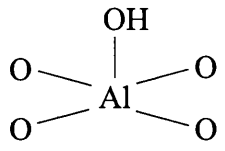

2. Octahedral

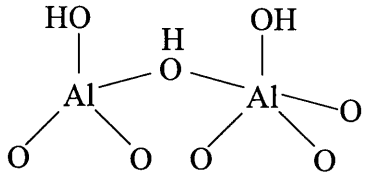

3. Tetra-O-Tetra

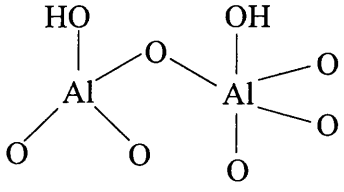

4. Tetra-O-Octa

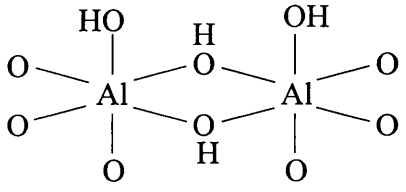

5. Octa-O-Octa

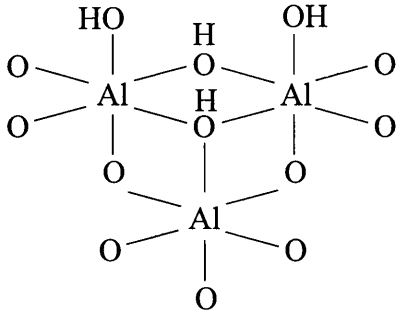

6. Octa-O-Octa
|
Octa

pyridine absorption studies the pyridine molecule was deemed to have been associated exclusively with Lewis acidic sites of the γ-alumina surface. The apparent lack of Brønsted acidity was attributed to the inability of the surface hydroxyl groups to hydrogen bond to electron pair donors.

1.7 Chemistry of the Halogenating Agents

In this section the chemistry of carbon tetrachloride and sulfur tetrafluoride will be reviewed, as they are key reagents used in the preparation of halogenated surfaces. Carbon tetrachloride is a colourless non-polar liquid (bp 349 K, mp 250 K), commonly used as a solvent in organic chemistry. Preparation of CCl_4 via chlorination of methane has been studied extensively in the liquid and vapour phases under both photochemical and thermal conditions (100-102). The generally accepted mechanism involves a free radical halogen reaction of the type shown in Eqn. 1.9 - 1.13 (103).

$$Cl_2 \rightleftharpoons 2Cl^{\bullet} \qquad \text{Eqn. 1.9}$$

$$Cl^{\bullet} + RH \rightleftharpoons HCl + R^{\bullet} \qquad \text{Eqn. 1.10}$$

$$R^{\bullet} + Cl_2 \longrightarrow RCl + Cl^{\bullet} \qquad \text{Eqn. 1.11}$$

$$R^{\bullet} + Cl^{\bullet} \longrightarrow RCl \qquad \text{Eqn. 1.12}$$

$$2R^{\bullet} \longrightarrow R_2 \qquad \text{Eqn. 1.13}$$

The chain reaction is initiated by the formation of a chlorine radical, $Cl^{\bullet}$ (Eqn. 1.9), with propagation steps resulting in chlorination of the alkyl component (Eqn. 1.10 and 1.11). The termination reactions in operation depend on the steady state concentrations of the radicals $R^{\bullet}$ and $Cl^{\bullet}$ (Eqn. 1.12 and 1.13).

Carbon tetrachloride has a tetrahedral geometry, with C-Cl bond lengths of 1.766 Å. It is more thermodynamically stable than CBr_4 or CI_4 but not as stable as CF_4 as reflected in the C-X bond energies (i.e. C-F 485, C-Cl 327, C-Br 285 and C-I 213 kJ mol^{-1}) (21). CCl_4 is thermodynamically unstable to hydrolysis, however its saturated nature makes the carbon acceptor orbitals inaccessible, therefore preventing hydrolysis. The photochemical decomposition of CCl_4 results in the formation of chlorine radicals especially at elevated temperature.

Transfer of chlorine to a variety of substrates takes place via highly reactive chlorine radicals. Species such as the $^{\bullet}CCl_3$ radical is known to possess pyramidal geometry with bond angles between tetrahedral and planar (104). A stabilisation energy of 12 Kcal mol^{-1} is associated with the availability of the chlorine d-orbitals for bonding with the carbon.

The use of CCl_4 as an effective chlorinating agent was discussed by Goble and Lawrence (105), for the interaction of CCl_4 on high surface area metal-alumina

catalysts at elevated temperature. They observed the production of CO_2, $COCl_2$ and HCl without the deposition of any carbonaceous material. Analysis of the solid after chlorination indicated up to 14 weight % of chlorine bound to the surface.

Carbonyl chloride ($COCl_2$) is a hydrolytically unstable gas. The reduction in CO bond order compared with that in a simple ketone is attributed to the partial double bond character of the chlorine to carbon bond. Goble and Lawrence proposed that the chlorination was a two stage mechanism involving CCl_4 initially, then $COCl_2$.

Sulfur tetrafluoride was first reported in the early 1900's (106). The direct fluorination of S_8 was an unsuitable method of preparation, yielding predominantly SF_6 with only trace quantities of SF_4 and S_2F_{10}. A number of methods of preparation for SF_4 have appeared in the literature (107) (Scheme 1.6), with the reaction of sulfur dichloride and sodium fluoride in acetonitrile emerging as the method of choice (108) (Eqn. 1.14)

$$SCl_2 + NaF \xrightarrow[343\text{-}353\ K]{\text{acetonitrile}} SF_4 + NaCl \qquad \text{Eqn. 1.14}$$

Sulfur tetrafluoride is a colourless gas (bp 165 K) which hydrolyses rapidly to hydrogen fluoride and thionyl fluoride. For this reason SF_4 must be handled in

completely dry apparatus and commonly in stainless steel or Monel metal equipment, which is inert to SF_4.

Investigation of the vibrational structure of SF_4 in 1956 suggested a C_{2v} symmetry (109). This led to the proposal of the now commonly accepted trigonal bipyramidal structure, in which one of the equatorial atoms was replaced by a lone pair of electrons (Figure 1.5). The structure was confirmed by NMR studies at 175 K with the observation of two identical triplets (110). Evidence for significant deviation from the C_{2v} symmetry was presented by Tolles and Gwinn in 1962 with the formation of a $BF_3.SF_4$ complex (111). The existence of an SF_3^+ ion (Figure 1.6) was proposed on the basis of the solid infrared spectroscopy studies on the BF_3 adduct ($SF_3^+BF_4^-$) (112). In contrast, however arsenic trifluoride gave no evidence for formation of an AsF_3^+ species (113).

Sulfur tetrafluoride can also act as a weak electron pair acceptor on interaction with caesium fluoride to form a stable anion pentafluorosulfate (SF_5^-) (114). The anion structure may be pseudo octahedral if the lone pair is considered (Figure 1.7) (115).

Sulfur tetrafluoride is widely used as a fluorinating agent in organic (Scheme 1.7) and inorganic chemistry (Scheme 1.8) (107). The fluorination is often highly

Scheme 1.6 : Methods of Preparation of Sulphur Tetrafluoride

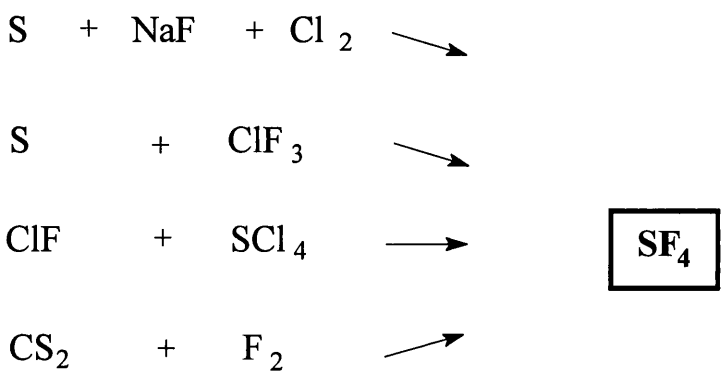

Figure 1.5 : Structure of SF_4

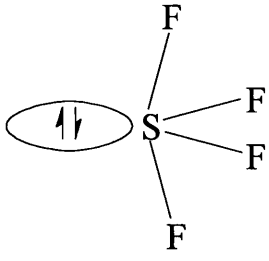

Figure 1.6 : Structure of SF_3^+

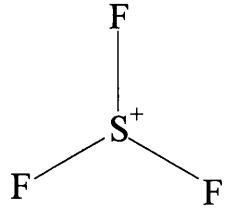

Figure 1.7 : Possible Structures of SF_5^- Species

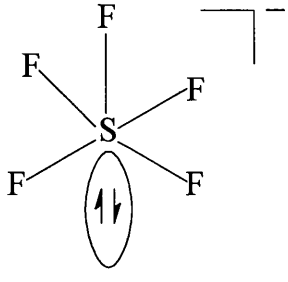

Scheme 1.7 : The Use of SF_4 in Organic Reactions

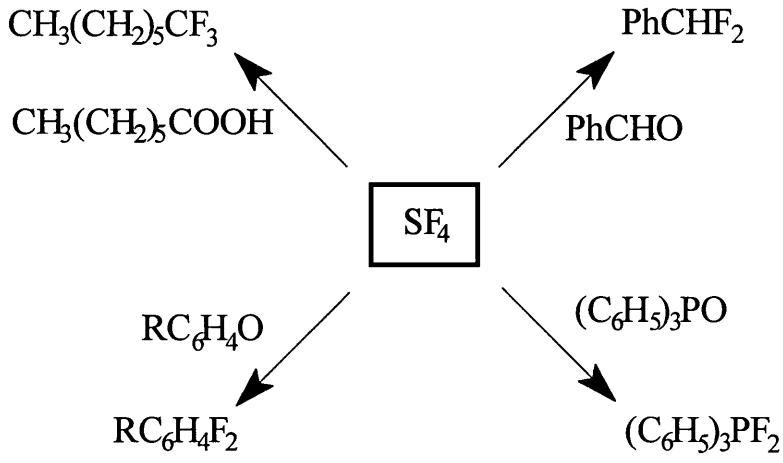

Scheme 1.8 : The Use of SF_4 in Inorganic Reactions

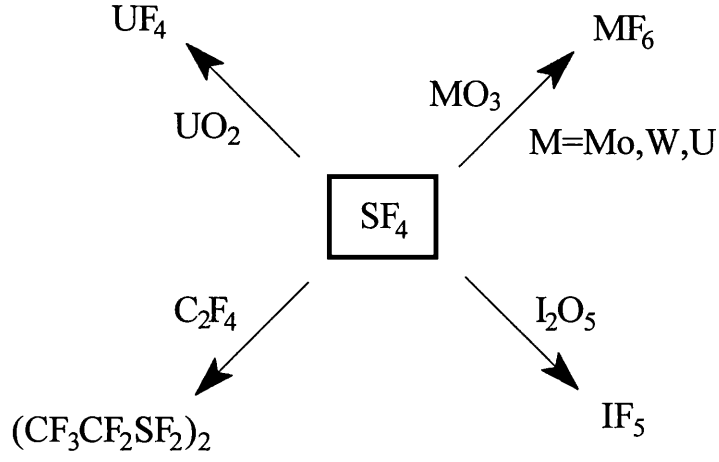

selective with C=O, P=O, COOH and POOH fluorinated to CF_2, PF_2, CF_3 and PF_3 respectively, without fluorination of other reactive functional groups (21).

1.8 Halogenation of γ-Alumina

The chlorination of inorganic oxides with carbon tetrachloride (CCl_4) was first reported in 1910 by Camboulives (116). Detailed discussion of the nature of the interaction and surface species involved was made by Goble and Lawrence, some years later, while studying their application in the low temperature isomerisation of paraffins (105). BET and X-ray diffraction data of the chlorine treated γ-aluminas indicated retention of a high porosity alumina structure consistent with reaction at selective surface species and not within the bulk. The amount of chlorine (c.a. 3.3 x 10^{-4} g/m^2) corresponded to 6 Cl atoms per 100 Å^2 and compared well with the theoretical maximum of 12 OH groups per 100 Å^2 for a full monolayer of alumina crystallites terminated in hydroxyl groups (81).

These observations in conjunction with the presence of oxygen containing species in the vapour phase following chlorination (i.e. $COCl_2$, CO_2) and the complete disappearance of OH bands in the infrared studies (94), was strong evidence for a chlorination mechanism involving the interaction of chlorine groups with surface oxygen containing species on the alumina. The Lewis acidic nature of the resultant aluminium sites, associated with the inductive effect of their

neighbouring electronegative chlorine species, was evident with carbenium ion formation observed on exposure to hydrocarbons.

Promotion of the surface acidity of γ-alumina depended on the nature of the chlorinating agent. Exposure of γ-alumina to anhydrous hydrogen chloride produced a surface which consists of Brønsted acid sites and non-acidic hydroxyl groups (117). The observed protonation of pyridine to the pyridinium ion as observed in infrared studies was a function of the hydrogen chloride chlorinated γ-aluminas Brønsted acidity.

A fundamental understanding of the nature of the acid sites may enable more efficient acid catalysts to be developed. Detailed investigation of the interaction of [^{36}Cl]-chlorine and [^{14}C]-carbon labelled carbon tetrachloride and [^{36}Cl]-chlorine and [^{2}H]-hydrogen labelled hydrogen chloride with γ-alumina enabled proposals to be made about the nature of the acid sites (75). The observed enhancement in Brønsted acidity, after HCl promotion, was attributed to dissociative adsorption of HCl in which terminal hydroxyl groups on Al^{3+} are replaced by chlorine and a neighbouring bridging oxygen is protonated (Eqn. 1.15).

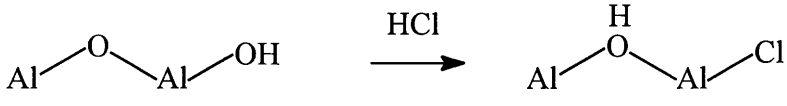

Eqn. 1.15

The surface model for hydrogen chloride promotion of γ-alumina was consistent with the facile hydrogen and chlorine exchange between surface species and HCl (> 90% exchange). The lack of Lewis acidity was associated with saturation of the Al^{3+} sites by the introduction of bulky chlorine groups.

Promotion of γ-alumina acidity by exposure to CCl_4 is thought to involve the initial rapid replacement of terminal hydroxyl groups by chlorine with formation of $COCl_2$ and HCl (Eqn. 1.16). The carbonyl chloride is then able to react further replacing the bridging oxygen by a two chlorine groups and producing CO_2 and HCl (Eqn. 1.17).

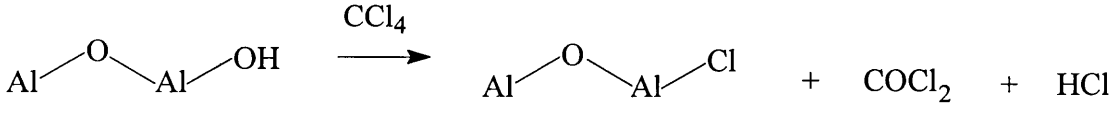

Eqn. 1.16

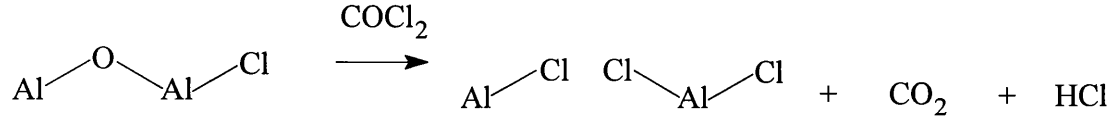

Eqn. 1.17

The existence of 2 distinct types of surface chlorine is supported by the exchange data, with only 70% of the surface chlorine facile with respect to [^{36}Cl]-chlorine labelled hydrogen chloride. Previous studies with the archetypal Lewis acid,

$AlCl_3$, indicated no observable exchange between [^{36}Cl]-chlorine and the solid anhydrous $AlCl_3$ (118). It was therefore concluded that the labile chlorine on γ-alumina, with respect to [^{36}Cl]-chlorine labelled hydrogen chloride, was associated with Brønsted acid sites, whereas the inert chlorine was complexed to Lewis acid sites.

Consideration of the model [110] face of γ-alumina promoted by hydrogen chloride, shows that replacement of terminal hydroxyl groups is possible for tetrahedral and octahedral aluminium(III) environments (Figure 1.8). In the model [110] face of γ-alumina promoted by CCl_4, however, both terminal hydroxyl groups and in plane oxygens that bridge three Al(III) sites are involved i.e. two surface Al^{3+} atoms and one immediately below the surface (Figure 1.9). The proposed Lewis acid sites consist of an octahedral Al^{3+}, two tetrahedral Al^{3+} and four chlorines. The coordinatively unsaturated Al^{3+} is bound to two chlorines each acting as a bridge to the neighbouring tetrahedral Al^{3+} and to an Al^{3+} beneath the plane. Each tetrahedral Al^{3+} has a terminal chlorine (75).

Fluorination of γ-alumina has been widely studied because the electronegative fluorine extends Brønsted acidity to alumina, which is used commercially in a variety of acid catalysed conversions of hydrocarbons (78,119, 120). The commercial importance and interest in fluorinated γ-alumina is reflected in the number of fluorinating agents reported including HF, SF_6, CF_4, CHF_3, F_2 etc

Figure 1.8 : Brønsted Acid Sites on Chlorinated γ-Alumina

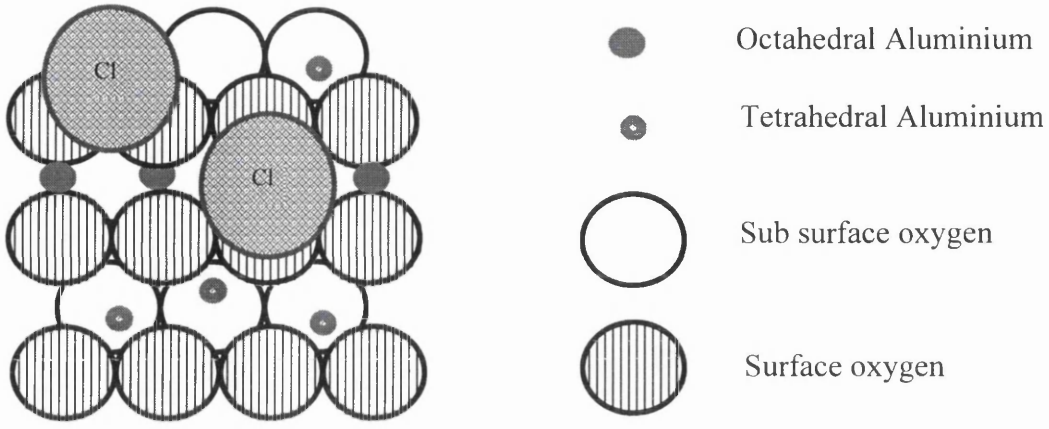

Coordinatively Saturated Al 4C and Al 6C Environment

Figure 1.9 : Lewis Acid Sites on Chlorinated γ-Alumina

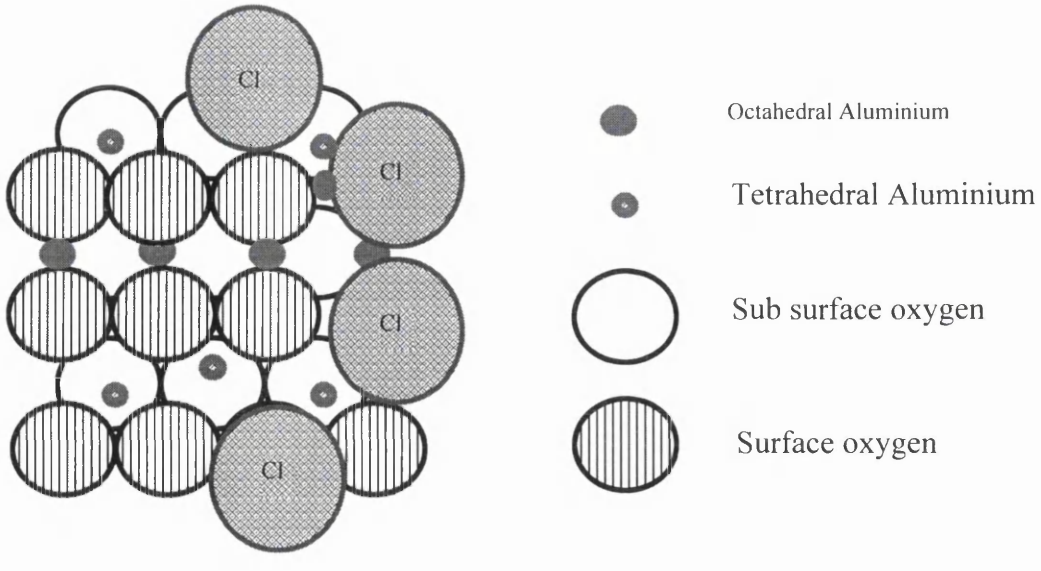

Coordinatively Unsaturated Al 6C Environment

(120-123). The most widely used fluorination procedure involves aqueous impregnation of γ-alumina with NH_4F, followed by calcination at high temperature. This treatment results in enhancements in Brønsted and Lewis acidity as determined by base adsorption studies (124), and solid state ^{19}F NMR indicates the presence of Al-F species (125).

The specific mechanism which results in modification of the hydroxyl groups on the γ-alumina surface during fluorination is not completely understood. It is generally accepted that the fluoride anions interact with the OH groups such that a significant number of the OH groups are replaced by fluorine atoms. Thereafter the high electronegativity of fluorine species on the solid, polarises the remaining O-H bonds via a strong inductive effect resulting in considerable increase in the acidity of the solid surface. The level of acidity of the fluorinated γ-alumina and hence the acidic properties depend on the method of fluorination and subsequent level of fluorine incorporated (119,126).

In the work discussed in this report, SF_4 fluorinated γ-alumina was evaluated as a Friedel-Crafts catalyst in model reactions. In previous radiochemical studies analogous to those discussed for CCl_4 chlorination of γ-alumina (75), γ-alumina was fluorinated with [^{18}F]-fluorine and [^{35}S]-sulfur labelled SF_4, SOF_2, COF_2 and anhydrous HF (121). Perhaps not surprisingly the HF behaved in an analogous

manner to HCl, resulting in the proposal that dissociative adsorption of H-F onto the γ-alumina surface, enhances the Brønsted acidity.

Carbonyl fluoride did not behave in an analogous fashion to carbonyl chloride, instead undergoing hydrolysis on the γ-alumina surface and increasing Brønsted acidity, presumably associated with the hydrolysis product HF. The behaviour of SF_4 fluorinated γ-alumina with respect to [^{18}F]-fluorine exchange with H^{18}F was completely consistent with the CCl_4 chlorination model in which two types of chlorine were proposed. It was therefore proposed that the facile fluoride species (c.a. 58%) was associated with Brønsted acid sites and the inert fluorine atoms were associated with Lewis acid sites.

The Lewis acid sites of solid acids were examined by exposure to the probe molecule 1,1,1-trichloroethane at room temperature. Notably, the archetypal Lewis acid $AlCl_3$ catalysed the dehydrochlorination and concomitant oligomerisation of CH_3CCl_3 resulting in the deposition of a coloured organic deposit (74). Temperatures in excess of 400 K are required for γ-alumina to exhibit dehydrochlorination properties (127). The CCl_4 chlorinated (75) and SF_4 fluorinated γ-alumina (76) displayed similar behaviour to the solid $AlCl_3$ at room temperature. This clearly indicated the Lewis acidic nature of the halogenated γ-alumina surface and the phenomena will be discussed later in this thesis (chapter 7).

1.9 Oxide Supported Organic Layer Catalysts as Potential Friedel-Crafts Catalysts

Activation of γ-alumina by halogenation with SF_4 and CCl_4 was discussed in section 1.8. The fluorinated and chlorinated surfaces dehydrochlorinate 1,1,1-trichloroethane producing 1,1-dichloroethene and HCl with further reaction resulting in the deposition of a highly coloured organic layer on the solid surface (75,76). Strong Lewis acids, such as the archetypal Lewis acid $AlCl_3$ also dehydrochlorinate 1,1,1-trichloroethane in a similar manner (74). The 1,1,1-trichloroethane probe molecule and its interaction with solid acids was adopted as a test for Lewis acidity.

The exact nature of the organic layer has not been conclusively established but it appears to be derived from polymerisation of the dehydrochlorination product CH_2CCl_2 (Scheme 1.9). Polymerisation of the alkene unit is possibly the result of cationic initiation by an intermediate carbocation species produced on interaction of an alkyl halide with the Lewis acid surface sites (Scheme 1.10). This type of mechanism is consistent with those reported for coke formation on chlorinated γ-alumina isomerisation catalysts used in the petrochemical industry (128,129).

In the reaction of 1,1,1-trichloroethane with SF_4 fluorinated γ-alumina, the formation of the organic layer was accompanied by the production of fluorinated products, $CH_3CCl_{3-n}F_n$ (n = 1-3) (77, 130). The organic layer catalyst was active in the fluorine for chlorine exchange of CH_3CCl_3 with anhydrous HF, at room

temperature, yielding a mixture of fluorinated products, $CH_3CCl_{3-n}F_n$ (n = 1-3). Similar reactions were observed for a variety of chlorocarbons including $CH_3CCl_2CH_3$, CH_3CCl_3, $CHCl_2CHCl_2$ and $CHCl{=}CCl_2$. The catalytically active fluorinated γ-alumina with an organic layer deposited on the surface is known as an oxide supported organic layer catalyst.

Scheme 1.9 : Layer Formation Observed in the Preparation of Oxide Supported Organic Layer Catalyst

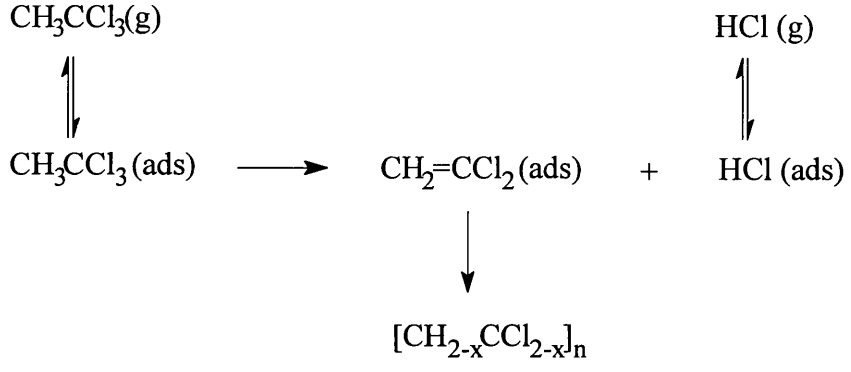

Scheme 1.10 : Cationic Initiation in the Formation of the Oxide Supported Organic Layer Catalyst

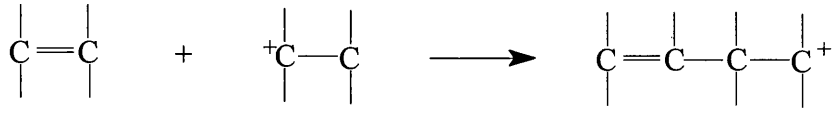

Interestingly, product distributions were consistent with the propensity of the hydrochlorocarbons to undergo dehydrochlorination, implying that the replacement of chlorine by fluorine is unlikely to be the result of a simple halogen exchange reaction. Protonation of the olefin, produced by dehydrochlorination, via surface Brønsted acidity is proposed as a suitably reactive intermediate in the formation of fluorinated products.

The catalytic activity of the oxide supported organic layer catalysts led to a proposed model in which the oligomeric layer does not block Lewis acid sites but acts as a quasi-liquid phase extending solubility to incoming reagents. The catalytic activity of such materials in model Friedel-Crafts reactions was studied within this work.

1.10 Potential of β-AlF_3 as a Friedel-Crafts Catalyst

The applications of aluminium fluorides and fluorinated aluminium oxides in the heterogeneous catalysis of fluorine for chlorine exchange are widely used. In the current climate of environmental protection, the best known examples are in the synthesis of hydrofluorocarbons (HFCs), for use as alternatives to the ozone depleting chlorofluorocarbons (76,77,131,132). Interconversions of fluorine for chlorine is thermodynamically possible but kinetic limitations require catalysts to achieve conversion. A good example is in the preparation of HFC-134a (1,1,1,2-tetrafluoroethane), a refrigerant used instead of CCl_3F and CCl_2F_2.

It is generally necessary to activate the metal fluorides and oxides via an HF or haloalkane pretreatment, before catalytic activity is observed. Kemnitz studied the activation process involved (133) and the nature of the catalyst surfaces formed following activation (78), for the dismutation of $CHClF_2$ to CHF_3. The catalytically active species in the solid surfaces were characterised by following changes in the solid phase on activation of certain aluminium oxides, hydroxyfluorides and fluorides by XRD and IR.

XRD analysis on γ-alumina activated at 675 K revealed the formation of the β-AlF_3 phase, traces of α-AlF_3 and $AlF_2(OH)$ pyrochlore structure. Synthesis of the specific fluoride phases enabled comparison of their catalytic activity pre and post activation. With the exception of β-AlF_3 all the solids required activation before they were catalytic.

Characterisation of the active site responsible for the β-AlF_3 activity was possible via FTIR photoacoustic spectroscopic studies of chemisorbed pyridine on the solid (134). The ability of the pyridine lone pair of electrons to bind coordinatively to Lewis acid sites or interact with acidic OH groups to form adsorbed pyridine or pyridium ions respectively, is a powerful tool in distinguishing between Lewis and Brønsted acid sites on a solid surface (98,99,135,136).

In the pyridine studies, β-AlF_3 exhibited exclusively Lewis acid sites with no Brønsted acidity detected. It was concluded that the dismutation of $CHClF_2$ to CHF_3 required Lewis acid coordination vacancies on the catalytic solid. The metastable β-AlF_3 solid phase is closely related to the hexagonal tungsten bronze structure and has a pseudo hexagonal crystal habit. The network is built up from very regular AlF_6 octahedra, rotated by 7.2° from the ideal HTB structure, with hexagonal hollow channels or cavities in the solid (137). The Al-F mean bond distance is very close to the sum of the Al^{3+} and F^- ionic radii, resulting in hexagonal hollow channels of ~350pm diameter (Figure 1.10). A cavity diameter of this size is sufficiently large for water and nitrogen molecules to enter but C_1 hydrocarbons are too large to penetrate the channels. BET surface area measurements of the β-AlF_3 solid have shown it to have a surface area of ~30m^2/g (78).

Figure 1.10 : Linking of the AlF_6 Octahedra in HTB structure of β-AlF_3 [001] face

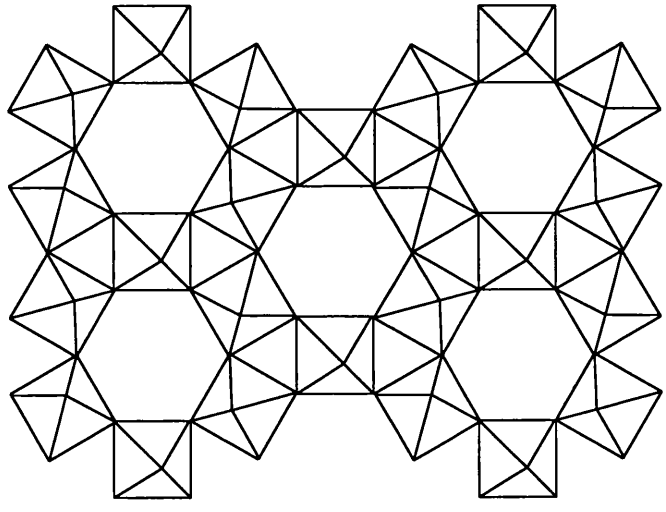

As discussed earlier the catalytic activity of Friedel-Crafts catalysts is a function of their vacant Lewis acid sites (i.e. the presence of coordinatively unsaturated Al^{3+} on the surface). The vacant orbitals afford interaction with electron pair donor species (Lewis bases), producing transient carbenium ion-catalyst complexes. It is the reactivity of such complexes which result in carbon to carbon bond formation between the carbenium ion and a π or σ donor molecule. The Lewis acid sites on β-AlF_3 were proposed for exploitation in Friedel-Crafts catalysis and studied within this work.

While this work was in progress a report appeared describing the enhancement of the catalytic activity of β-AlF_3 in dismutation reactions by replacement of aluminium by magnesium or chromium (138). Maximum catalytic activity was achieved at 10-20 atom % magnesium doping with a decrease in catalytic activity above this threshold attributed to distortion of the β-AlF_3 structure and lowering of Lewis acidity (139).

CHAPTER 2

EXPERIMENTAL

The hygroscopic nature of the materials examined during this work, made it essential to exclude air and moisture. All work was performed *in vacuo* (10^{-4} Torr), or in an inert atmosphere box ($H_2O \leq 3$ppm).

2.1 Equipment

2.1.1 The Vacuum Systems

Two distinct vacuum systems were used depending on the nature of the volatile material in use, a Pyrex glass system for handling volatile organic materials and a Monel metal system for handling corrosive materials such as sulfur tetrafluoride.

Each system consisted of a rotary pump connected to a line with gas handling facilities. A series of waste traps, cooled with liquid nitrogen, prevented damage to the pump from exposure to volatile materials. The vacuum lines were calibrated by attaching Pyrex glass bulbs of known volume and recording the resultant pressure in various portions of the line. This process was repeated several times to minimise any error in volume, before calculating line volumes via the ideal gas equation (Eqn. 2.1).

$$PV = nRT \qquad \text{Eqn. 2.1}$$

where P = Pressure (atmosphere)

V = Volume (litre)

n = Quantity of gas (mol)

R = Gas constant (0.082058 L.atm/(K.mol))

T = Absolute temperature (K)

2.1.2 Pyrex Glass Vacuum Line

The Pyrex glass enclosed system consisted of a gas handling manifold, pressure gauge and a mercury vacustat (Figure 2.1). Evacuation of the line to 10^{-4} Torr was achieved by a rotary vacuum pump in conjunction with a water cooled mercury diffusion pump. The vacustat measured the vacuum achieved by the pump, while a Bourden tube pressure gauge (Heise) enabled pressure in the manifold to be measured to ± 0.5 Torr. The manifold had several B14 sockets, isolated from the system by high vacuum stopcocks (Young or Rotaflow). Vacuum flasks and ampoules, containing reagents, equipped with high vacuum stopcocks and B14 cones were connected to the manifold using Kel-F grease. All the vessels and the vacuum system, were flamed out to reduce adsorbed moisture levels on the glass surface.

2.1.3 Monel Metal Vacuum Line

Monel is a nickel/copper based alloy, chosen for its chemical resistance to corrosive chemicals such as sulfur tetrafluoride. The Monel system (Figure 2.2) was constructed from 2/5 inch Monel tubing and Monel metal valves. Nipple and collar

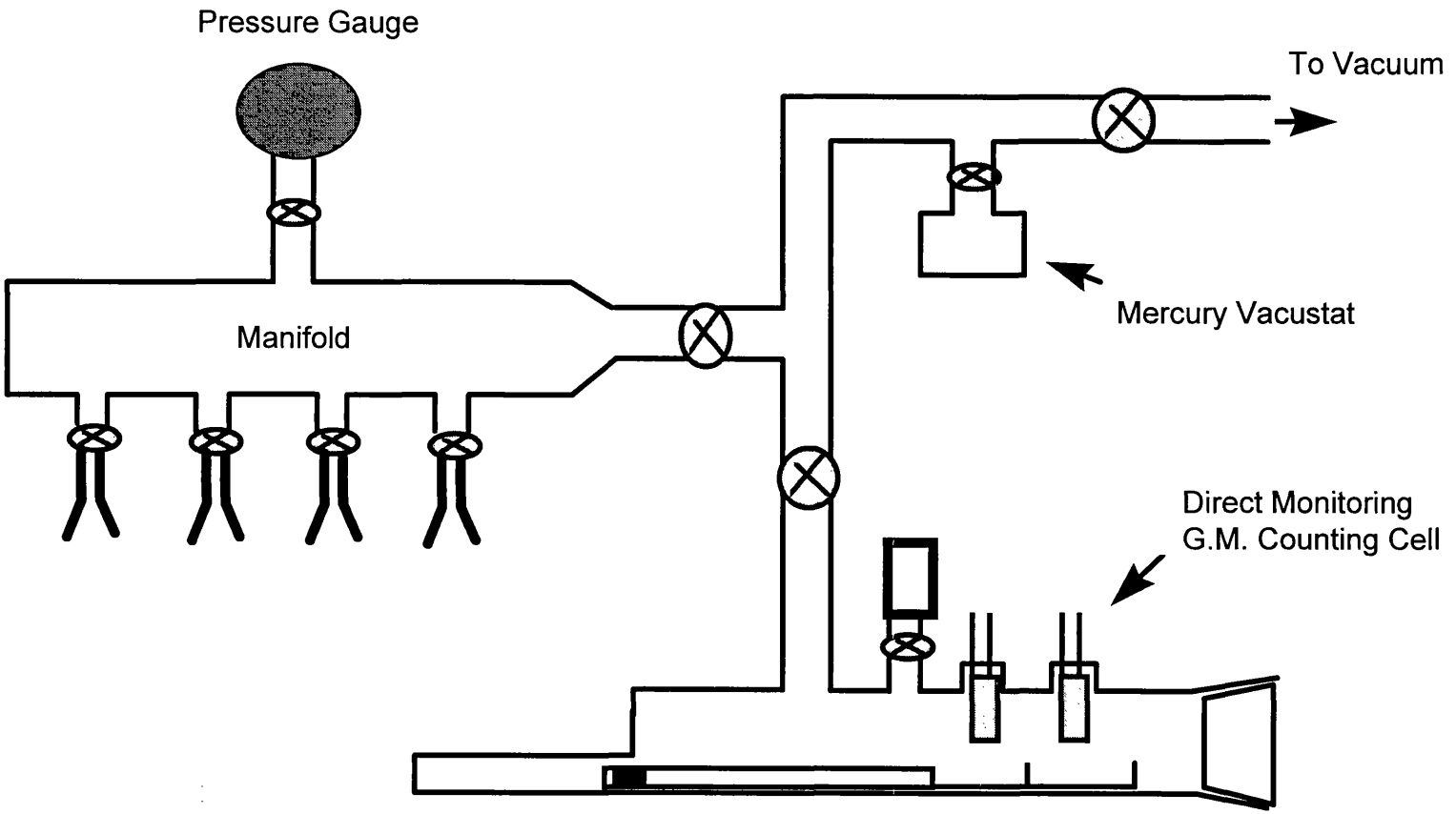

Figure 2.1 : Pyrex Glass Vacuum Line

screw couplings enabled connection of Monel metal or stainless steel bombs to the manifold. The Monel section was connected to the rotary pump and waste traps via a 1/4 inch glass/Monel seal. A cylinder of SF_4 and a Monel metal waste trap were connected to the manifold, with pressures in the line monitored on an inline pressure gauge (Heisse).

2.1.4 Inert Atmosphere Box

A nitrogen atmosphere glove box ($H_2O \leq 3$ ppm) was used when handling and storing all solid samples. Glass vessels were evacuated and flamed out before transferring to the box. An analytical balance within the box enabled samples to be weighed to two decimal places, in a dry atmosphere.

2.1.5 Catalyst Microreactor

Friedel-Crafts solid/liquid phase reactions were studied using the reactor shown in Figure 2.3. The reactor consisted of three ports - (i) a gas inlet port, (ii) a gas outlet port and (iii) a septum cap. The gas outlet port was fitted with a condenser exiting to a gas scavenger system. A flow of inert gas (He) was passed through the reactor during catalytic runs, in order to minimise H_2O vapour due to the hygroscopic nature of the solids under investigation. Loading of catalysts into the reactor in an inert atmosphere box and injection of reactants through the septum cap, minimised exposure to air and moisture. A magnetic stirrer hotplate was used to agitate the

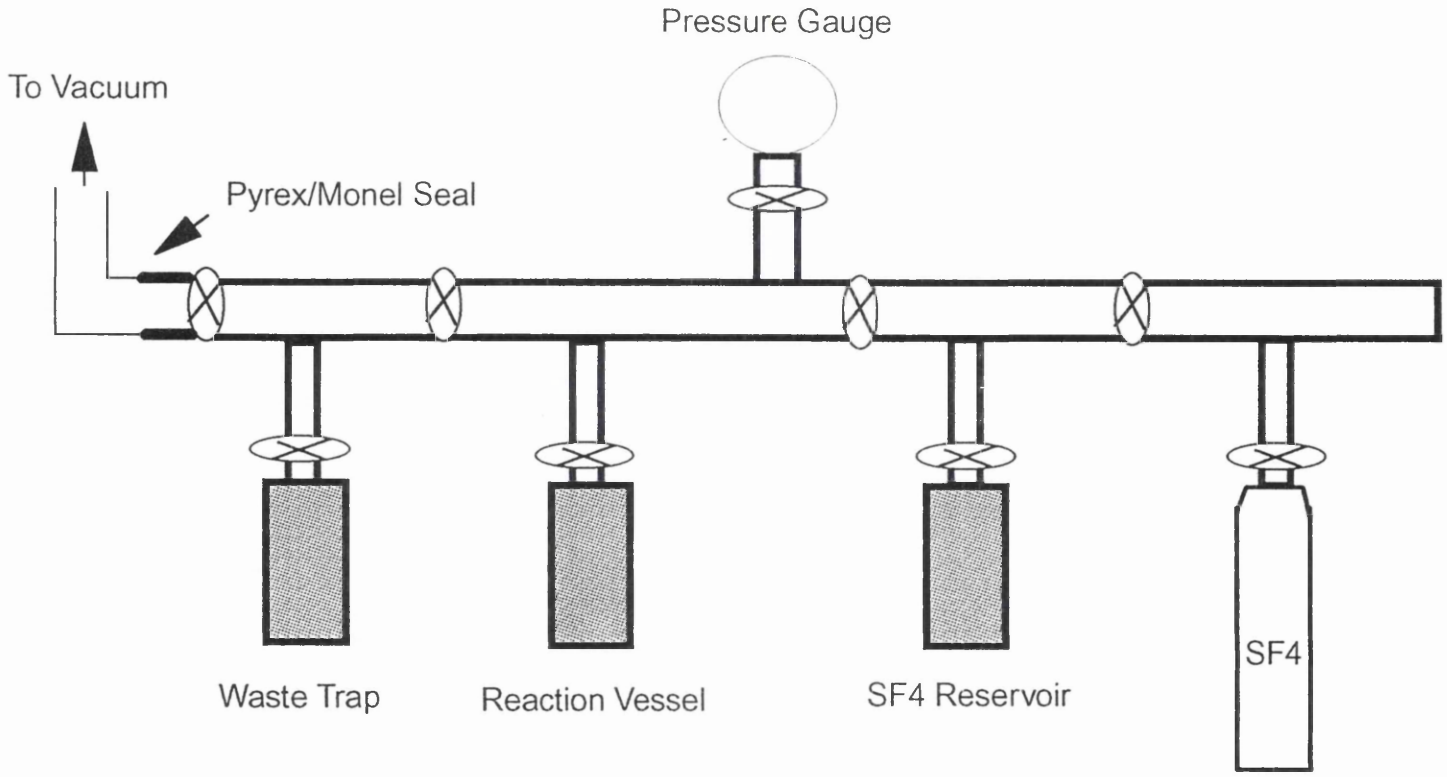

Figure 2.2 : Monel Metal Vacuum Line

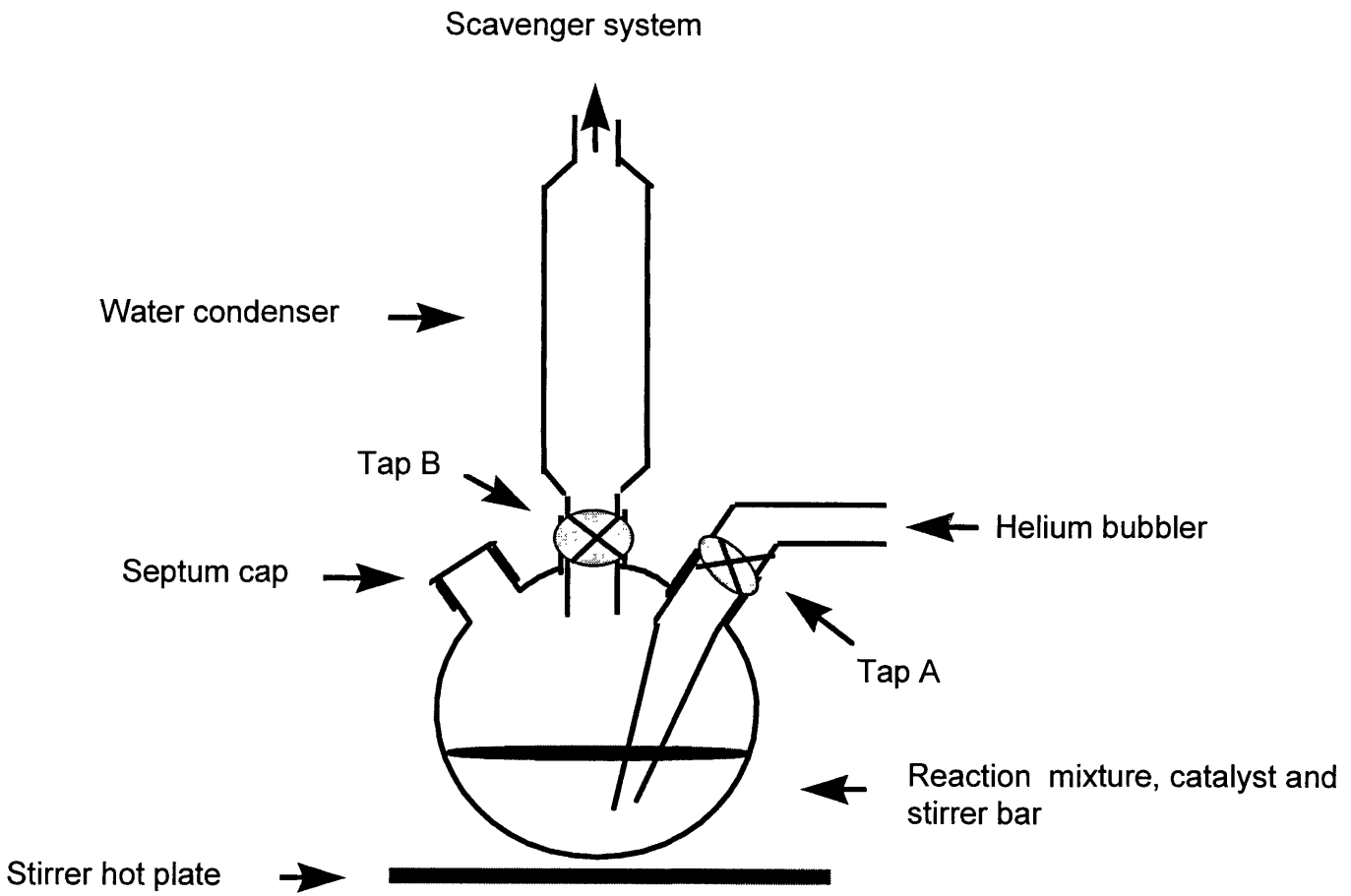

Figure 2.3 : Catalyst Microreactor

reaction mixture and therefore limit diffusion effects. Samples of the reaction mixture were taken by syringe via the septum cap and analysed by GC and GCMS.

2.2 Preparation and Purification of Reagents

2.2.1 Sulfur Tetrafluoride

Sulfur tetrafluoride (94% pure, Fluorochem) supplied in a cylinder was connected to the manifold of a Monel metal vacuum system. Sulfur tetrafluoride is a colourless gas (bp 233 K), susceptible to hydrolysis yielding thionyl fluoride and hydrogen fluoride. For this reason stainless steel or Monel apparatus were used when handling SF_4.

2.2.2 Carbon Tetrachloride

Carbon tetrachloride (99.99% pure, Pronalys) was stored over 3 Å molecular sieves, *in-vacuo*, under subdued light to prevent degradation. Carbon tetrachloride is a colourless liquid which boils at 349 K.

2.2.3 Purification of 1,1,1-Trichloroethane

1,1,1-Trichloroethane (99% pure, Aldrich) was stored over 3 Å molecular sieves, *in-vacuo,* under subdued light to inhibit photopolymerisation. The 1,4-dioxane stabilizer present to inhibit polymerisation and oxidation, was removed by vacuum distillation. 1,1,1-Trichloroethane is a colourless liquid which boils at 349 K.

2.2.4 Purification of 1,1-Dichloroethene

1,1-Dichloroethene (99% pure, Aldrich) was stored over 3 Å molecular sieves, *in-vacuo*, under subdued light to inhibit photopolymerisation. The hydroquinone monomethyl ether present to inhibit polymerisation and oxidation, was removed by vacuum distillation. 1,1-Dichloroethene is a colourless liquid which boils at 303-305 K.

2.2.5 Preparation of Anhydrous Hydrogen Chloride

Anhydrous hydrogen chloride was generated by the reaction of concentrated hydrochloric acid with concentrated sulfuric acid (Eqn. 2.2) (140).

$$Cl^-_{(aq)} + H_2SO_{4(aq)} \rightarrow HCl_{(g)} + HSO_4^-{}_{(aq)} \qquad \text{Eqn. 2.2}$$

The apparatus consisted of a reaction vessel with a dropping funnel and a pressure equilibrating arm, to which a series of cooled traps were attached (Figure 2.4). Traps (i) and (ii) contained the drying agent P_2O_5 and were cooled to 213 K in dichloromethane/dry ice. Trap (iii) was used as a collection vessel, cooled to 153 K in isopentane/liquid nitrogen slush.

Concentrated HCl (10 cm^3) and concentrated H_2SO_4 (15 cm^3) were loaded into the upper and lower limbs of the vessel respectively. Drop wise addition of the conc. HCl into the conc. H_2SO_4, liberated hydrogen chloride which was distilled

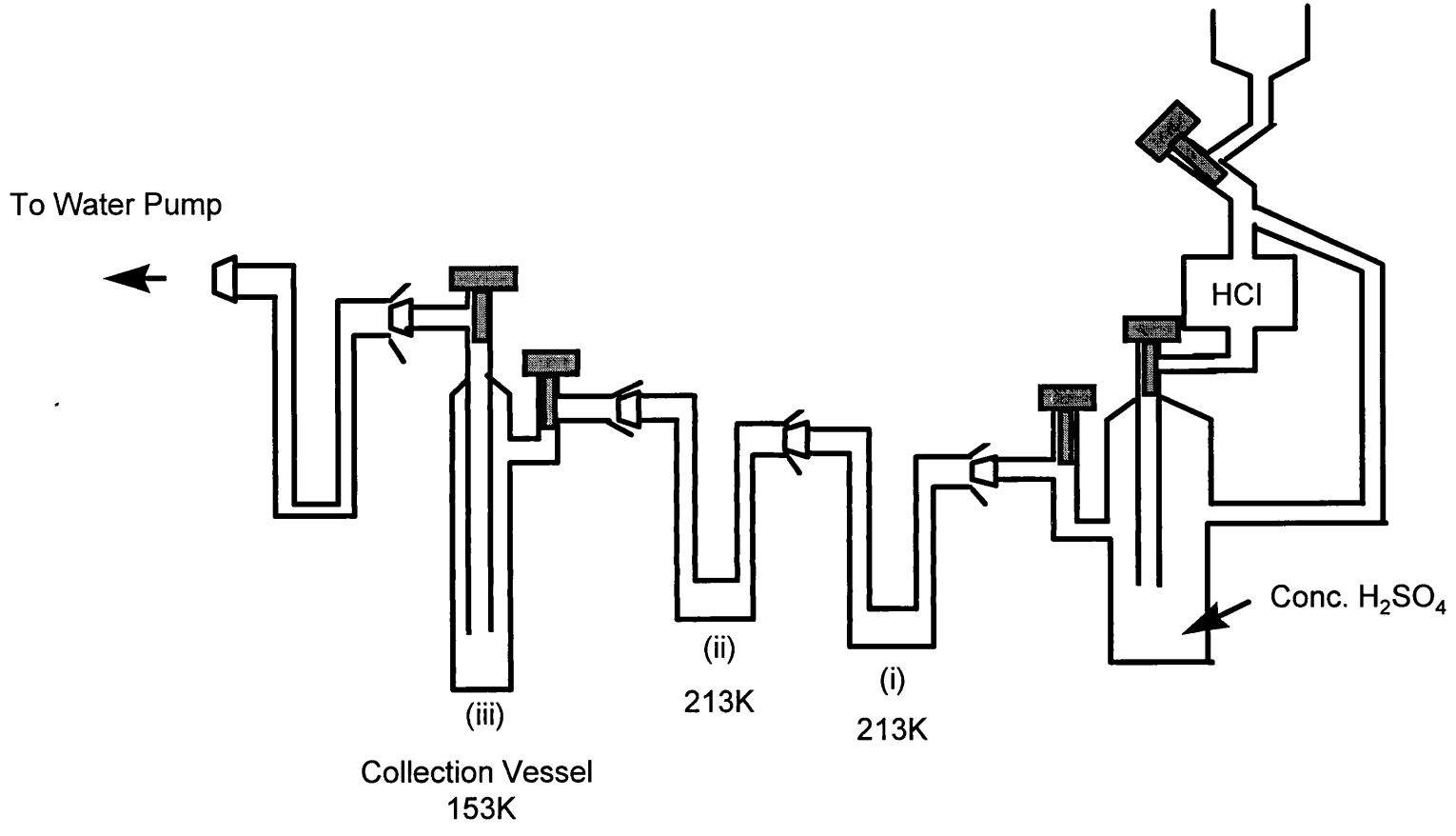

Figure 2.4 : Hydrogen Chloride Preparation Apparatus

through traps (i) and (ii) and was collected in trap (iii). The vessel was transferred to a vacuum line where the HCl was degassed before vacuum distilling into a Monel metal bomb containing P_2O_5.

2.2.6 [^{36}Cl]-Chlorine Radioisotope

Radio-labelling specific reactants of interest enabled a radiotracer technique known as direct monitoring Geiger Müller counting, to be used to study reactant-catalyst interactions (79,80).

The [^{36}Cl]-chlorine isotope decays by β^- emission (Eqn. 2.3) with a half life of $3x10^5$ y.

$$^{36}Cl \rightarrow {}^{36}Ar + e^- + \nu^- \qquad \text{Eqn. 2.3}$$

The [^{36}Cl]-chlorine isotope was supplied as a solution of [^{36}Cl]-NaCl (Amersham International p.l.c.). A 1 cm^3 sample of the $Na^{36}Cl$ solution was diluted with concentrated HCl (9 cm^3), giving a solution with specific [^{36}Cl]-chlorine activity of *c.a.* 9.3 x 10^5 Bq cm^{-3}.

2.2.7 Preparation of [^{36}Cl]-Chlorine Labelled Hydrogen Chloride (140)

Anhydrous [^{36}Cl]-chlorine labelled hydrogen chloride was generated by the reaction of concentrated hydrochloric acid (containing the [^{36}Cl]-chlorine isotope) with concentrated sulfuric acid (Eqn. 2.4).

$$^{36}Cl^-_{(aq)} + H_2SO_{4(aq)} \rightarrow H^{36}Cl_{(g)} + HSO_4^-{}_{(aq)} \qquad \text{Eqn. 2.4}$$

The apparatus and procedure described for the preparation of anhydrous hydrogen chloride in section 2.2.5 was followed. The [^{36}Cl]-chlorine label was introduced via the addition of a sample (1 cm^3, 25μCi) of the [^{36}Cl]-chlorine solution, prepared in section 2.2.6, to the concentrated HCl in the upper limb of the reactor prior to reaction.

2.2.8 Preparation of [^{36}Cl]-Chlorine Labelled 2-Chloropropane (141)

A sample of CCl_4 chlorinated γ-alumina (0.5 g), as prepared in section 2.3.2, was loaded into a stainless steel bomb in an inert atmosphere box. The bomb was transferred to a Pyrex vacuum line and degassed. Propene vapour was expanded into a calibrated manifold (254 cm^3) to a pressure of 660 Torr, giving 9.0 mmol of propene, which was condensed into the bomb at 77 K. The bomb was isolated before expanding [^{36}Cl]-chlorine labelled hydrogen chloride vapour into the calibrated manifold to a pressure of 600 Torr, giving 8.1 mmol of H^{36}Cl, which was condensed into the bomb at 77 K. Reaction was initiated by warming the bomb to

room temperature and holding for 18 h. The reaction mixture was analysed following reaction by infrared and gas chromatography of the vapour phase.

2.2.9 Preparation of [^{36}Cl]-Chlorine Labelled *t*-Butyl Chloride (142)

2-Methylpropan-2-ol (1.66 g : 23.0 mmol) was added to a 100 cm^3 separating funnel to which concentrated hydrochloric acid (5.66 cm^3) containing [^{36}Cl]-chlorine labelled hydrogen chloride (1 cm^3, 25 μCi) was added. The mixture was shaken occasionally over a 2 h period, loosening the stopper to relieve pressure build up. The mixture was allowed to stand until the layers separated sharply, discarding the lower acidic layer. The halide portion was washed with sodium hydrogen carbonate solution (5 cm^3 of 5% solution) and water (5 cm^3). The product was dried over anhydrous calcium sulfate (0.4 g : 3.0 mmol), isolated via vacuum distillation and stored over 3 Å molecular sieves. The reaction mixture was analysed following reaction by ^{13}C and ^{1}H N.M.R.

2.2.10 Preparation of [^{36}Cl]-Chlorine Labelled Acetyl Chloride (143)

[^{36}Cl]-chlorine labelled acetyl chloride was prepared via chlorine exchange of acetyl chloride with [^{36}Cl]-chlorine labelled hydrogen chloride. A quantity of CH_3COCl (4.0 mmol) was isolated in the calibrated manifold (254 cm^3) by allowing the vapour to expand to a pressure of 300 Torr. The acetyl chloride vapour was then condensed into a stainless steel bomb at 77 K. The bomb was isolated before expanding a quantity of [^{36}Cl]-chlorine labelled hydrogen chloride (4.0 mmol), as

prepared in section 2.2.7, into the calibrated manifold (254 cm^3) by allowing the vapour to expand to a pressure of 300 Torr. The [^{36}Cl]-chlorine labelled hydrogen chloride was then condensed into the bomb at 77 K, and the bomb warmed to room temperature and held for 2 h to promote the exchange reaction.

Following the exchange reaction, HCl was removed from the [^{36}Cl]-chlorine labelled acetyl chloride in the reaction vessel by vacuum distillation at 193 K, in a dry ice/acetone bath. Removal of residual HCl from the [^{36}Cl]-chlorine labelled acetyl chloride proved somewhat difficult. Complete removal of HCl was achieved by repeatedly pumping the reaction mixture under dynamic vacuum at 193 K. This process was repeated five times, with the infrared spectrum of the vapour phase used to confirm removal of the HCl. Removal of the HCl was critical as it would have interfered with radiochemical studies, due to interaction with the solid surfaces.

2.3 Preparation and Pretreatment of Catalysts

The hygroscopic properties of the solids under investigation made it necessary to exclude moisture and air at all times. Catalyst preparations were carried out *in vacuo* (10^{-4} Torr), with catalyst manipulations being performed in an inert atmosphere box ($H_2O \leq 3$ ppm).

Degussa γ-alumina was obtained as a fine powder with its associated handling difficulties. To facilitate the handling of this material it was pelletized. The

procedure involved preparing an alumina paste with deionised water (400 g powder and 250 cm^3 water). The paste was heated in an evaporating dish on a hot plate until a dry cake was obtained, which was then sieved to give pellets of particle size 400 - 1680 μm.

2.3.1 Calcination of γ-Alumina

A sample of γ-Alumina (10.0 g) was loaded into a dry stainless steel bomb which was fitted with a cone and valve. The bomb was attached to a Pyrex vacuum line and degassed. An electrically heated furnace and a thermocouple to monitor temperature were fitted round the bomb. The bomb was heated to 523 K and held for 6 h under dynamic vacuum to dehydrate the γ-alumina surface. The calcined γ-alumina sample was transferred to an inert atmosphere box and stored under nitrogen.

2.3.2 Chlorination of γ-Alumina (75)

A sample of calcined γ-alumina (2.10 g) was loaded into a Monel metal bomb and fitted with a cone and valve, in an inert atmosphere box. The bomb was transferred to a Pyrex vacuum line and degassed. A quantity of carbon tetrachloride (8.0 mmol) was isolated in the calibrated manifold (254 cm^3) by allowing the vapour to expand to a pressure of 584 Torr. The carbon tetrachloride was then condensed into the bomb at 77 K. The reaction bomb was isolated and warmed to room temperature before being fitted with an electrically heated furnace and a

thermocouple to monitor temperature. The bomb was heated to 473 K and held for 4 h. After cooling to room temperature, the volatile material from the bomb was expanded into a gas infrared cell and the infrared spectrum recorded. The bomb was pumped out to remove remaining volatile material before the chlorinated γ-alumina was transferred to an inert atmosphere box and stored under nitrogen.

2.3.3 Fluorination of γ-Alumina (121)

A sample of calcined γ-alumina (1.5 g) was loaded into a Monel metal bomb and fitted with a cone and valve in an inert atmosphere box. The bomb was transferred to a Monel metal vacuum line and degassed. A quantity of sulfur tetrafluoride (9.0 mmol) was isolated in the calibrated manifold by allowing the vapour to expand to a pressure of 1084 Torr. The sulfur tetrafluoride was then condensed into the Monel bomb at 77 K. The bomb was warmed to room temperature to initiate reaction and held for 2 h. The volatile material from the bomb was expanded into a gas infrared cell and the infrared spectrum recorded before pumping out the bomb to remove remaining volatiles. The fluorination process was repeated a further twice to ensure efficient fluorination of the γ-alumina. The fluorinated γ-alumina was transferred to an inert atmosphere box and stored under nitrogen.

2.3.4 Formation of Oxide Supported Organic Layer Catalysts (144)

A sample of halogenated γ-alumina (0.75 g) was loaded into a stainless steel bomb and fitted with a cone and valve, in an inert atmosphere box. The bomb was transferred to a Pyrex vacuum line and degassed. A quantity of 1,1,1-trichloroethane (1.5 mmol) was isolated in the calibrated manifold (254 cm^3) by allowing the vapour to expand to a pressure of 110 Torr. The 1,1,1-trichloroethane was then condensed into the bomb at 77 K and the bomb isolated. The contents of the bomb were heated to room temperature and held for 3 h. Volatile material from the bomb was expanded into a gas infrared cell and the infrared spectrum recorded, before pumping out the bomb. The oxide supported organic layer catalyst produced was transferred to an inert atmosphere box and stored under nitrogen.

2.3.5 Sublimation of Aluminium(III) Chloride (145)

An evacuated Pyrex vessel was flamed out under dynamic vacuum, before placing in an inert atmosphere box. A sample (1-2 g) of aluminium(III) chloride (anhydrous > 99% pure, Fluka AG) and a piece of aluminium wire (99.99% pure, Fluka AG) were weighed into the vessel. The function of aluminium wire was to reduce any iron chloride impurities during sublimation. The aluminium(III) chloride was degassed before attaching to the sublimation apparatus (Figure 2.5) via the breakseal. The sublimation apparatus was flamed out and the breakseal broken, before heating the aluminium(III) chloride to 393 K with an electrically heated furnace (thermocouple used to monitor temperature). The sublimate was condensed

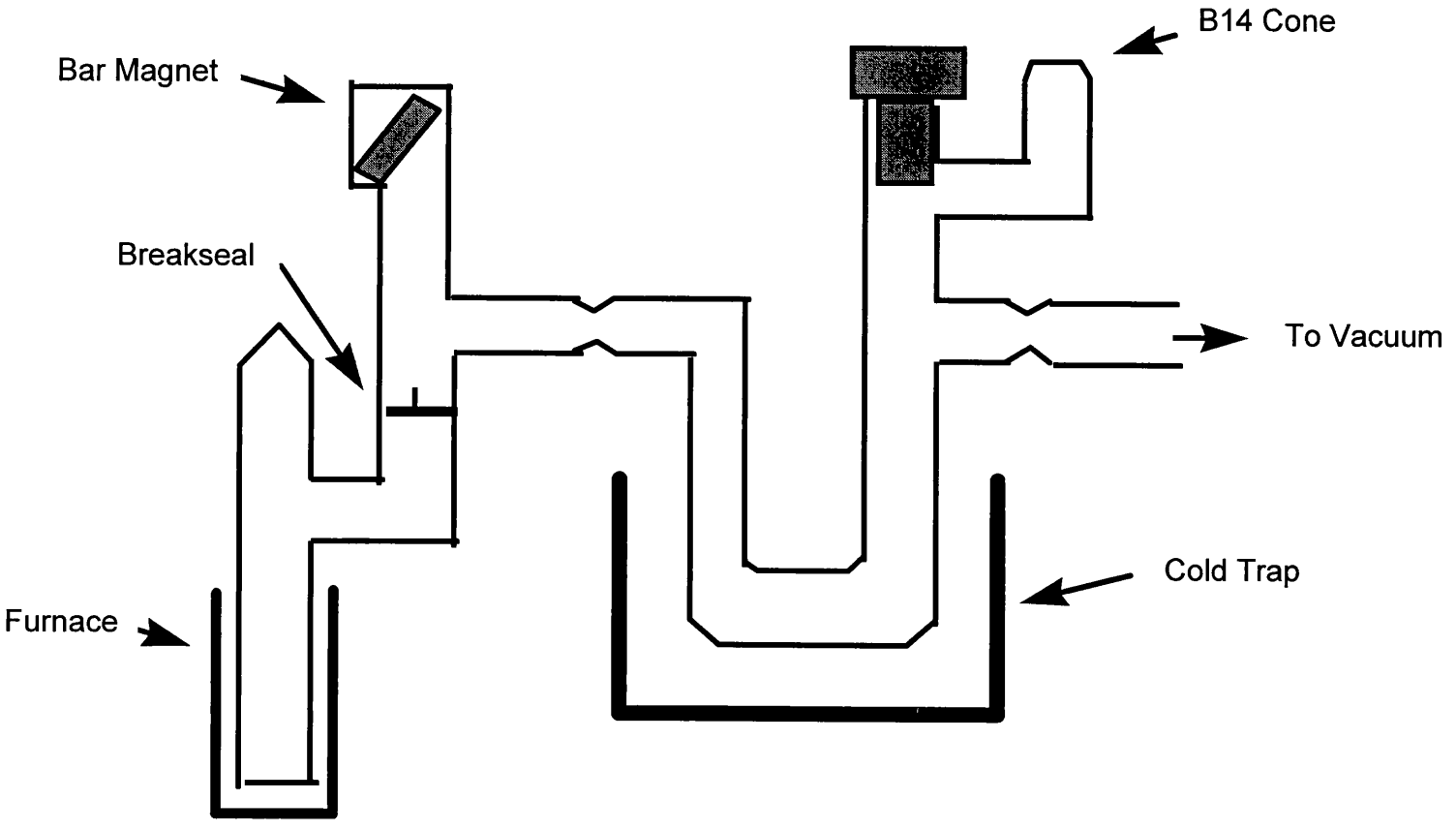

Figure 2.5 : Sublimation Apparatus

in the Pyrex U-bend of the system at 77 K, under dynamic vacuum. The apparatus was heated during the sublimation process to prevent sublimate condensing on the inner walls of the Pyrex glass.

On completion of the sublimation process, the Pyrex U-tube containing the sublimed aluminium(III) chloride was sealed under vacuum at the constrictions, with a gas/oxygen flame. The sealed U-tube was transferred to an inert atmosphere box and the aluminium(III) chloride used as soon as possible.

2.3.6 Preparation of β-AlF_3 (137)

A sample of α-$AlF_3.3H_2O$ (5.0 g) was loaded into a Pyrex flow vessel (Figure 2.6). An electrically heated furnace and a thermocouple, connected to a temperature programmer were fitted around the vessel and heated (5 K min^{-1}) to 493 K under dynamic vacuum, to give an amorphous solid ($AlF_3.xH_2O$, where $x < 0.5$). Pure crystalline β-AlF_3 was obtained by passing a flow of inert gas (He) over the amorphous solid as it was heated (5 K min^{-1}) to 723 K. The β-AlF_3 was transferred to an inert atmosphere box and stored under nitrogen.

2.4 Friedel-Crafts Reactions

Friedel-Crafts alkylation or acylation reactions involve the addition of an alkyl or acyl halide respectively to a nucleophilic, electron rich, molecule in the

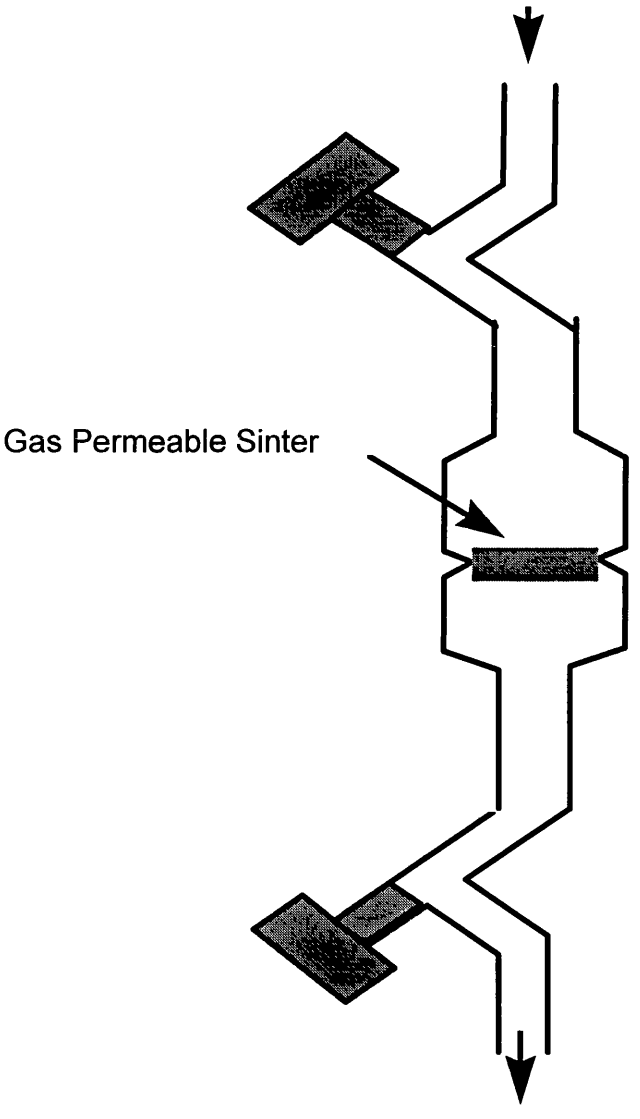

Figure 2.6 : Flow Reactor

presence of a Lewis acid catalyst. The catalytic activity of a variety of solid materials in model Friedel-Crafts reactions was investigated during this work.

2.4.1 Experimental Method

The solid materials of interest were examined for catalytic behaviour in the model Friedel-Crafts reactions using the catalyst microreactor described in section 2.14. The hygroscopic nature of the solid materials being examined made it essential to avoid contact with air or moisture. The solid of interest (0.5 g) was loaded into the catalyst microreactor in an inert atmosphere box, in order to prevent the solids becoming deactivated due to contact with air or moisture.

The reagents, i.e. alkyl or acyl halide (22.4 mmol) and aromatic compounds (224.0 mmol), were injected directly into the reactor via the septum cap, such that they covered the solid. It was hoped that coverage of the solid by the reactants made the solids less susceptible to deactivation from air and moisture. A helium bubbler and condenser were fitted to the reactor and a positive pressure of helium introduced before opening the system to the condenser and scavenger system. The liquid-solid reaction mixture was stirred at a constant rate with a magnetic stirrer bar and magnetic stirrer hotplate. Samples (0.5 cm^3) of the reaction mixture were taken by syringe at timed intervals and analysed by GC and GCMS (discussed in section 2.6 and 2.7). A ratio of 1:10 alkyl or acyl halide to aromatic was designed to minimise the effects of multiple alkylation and facilitated ease of sampling.

2.5 Infrared Spectroscopy

2.5.1 Infrared Spectroscopy in the Vapour Phase Over Surface Reactions

Infrared spectroscopic analysis of material in the vapour phase of gas/solid systems was performed using an *in-situ* gas infrared cell (Figure 2.7). The cell consisted of KBr windows, a 10 cm path length, B14 socket (to host a dropping ampoule for delivery of solid material) and a trough to prevent the solid from affecting the spectrometer beam. Attachment of the cell to the calibrated manifold of a vacuum system enabled expansion of known quantities of vapour into the cell. A specially designed cell holder, afforded reproducible positioning of the cell in the spectrometer beam. The cell was also used without the solid dropping facility to analyse gaseous reaction products from other reactions.

2.5.2 Experimental Procedure

A sample (0.5 g) of the solid catalyst of interest was loaded into a dropping ampoule in an inert atmosphere box. The ampoule was transferred to the limb of an *in-situ* gas infrared cell (Figure 2.7) and the vessel degassed. A known pressure of vapour (20 Torr) was expanded into the manifold and the infrared cell before isolating the cell. The cell was transferred to an infrared spectrophotometer and the spectrum of the vapour phase recorded in the absorbance mode. The solid material of interest was then dropped into the infrared cell, via the dropping ampoule, where it was exposed to the vapour. The reaction between the vapour and the solid was

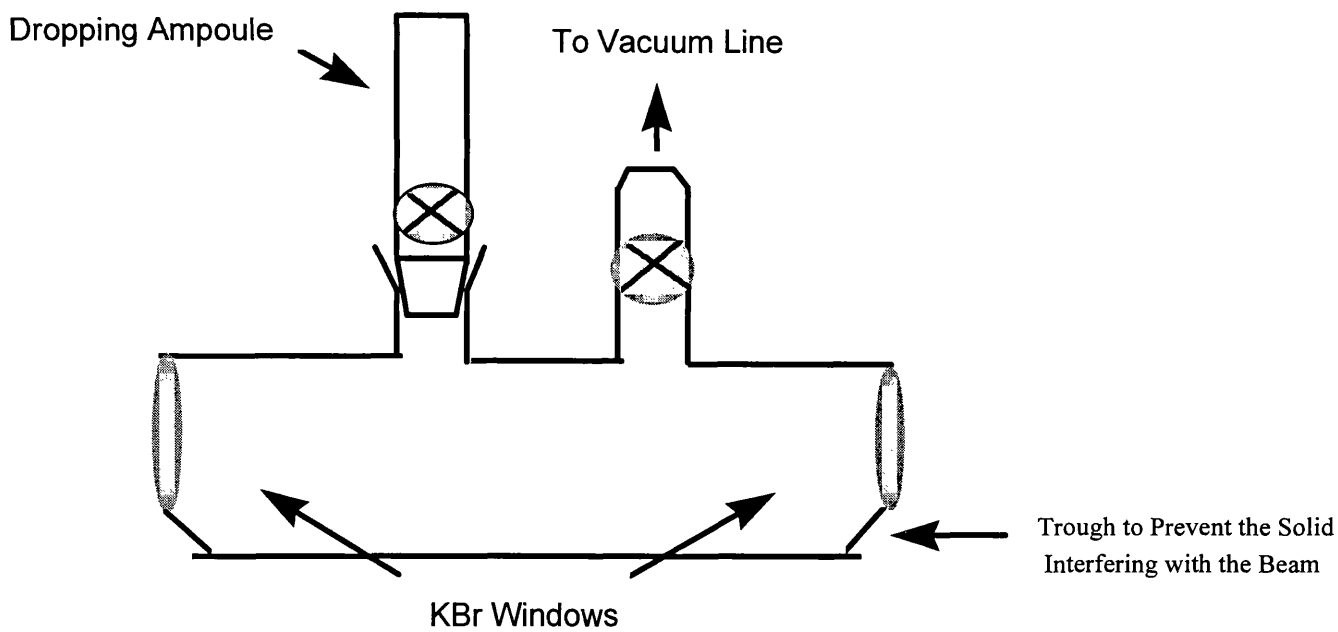

Figure 2.7 : "in-situ" Gas Infrared Cell

followed by recording the infrared spectra of the vapour phase at specific time intervals following the dropping of the solid into the cell (i.e. 1, 15, 30, 60 min and finally at 20 h).

2.5.3 Identification of Gaseous Samples

Infrared spectroscopic assignments of reagents and reaction products were made by comparison with standard literature assignments from the 'Aldrich Library of Infrared Spectra' or vapour phase spectra of the authentic materials. Principal peak positions for the reagents used and possible reaction products are presented in Table 2.1.

2.6 Gas Chromatography (GC)

An A.M.S. Model 93 Gas Chromatograph fitted with a 15 m capillary column and a flame ionisation detector (FID) was used in the analysis of Friedel-Crafts reaction products. The FID was connected to an electronic integrator and chart recorder. Carrier gas flow rates were set at 25 cm^3 min^{-1} nitrogen, 40 cm^3 min^{-1} hydrogen and 300 cm^3 min^{-1} air. Initial Column Temperature : 313 K (benzene system) and 333 K (toluene system) ; Column Hold Time : 2 min ; Final Temperature : 473 K ; Hold Time : 2 min ; Ramp Rate : 20 K min^{-1} ; Injector Temperature : 473 K ; Detector Temperature : 498 K.

Table 2.1 : Principal Infrared Peaks

Compound	Wavelength (cm^{-1})
CCl_4	795
SF_4	892, 867, 730, 558, 532, 475
SOF_2	1339, 1329, 807, 747, 530, 393
HCl	2900-2800
SiF_4	1030
CH_3CCl_3	3010, 950, 1440, 385, 1085, 1010, 720, 520
CH_2CCl_2	1730, 1620, 1570, 1140, 1090, 865, 790, 595
$CH_3CH=CH_2$	3080, 3040, 2980, 1690, 1440, 1010, 950, 740
$(CH_3)_3CCl$	2992, 2937, 1374, 1155, 740, 585
$CH_3CHClCH_3$	2997, 2989, 2944, 1471, 1390, 1268, 1163, 1075, 887, 740, 640
CH_3COCl	1827, 1810, 1117, 1108, 962, 614, 605

Samples were injected directly onto the column with a 5 μl syringe. The instrument response was calibrated with standard concentrations of the Friedel-Crafts alkylation products (i.e. *t*-butylbenzene and *t*-butyltoluene). Response Factor : Linear ; Retention Times - $(CH_3)_3CCl$: 0.6 min ; C_6H_6 : 1.9 min ; $C_6H_6CH_3$: 2.1 min ; *t*-butylbenzene : 4.9 min ; di-*t*-butylbenzene : 6.9 and 7.6 min ; 4-*t*-butyltoluene : 4.9 min ; 3-*t*-butyltoluene : 4.9 min ; di-t-butyltoluene : 7.7 min.

2.7 Gas Chromatography Mass Spectrometry (GCMS)

GCMS analysis was performed with a Hewlett Packard 5971 Mass selective detector (quadrupole), interfaced to a Hewlett Packard 5890 series II gas chromatograph. An HP1 non polar fused silica 15 m capillary column (0.20 mm i.d. and 0.33 μm film thickness) was used. Mass spectra were recorded at 70 eV under continuous scanning conditions.

Sampling was via a split injection system (50 : 1) with a 1 cm^3 min^{-1} flow of carrier gas (He). Initial Column Temperature : 353 K ; Hold Time : 2 min ; Final Temperature : 423 K ; Ramp Rate : 5 K min^{-1} ; Injector Temperature : 523 K ; Detector Temperature : 458 K ; Interface Transfer Line Temperature : 553 K. Retention Time : *t*-butylbenzene : 2.7 min ; di-*t*-butylbenzene : 6.9 and 7.9 min ; 4-*t*-butyltoluene : 3.5 min ; 3-*t*-butyltoluene : 3.4 min ; di-*t*-butyltoluene : 8.7 min.

2.8 Radiochemical Counting

2.8.1 Geiger Müller Counters (146,147)

Geiger Müller counters are used in the detection of ionising radiation and consist of a Geiger Müller tube connected to an electronic scaler output. A Geiger Müller tube is a gas-tight chamber with a thin mica window at one end and a centrally mounted counter wire at the other (Figure 2.8). The inside wall of the tube acts as a cathode with the central wire behaving as an anode. The gas contained within the tube is composed of 90% noble gas (argon) and 10% quenching agent (methane or alcohol). The presence of a quenching agent minimises electrical discharge from the casing of the tube, which would result in spurious discharge from the counter.

Ionising radiation entering the tube via the mica window partially ionises the counter gas producing positive ions and electrons. The electrons move rapidly towards the high positive potential of the counter wire while the positive ions move slowly towards the cathodic inner wall of the tube. As the potential difference between the wire and the inner wall increases, electrons gain energy raising the collision frequency with the gas molecules and hence producing greater ionisation and a greater number of electrons. This process of electron multiplication continues until the number of electrons collected on the wire is greater than the number created by the passage of radiation through the counter gas, and is known as 'ion multiplication'.

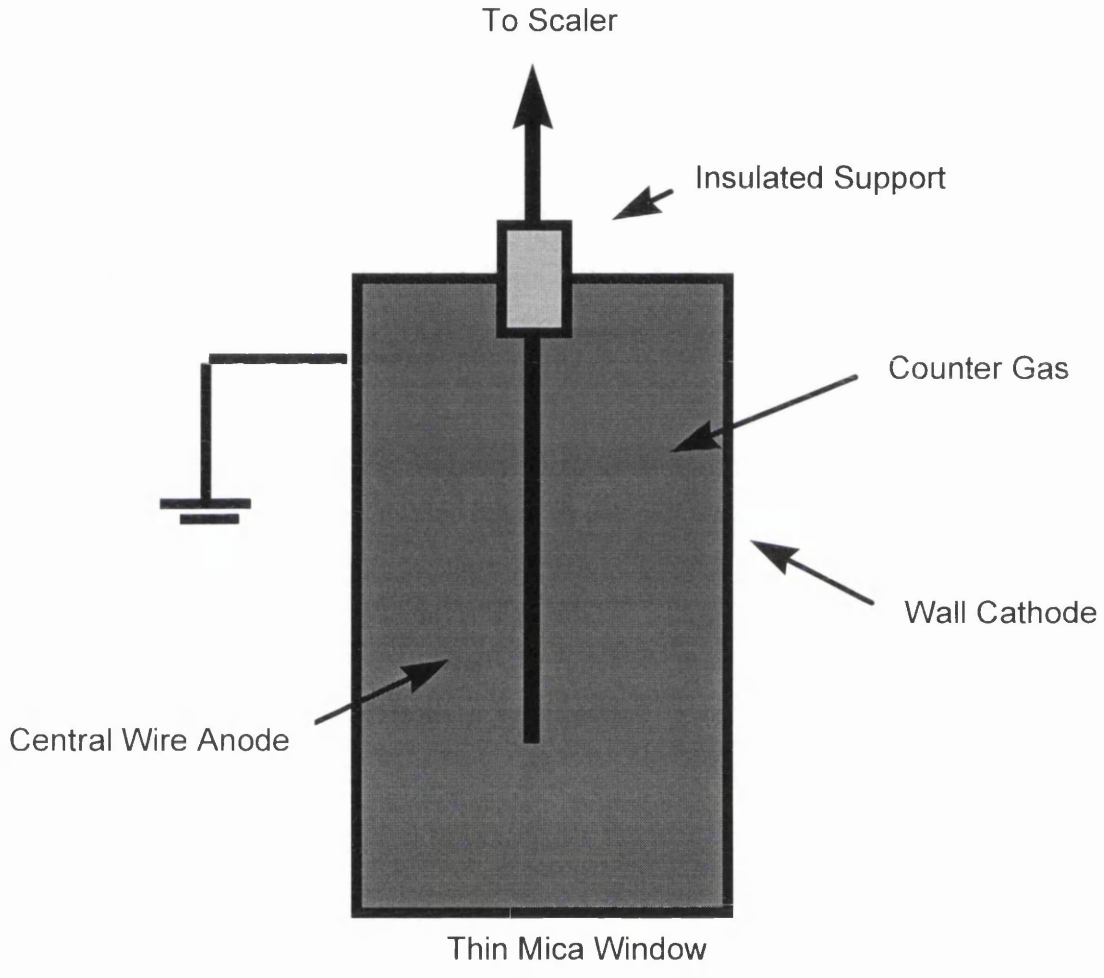

Figure 2.8 : Geiger Müller Tube

Increasing the counter wire voltage increases the extent of ion multiplication until a saturated state known as the Geiger region is reached, where, the number of electrons collected on the wire and hence the magnitude of the resultant voltage pulse is independent of the number of electrons created by the initial radiation passing through the counter gas. The Geiger Region is reached when the number of electrons produced by ion multiplication per primary electron produced by ionisation radiation becomes so great that an 'electron avalanche' is created which spreads along the wire.

2.8.2 Dead Time

Electrons produced in the Geiger Müller tube travel rapidly to the central anode wire whereas the positive ions move comparatively slowly towards the cathodic inner wall of the tube (2.8.1). During this initial lag time the potential difference is below the Geiger threshold (V_o) and hence ion multiplication is prohibited. Once the positive ions are sufficiently far away from the central wire, the counter can operate normally. The period of non-detection resulting from this, is known as the 'dead-time' and has been calculated for short half life species such as [^{18}F]-fluorine at 6.49 x 10^{-4} s. (148). Inclusion of dead time count correction during this work was not necessary as it is less significant than the statistical error in counting.

2.8.3 Plateau Region

The applied voltage on a Geiger Müller counter wire must be large enough to attract electrons to the anode before ionisation radiation can be detected (V_o - 'Geiger threshold'). Above this voltage the count rate increases rapidly until a plateau region is reached where the count rate is independent of the applied voltage. Further increases in the applied voltage will result in a rapid increase in the count rate as the quenching gas within the tube is unable to prevent spurious discharge caused by secondary electron emission at the cathode wall. It is desirable to operate at a voltage in the middle of the plateau region, as the counters are most stable under this condition.

The plateau region was determined for each Geiger Müller counter by constructing a plot of counts vs. voltage on exposure to a solid β source (Figure 2.9). Typical plateau regions in this work ranged from 400 - 500 V, resulting in operating voltages of around 450 V.

2.8.4 Background

Geiger Müller counters will detect ionising radiation in the absence of a radioactive source, as they detect naturally occurring radioisotopes present in the environment. Such radiation is referred to as background radiation and must be subtracted from radiochemical counting experiments. Typical background count rates were in the range, 20 - 40 count min^{-1}.

Figure 2.9 : Typical Plateau Curve (Applied Voltage vs G.M. Counter)

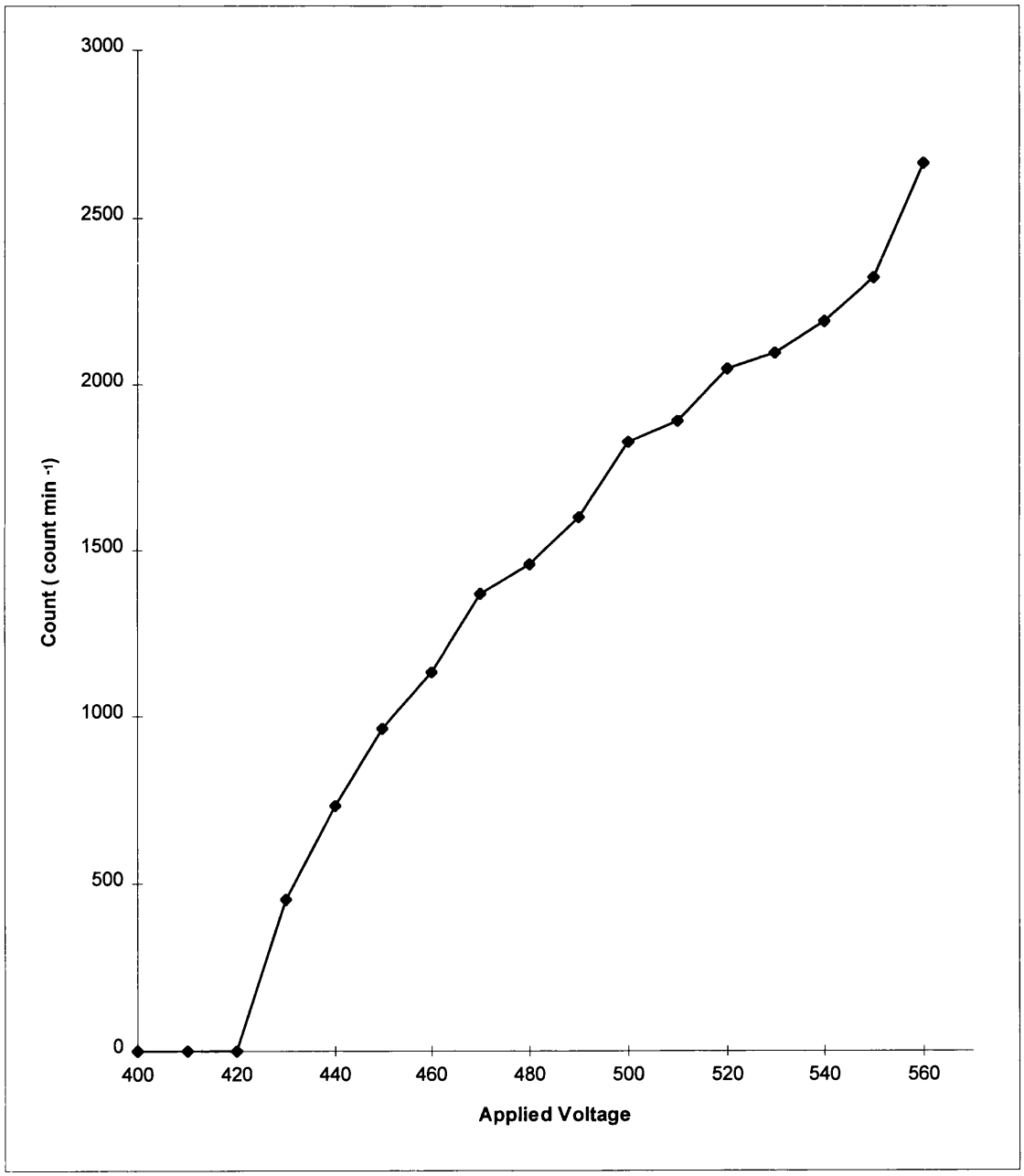

2.8.5. Self Absorption

Ionising radiation (Alpha, Beta and Gamma) interact with matter to varying degrees. α-Radiation for example is completely absorbed by a few centimetres of air. The α-particles lose their energy as a result of electronic interaction in atomic orbitals, in essence, the collision of the α-particle with an electron. Low energy β^- emitters, such as [^{36}Cl]-chlorine, undergo significant self absorption and hence their use in radiochemical experiments, such as the direct monitoring Geiger Müller technique (section 2.9), requires special considerations:

(i) The distance between the counter and the solid material under investigation must always be the same..

(ii) A constant weight of solid material must be used.

(iii) [^{36}Cl]-Chlorine within the bulk of the solid may not be detected.

If these conditions are met and considered when handling the data produced, reliable information can be collected for the surface interactions on a solid, without the need to correct for self-absorption.

2.9 Direct Monitoring Geiger Müller Counting Technique

The direct monitoring Geiger Müller radiochemical counting technique was developed by Thomson and modified by Al-Ammar and Webb (79,80) to determine surface radioactivity on solids exposed to radiolabelled gases. The ability to monitor

in-situ the reaction between a radiolabelled gas and the solid surface of a heterogeneous catalyst has offered mechanistic information in a variety of catalytic processes (76,77).

2.9.1 Equipment

The direct monitoring counting vessel consisted of a Pyrex reaction vessel (Figure 2.10) containing two mounted Geiger Müller tubes, a B14 socket for attachment of a dropping vessel and a Pyrex glass boat containing two sections. The vessel was connected via a manifold to a vacuum system consisting of a constant volume manometer and gas handling facilities. Solid samples of interest were introduced to the counting vessel, under vacuum, by connection of an ampoule containing the solid to the B14 socket. The Pyrex boat could be moved along the length of the vessel using a magnet and hence the solid sample placed below a specific Geiger Müller tube.

The Geiger Müller tubes were calibrated before use, by expanding known pressures of radioactive gas into the vessel and recording the counts. A plot of pressure of gas against counts gave a linear response passing through the origin (Figure 2.11). It was also important to plot the counts from the Geiger Müller tubes against each other to obtain the counting ratio between the tubes. The plot gave a straight line with the gradient equal to the counter ratio (Figure 2.12). The typical

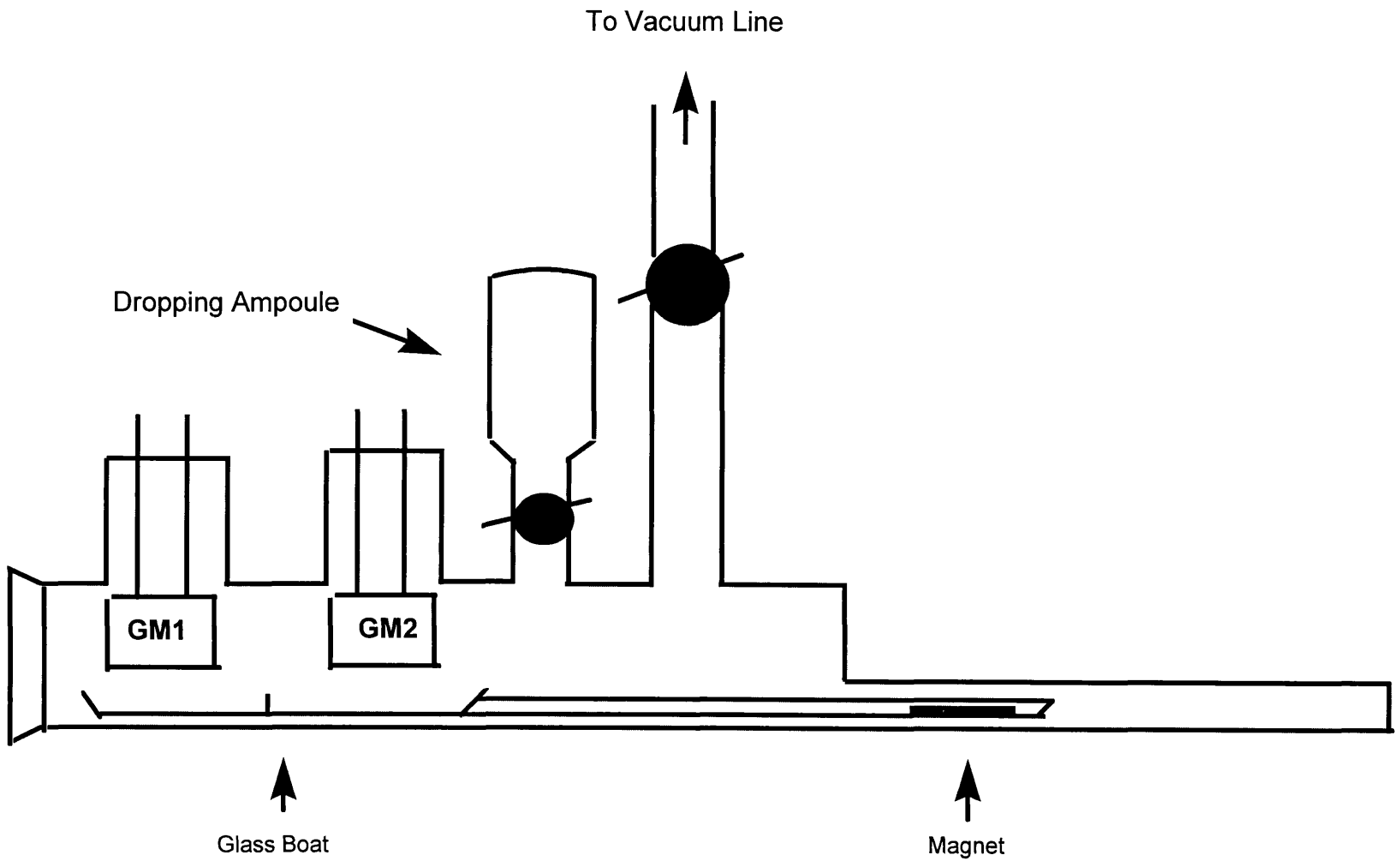

Figure 2.10 : Direct Monitoring Geiger Muller Vessel

Figure 2.11 : Plot of G.M. Counter vs Pressure (atm.)
(for various pressures of $CH_3CO^{36}Cl$)

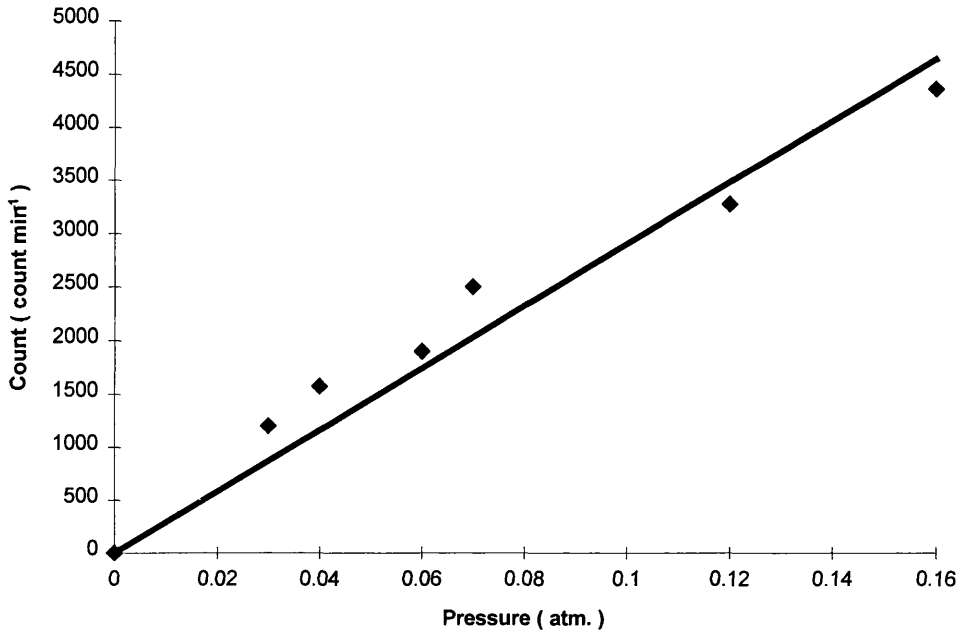

Figure 2.12 : Intercalibration Plot -
G.M.1 Count vs G.M.2 Count
(for various pressures of $CH_3CO^{36}Cl$)

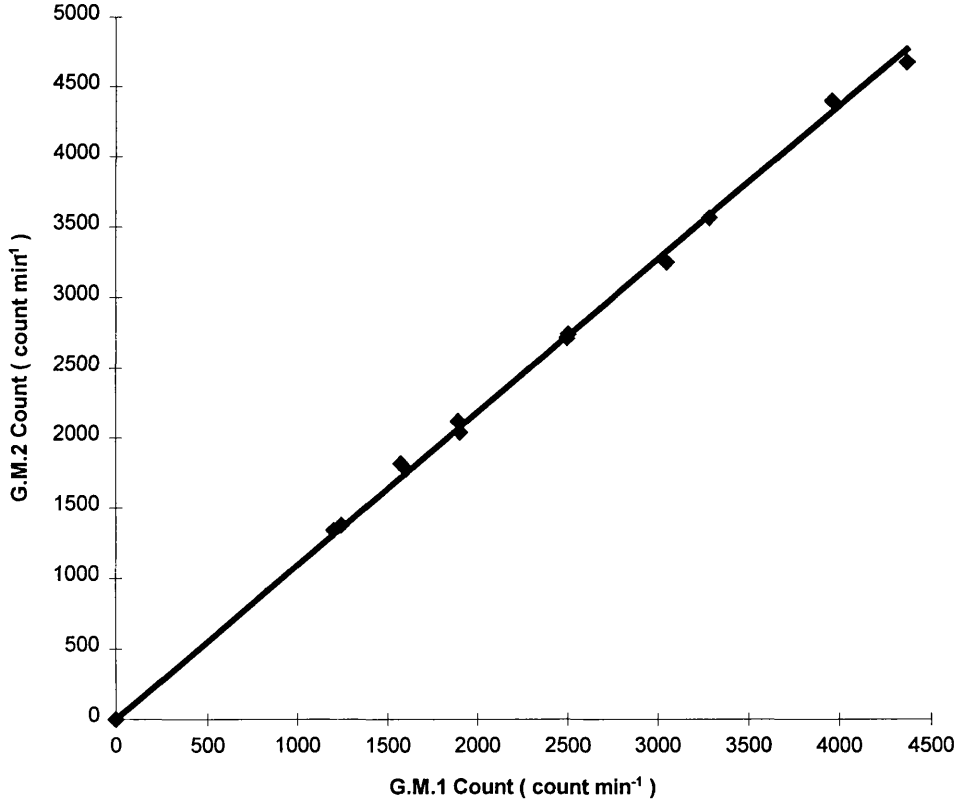

intercalibration ratio was in the region 1 : 1.15, remaining constant throughout the counting period.

2.9.2 Experimental Method

A sample of the solid material of interest was loaded into a dropping ampoule in an inert atmosphere box, degassed and attached to the evacuated counting vessel via the B14 socket. The solid was dropped from the ampoule into the left hand section of the glass boat, which was then positioned such that the left hand section was directly below G.M.1 and the right hand section below G.M.2. G.M.1 recorded gas and solid counts while G.M.2 recorded the gas only count.

Desired pressures of radioactive gas were introduced to the counting vessel, the vessel isolated and the counts from both Geiger Müller tubes recorded over a specific time interval. The recorded counts were corrected for background and intercalibration. A surface count for the solid of interest was obtained by subtracting the counts for G.M.2 (gas only) from the G.M.1 counts (solid and gas).

2.9.3 Statistical Errors

The decay of a radioisotope is a random process and is therefore subject to fluctuation due to the statistical nature of the process. The number of disintegrations observed for a given source, if repeatedly counted over a specified time, will not remain constant, even if the half life of the species is too long to make it relevant to

the recorded count. The probability W(m) of obtaining M disintegrations in time t from N_0 original radioactive atoms, is given by the binomial expression (Eqn. 2.5):

$$W(m) = \{ N_o!(N_o\text{-}m)!m!\} \; P^m (1\text{-}p)^{No-m} \qquad \text{Eqn. 2.5.}$$

where p is probability of a disintegration occurring within the time of observation.

It can be shown from this expression (149,150) that the expected standard deviation for radioactive disintegration, σ, is given by Eqn. 2.6:

$$\sigma = \sqrt{m}e^{-\lambda t} \qquad \text{Eqn.2.6}$$

In practice, the observed time t is short in comparison to the half life so Eqn. 2.6 is reduced to Eqn. 2.7 :

$$\sigma = \sqrt{m} \qquad \text{Eqn. 2.7}$$

where m is the number of counts obtained.

In this study errors quoted are a combination of the uncertainty of counts obtained and variations in physical measurements such as mass of sample and pressure of gas. Surface counts recorded on solids after the treatment outlined above

are often small. In order to use the data with confidence, we carry out repetitive determinations of the surface count rate and take account of statistical error (i.e. the square root of recorded counts).

CHAPTER 3

PREPARATION AND CHARACTERISATION OF [^{36}Cl]-CHLORINE LABELLED *t*-BUTYL CHLORIDE, 2-CHLOROPROPANE AND ACETYL CHLORIDE

3.1 Introduction

This chapter is concerned with the synthesis of [^{36}Cl]-chlorine labelled alkyl and acyl halides for use in the direct monitoring Geiger Müller technique (79,80), discussed in section 2.9. The technique was used to study the interactions between alkyl and acyl halides with solid materials of interest. The information obtained from the direct monitoring studies allowed us to develop an understanding of the nature of the surface interactions in the heterogeneous catalytic systems (chapter 6).

Before preparing radiolabelled compounds, two key questions were addressed:

(i) Which specific alkyl or acyl halides were pertinent to the study?

(ii) Did suitable routes exist for incorporation of the [^{36}Cl]-chlorine radioisotope into the alkyl and acyl halides?

The considerable diversity of Friedel-Crafts reactions made it important to focus on specific model reactions. The radiolabelled alkyl and acyl halides selected had to complement the Friedel-Crafts studies in order to develop working models for the catalytic systems.

The combination of a tertiary and secondary alkyl halide with two aromatic compounds, possessing different propensities towards electrophilic aromatic substitution, offered both an activated system for screening of the solid materials and a more demanding system for assessing catalytic activity. The alkyl halides, *t*-butyl chloride and 2-chloropropane were selected as they could be easily labelled with [^{36}Cl]-chlorine and were sufficiently volatile for use in the direct monitoring technique and Fourier transform infrared studies.

Problems associated with conventional Friedel-Crafts acylation reactions are the focus of considerable interest within the academic and industrial communities (refer to section 1.3) (36). The strong binding interaction of acyl carbonyl functional groups to Friedel-Crafts catalysts such as the archetypal Lewis acid, $AlCl_3$, are well documented. Synthesis of [^{36}Cl]-chlorine labelled acetyl chloride was an important goal, as it would enable the interaction between the acyl halide and the catalyst surfaces to be studied.

The development of experimental procedures to prepare [^{36}Cl]-chlorine labelled *t*-butyl chloride, 2-chloropropane and acetyl chloride, is discussed within this chapter. The radiochemical data obtained, were used to explain experimental observations made in the Friedel-Crafts systems and are discussed in chapter 6.

Toluene and benzene were chosen as the aromatic reagents, the inductive effect (+I) of the methyl group on toluene activates the ring system towards electrophilic aromatic substitution, and makes benzene vs. toluene excellent substrates for studying different levels of Friedel-Crafts catalytic activity.

3.2 Experimental Strategy

Alkyl halides are commonly prepared in industry by direct halogenation of hydrocarbons at high temperature via free radical reactions, resulting in a mixture of products, separated by distillation. In order to synthesise [^{36}Cl]-chlorine labelled *t*-butyl chloride, 2-chloropropane and acetyl chloride, synthetic routes for incorporation of the [^{36}Cl]-chlorine radioisotope were investigated. The experimental procedures were examined initially with unlabelled hydrogen chloride in order to minimise the potential exposure to the [^{36}Cl]-chlorine radioisotope. The physical form of the [^{36}Cl]-chlorine labelled hydrogen chloride available and an appreciation of the synthetic routes to alkyl and acyl halides, led to proposal of the following procedures. The [^{36}Cl]-chlorine radioisotope was available in concentrated hydrochloric acid (as prepared in section 2.2.6) or as anhydrous hydrogen chloride (as prepared in section 2.2.7).

Preparation of 2-chloropropane via electrophilic addition of anhydrous hydrogen chloride across the double bond in propene (141), was examined (Scheme 3.1). Interaction between the electronegative character of the weak π bond

of the alkene and the electron deficient (i.e. electrophilic) proton of the hydrogen chloride, is hindered by a considerable activation energy. The presence of a strong Lewis acid catalyst, however, provides a low energy pathway from reactants to products. Markovnikov addition, is favoured due to the stability of the intermediate carbenium ion and results in formation of 2-chloropropane (experimental observations discussed in section 3.5).

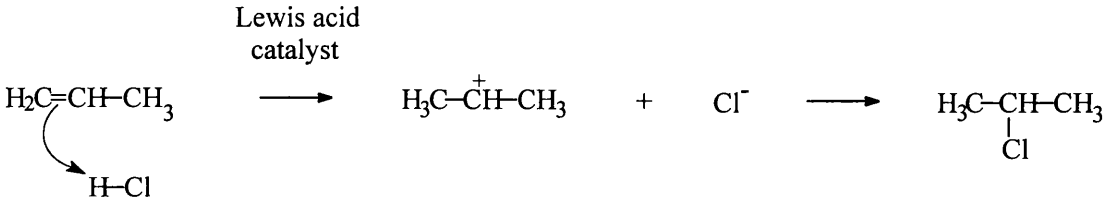

Scheme 3.1

The preparation of *t*-butyl chloride, via the nucleophilic substitution of 2-methyl propan-2-ol in concentrated hydrochloric acid, was examined (Scheme 3.2). 2-Methyl propan-2-ol should undergo a unimolecular (S_N1) reaction forming an intermediate *t*-butyl carbenium ion (142). The inherent stability of the *t*-butyl carbenium ion prevents rearrangements, and subsequent attack by the nucleophilic chlorine species should yield *t*-butyl chloride (experimental observations discussed in section 3.4).

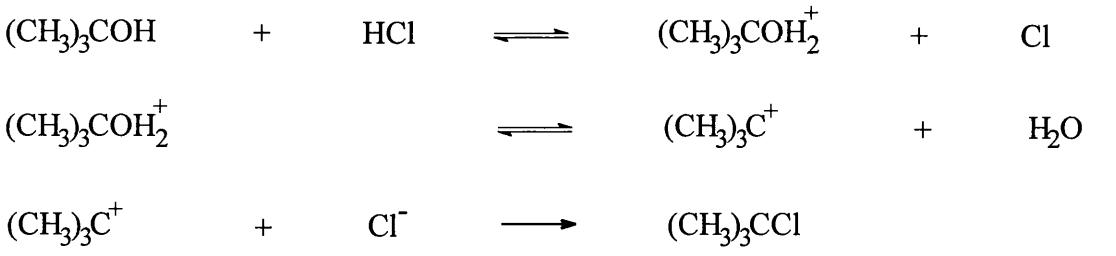

Scheme 3.2

A direct synthetic route for the preparation of acetyl chloride incorporating the [^{36}Cl]-chlorine radioisotope from concentrated hydrochloric acid or anhydrous hydrogen chloride, apparently does not exist. Exchange of chlorine between anhydrous hydrogen chloride and acetyl chloride in the vapour phase, however, affords a potential means of incorporating the [^{36}Cl]-chlorine radioisotope (143). The mechanism shown in scheme 3.3, is consistent with the observed rate law from kinetic studies (experimental observations discussed in section 3.6).

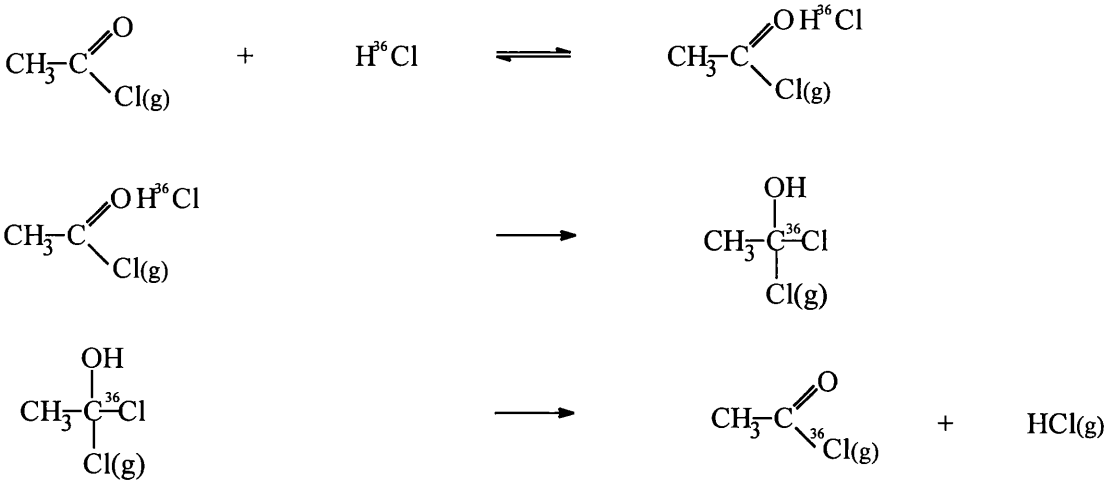

Scheme 3.3

The development of experimental procedures for preparing 2-chloropropane, *t*-butyl chloride and acetyl chloride, are reviewed within this chapter.

3.3 Methods of Analysis

2-Chloropropane, *t*-butyl chloride and acetyl chloride (bp 309 K, 324 K and 324 K respectively) are sufficiently volatile that Fourier transform infrared spectroscopy of the vapour phase, in a gas infrared cell (described in section 2.5.1), was used for identification. Samples were taken by expansion of the volatile material from the reaction vessel following reaction, into a vacuum line with a gas infrared cell fitted. Key functional infrared active absorbances of the reactants and products were monitored to determine whether or not reaction had occurred. The wavenumber of key absorbance modes and the functional group assignments of standard *t*-butyl chloride, 2-chloropropane and acetyl chloride (Table 3.1), were used in comparison with the reaction products. The distinctive rotational fine structure of hydrogen chloride in the vapour phase was used diagnostically to assess whether reactions and/or separation procedures had been successful.

^{1}H and ^{13}C NMR spectroscopy were used to analyse products from the nucleophilic substitution reaction of 2-methyl propan-2-ol with concentrated hydrochloric acid. The reaction product and the authentic *t*-butyl chloride were

Table 3.1 : Characteristic Infrared bands (151,152)

Sample	ν max/cm^{-1}	Assignment
HCl	2900	H-Cl rot.
$(CH_3)_3CCl$	2992	C-H str.
	2937	C-H str.
	1374	C-H deform.
	1155	C-C str.
	740	C-Cl str.
CH_3COCl	3030	C-H str.
	1827	C=O str.
	1810	C=O str.
	1360	C-H deform.
	1117	C-C str.
	962	C-Cl str.
$CH_3CHClCH_3$	2997	C-H str.
	2944	C-H str.
	1471	C-H deform.
	1390	C-H deform.
	1163	C-C str.
	890	C-Cl str.

Table 3.2 : Standard ^1H and ^{13}C NMR, Reference TMS (153)

Sample	Shift/ppm		Assignment
$(CH_3)_3CCl$	(^1H)	1.6	Cl-C-CH_3
	(^{13}C)	35	CH_3-
		67	C-Hal
$(CH_3)_3COH$	(^1H)	1.2	-CH_3
		1.9	-OH
	(^{13}C)	31	CH_3-
		70	C-OH

recorded in $CDCl_3$. Literature assignments for the ^1H and ^{13}C NMR of authentic *t*-butyl chloride (Table 3.2) were used for comparison with the reaction product.

3.4 Synthesis of [^{36}Cl]-Chlorine Labelled *t*-Butyl Chloride

The experimental procedure for the synthesis of [^{36}Cl]-chlorine labelled *t*-butyl chloride, detailed in section 2.2.9, was developed from the following investigation. The nucleophilic substitution reaction of 2-methyl propan-2-ol with [^{36}Cl]-chlorine labelled hydrochloric acid (as prepared in section 2.2.6), offered a potential route for incorporation of the [^{36}Cl]-chlorine radioisotope (mechanism outlined in section 3.2).

Initial attempts to prepare *t*-butyl chloride were based on a standard literature procedure (142). 2-Methyl propan-2-ol (1.66 g) was added to concentrated hydrochloric acid (5.66 cm^3) in a separating flask and shaken occasionally over a 2 h period, releasing the stopper occasionally to release any pressure build up. After approximately 2 h the evolution of gas appeared to have stopped and the lower acidic layer was discarded. The halide portion remaining was washed with sodium hydrogencarbonate solution (5 cm^3 of 5% solution), before drying the product over anhydrous calcium sulfate. The ^1H and ^{13}C NMR spectra of the product were recorded in $CDCl_3$ (Table 3.3 and 3.4) and compared with standard literature assignments for *t*-butyl chloride (Table 3.2).

Table 3.3 : ^{1}H NMR Spectra of the Reaction Product vs. *t*-Butyl Chloride

Sample	^{1}H Shift/ppm	Assignment
Reaction Product	1.62	Cl-C-CH_3
***t*-Butyl Chloride** (literature)	1.6	Cl-C-CH_3

Table 3.4 : ^{13}C NMR Spectra of the Reaction Product vs. *t*-Butyl Chloride

Sample	^{13}C Shift/ppm	Assignment
Reaction Product	34.5 67	CH_3- C-Hal
***t*-Butyl Chloride** (literature)	35 67	CH_3- C-Hal

The functional group assignments for the reaction product gave agreement with the *t*-butyl chloride literature, notably the disappearance of the 2-methyl propan-2-ol ^{1}H NMR signals at 1.2 and 1.9 ppm for -CH_3 and -OH respectively (Table 3.2) and the appearance of the single ^{1}H signal at 1.62 ppm (Table 3.3), corresponding to *t*-butyl chloride. The disappearance of ^{13}C NMR signals at 71 ppm and 31 ppm for C-OH and CH_3- respectively (Table 3.2) and the appearance of signals at 67 ppm and 35 ppm consistent with *t*-butyl chloride formation (Table 3.4).

In the initial attempts to prepare *t*-butyl chloride problems were encountered during the drying stage as the product became absorbed on the drying agent, anhydrous calcium sulfate, reducing the yield. The volatility of the product, however, enabled removal and isolation via vacuum distillation, increasing product yields from 10-20 % up to approximately 70%. FTIR of the reaction product in the vapour phase (Table 3.5), was consistent with the infrared spectrum of authentic *t*-butyl chloride (Table 3.1).

Table 3.5 : Infrared Spectra of the Reaction Product vs. *t*-Butyl Chloride

Sample	ν max/cm^{-1}	Assignment
Reaction Product	2994	C-H str.
	2938	C-H str.
	1377	C-H deform.
	1160	C-C str.
	740	C-Cl str.
***t*-Butyl Chloride** (literature)	2992	C-H str.
	2937	C-H str.
	1374	C-H deform.
	1155	C-C str.
	740	C-Cl str.

The nucleophilic substitution reaction of 2-methyl propan-2-ol with concentrated hydrochloric acid afforded an effective synthetic route for the preparation of *t*-butyl chloride. This procedure was adopted in the preparation of

[^{36}Cl]-chlorine labelled *t*-butyl chloride to produce material with a specific count rate of approximately 43 count s^{-1} per 100 Torr.

3.5 Synthesis of [^{36}Cl]-Chlorine Labelled 2-Chloropropane

The experimental procedure for the synthesis of [^{36}Cl]-chlorine labelled 2-chloropropane, detailed in section 2.2.8, was developed from the following investigation. The electrophilic addition reaction of anhydrous hydrogen chloride across the double bond in propene (mechanism outlined in section 3.2), offered a potential means of incorporating the [^{36}Cl]-chlorine radioisotope in 2-chloropropane (141). The reaction requires a Lewis acid catalyst to overcome the considerable activation energy barrier. Development of a catalytic system which provides a low energy pathway for the electrophilic addition of anhydrous hydrogen chloride to propene is reviewed within this section. The acidic properties of (i) HCl chlorinated γ-alumina, and (ii) CCl_4 chlorinated γ-alumina, led to them being proposed as potential catalysts (75).

The catalytic activities of the chlorinated γ-aluminas were evaluated by condensing propene and hydrogen chloride into a bomb containing the solid of interest. The propene vapour was expanded into a calibrated manifold (254 cm^3) to a pressure of 660 Torr, giving 9.0 mmol of propene, which was condensed into the bomb at 77 K. The bomb was isolated before expanding hydrogen chloride vapour into the calibrated manifold to a pressure of 600 Torr, giving 8.1 mmol of HCl,

which was condensed into the bomb at 77 K. Reaction was initiated by warming the bomb to room temperature and holding for 18 h.

FTIR of the vapour phase from the reaction mixture after 20 h was recorded, in a gas infrared cell, to determine whether reaction had occurred. Spectra from the HCl chlorinated γ-alumina system (Table 3.6) and the CCl_4 chlorinated γ-alumina system (Table 3.7), were compared with the spectral assignments of authentic 2-chloropropane (data from Table 3.1).

Table 3.6 : Infrared Spectra of the Reaction Product from the HCl Chlorinated γ-Alumina System vs. 2-Chloropropane

Sample	**ν max/cm^{-1}**	**Assignment**
Reaction Product	3080	C-H str. ($C=CH_2$)
	3032	C-H str. (C-CH)
	2984	C-H str. ($-CH_3$)
	1685	C=C str.
	1438	C-H deform.
	1018	C-Cstr.
	952	CH=CH trans.
	745	CH=CH cis
2-Chloropropane (literature)	2997	C-H str.
	2944	C-H str.
	1471	C-H deform.
	1390	C-H deform.
	1163	C-C str.
	890	C-Cl str.

Table 3.7 : Infrared Spectra of the Reaction Product from the CCl_4 Chlorinated γ-Alumina System vs. 2-Chloropropane

Sample	ν max/cm^{-1}	Assignment
Reaction Product	2991	C-H str.
	2940	C-H str.
	1470	C-H deform.
	1382	C-H deform.
	1158	C-C str.
	886	C-Cl str.
2-Chloropropane (literature)	2997	C-H str.
	2944	C-H str.
	1471	C-H deform.
	1390	C-H deform.
	1163	C-C str.
	890	C-Cl str.

Analysis of the infrared spectra indicates that propene and hydrogen chloride, did not react together, in the presence of HCl chlorinated γ-alumina (Table 3.6). The characteristic modes for propene (data from Table 2.1) and the distinctive rotational fine structure of hydrogen chloride were still observed following the 20 h reaction period. Comparison of the infrared spectra of the reaction mixture with the standard 2-chloropropane, showed the absence of the infrared active modes pertaining to 2-chloropropane. The lack of catalytic activity of the HCl chlorinated γ-alumina, in the electrophilic addition reaction, is probably due to insufficient Lewis acidity of the solid surface.

Reaction of propene and hydrogen chloride in the presence of CCl_4 chlorinated γ-alumina (Table 3.7) resulted in the disappearance of diagnostic functional group modes of the propene molecule (data in Table 2.1) and the appearance of modes characteristic of the 2-chloropropane molecule.

Purity of the synthesised 2-chloropropane was determined by comparison with the authentic 2-chloropropane via GC. The reaction product had a similar retention time to the standard (i.e. 1.11 vs. 1.15 min) and no significant impurities were observed. Yields varied between 35 % and 60 %, with the variability believed to be associated with the strong affinity of the catalyst surface for the 2-chloropropane (i.e. Lewis acid sites on the solid binding the Lewis basic reactant molecules).

The electrophilic addition reaction of anhydrous hydrogen chloride and propene, catalysed by CCl_4 chlorinated γ-alumina, afforded an effective synthetic route for the preparation of 2-chloropropane. This procedure was adopted in the preparation of [^{36}Cl]-chlorine labelled 2-chloropropane to produce material with a specific count rate of approximately 18 count s^{-1} per 100 Torr.

3.6 Synthesis of [^{36}Cl]-Chlorine Labelled Acetyl Chloride

The experimental procedure for the preparation of [^{36}Cl]-chlorine labelled acetyl chloride, detailed in section 2.2.10, was developed from the following

investigation. The chlorine exchange reaction between acetyl chloride and [^{36}Cl]-chlorine labelled hydrogen chloride (mechanism outlined in section 3.2), offered a potential route for incorporation of the [^{36}Cl]-chlorine radioisotope in acetyl chloride. Preparation of the [^{36}Cl]-chlorine labelled hydrogen chloride has been described in section 2.2.7.

Initial attempts to prepare [^{36}Cl]-chlorine labelled acetyl chloride were based on the procedure outlined in the kinetic study of chlorine exchange in the vapour phase between acetyl chloride and [^{36}Cl]-chlorine labelled hydrogen chloride (143). The acetyl chloride vapour was expanded into a calibrated manifold (254 cm^3) to a pressure of 290 Torr, giving 4.0 mmol of acetyl chloride, which was condensed into the bomb at 77 K. The bomb was isolated before expanding hydrogen chloride vapour into the calibrated manifold to a pressure of 290 Torr, giving 4.0 mmol of HCl, which was condensed into the bomb at 77 K. The vessel was then warmed to room temperature and allow to stand for 1 h. Removal of hydrogen chloride from the acetyl chloride following the exchange reaction was necessary, as any residual hydrogen chloride would interfere with radiochemical counting experiments.

Separation of hydrogen chloride (bp 193 K, mp 159 K) from acetyl chloride (bp 325 K, mp 161 K), was based on their relative volatility. The reaction vessel was immersed in a dry ice/acetone bath (195 K), in order to condense the acetyl chloride and enable removal of the volatile hydrogen chloride. Following the initial

separation stage, analysis of the product by FTIR, in the gas infrared cell, indicated that hydrogen chloride was still present. The similarity between the separation temperature and the boiling point of hydrogen chloride, may result in liquid hydrogen chloride present and hence account for its incomplete removal.

An effective separation procedure was developed in which consecutive separations were performed. The procedure involved condensing the reaction mixture in a dry ice/acetone bath, removing the volatile hydrogen chloride, sealing the vessel and warming to room temperature. This procedure was repeated a further five times, with the quantity of the volatile hydrogen chloride recorded by expansion into a calibrated manifold of known volume (Table 3.8).

Table 3.8 : Separation of Hydrogen Chloride from Acetyl Chloride

Separation	**HCl/mmol**
1	1.6
2	1.2
3	0.6
4	0.4
5	0.2
6	0
Total	4.0

A decrease in the quantity of hydrogen chloride removed on each consecutive separation step was observed. Comparison of the total hydrogen chloride removed

(i.e. 4.0 mmol) with the input quantity (4.0 mmol), indicated the efficiency of the separation technique. Following the last separation step, the product was expanded into a gas infrared cell and the FTIR spectrum recorded (Table 3.9). The spectrum of the reaction product was consistent with the authentic acetyl chloride and no hydrogen chloride was observed.

Table 3.9 : Infrared Spectra of the Reaction Product vs. Acetyl Chloride

Sample	ν max/cm^{-1}	Assignment
Reaction Product	3027	C-H str.
	1824	C=O str.
	1807	C=O str.
	1354	C-H deform.
	1119	C-C str.
	960	C-Cl str.
Acetyl Chloride (literature)	3030	C-H str.
	1827	C=O str.
	1810	C=O str.
	1360	C-H deform.
	1117	C-C str.
	962	C-Cl str.

The success of the chlorine exchange reaction is reflected in the magnitude of the [^{36}Cl]-chlorine labelled acetyl chloride specific count rate (i.e. approximately 63 count s^{-1} per 100 Torr), produced following exposure of acetyl chloride to [^{36}Cl]-chlorine labelled hydrogen chloride. The use of this material as a radiotracer in the direct monitoring radiochemical studies is discussed extensively within chapter 6.

CHAPTER 4

EVALUATION OF HALOGENATED SURFACES AS CATALYSTS IN MODEL FRIEDEL-CRAFTS REACTIONS

4.1. Introduction

The considerable diversity of Friedel-Crafts reaction chemistry made it important to focus on specific model reactions. Friedel-Crafts systems were selected which allowed investigation of the catalytic activity of the solid materials of interest and which were compatible with the other key techniques employed in this work i.e. *in-situ* infrared studies and the direct monitoring Geiger Müller technique (79,80).

The Friedel-Crafts reactions studied involved the electrophilic aromatic substitution of an alkyl or acyl halide on to a nucleophilic or electron rich molecule, under the catalytic influence of a solid acid catalyst. This chapter is concerned with the evaluation of solid materials as potential Lewis acid catalysts in model Friedel-Crafts reactions. The solid materials of interest, i.e. chlorinated and fluorinated γ-aluminas, oxide supported organic layer catalysts and β-AlF_3, were prepared as outlined in section 2.3.

Examining the Friedel-Crafts alkylation reactions of the tertiary alkyl halide, *t*-butyl chloride, with two aromatic compounds possessing different propensities towards electrophilic aromatic substitution, offered an activated system for screening the solid materials and a more demanding system for assessing catalytic activity.

The tertiary alkyl halide, *t*-butyl chloride, was chosen due to the stability of the transient cabenium ion minimising the effects of rearrangements. Toluene and benzene were selected as the aromatic reagents, with the inductive effect (+I) of the methyl group on toluene resulting in an activated system which we could compare vs. the more catalytically demanding alkylation of benzene. The solid materials of interest were examined in the Friedel-Crafts systems (i) *t*-butyl chloride/toluene and (ii) *t*-butyl chloride/benzene; catalytic performance was compared with the archetypal Lewis acid catalyst $AlCl_3$.

The general experimental procedure adopted for the evaluation of potential solid catalysts is described in section 2.4.1. The model Friedel-Crafts alkylation reactions studied employed an alkyl halide to aromatic mole ratio of (1:10), in order to minimise the effects of multiple alkylation. Samples from the solid/liquid reaction mixtures were analysed by gas chromatography (GC) during the catalytic runs and by gas chromatography mass spectrometry (GCMS) once the catalytic run was finished (conditions described in sections 2.6 and 2.7 respectively).

Friedel-Crafts alkylation reactions such as the model reactions studied in this work represent the simplest examples of Friedel-Crafts catalysis. They generally result in high yield and selectivity. In more catalytically demanding systems, including benzoylation and acetylation, there is generally considerable reduction in yield and selectivity vs. the alkylation reactions, even with the highly active $AlCl_3$

catalyst (36). For a new Friedel-Crafts catalyst to successfully replace $AlCl_3$, it must display high catalytic activity in even the more demanding systems. The solid with the greatest catalytic activity in the model Friedel-Crafts alkylation reactions studied, was examined in the benzoylation of benzene.

4.2 Experimental Procedure

The following general experimental procedure was adopted to study the Friedel-Crafts catalytic activity of solid materials of interest. A sample of the solid (0.5g) was loaded into the catalyst microreactor (described in section 2.1.5) in an inert atmosphere box. The reactor was transferred to the laboratory where a helium bubbler and condenser were connected. The reactants were injected into the microreactor via a septum cap i.e. 22.4 mmol of alkyl halide and 224.0 mmol of aromatic, such that the solid was covered by the liquors. It was important to exclude moisture and air to prevent deactivation of the active sites on the solid, which could occur via coordination of water molecules.

A positive pressure of helium was introduced into the reactor before opening the system to the condenser and scavenger. The solid/liquid reaction mixture was agitated at a constant rate with an electrically powered magnetic stirrer. Samples of the reaction mixture were taken by syringe, via the septum cap, from the start of the reaction at 30 min intervals. The reaction mixtures were analysed by injecting 5µl samples directly into the GC (conditions described in section 2.6). The reactions

were typically monitored over the first 5-6 h, with a further sample taken at approximately 20 h to determine the final product composition by GCMS (conditions described in section 2.7).

4.3. Methods of Analysis

The Friedel-Crafts reactions were followed during the catalytic run by GC (chromatographic conditions and standard retention times are detailed in section 2.6). GC was a powerful analytical tool, affording separation of the reactants from the products on the basis of their relative volatility. Retention times of the standard components and authentic samples of the desired Friedel-Crafts products were recorded, for comparison with the data from the chromatograms taken during the catalytic runs. Samples were taken from the catalyst microreactor by syringe and filtered through cotton wool packed pipettes, before direct injection onto the column with a 5 μl syringe.

The GC instrument response was calibrated prior to use by injection of the standard Friedel-Crafts alkylation products, *t*-butylbenzene and 4-*t*-butyltoluene, of known concentrations. Percentage conversion to Friedel-Crafts products was calculated by comparison of the integrator data recorded during the catalytic runs, with the standard calibration data. The consumption of *t*-butyl chloride both on initial exposure to the solids and over the course of the reaction was an important

consideration in understanding the nature of the interactions between the alkyl halide and the solid surfaces.

When no further change in GC composition was observed, samples were taken for analysis by GCMS, to confirm identity and establish final product composition. GCMS proved to be a very sensitivity analytical technique, being able to differentiate between the product stereoisomers i.e. para vs. meta (conditions and standard retention times are detailed in section 2.7). The reproducibility of retention times for the authentic Friedel-Crafts products enabled identification of the specific isomers present in the product mixture. The use of NMR in identification of the isomers proved problematic due to the presence of polymeric residues, believed to be the result of interaction of the solid with the reagents.

4.4 Results

The catalytic activity of the solid materials of interest as Friedel-Crafts catalysts, in Friedel-Crafts reactions was compared to that of the industry standard catalyst, solid $AlCl_3$. The catalytic performance of the following solid materials was examined primarily in two key Friedel-Crafts alkylation reactions (i) *t*-butyl chloride/toluene and (ii) *t*-butylchloride/benzene:

(i) Calcined γ-alumina.

(ii) CCl_4 chlorinated γ-alumina

(iii) Oxide supported organic layer catalyst derived from exposure of CCl_4 chlorinated γ-alumina to 1,1,1-trichloroethane

(iv) Oxide supported organic layer catalyst derived from exposure of CCl_4 chlorinated γ-alumina to 1,1-dichloroethene

(v) SF_4/SOF_2 fluorinated γ-alumina

(vi) SF_4 fluorinated γ-alumina

(vii) Solid β-AlF_3

(viii) Solid $AlCl_3$

4.4.1 Friedel-Crafts Reaction of *t*-Butyl Chloride with Toluene on Solid Surfaces

The Friedel-Crafts alkylation of toluene by *t*-butyl chloride is a relatively active Friedel-Crafts system due to the inductive effect (+I) of the methyl substituent on the toluene ring system, activating the molecule towards electrophilic aromatic substitution, and the propensity of the *t*-butyl chloride to form a stable tertiary carbenium ion. This system was used to screen the solids of interest to determine whether they exhibited potential as Friedel-Crafts catalysts. The use of *t*-butyl chloride complemented the radioisotope studies, in which the interaction of [^{36}Cl]-chlorine labelled *t*-butyl chloride with the solid surfaces was examined (discussed in chapter 6).

The experimental procedure and analysis techniques adopted for evaluating the solids in the model Friedel-Crafts reactions are detailed in sections 4.2 and 4.3 respectively. The catalytic performance of the solid materials (0.5 g) was evaluated by adding 22.4 mmol of *t*-butyl chloride and 224.0 mmol of toluene in the microreactor. Percentage conversion to Friedel-Crafts products was calculated from GC calibration standards and the product distributions determined after 20 h by GCMS, by comparison with the authentic products (data in Table 4.1).

Table 4.1 : Friedel-Crafts Reaction of *t*-Butyl Chloride and Toluene (1:10) on Solid $AlCl_3$, Calcined γ-Alumina and Chlorinated γ-Alumina Surfaces

Solid	**% Conversion to Friedel-Crafts Products***	**Distribution of Friedel-Crafts Products**	
		t-butyltoluene (para : meta)	di-*t*-butyltoluene
$AlCl_3$	100	66 : 34	0
Calcined γ-Alumina	0	0	0
CCl_4 Chlorinated γ-Alumina	100	63 : 35	2
Oxide Supported Organic Layer Catalyst Derived from CCl_4 Chlorinated γ-Alumina/ 1,1,1-trichloroethane	45	78 : 22	0
Oxide Supported Organic Layer Catalyst Derived from CCl_4 Chlorinated γ-Alumina/ 1,1-dichloroethene	50	53 : 47	0

* 0.5g solid / 22.4 mmol $(CH_3)_3CCl$ / 224.0 mmol $C_6H_5CH_3$. % Conversion based on GC calibration.

Aluminium trichloride catalysis of the alkylation of toluene with t-butyl chloride was a vigorous exothermic reaction, resulting in 100% conversion to the Friedel-Crafts products 4-*t*-butyltoluene (66%) and 3-*t*-butyltoluene (34%), in ~1 h. Predominant substitution at the para position, giving 4-*t*-butyl toluene, is consistent with the electronic and steric effects of the methyl substituent on the ring system and the size of the bulky *t*-butyl chloride molecule (154). The meta substitution of the ring, giving 3-*t*-butyltoluene, is favoured over substitution at the ortho position due to steric hindrance preventing the large *t*-butyl chloride from attacking at the ortho position. The activity of $AlCl_3$ in the Friedel-Crafts alkylation reaction is attributed to the Lewis acidic character of coordinatively unsaturated Al^{3+} sites and is discussed later within this thesis.

Calcined γ-alumina was not catalytically active in the reaction of *t*-butyl chloride with toluene. This lack of activity in what is a relatively activated Friedel-Crafts system, suggests that calcined γ-alumina does not possess acid sites which allow it to function as a Friedel-Crafts catalyst. The performance of CCl_4 chlorinated γ-alumina in the alkylation of toluene with *t*-butyl chloride, is very similar to that of $AlCl_3$, resulting in 100% conversion to the Friedel-Crafts products 4-*t*-butyltoluene (63%) and 3-*t*-butyltoluene (35%) and a small quantity of the dialkylated product, in ~1 h. The catalytic reaction involving CCl_4 chlorinated γ-alumina, however, was not as visibly vigorous as the $AlCl_3$ catalysed reaction. The observed differences

between the solids during catalysis may be a function of the apparently more soluble nature of $AlCl_3$ compared with the chlorinated γ-alumina.

The two solids, aluminium trichloride and CCl_4 chlorinated γ-alumina achieved 100% conversion of *t*-butyl chloride and toluene to Friedel-Crafts products, corresponding to 22.4 mmol, in approximately 1 h (Figure 4.1). The comparable catalytic activity of $AlCl_3$ and CCl_4 chlorinated γ-alumina, is very significant, as $AlCl_3$ is regarded as the classic Friedel-Crafts catalyst. The catalytic activity of CCl_4 chlorinated γ-alumina in the Friedel-Crafts alkylation of toluene with *t*-butyl chloride was a key finding and will be discussed later (chapter 7).

The deposition of a supported organic layer on CCl_4 chlorinated γ-alumina following treatment with 1,1,1-trichloroethane and 1,1-dichloroethene respectively, results in a decrease in the catalytic activity of the halogenated γ-alumina, as reflected in percentage conversion to Friedel-Crafts products of 45% and 50% (Table 4.1). Preliminary selectivity data may indicate a higher degree of selectivity for the para over meta isomer, on the 1,1,1-trichloroethane based supported layer, than the 1,1-dichloroethene based layer i.e. 78% : 22% vs. 53% : 47% of 4-*t*-butyltoluene to 3-*t*-butyltoluene respectively. Selectivity effects were not studied further, as the objective of this work was to screen the solids for catalytic activity and develop an understanding of the surface interactions via radiochemical and infrared studies.

Figure 4.1 : Friedel-Crafts Reaction of *t*-Butyl Chloride and Toluene (1:10) on Solid $AlCl_3$, CCl_4 Chlorinated γ-Alumina and Oxide Supported Organic Layer Catalyst

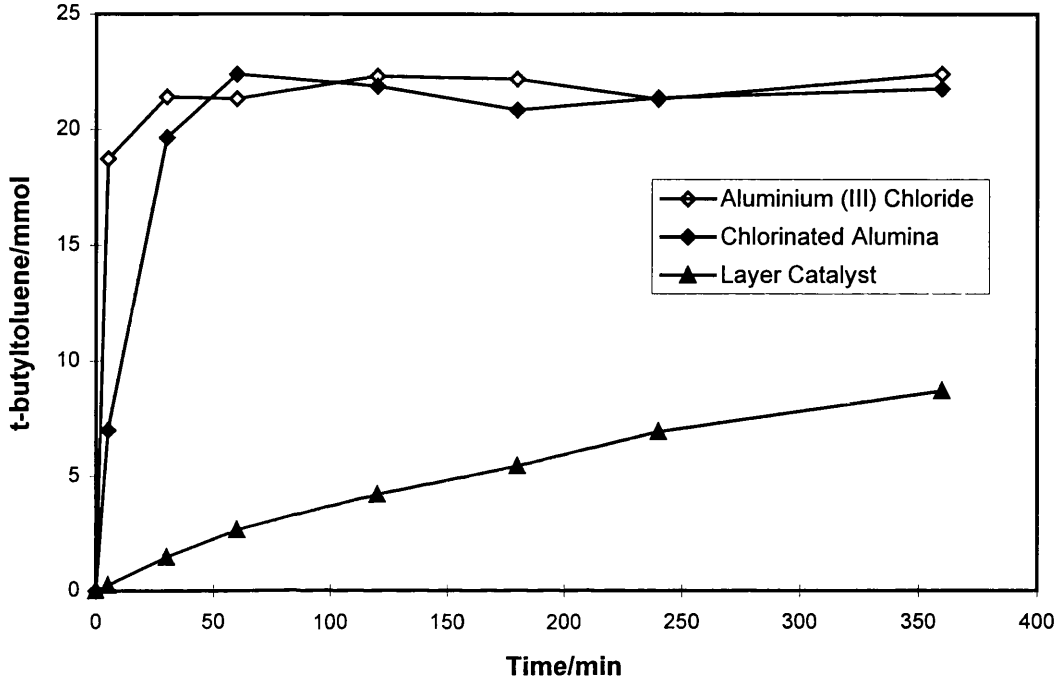

The distinctive purple layer associated with the oxide supported organic layer catalysts (75) remained throughout the catalytic run. It is believed that the presence of the supported organic layer on the chlorinated γ-alumina surface, alters the nature of surface interactions with reactant molecules and may account for some selectivity effects. The reduction in catalytic activity of the layer catalysts compared with their halogenated precursor, CCl_4 chlorinated γ-alumina, is evident in the relative conversion to Friedel-Crafts products (Figure 4.1).

It was hoped that the fluorinated solid materials would offer similar or superior Friedel-Crafts catalytic activity to the chlorinated materials discussed, due to the enhanced electronegativity of fluorine vs. chlorine, creating stronger active sites on the solid (121). The SF_4 fluorinated γ-alumina, however, was completely inactive in the Friedel-Crafts alkylation of toluene with *t*-butyl chloride (Table 4.2).

Table 4.2 : Friedel-Crafts Reaction of *t*-Butyl Chloride and Toluene (1:10) on Solid Chlorinated γ-Alumina and Fluorinated γ-Alumina Surfaces

Solid	**% Conversion to Friedel-Crafts Products***	**Distribution of Friedel-Crafts Products**	
		t-butyltoluene (para : meta)	di-*t*-butyltoluene
CCl_4 Chlorinated γ-Alumina	100	63 : 35	2
SF_4 Fluorinated γ-Alumina	0	0	0
SOF_2/SF_4 Fluorinated γ-Alumina	36	97 : 3	0
β-AlF_3	46	84 : 16	0

* 0.5g solid / 22.4 mmol $(CH_3)_3CCl$ / 224.0 mmol $C_6H_5CH_3$. % Conversion based on GC calibration.

Exposure of the SF_4 fluorinated γ-alumina to the reactants resulted in the deposition of an orange deposit on the surface of the solid. The GC data indicated a significant reduction in the *t*-butyl chloride concentration (Figure 4.2), notably, without the formation of Friedel-Crafts products. The formation of a coloured deposit on the solid surface is believed to be analogous to the layer formation

observed on the oxide supported organic layer catalysts (76,77). It would appear that deposition of a supported organic layer derived from *t*-butyl chloride is favoured over its conversion to Friedel-Crafts products. The apparent lack of catalytic activity of the SF_4 fluorinated γ-alumina is discussed later in conjunction with mechanistic proposals for the layer formation (Chapter 7).

Figure 4.2 : Friedel-Crafts Reaction of *t*-Butyl Chloride and Toluene (1:10) on Solid SF_4 Fluorinated γ-Alumina

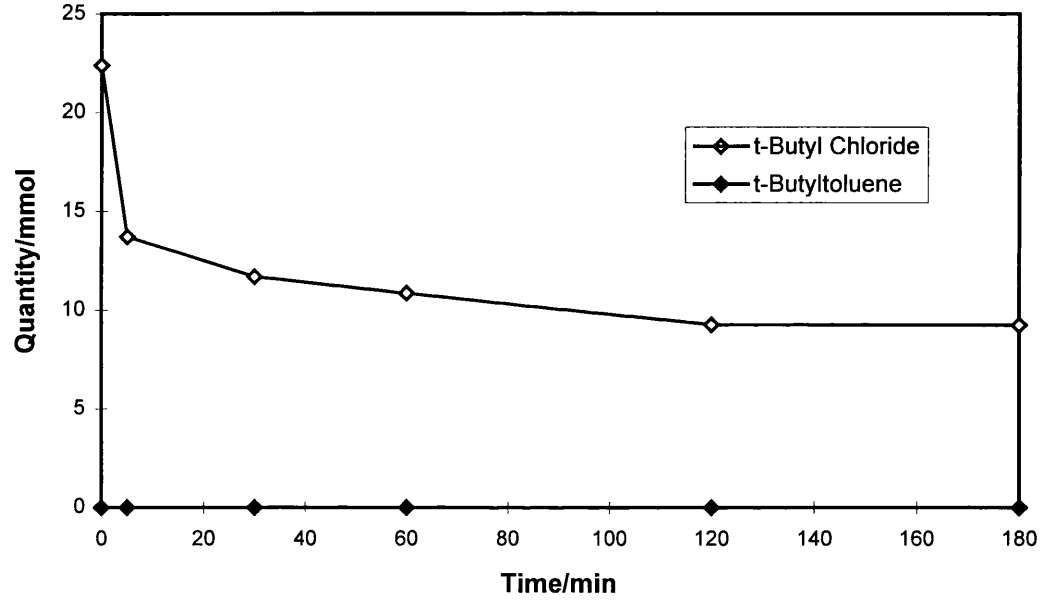

Fluorination of γ-alumina with an SF_4/SOF_2 mixture resulted in a solid material with some degree of catalytic activity in the Friedel-Crafts alkylation reaction of toluene with *t*-butyl chloride (Table 4.2). Conversion to Friedel-Crafts products of 36%, represents a significant improvement over the catalytic

performance of the γ-alumina fluorinated with SF_4. Interestingly, SOF_2 is a hydrolysis product of SF_4 and generally accepted to be a weaker fluorinating agent than SF_4. Exposure of γ-alumina to SOF_2 produces surface sites which apparently differ from the SF_4 fluorinated γ-alumina, and which are capable of catalysing the alkylation of toluene with *t*-butyl chloride. The apparent high selectivity for the para isomer i.e. 4-*t*-butyltoluene (97%) vs. 3-*t*-butyltoluene (3%), by γ-alumina fluorinated with SF_4/SOF_2, may be associated with the acidity of the solid surface and/or the presence of a supported organic layer inducing orientation of incoming reactant molecules.

The β-AlF_3 solid is the only material which did not receive a conditioning treatment (137), which displayed catalytic activity in the Friedel-Crafts alkylation reaction of toluene with *t*-butyl chloride (Table 4.2). The percentage conversion to Friedel-Crafts products of 46%, was considerably higher than SF_4 fluorinated γ-alumina and comparable to the performance of the SF_4/SOF_2 fluorinated material. Interestingly the solid β-AlF_3, like SF_4/SOF_2 fluorinated γ-alumina, showed a preference for formation of the para over meta isomer i.e. 4-*t*-butyltoluene (84%) vs. 3-*t*-butyltoluene (16%). The apparent selectivity may be a function of interaction of reactant molecules with the solid catalyst surfaces, in specific orientations due to the nature of the active sites on the solid surfaces.

The conversion to Friedel-Crafts products over β-AlF_3 and SF_4/SOF_2 fluorinated γ-alumina, indicate significant differences in the respective catalytic reactions (Figure 4.3). Solid β-AlF_3 results in rapid initial conversion to Friedel-Crafts products, in the first five minutes of the reaction, followed by no further conversion thereafter. This type of behaviour implies that the β-AlF_3 surface becomes blocked or deactivated on interaction with the reactant molecules. The catalytic reaction of SF_4/SOF_2 fluorinated γ-alumina, however, results in a slower conversion to Friedel-Crafts products over approximately 2 - 4 h.

Figure 4.3 : Friedel-Crafts Reaction of *t*-Butyl Chloride and Toluene (1:10) on Solid Chlorinated γ-Alumina and Fluorinated γ-Alumina Surfaces

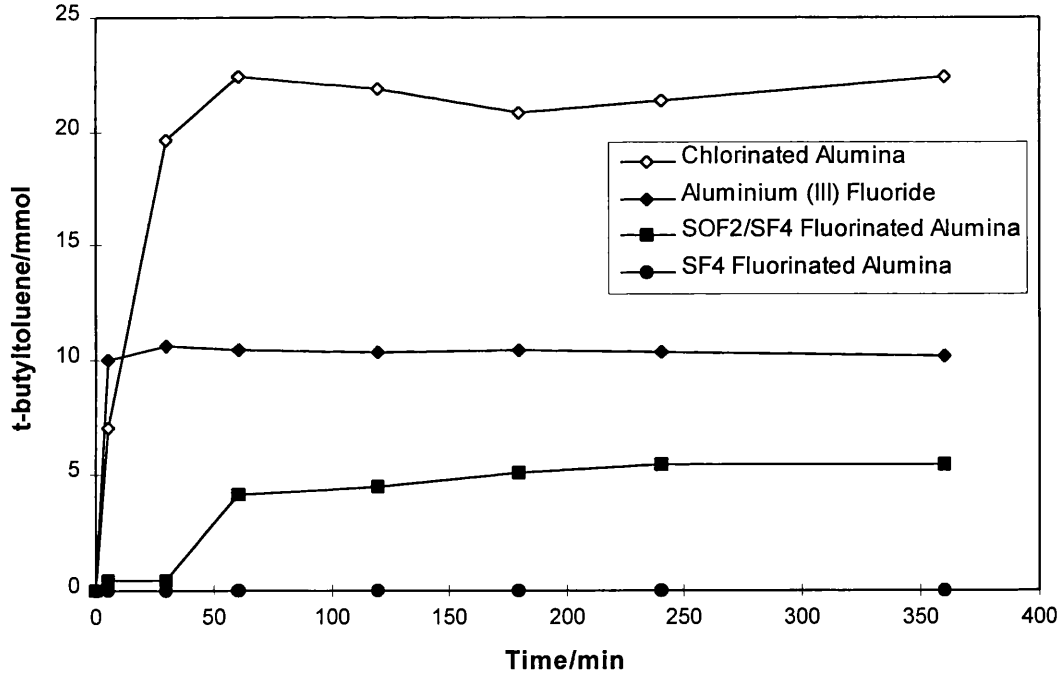

4.4.2 Friedel-Crafts Reaction of *t*-Butyl Chloride with Benzene on Solid Surfaces

The Friedel-Crafts alkylation of benzene with *t*-butyl chloride is a more demanding test for the solids than the toluene based system discussed in section 4.4.1. This system was studied to give a more discriminating evaluation of the catalytic activity of the solid materials. The same experimental procedure was adopted to study the alkylation of benzene by *t*-butyl chloride i.e. *t*-butyl chloride (22.4 mmol), benzene (224.0 mmol) and 0.5 g catalyst; findings are summarised in Table 4.3. Product conversions were calculated by comparison with standard GC calibration data from authentic samples of the desired Friedel-Crafts products and the product distributions determined after 20 h by GCMS.

Aluminium trichloride catalysis of the Friedel-Crafts alkylation of benzene with *t*-butyl chloride, was a vigorous exothermic reaction resulting in 100% conversion to Friedel-Crafts products, *t*-butylbenzene and di-*t*-butylbenzene, in approximately 1-2 h (Figure 4.4) with 98% of the monoalkylated product *t*-butylbenzene formed (Table 4.3). Interestingly, the catalytic activity of CCl_4 chlorinated γ-alumina in the *t*-butyl chloride/benzene system, is similar to that of the $AlCl_3$ giving 100% conversion to the Friedel-Crafts products, *t*-butylbenzene and di-*t*-butylbenzene, except taking approximately 6 h (Figure 4.4), with 92% of the monoalkylated product *t*-butylbenzene formed (Table 4.3). The apparent slower production of Friedel-Crafts products over CCl_4 chlorinated γ-alumina, may be

reflected in the fact that the reaction is visibly less vigorous than $AlCl_3$ catalysis. The behaviour of the solids in the alkylation of benzene with *t*-butyl chloride, may suggest that $AlCl_3$ is a stronger Lewis acid than CCl_4 chlorinated γ-alumina. This is examined later in the thesis via infrared and radiochemical studies (chapters 5 and 6).

Table 4.3 : Friedel-Crafts Reaction of *t*-Butyl Chloride and Benzene (1:10) on Solid $AlCl_3$, Calcined γ-Alumina, Chlorinated γ-Alumina and Fluorinated γ-Alumina Surfaces

Solid	**% Conversion to Friedel-Crafts Products***	**Distribution of Friedel-Crafts Products**	
		t-butylbenzene	di-*t*-butylbenzene
$AlCl_3$	100	98	2
Calcined γ-Alumina	0	0	0
CCl_4 Chlorinated γ-Alumina	100	92	8
Oxide Supported Organic Layer Catalyst Derived from CCl_4 Chlorinated γ-Alumina / 1,1,1-trichloroethane	0	0	0
Oxide Supported Organic Layer Catalyst Derived from CCl_4 Chlorinated γ-Alumina / 1,1-dichloroethene	0	0	0
SF_4 Fluorinated γ-Alumina	0	0	0
SOF_2/SF_4 Fluorinated γ-Alumina	8	89	11
β-AlF_3	5	79	21

* 0.5g solid / 22.4 mmol $(CH_3)_3CCl$ / 224.0 mmol C_6H_6. % Conversion based on GC calibration.

Figure 4.4 : Friedel-Crafts Reaction of *t*-Butyl Chloride and Benzene (1:10) on Solid $AlCl_3$ and CCl_4Chlorinated γ-Alumina

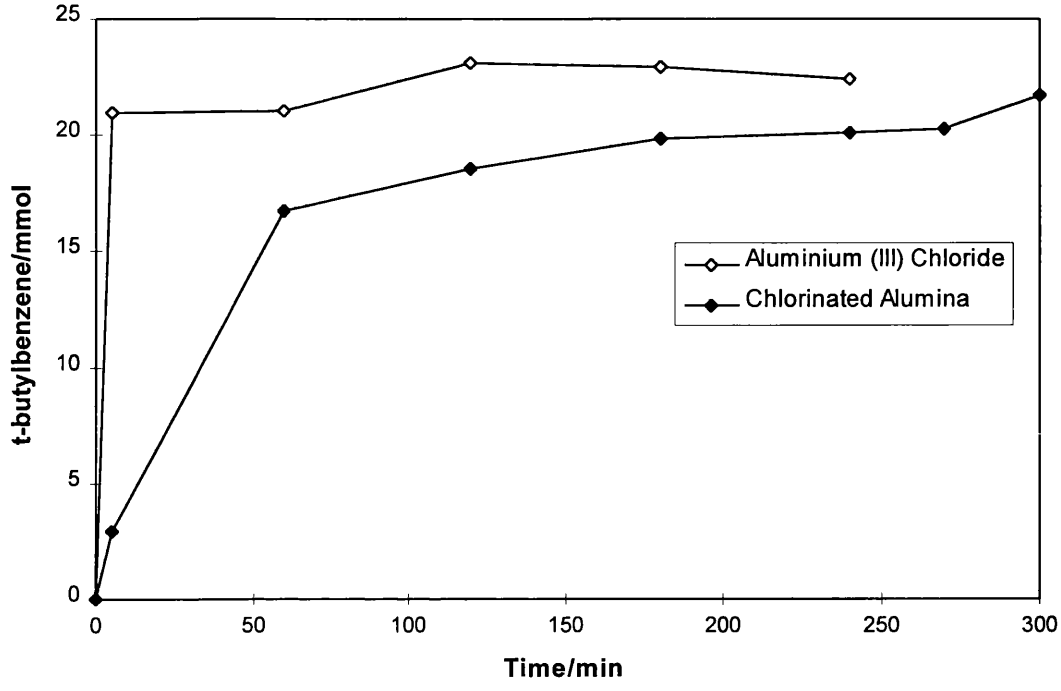

Deposition of a supported organic layer on CCl_4 chlorinated γ-alumina, following treatment with 1,1,1-trichloroethane and 1,1-dichloroethene respectively, rendered the solid catalytically inactive in the Friedel-Crafts alkylation of benzene with *t*-butyl chloride (Table 4.3). The distinctive purple coloured layer, characteristic of the oxide supported organic layer catalysts, was observed throughout the catalytic run. The exact role of the supported organic layer in deactivating the halogenated γ-alumina is discussed in chapter 7.

Solid γ-alumina fluorinated with SF_4 was not catalytically active in the alkylation of benzene with *t*-butyl chloride (Table 4.3). Although no Friedel-Crafts products were formed, an orange coloured layer was seen to form on the solid within 5-10 min of the reactants being added, and analysis of the GC data showed considerable reduction in the *t*-butyl chloride concentration in the reaction mixture over time (Figure 4.5). The consumption of *t*-butyl chloride in the Friedel-Crafts alkylation of benzene with *t*-butyl chloride, in the presence of different solid materials examined is shown in Figure 4.5. Two very interesting observations were made from the *t*-butyl chloride GC consumption data:

(i) The *t*-butyl chloride/SF_4 fluorinated γ-alumina system shows ~60% reduction in the *t*-butyl chloride after 1 h (i.e. from 22.4 to ~9.5 mmol), without formation of Friedel-Crafts products.

(ii) Comparison of the initial drop in the *t*-butyl chloride level over the various solids showed the greatest initial uptake i.e. ~40% after 5 min on the SF_4 fluorinated γ-alumina (i.e. from 22.4 to ~14 mmol).

This information indicates that there is a strong interaction/affinity between *t*-butyl chloride and SF_4 fluorinated γ-alumina, resulting in the deposition of an organic layer derived from *t*-butyl chloride. On removal of the reaction mixture from the inert atmosphere following reaction, the orange colouration disappeared from the solid. GCMS of the reaction mixture showed the presence of two non-

Figure 4.5 : Friedel-Crafts Reaction of *t*-Butyl Chloride and Benzene (1:10) on Solid Chlorinated γ-Alumina and Fluorinated γ-Alumina Surfaces

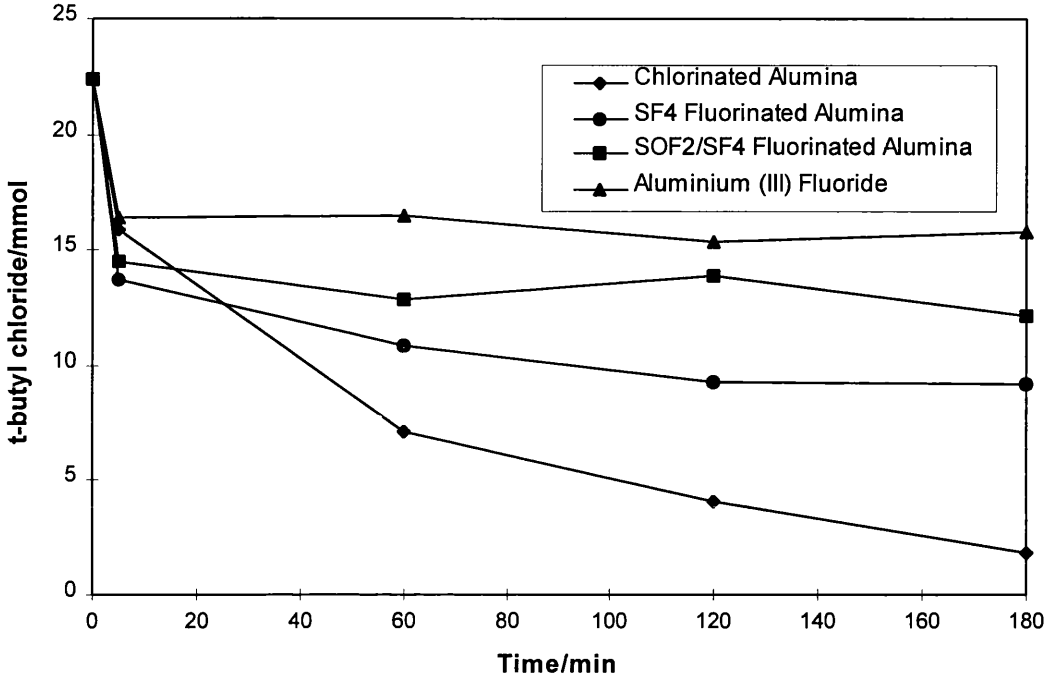

chlorine containing features of molecular weight 224 a.m.u and 56 a.m.u. The characteristic features were observed for all work involving SF_4 fluorinated γ-alumina and *t*-butyl chloride, and when SF_4 fluorinated γ-alumina was stirred in the reactor with only *t*-butyl chloride present (Table 4.4).

It was concluded that the fractions were a C_4 hydrocarbon unit or 'building block', consistent with the $(CH_3)_3CCl$ dehydrochlorination product, $(CH_3)_2C{=}CH_2$ (56 a.m.u.), and a C_{16} hydrocarbon polymerisation product of the 'building block'. It is difficult to determine the exact mechanism of layer formation, but it appears to

be analogous to formation of the oxide supported organic layer catalysts, via dehydrochlorination and oligomerisation of CH_3CCl_3 on SF_4 fluorinated γ-alumina (76,77). The proposed mechanism for formation of the supported layer is discussed in chapter 7.

Table 4.4 : GCMS Analysis Following Reaction of *t*-Butyl Chloride with SF_4 Fluorinated γ-alumina

Fraction	**Mass/a.m.u.**	**Assignment**
1	56	$(CH_3)_2C=CH_2$
2	224	$-[(CH_3)_2C-CH_2]-_n$

The β-AlF_3 and SF_4/SOF_2 fluorinated γ-alumina solids were considerably less catalytically active, in the Friedel-Crafts alkylation of benzene with *t*-butyl chloride, than in the alkylation of toluene (Tables 4.3 and 4.2 respectively). Conversion to Friedel-Crafts products dropped from 46% to 5% for β-AlF_3 and from 36% to 8% for SF_4/SOF_2 fluorinated γ-alumina on moving from the alkylation of toluene to benzene. These solid exhibited considerably lower catalytic activity in the model Friedel-Crafts reaction studied, compared to the high activity CCl_4 chlorinated γ-alumina catalyst, and therefore there catalytic properties were not examined further.

4.4.3 Friedel-Crafts Reaction of *t*-Butyl Chloride with Benzene on CCl_4 Chlorinated γ-Alumina

The solid γ-alumina chlorinated with CCl_4, displayed a high level of catalytic activity in the Friedel-Crafts alkylation of toluene and benzene with *t*-butyl chloride respectively (sections 4.4.1 and 4.4.2). The activity of the CCl_4 chlorinated γ-alumina, was similar to the archetypal Lewis acid catalyst $AlCl_3$, and considerably more active than any of the other solids examined as potential catalysts. A preliminary study was made to determine whether the CCl_4 chlorinated γ-alumina catalyst (i) catalysed consecutive alkylation reactions, (ii) resulted in the same product distribution depending on the sample of chlorinated γ-alumina used, and (iii) to ascertain whether the catalyst loading affected the conversion to Friedel-Crafts products.

Two samples of CCl_4 chlorinated γ-alumina ('named' Sample 1 and 2), prepared as detailed in section 2.3.2 were stored in an inert atmosphere box for approximately 24 h, before examining their catalytic activity in the Friedel-Crafts alkylation of benzene with *t*-butyl chloride. The experiments were run with the same catalyst loading as used in sections 4.3.1 and 4.3.2 (i.e. 0.5 g catalyst / 22.4 and 224 mmol of *t*-butyl chloride and benzene respectively), in addition to running at double the catalyst loading for one sample in order to study the effect of catalyst loading (i.e. 1.0 g catalyst : 22.4 and 224 mmol of *t*-butyl chloride and benzene respectively). The experimental procedure and analysis techniques adopted are detailed in sections

4.2 and 4.3. Table 4.5 summarises the conversion to Friedel-Crafts products and the product distributions (calculated by comparison with standard GC data from authentic samples of known concentration and GCMS respectively) for three separate *t*-butyl chloride/benzene catalytic experiments with the chlorinated γ-alumina samples detailed above.

Table 4.5 : Friedel-Crafts Reaction of *t*-Butyl Chloride with Benzene (1:10) on Solid CCl_4 Chlorinated γ-alumina Samples

CCl_4 Chlorinated γ-Alumina Sample	**% Conversion to Friedel-Crafts Products[#]**	**Distribution of Friedel-Crafts Products**	
		t-butylbenzene	di-*t*-butylbenzene
Sample 1*	100	92	8
Sample 2[Δ]	100	61	39
Sample 2[•]	100	70	30

[#] % Conversion based on GC calibration of authentic Friedel-Crafts products of known concentration.
* 0.5g Chlorinated γ-alumina from Sample 1.
[Δ] 0.5g Chlorinated γ-alumina from Sample 2.
[•] 1.0g Chlorinated γ-alumina from Sample 2.

Differences in the product distribution were observed depending on the sample of chlorinated γ-alumina used (i.e. 92% and 61% monoalkylated product, *t*-butylbenzene, from 0.5 g of Sample 1 and Sample 2 respectively). Variations in the

product selectivity may be associated with different levels of chlorine present on the solids due to the nature of the chlorination process (75). Interestingly, increasing the catalyst loading of sample 2 from 0.5 to 1.0 g, resulted in similar Friedel-Crafts product distribution i.e. 61% and 70% of the monoalkylated product *t*-butylbenzene respectively. The fact that the product distribution is not dependent on the amount of the CCl_4 chlorinated γ-alumina solid used, indicates that the solid is behaving as a catalyst and not simply a 'reagent'. Conversion to the Friedel-Crafts products, *t*-butylbenzene and di-*t*-butylbenzene, as a function of time shows the difference in product distribution for different chlorinated γ-alumina samples (Figure 4.6 vs. 4.7), and the similarity in product distribution at different catalyst loading (Figure 4.7 vs. 4.8).

A catalyst by definition is capable of promoting a chemical reaction without being used up in the process. A key requirement of an effective catalyst, therefore, is the ability to catalyse repetitive reactions without the need to be replaced. The standard industrial Friedel-Crafts catalyst, $AlCl_3$, is unable to catalyse repetitive reactions as it becomes bound to the reactant and products, preventing further catalysis (36).

The ability of CCl_4 chlorinated γ-alumina to catalyse repetitive reactions was examined in the alkylation of toluene and benzene with *t*-butyl chloride. The experimental procedure and analysis techniques adopted, were as outlined in section

Figure 4.6 : Friedel-Crafts Reaction of *t*-Butyl Chloride with Benzene (1:10) on Solid CCl_4 Chlorinated γ-Alumina - **Sample 1 (0.5 g)**

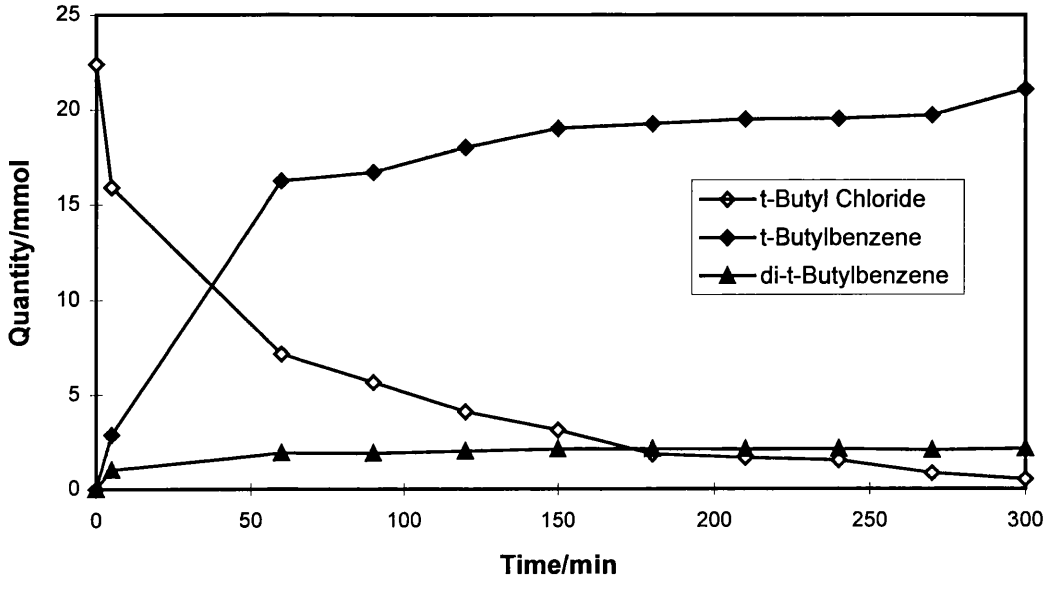

Figure 4.7 : Friedel-Crafts Reaction of *t*-Butyl Chloride with Benzene (1:10) on Solid CCl_4 Chlorinated γ-Alumina - **Sample 2 (0.5 g)**

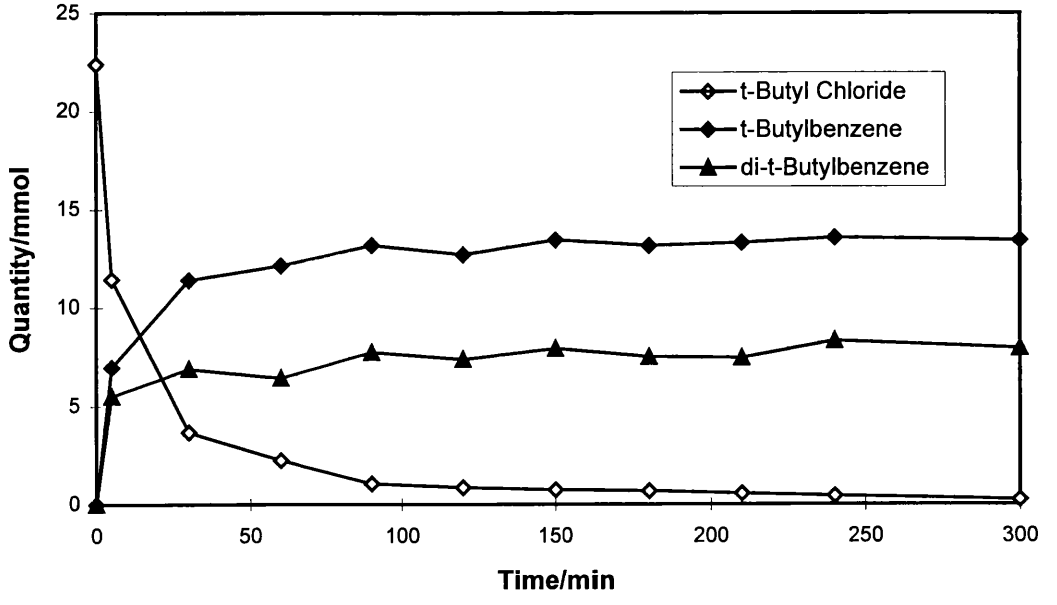

Figure 4.8 : Friedel-Crafts Reaction of *t*-Butyl Chloride with Benzene (1:10) on Solid CCl_4 Chlorinated γ-Alumina - **Sample 2 (1.0 g)**

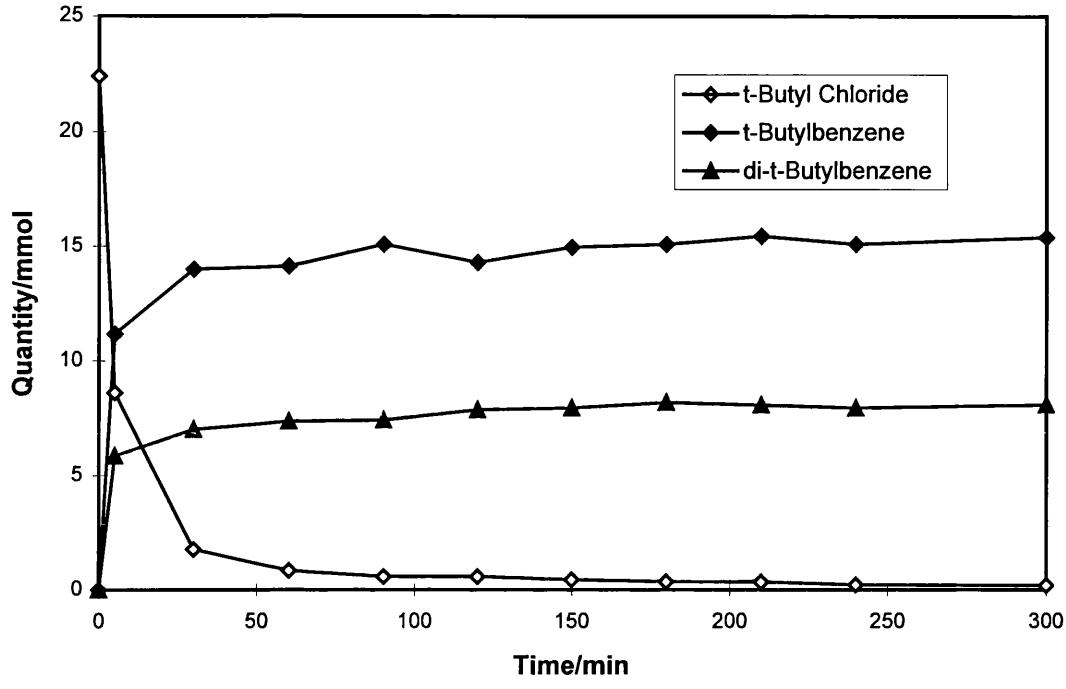

4.2 and 4.3. Following complete conversion of *t*-butyl chloride to Friedel-Crafts products (i.e. varied from 2 - 5 h depending on the system), a second aliquot of *t*-butyl chloride (22.4 mmol) was introduced to the reaction vessel. Analysis of the reaction system by GC, showed no increase in the quantity of Friedel-Crafts products and a constant level of *t*-butyl chloride. It is important to note that halogenated γ-aluminas are susceptible to moisture and air and may have become effectively deactivated due to residual moisture in the gas inlet or reagents, binding strongly to the active sites on the solid (94-96).

The inability of chlorinated γ-alumina to catalyse repetitive reactions is similar to the catalytic behaviour of $AlCl_3$. Interestingly, the two catalytic systems were visually very different, with the $AlCl_3$ appearing to be very soluble in the reaction mixture (i.e. 'pseudo homogeneous') compared with the relatively insoluble chlorinated γ-alumina.

4.4.4 Friedel-Crafts Reaction of Benzoyl Chloride with Benzene on CCl_4 Chlorinated γ-Alumina

The high catalytic activity of the CCl_4 chlorinated γ-alumina solid in the model Friedel-Crafts alkylation reactions studied in sections 4.4.1 and 4.4.2, led to a preliminary study being made of its activity in the more demanding reaction of benzoyl chloride with benzene. Benzoylation and acylation reactions are known to be problematic, due to complexation of the oxygen species to active catalytic sites on solid catalysts (36). Enhanced electrophilicity of the acylium ion often results in the species becoming strongly bound to the Lewis acid sites of Friedel-Crafts catalysts, deactivating the catalysts.

The experimental procedure and analysis techniques adopted are detailed in section 4.2 and 4.3 respectively. Initial attempts to prepare benzophenone by stirring benzoyl chloride (22.4 mmol) and benzene (224.0 mmol) at room temperature in the presence of CCl_4 chlorinated γ-alumina (0.5 g) were unsuccessful. GC analysis indicated two broad features, whose retention times (8.3 and 11.5 min) were not

consistent with benzene (1.1 min), benzoyl chloride (5.5 min) or the desired Friedel-Crafts product benzophenone (10.1 min). The absence of the desired product was initially thought to be the result of complexation of the acylium ion, derived from benzoyl chloride, to the active sites on the surface of the CCl_4 chlorinated γ-alumina solid. Previous workers, had successfully employed elevated temperature to degrade the product-catalyst complexes formed and recover the Friedel-Crafts products (155).

Several attempts were made to develop a high temperature system, with chlorinated γ-alumina suspended in benzoyl chloride at 438 K, with dry benzene added slowly, in order to minimise the temperature drop. In all cases GC analysis showed the presence of the two broad features and unreacted starting material, but no band corresponding to benzophenone.

GCMS analysis of the reaction mixtures identified two broad bands, retention times 5.5 and 21.0 min and molecular masses 122 a.m.u. and 226 a.m.u. respectively (Table 4.6). Benzoyl chloride is susceptible to hydrolysis, to benzoic acid and benzoic anhydride, whose molecular masses are consistent with those obtained from the GCMS. It was therefore concluded that the two broad features were due to benzoic acid and benzoic anhydride. The formation of hydrolysis products may indicate that the lack of catalytic activity of the CCl_4 chlorinated γ-alumina, in the benzoylation reaction, is the result of the solid surface becoming deactivated due to coordination of water molecules. It is equally possible however that the CCl_4

chlorinated γ-alumina solid does not possess sufficient surface acidity for it to function as a Friedel-Crafts catalyst in the demanding benzoylation reaction.

Table 4.6 : GCMS Analysis of the Friedel-Crafts Reaction of Benzoyl Chloride with Benzene (1:10) on CCl_4 Chlorinated γ-Alumina

Fraction	Retention Time/min	Mass/a.m.u.	Assignment
1	5.5	122	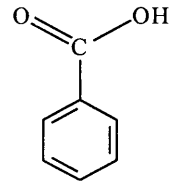 Benzoic Acid
2	21.0	226	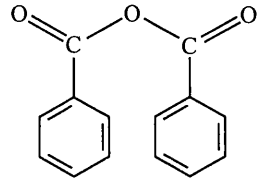 Benzoic Anhydride

CHAPTER 5

INFRARED SPECTROSCOPIC STUDIES OF THE VAPOUR PHASE IN SOLID/VAPOUR SYSTEMS

5.1 Introduction

This short chapter summarises infrared spectroscopic analysis of the vapour phase in solid/vapour systems and was designed to act as reference material for developing understanding of the nature of the solid/reagent interactions. Interactions of the Friedel-Crafts reagents *t*-butyl chloride, 2-chloropropane and acetyl chloride with a variety of solid materials of catalytic interest were studied by following changes in the infrared spectra of the alkyl or acyl halide with time. The alkyl and acyl halide systems studied were chosen to complement both the Friedel-Crafts and [^{36}Cl]-chlorine radiochemical studies (chapters 4 and 6 respectively). The following solid materials were examined within this work:

(i) Calcined γ-alumina

(ii) CCl_4 chlorinated γ-alumina

(iii) SF_4 fluorinated γ-alumina

(iv) SOF_2/SF_4 fluorinated γ-alumina

(v) Oxide supported organic layer catalyst derived from dehydrochlorination and oligomerisation of 1,1,1-trichloroethane on CCl_4 chlorinated γ-alumina

(vi) Oxide supported organic layer catalyst derived from dehydrochlorination and oligomerisation of 1,1,1-trichloroethane on SF_4 fluorinated γ-alumina

(vii) Solid β-AlF_3

(viii) Solid $AlCl_3$

The solid/vapour interactions were studied by monitoring a specific infrared active mode for each alkyl or acyl halide. Changes in the absorbance of the selected mode and the appearance of any new infrared active modes when the vapour was exposed to solid materials were recorded. The infrared active mode chosen for each compound was the stretching mode with the largest dynamic dipole moment (i.e. greatest absorbance in the infrared). Direct comparison of the infrared spectra of a given alkyl or acyl halide on different solid materials was possible as the experiments were performed in the same infrared cell, with identical pressures of volatile material.

It is important to note that the solid materials examined within this section have different surface areas. The potential for a solid surface to interact with an alkyl or acyl halide in the vapour phase will be a function of the number of active surface sites available on the solid. This will depend on the surface area of a solid and is therefore an important consideration when interpreting data. Surface areas of the solids investigated are given in Table 5.1.

The one point BET surface area measurements were performed on a Coulter SA 3100 instrument.

Table 5.1 : Surface Areas of the Solid Materials (78,121,145)

Solid	Surface Area/m^2g
Calcined γ-Alumina	110
CCl_4 Chlorinated γ-Alumina	80-90
SF_4 Fluorinated γ-Alumina	80-90
β-AlF_3	31
$AlCl_3$	~30

5.2 Experimental Procedure

A sample (0.5g) of the solid material of interest was loaded into a Pyrex glass dropping ampoule, in a inert atmosphere box. The ampoule was transferred to the limb of an *in-situ* gas infrared cell (described in section 2.5.1) and the vessel degassed. A known pressure of the alkyl or acyl halide (20 Torr) was expanded into the infrared cell via a calibrated manifold. The cell was transferred to an FTIR spectrophotometer and the infrared spectrum of the volatile material recorded in the absorbance mode. The solid material was then dropped into the cell, in contact with the alkyl or acyl halide vapour, and the resultant infrared spectra recorded at timed intervals (i.e. 1, 15, 30, 60 min and finally 20 h).

The degree and nature of the interaction between the alkyl or acyl halide vapour and the solids were studied by monitoring changes in the absorbance value of a key functional infrared active mode. Appearance of new infrared active modes and any changes in the physical appearance of the solid following exposure to the alkyl or acyl halide were recorded.

5.3 *t*-Butyl Chloride in the Vapour Phase over Solid Surfaces

The interaction of *t*-butyl chloride vapour with the solids listed in section 5.1 was studied by monitoring the infrared active C-H stretching mode of the $-CH_3$ functional group (at ~2996 cm^{-1} wavenumbers) in the vapour phase. Infrared experiments were performed in the *in-situ* gas infrared cell via the procedure detailed in section 5.2. Infrared spectra were recorded in the absorbance mode over the first hour of exposure, with the absorbance value of the C-H stretching mode plotted as a function of time. Intensity of the infrared active C-H stretching mode absorbance for the vapour-solid system examined was normalised by correcting for the baseline absorbance. Figure 5.1 shows the infrared spectrum of standard *t*-butyl chloride recorded at 20 Torr in the *in-situ* gas infrared cell, prior to introduction of solid material (standard assignments are shown in Table 3.1).

The interaction of *t*-butyl chloride vapour with $AlCl_3$ exhibited unique behaviour compared with the other solids examined (Figure 5.2). Exposure of $AlCl_3$ to *t*-butyl chloride, resulted in an initial decrease in the absorbance intensity of the

C-H stretch (i.e. 1.2→0.35 absorbance units), followed by a sharp increase in absorbance almost back to the level of the initial absorbance (i.e. 0.35→1.1 absorbance units, between the 5 and 15 min readings). A distinctive yellow deposit was formed on the surface of the $AlCl_3$. Thereafter a gradual rise in the C-H absorbance intensity was observed and HCl rotational fine structure detected on analysis of the infrared spectra. The infrared spectrum of the material present in the vapour phase over $AlCl_3$, after 60 min exposure, was consistent with the spectra of *t*-butyl chloride and the rotational fine structure characteristic of HCl.

Figure 5.1 : Infrared Spectrum of *t*-Butyl Chloride (20 Torr)

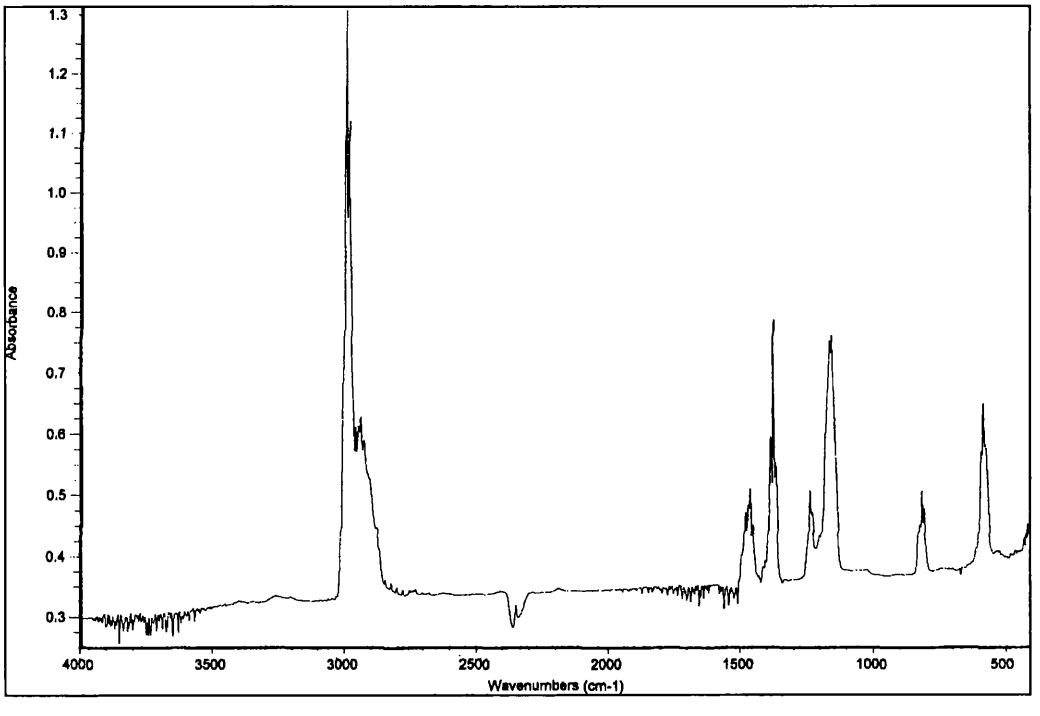

Infrared spectroscopic analysis and observations of the solid/vapour systems studied, highlighted the distinctive behaviour of $AlCl_3$. Formation of a coloured deposit on the surface of the solid on interaction with *t*-butyl chloride, was not observed on the chlorinated γ-alumina solid.

The vapour/solid interaction of chlorinated γ-alumina with *t*-butyl chloride was very different to that observed for the $AlCl_3$ (Figure 5.2). Initial exposure of *t*-butyl chloride to the chlorinated solid resulted in complete removal of the *t*-butyl chloride from the vapour phase, with the evolution of HCl evident in the infrared spectra. Monitoring the vapour phase by infrared thereafter, growth of HCl with time was observed without detecting *t*-butyl chloride. No visible change in the appearance of the chlorinated γ-alumina surface was observed on interaction with *t*-butyl chloride. The different behaviour of *t*-butyl chloride over $AlCl_3$ and chlorinated γ-alumina is interesting, as both solids exhibited similar catalytic activity in the model Friedel-Crafts alkylation reactions, reviewed in chapter 4.

Calcined γ-alumina, the precursor to many of the solids examined was a useful solid to benchmark the solid/vapour interactions against. In contrast to chlorinated γ-alumina, exposure of calcined γ-alumina to *t*-butyl chloride did not result in complete removal of the *t*-butyl chloride from the vapour phase and HCl was not evident on analysis of the infrared spectra (Figure 5.2). The apparent

lower affinity of the calcined γ-alumina for *t*-butyl chloride is probably due to the weaker surface acidity of the oxide vs. the halogenated solids.

Exposure of β-AlF_3 to *t*-butyl chloride behaved similarly to chlorinated γ-alumina, but *t*-butyl chloride was not removed completely from the vapour phase (Figure 5.2). The evolution of a small quantity of HCl was observed, without any visual change in the appearance of the solid.

Figure 5.2 : *t*-Butyl Chloride Infrared Active C-H Stretch (at ~2996 cm^{-1}) Over Solid Surfaces

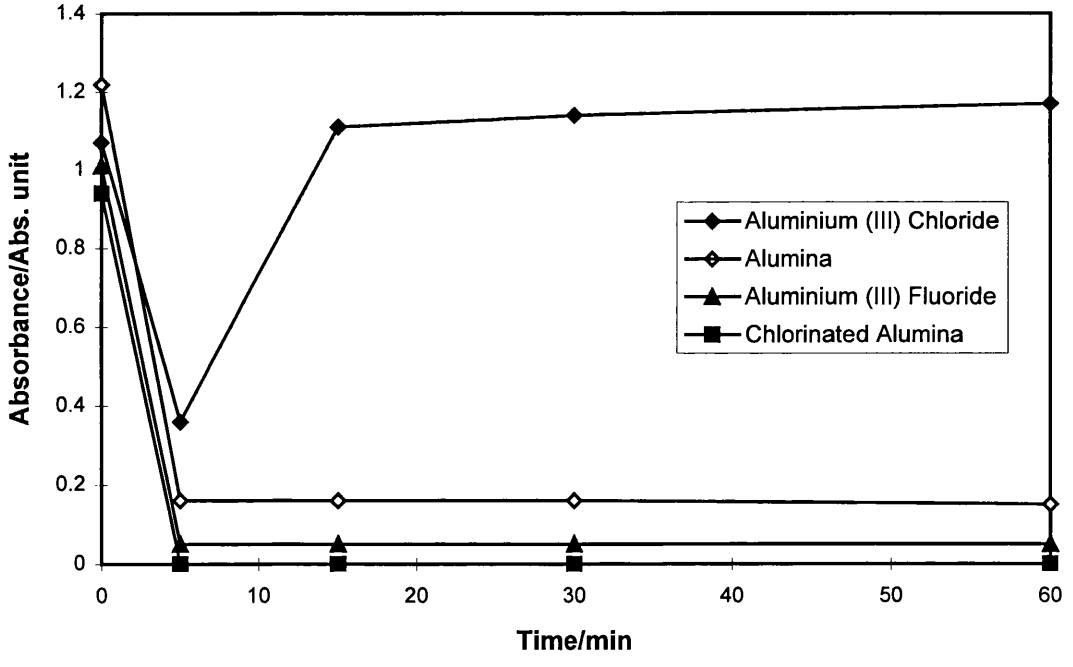

Exposure of *t*-butyl chloride to SF_4 fluorinated γ-alumina resulted in similar behaviour to chlorinated γ-alumina, leading to complete removal of the *t*-butyl

chloride from the vapour phase (Figure 5.3). Interestingly, a characteristic yellow deposit was formed on the surface of the fluorinated γ-alumina and no HCl was detect in the vapour phase. The behaviour over the SF_4 fluorinated γ-alumina will be discussed later.

Samples of γ-alumina fluorinated with an SOF_2/SF_4 mixture did not display as strong an affinity for the *t*-butyl chloride as γ-alumina fluorinated with predominantly SF_4 (Figure 5.3). Initial exposure of SOF_2/SF_4 fluorinated γ-alumina to *t*-butyl chloride, resulted in partial removal of the material from the vapour phase (i.e. 1.2 to 0.2 absorbance units), compared with complete removal of the *t*-butyl chloride from the vapour phase over SF_4 fluorinated γ-alumina. A purple deposit was formed on the surface of the γ-alumina fluorinated with the SOF_2/SF_4 mixture. The apparent lower affinity of the SOF_2/SF_4 fluorinated γ-alumina for *t*-butyl chloride is perhaps not surprising as SOF_2 is a weaker fluorinating agent than SF_4 and therefore may result in a surface of reduced acidity vs. the SF_4 fluorinated γ-alumina.

The oxide supported organic layer catalysts, derived from exposure of CCl_4 chlorinated γ-alumina and SOF_2/SF_4 fluorinated γ-alumina to 1,1,1-trichloroethane respectively, were examined in order to investigate the effect of the supported layer, on the vapour-solid interactions. The supported organic layer catalyst prepared from γ-alumina fluorinated with SOF_2/SF_4 behaved in a similar manner to its precursor (Figure 5.3). In contrast, the supported organic layer on chlorinated γ-alumina

modified the nature of the vapour-solid interaction. The layer catalyst did not completely remove *t*-butyl chloride from the vapour phase (Figure 5.3), as had been previously observed for the chlorinated γ-alumina (Figure 5.2). Interestingly, HCl rotational fine structure was observed on analysis of the infrared spectra of the vapour phase above both the chlorinated and fluorinated layer catalysts. The layer catalysts are highly coloured due to the presence of the supported organic layer and therefore any colour changes due to deposition of *t*-butyl chloride on the solid surfaces are not observed.

Figure 5.3 : *t*-Butyl Chloride Infrared Active C-H Stretch (at ~2996 cm^{-1}) Over Solid Surfaces

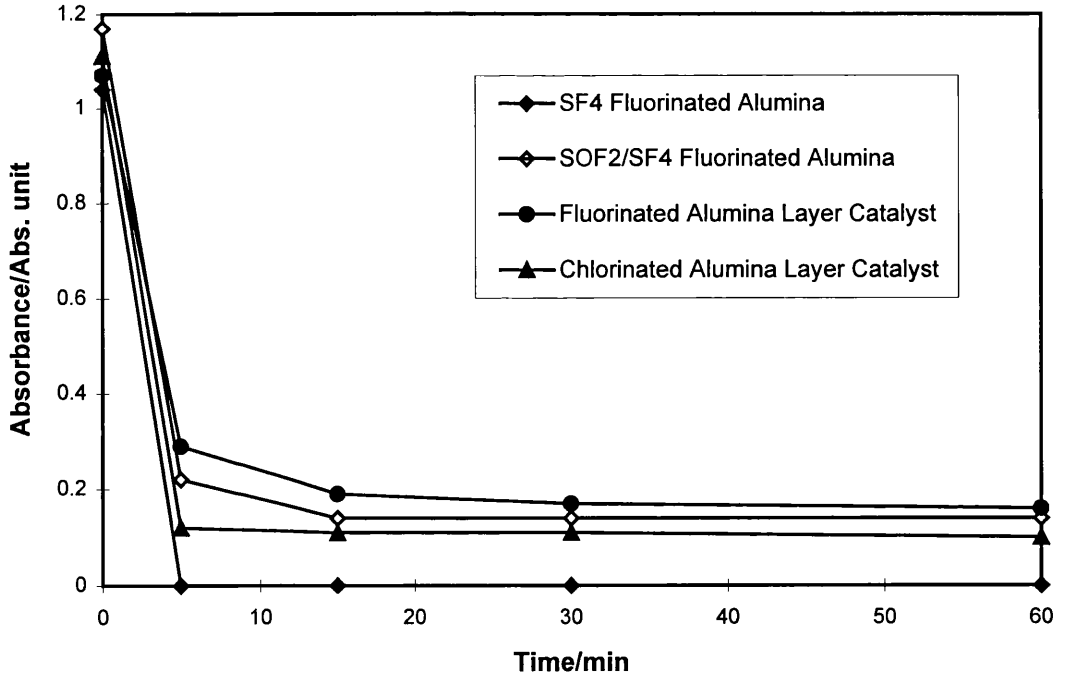

5.4 2-Chloropropane in the Vapour Phase over Solid Surfaces

The interaction of 2-chloropropane vapour with the solids listed in section 5.1 were studied by monitoring the infrared active C-H stretching mode of the $-CH_3$ functional group (at ~2989 cm^{-1} wavenumbers) in the vapour phase. Infrared experiments were performed in the *in-situ* gas infrared cell, via the procedure detailed in section 5.2. Infrared spectra were recorded in the absorbance mode over the first hour of exposure, with the absorbance value of the C-H stretching mode plotted as a function of time. The intensity of the infrared active C-H stretching mode absorbance for the vapour-solid systems examined was normalised by correcting for the baseline absorbance. Figure 5.4 shows the standard infrared spectrum of 2-chloropropane recorded at 20 Torr in the *in-situ* gas infrared cell, prior to introduction of solid material (standard assignments are shown in Table 3.1).

Exposure of 2-chloropropane vapour to solid $AlCl_3$ did not appear to result in any significant change in the absorbance intensity of the C-H stretching mode (Figure 5.5). Interestingly, however, a yellow deposit formed on the surface of the $AlCl_3$ and HCl rotational fine structure was observed in the infrared spectra of the vapour phase. Absorbance due to HCl increased with time. This apparently contradictory data may suggest that 2-chloropropane interacts very rapidly with the $AlCl_3$ surface, producing a surface species which releases HCl thereafter and effectively blocks the surface towards further interaction with 2-chloropropane vapour.

Figure 5.4 : Infrared Spectrum of 2-Chloropropane (20 Torr)

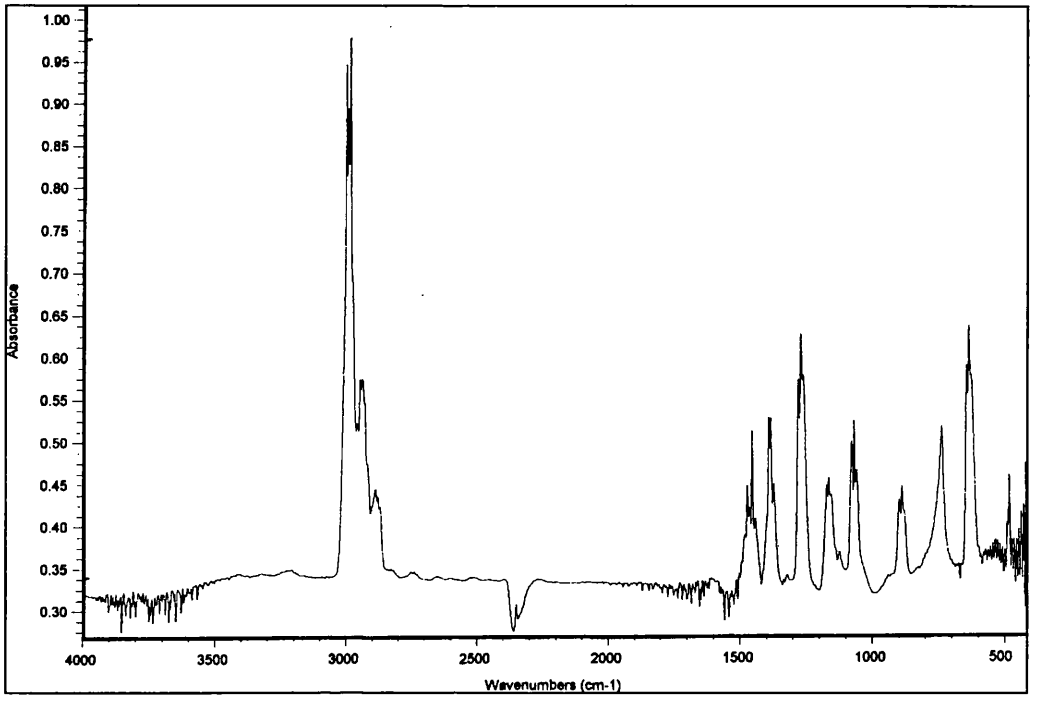

On the basis of the C-H absorbance intensity profile, β-AlF_3 appears to interact with 2-chloropropane in a similar manner to $AlCl_3$. An initial drop in the level of 2-chloropropane in the vapour phase over β-AlF_3 was followed by a period in which no further material was removed from the vapour phase (Figure 5.5). The β-AlF_3 and $AlCl_3$ surfaces actually behaved quite differently, with no coloured layer surface deposit formed or HCl released for β-AlF_3. Monitoring the absorbance intensity of the infrared active C-H stretching mode of 2-chloropropane over $AlCl_3$ and β-AlF_3, apparently does not truly reflect the different nature of the vapour-solid interactions which occur.

Exposing CCl_4 chlorinated γ-alumina to 2-chloropropane vapour resulted in a considerable decrease in the volatile 2-chloropropane (0.65→0.30 absorbance units) (Figure 5.5). Surprisingly a greater drop in the absorbance intensity of the C-H stretching mode was observed for calcined γ-alumina exposed to 2-chloropropane (i.e. 0.65→0.05 absorbance units). The apparent high removal of 2-chloropropane from the vapour phase over calcined γ-alumina would not have been predicted based on the relatively low acidity of the oxide surface.

Figure 5.5 : 2-Chloropropane Infrared Active C-H Stretch (at ~2989 cm^{-1}) Over Solid Surfaces

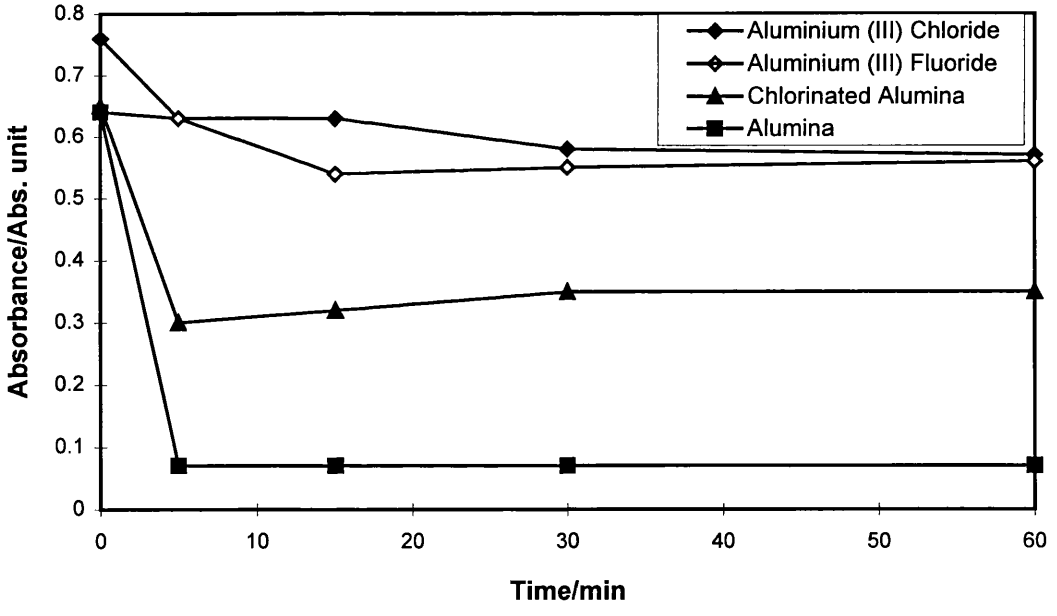

Analysis of the infrared spectra indicated that HCl was being released from the chlorinated γ-alumina surface during exposure to 2-chloropropane, whereas no HCl was evident in the vapour phase over calcined γ-alumina. This may indicate that

2-chloropropane reacts with the CCl_4 chlorinated γ-alumina effectively blocking surfaces sites on the solid, whereas adsorption on the surface of the calcined γ-alumina results in greater removal of volatile material due to the surface sites remaining active.

2-Chloropropane exposed to γ-alumina fluorinated with SF_4 or an SOF_2/SF_4 mixture behaved very similarly (Figure 5.6), with gradual removal of material from the vapour phase (i.e. from ~0.65→0.4 absorbance units in ~30 min). Analysis of the infrared spectra indicated the presence of HCl in the vapour phase of both systems. The absorbance intensity due to HCl increased with time.

Figure 5.6 : 2-Chloropropane Infrared Active C-H Stretch (at ~2989 cm^{-1}) Over Solid Surfaces

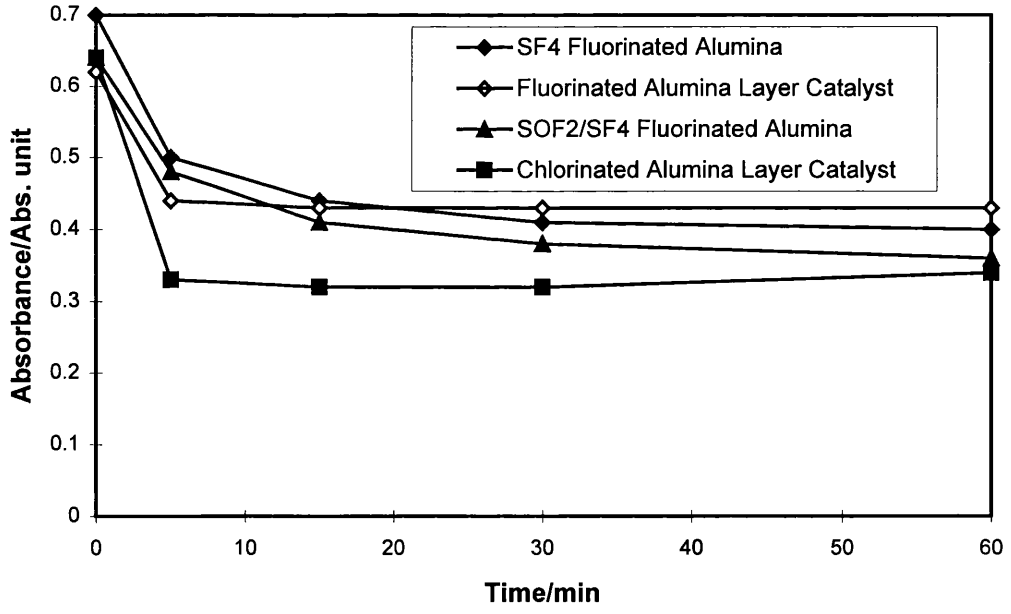

Exposing oxide supported organic layer catalysts derived from chlorinated and fluorinated γ-alumina to 2-chloropropane resulted in very similar C-H absorbance intensity profiles as a function of time (Figure 5.6). Analysis of the infrared spectra indicated that the chlorinated γ-alumina supported organic layer released HCl into the vapour phase over time. In contrast, the fluorinated supported organic layer did not appear to produce HCl in the vapour phase.

5.5 Acetyl Chloride in the Vapour Phase over Solid Surfaces

The interaction of acetyl chloride vapour with the solids listed in section 5.1 were studied by monitoring the infrared active C=O stretching mode of the acyl functional group (at ~1827cm^{-1}) in the vapour phase. Infrared experiments were performed in the *in-situ* gas infrared cell, via the procedure detailed in section 5.2. Infrared spectra were recorded in the absorbance mode over the first hour of exposure, with the absorbance value of the C=O stretching mode plotted as a function of time. Intensity of the infrared active C=O stretching mode absorbance for the vapour-solid systems was normalised by correcting for the baseline absorbance. Figure 5.7 shows the standard infrared spectrum of acetyl chloride recorded at 20 Torr in the *in-situ* gas infrared cell, prior to introduction of solid material (standard assignments are shown in Table 3.1).

Interaction of the acetyl chloride vapour with the solid materials was the least discriminating of the solid/vapour systems studied by *in-situ* infrared analysis. All

the solids examined showed a strong affinity for the acetyl chloride vapour, resulting in complete removal of the vapour phase within the first 5 min of exposure. Figure 5.8 shows the characteristic profile of the absorbance intensity of the infrared active C=O stretching mode of the acetyl chloride, observed in all the vapour-solid systems studied. The strong affinity of the solid materials for the volatile acetyl chloride, notably was even observed for calcined γ-alumina.

Figure 5.7 : Infrared Spectrum of Acetyl Chloride (20 Torr)

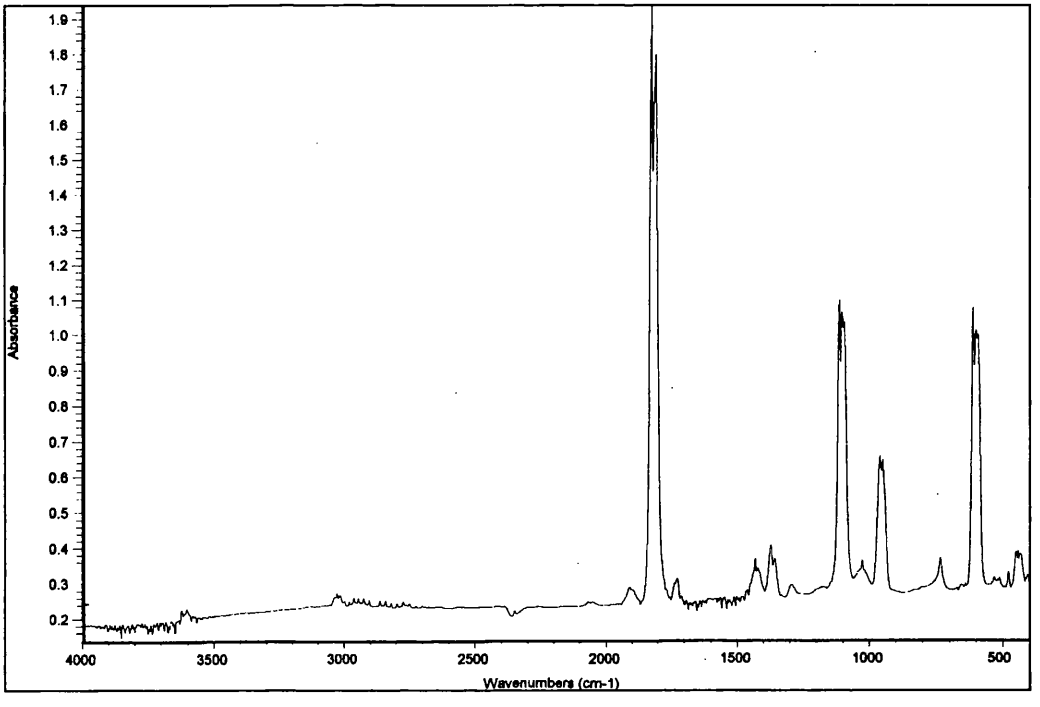

Interestingly, in the acetyl chloride vapour-solid systems no coloured deposits were observed on any of the solid surfaces following interaction. This strongly

implies that the coloured deposits observed on the solid surfaces exposed to *t*-butyl chloride or 2-chloropropane are the result of reaction of the alkyl halides on the solid surfaces. The strong solid/vapour interactions observed between acetyl chloride and the solid materials examined, highlight the problem often encountered in Friedel-Crafts acylation reactions (36). The lone pairs of electrons on the acyl oxygen give the molecule strong Lewis basic character and result in it binding strongly to acidic solids. The interaction of the solids with the acetyl chloride, highlights how difficult it is to get a catalytic system which is sufficiently acidic to catalyse acylation reactions, but which does not suffer deactivation due to complexation of reactants.

Figure 5.8 : Acetyl Chloride Infrared Active C=O Stretch (at ~1827 cm^{-1}) Over Solid Surfaces

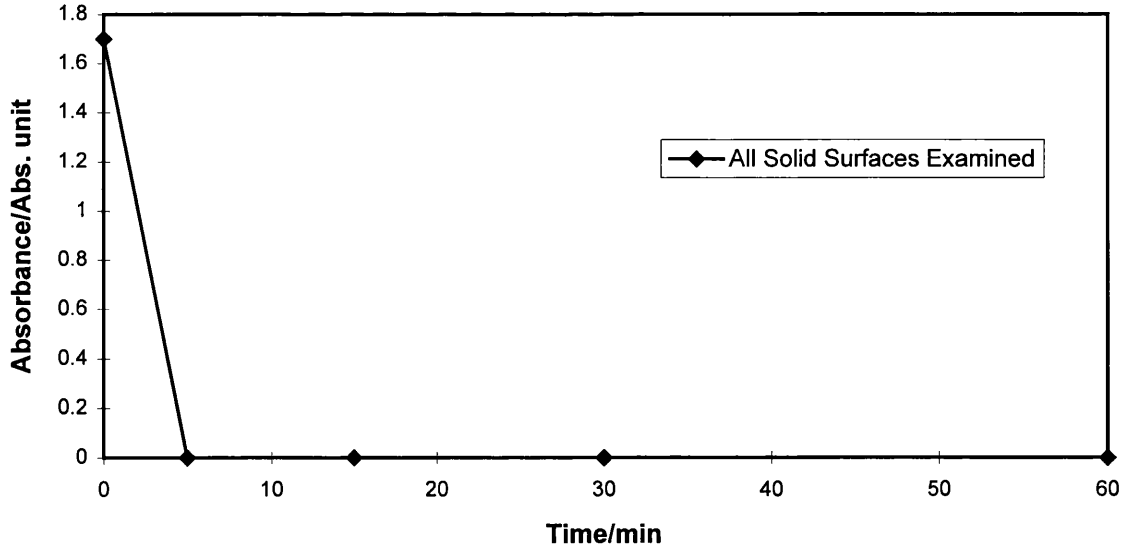

CHAPTER 6

RADIOCHEMICAL STUDIES – INTERACTIONS OF [^{36}Cl]–CHLORINE LABELLED *t*-BUTYL CHLORIDE, 2-CHLOROPROPANE AND ACETYL CHLORIDE WITH HALOGENATED SURFACES

6.1 Introduction

This chapter is concerned with the nature of the vapour-solid interactions that occur between alkyl and acyl halides with solid materials of interest as Friedel-Crafts catalysts. The radiolabelled compounds [^{36}Cl]–chlorine labelled *t*-butyl chloride, 2-chloropropane and acetyl chloride were prepared as described in sections 2.2.9, 2.2.8 and 2.2.10 respectively. Development of the experimental procedures for preparation of the radiolabelled compounds was reviewed in chapter 3. The key probe molecule, [^{36}Cl]–chlorine labelled *t*-butyl chloride, was used predominantly in these studies to gain a fundamental understanding of the model Friedel-Crafts reactions studied in chapter 4.

Vapour-solid interactions between the [^{36}Cl]–chlorine labelled alkyl and acyl halides and the solid surfaces were investigated via the direct monitoring Geiger Müller radiochemical counting technique (79,80). This technique enables *in-situ* monitoring of the reaction between a radiolabelled gas and a solid surface, via detection of [^{36}Cl]–chlorine on the solid surface (discussed in section 2.9). The [^{36}Cl]–chlorine radiochemical count recorded on a solid surface after exposure to a radiolabelled compound reflects the degree and nature of the vapour-solid interaction between the labelled species and the solid surface.

A fundamental understanding of the nature of the vapour-solid interactions is developed by examining the effects which a dynamic vacuum or exposure to unlabelled HCl have on the [^{36}Cl]-chlorine surface count of the solid. The use of radiolabelled species in this manner can yield useful information regarding the nature of the interaction between reactant molecules and catalytic surfaces. The direct monitoring Geiger Müller radiochemical counting technique has been successfully used to clarify the catalytic role of the oxide supported organic layer catalysts in halogen exchange reactions (75-77).

It is important to note the limitations of the direct monitoring Geiger Müller radiochemical counting technique in the study of vapour-solid interactions. The [^{36}Cl]-chlorine surface count for a given solid can not be directly compared with another solid sample. This is primarily due to variations in geometrical factors which will result in variations in the surface area available to interact with the [^{36}Cl]-chlorine labelled species present. Reproducibility from sample to sample is further complicated by variable elements in both the preparation of the halogenated solids and the [^{36}Cl]-chlorine labelled compounds. Interpretation of the [^{36}Cl]-chlorine solid surface count data, however, indicates whether a given radiolabelled compound interacts with a solid surface, and to what extent (i.e. weak or strongly bound).

Uptake and lability of [^{36}Cl]–chlorine labelled alkyl and acyl halides on the following solid materials, which exhibit a range of catalytic activity in model Friedel-Crafts reactions (Chapter 4), are reviewed within this chapter.

(i) Calcined γ-alumina

(ii) CCl_4 chlorinated γ-alumina

(iii) Oxide supported organic layer catalyst derived from dehydrochlorination/ oligomerisation of 1,1,1-trichloroethane on CCl_4 chlorinated γ-alumina

(iv) SF_4 fluorinated γ-alumina

(v) Solid β-AlF_3

(vi) Oxide supported organic layer catalyst derived from dehydrochlorination/ oligomerisation of 1,1,1-trichloroethane on SF_4 fluorinated γ-alumina

(vii) Solid $AlCl_3$

6.2 Experimental

6.2.1 Uptake of [^{36}Cl]–Chlorine on Solid Surfaces

Radiochemical experiments to investigate interactions between radiolabelled alkyl and acyl halides and solid surfaces were performed at room temperature, *in vacuo*, under vapour-solid conditions (79,80). The direct monitoring Geiger Müller counting vessel used consists of a Pyrex reaction vessel with two Geiger Müller tubes mounted over a Pyrex glass boat containing two sections (Figure 2.10). The vessel was connected via a manifold to a vacuum system consisting of a

constant volume manometer and gas handling facilities (Figure 2.1). Intercalibration of the Geiger Müller tubes and the experimental procedure adopted are detailed in section 2.9.

A sample (0.5g) of the solid material of interest was loaded into an ampoule in an inert atmosphere box, degassed and attached to the counting vessel. The vessel was evacuated before dropping the solid into one half of the glass boat. The solid was then positioned directly below a specific Geiger Müller tube, with the empty half of the boat below the second Geiger Müller tube. An aliquot of the [^{36}Cl]–chlorine labelled alkyl or acyl halide (100 Torr : 1.2 mmol) was expanded into the counting vessel via the calibrated manifold. The vessel was isolated and the [^{36}Cl]–chlorine count from both Geiger Müller tubes recorded over a specified time interval. Count duration was set to minimise the counting error experienced in radiochemical counting due to the random nature of the decay process (discussed in section 2.9.3).

One Geiger Müller tube records the [^{36}Cl]–chlorine gas phase count, while the second Geiger Müller tube records both the [^{36}Cl]–chlorine gas and solid surface count. Subtraction of the [^{36}Cl]–chlorine gas phase count from the gas/solid count gives a [^{36}Cl]–chlorine surface count for the solid. Uptake of [^{36}Cl]–chlorine, from labelled alkyl or acyl halides, on solid surfaces reflects the affinity of the solid for the Friedel-Crafts reactants. The [^{36}Cl]–chlorine radiochemical data were used to

develop a fundamental understanding of the interaction between Friedel-Crafts reactant molecules and solid catalytic surfaces.

6.2.2 Lability of [^{36}Cl]–Chlorine on Solid Surfaces

The ability of a catalyst to turnover reactant molecules on its surface is a prerequesit of an effective catalytic system. The ease with which [^{36}Cl]–chlorine species adsorbed on solid surfaces, were removed or displaced was investigated in order to develop an understanding of the nature of the interactions between the alkyl and acyl halides and the solids. Following interaction of the [^{36}Cl]–chlorine labelled species with the solid surfaces, the systems were pumped under dynamic vacuum to remove volatile and weakly adsorbed [^{36}Cl]–chlorine species from the solid surface. The solid was then recounted to measure the [^{36}Cl]–chlorine retained on the surface. Comparison of the initial [^{36}Cl]–chlorine surface count with the retained surface count gave a percentage retention. The level of [^{36}Cl]–chlorine retained on the solid surface is a function of the affinity of the solid for the alkyl or acyl halide species being studied. From this information, conclusions were made about the strength of the reagent-solid interaction.

Introduction of unlabelled HCl to solid surfaces labelled with [^{36}Cl]–chlorine, following interaction with labelled alkyl or acyl halides, was investigated to determine the lability of the [^{36}Cl]–chlorine species towards exchange/displacement. The [^{36}Cl]–chlorine surface count on the solids was monitored to assess whether

unlabelled HCl exchanged with/displaced the [^{36}Cl]–chlorine from the surface. It is important to note that only solid materials with appreciable [^{36}Cl]–chlorine surface counts can be studied by this technique, as it is based on changes in the magnitude of the [^{36}Cl]–chlorine count rate of material associated with the solid surface.

6.3 Results

Radiochemical data in this section summarise findings from the study of vapour-solid interactions between [^{36}Cl]–chlorine labelled alkyl and acyl halides and solid materials of catalytic interest. Interaction of [^{36}Cl]–chlorine labelled *t*-butyl chloride with the solid materials of interest was studied primarily to gain a fundamental understanding of the catalytic behaviour observed in the model Friedel-Crafts reactions discussed in chapter 4. [^{36}C1]–chlorine labelled 2-chloropropane and acetyl chloride were used as probe molecules to a lesser extent. The experimental procedure adopted for studying the vapour-solid systems, via the direct monitoring Geiger Müller technique, are detailed in sections 6.2.1 and 6.2.2.

6.3.1 Uptake of [^{36}Cl]–Chlorine Labelled *t*-Butyl Chloride on $AlCl_3$

The archetypal Lewis acid $AlCl_3$ is commonly used in industry as a Friedel-Crafts catalyst. The principal aim of the work reviewed within this thesis was to identify solids which display catalytic activity comparable with $AlCl_3$, without the environmental negatives associated with its use (36). Study of the vapour-solid interactions between [^{36}Cl]–chlorine labelled alkyl and acyl halides with new

alternative catalysts were benchmarked vs. $AlCl_3$. Behaviour of [^{36}Cl]–chlorine labelled *t*-butyl chloride on exposure to $AlCl_3$ was examined via the direct monitoring Geiger Müller technique (discussed in section 2.9).

Anhydrous $AlCl_3$ was prepared as described in section 2.3.5. Preparation of [^{36}Cl]–chlorine labelled *t*-butyl chloride, with a specific count rate of 54 count s^{-1} per 100 Torr, was prepared as detailed in section 2.2.9. A sample (0.5g) of $AlCl_3$ was loaded into the direct monitoring vessel and an aliquot of [^{36}Cl]–chlorine labelled *t*-butyl chloride (100 Torr : 1.2 mmol) introduced via a calibrated gas handling manifold (254 cm^3). The counts from the Geiger Müller tubes were recorded at specific time intervals to minimise counting error due to the random nature of the decay process. The white $AlCl_3$ solid turned yellow and began to bubble vigorously when exposed to the [^{36}Cl]–chlorine labelled *t*-butyl chloride. After approximately fifteen minutes the reaction became less vigorous and the appearance of the $AlCl_3$ changed to a brown viscous liquid.

A plot of the [^{36}Cl]–chlorine surface count of $AlCl_3$ and the [^{36}Cl]–chlorine gas phase count vs. time (Figure 6.1), showed an initial rapid deposition of the [^{36}Cl]–chlorine species on the solid surface. Thereafter the [^{36}Cl]–chlorine labelled *t*-butyl chloride was not removed from the vapour phase to any appreciable extent and the [^{36}Cl]–chlorine surface count on the solid remained essentially constant.

The [^{36}Cl]–chlorine radiochemical data indicate that there is a considerable interaction between the [^{36}Cl]–chlorine labelled *t*-butyl chloride and the $AlCl_3$ surface. Affinity of the $AlCl_3$ for the *t*-butyl chloride is evident from the large [^{36}Cl]–chlorine surface count on $AlCl_3$ after 1 h exposure (Table 6.1). The vigorous reaction between $AlCl_3$ and [^{36}Cl]–chlorine labelled *t*-butyl chloride is discussed later.

Figure 6.1 : Exposure of Solid $AlCl_3$ to [^{36}Cl]–Chlorine Labelled *t*-Butyl Chloride

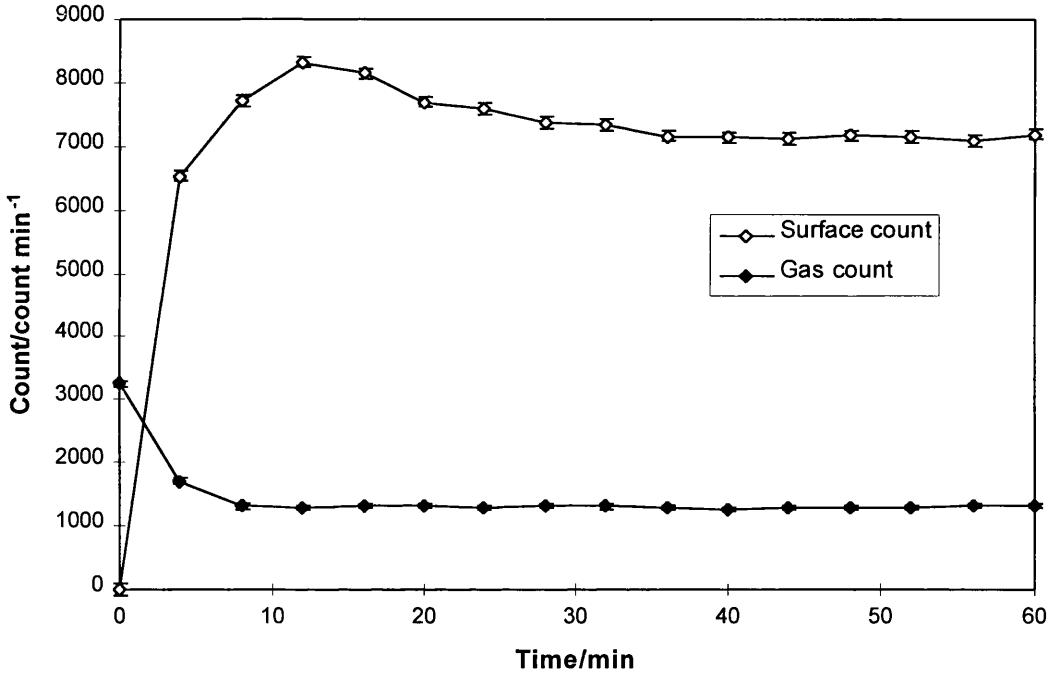

Table 6.1 : Uptake of [^{36}Cl]–Chlorine Labelled *t*-Butyl Chloride on Solid $AlCl_3$

Surface+Gas Count	Gas Count	Surface Count*
34846 ± 1592	5064 ± 88	29769 ± 1589

* Data from 14 readings of 4min count duration, standard deviation of mean quoted.

6.3.2 Uptake of [^{36}Cl]–Chlorine Labelled *t*-Butyl Chloride on Calcined γ-Alumina and CCl_4 Chlorinated γ-Alumina

This section is concerned with the vapour-solid interaction between [^{36}Cl]–chlorine labelled *t*-butyl chloride and the solids calcined γ-alumina and CCl_4 chlorinated γ-alumina (solids prepared as detailed in sections 2.3.1 and 2.3.2 respectively). Halogenation of calcined γ-alumina is known to result in surfaces which induce dehydrochlorination and oligomerisation of 1,1,1-trichloroethane to form a purple organic layer deposit on the halogenated surface (75,76). It was of interest to study interaction of the Lewis basic probe molecule, [^{36}Cl]–chlorine labelled *t*-butyl chloride, with both calcined γ-alumina and chlorinated γ-alumina.

Vapour-solid interactions between the [^{36}Cl]–chlorine labelled *t*-butyl chloride and the solid oxides were examined via the direct monitoring Geiger Müller counting technique (79,80). Limitations of the radiochemical technique (i.e. geometrical factors) in conjunction with variations in the specific count rate of the [^{36}Cl]–chlorine labelled probe molecule, made it impossible to compare directly [^{36}Cl]–chlorine surface counts from separate experiments. The technique was used successfully however to indicate whether [^{36}Cl]–chlorine labelled *t*-butyl chloride molecules interact with the solid surfaces of interest.

Calcined γ-alumina (0.5g) was exposed to an aliquot of [^{36}Cl]–chlorine labelled *t*-butyl chloride (100 Torr : 1.2 mmol), with a specific count rate of 28

count s^{-1} per 100 Torr, in the direct monitoring vessel. The counts from the two Geiger Müller tubes were recorded over a specific time interval, to minimise the counting error. Initial removal of the [^{36}Cl]–chlorine labelled *t*-butyl chloride from the vapour phase and deposition on the surface of the solid γ-alumina was observed (Figure 6.2). Initial deposition of the [^{36}Cl]–chlorine labelled *t*-butyl chloride was not visible on the solid surface. Thereafter the [^{36}Cl]–chlorine count of the gas and surface remained essentially constant. Identical behaviour was observed for a second sample of calcined γ-alumina examined.

Figure 6.2 : Exposure of Calcined γ-Alumina to [^{36}Cl]–Chlorine Labelled *t*-Butyl Chloride

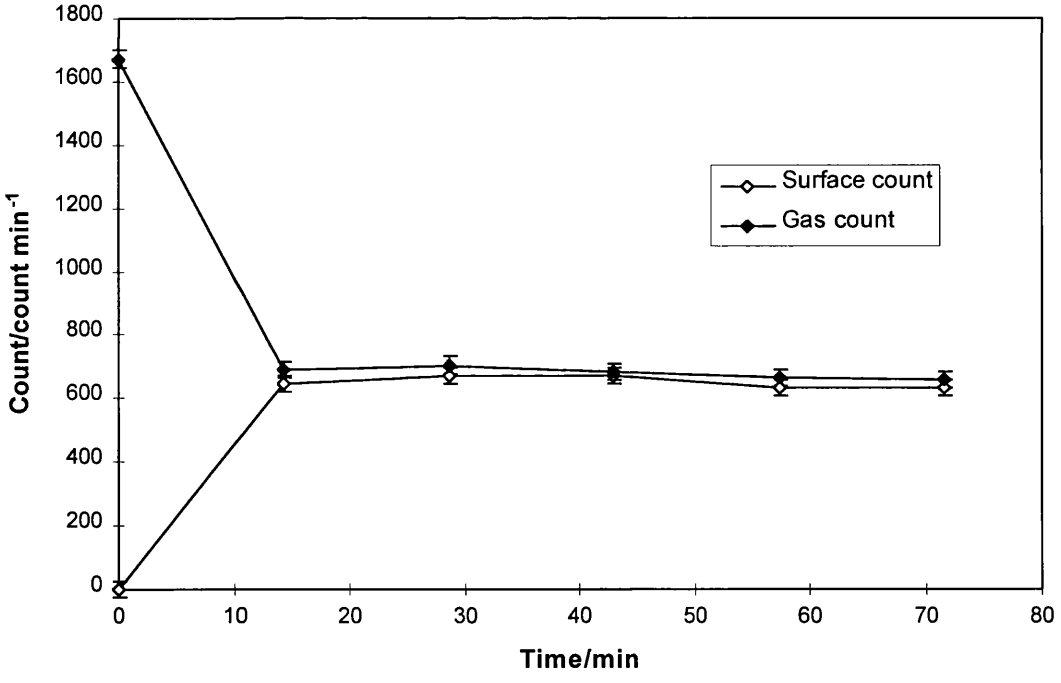

It is important to note that although the [^{36}Cl]–chlorine surface count on the calcined γ-alumina samples is relatively small, repeated counting and compensation for counting error, allows us to confirm the presence of [^{36}Cl]–chlorine species on the surface (Table 6.2). It was concluded that the γ-alumina surface has an affinity for the Lewis basic [^{36}Cl]–chlorine labelled *t*-butyl chloride probe molecule.

Table 6.2 : Uptake of [^{36}Cl]–Chlorine Labelled *t*-Butyl Chloride on Calcined γ-Alumina

Experiment	Surface+Gas Count	Gas Count	Surface Count
1*	19001 ± 547	9717 ± 303	9329 ± 218
2$^{\Delta}$	20508 ± 312	12180 ± 358	8328 ± 121

* Data from 5 readings of 14min count duration, standard deviation of mean quoted.
$^{\Delta}$ Data from 4 readings of 32min count duration, standard deviation of mean quoted.

Interaction between a halogenated γ-alumina and the probe molecule [^{36}Cl]–chlorine labelled *t*-butyl chloride was investigated firstly by examining CCl_4 chlorinated γ-alumina. Chlorinated γ-alumina was exposed to [^{36}Cl]–chlorine labelled *t*-butyl chloride (100 Torr : 1.2 mmol), with a specific count rate of 28 count s^{-1} per 100 Torr, in the direct monitoring cell via the same procedure used for the calcined γ-alumina. Initial exposure of the [^{36}Cl]–chlorine labelled *t*-butyl chloride to CCl_4 chlorinated γ-alumina resulted in a significant decrease in [^{36}Cl]–chlorine in the vapour phase as [^{36}Cl]–chlorine was deposited on the surface of the solid (Figure 6.3).

Following initial removal of [^{36}Cl]–chlorine labelled *t*-butyl chloride from the vapour phase, the [^{36}Cl]–chlorine gas phase count continued to drop slowly, without a corresponding increase in the [^{36}Cl]–chlorine surface count on the CCl_4 chlorinated γ-alumina solid. This apparent contradiction in behaviour, is probably associated with self absorption of the weak β^- decay (discussed in chapter 7). Exposure of the [^{36}Cl]–chlorine labelled *t*-butyl chloride to the CCl_4 chlorinated γ-alumina surfaces did not alter the appearance of the solid.

Figure 6.3 : Exposure of CCl_4 Chlorinated γ-Alumina to [^{36}Cl]–Chlorine Labelled *t*-Butyl Chloride

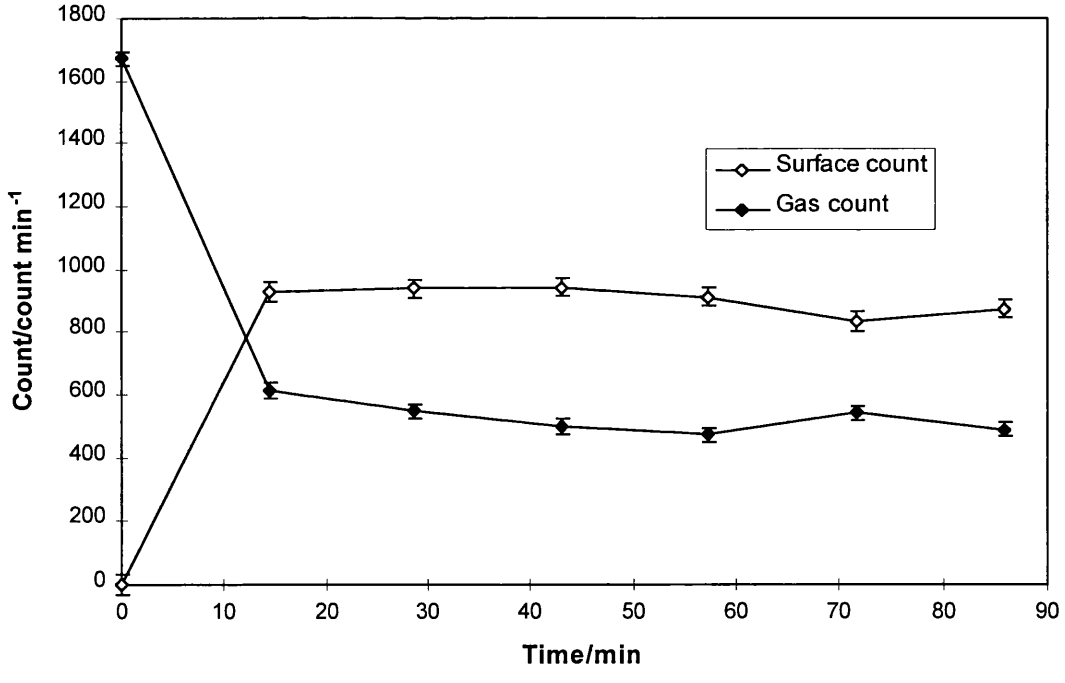

Investigation of the vapour-solid interaction between the CCl_4 chlorinated γ-alumina samples and [^{36}Cl]–chlorine labelled *t*-butyl chloride, showed similar

behaviour to that observed in Figure 6.3. Appreciable [^{36}Cl]–chlorine surface counts recorded for three different samples of CCl_4 chlorinated γ-alumina, indicate that the solid has an affinity for the [^{36}Cl]–chlorine labelled *t*-butyl chloride (Table 6.3). Even with the limitations of the radiochemical technique and variations in the reagent and sample preparation (as discussed earlier), we observed significant uptake of the [^{36}Cl]–chlorine labelled *t*-butyl chloride probe molecule in all cases.

Table 6.3 : Uptake of [^{36}Cl]–Chlorine Labelled *t*-Butyl Chloride on CCl_4 Chlorinated γ-Alumina

Experiment	Surface+Gas Count	Gas Count	Surface Count
1*	20631 ± 753	7297 ± 477	13334 ± 664
2$^{\Delta}$	23925 ± 193	12608 ± 556	11204 ± 518
3$^{\bullet}$	14563 ± 468	9789 ± 646	4866 ± 339

* Data from 6 readings of 14min count duration, standard deviation of mean quoted.
$^{\Delta}$ Data from 5 readings of 32min count duration, standard deviation of mean quoted.
$^{\bullet}$ Data from 16 readings of 14min count duration, standard deviation of mean quoted.

Although individual experiments can not be directly compared quantitatively, it is worth noting that the [^{36}Cl]–chlorine labelled *t*-butyl chloride exposed to calcined γ-alumina and chlorinated γ-alumina (Figure 6.2 and 6.3 respectively) was from the same batch (i.e. specific count rate of 28 count s^{-1} per 100 Torr). On the basis of the [^{36}Cl]–chlorine surface count data the calcined γ-alumina and chlorinated γ-alumina have similar affinities for the [^{36}Cl]–chlorine labelled *t*-butyl chloride probe molecule.

This is particularly interesting as the two solids displayed very different catalytic activity in the model Friedel-Crafts reactions studied in chapter 4. These findings are discussed in chapter 7.

6.3.3 Uptake of [^{36}Cl]–Chlorine Labelled *t*-Butyl Chloride on Oxide Supported Organic Layer Catalyst Derived from CCl_4 Chlorinated γ-Alumina

This section is concerned with the interaction between [^{36}Cl]–chlorine labelled *t*-butyl chloride and the oxide supported organic layer catalyst derived from exposure of CCl_4 chlorinated γ-alumina to 1,1,1-trichloroethane. The use of layer materials of this nature as halogen exchange catalysts, was reviewed in section 1.9, and resulted in interest in their potential application as Friedel-Crafts catalysts. These catalysts are referred to as oxide supported organic layer catalysts and were prepared as detailed in section 2.3.4.

The oxide supported organic layer catalyst (0.5g) was exposed to [^{36}Cl]–chlorine labelled *t*-butyl chloride (100 Torr : 1.2 mmol), with a specific count rate of 32 count s^{-1} per 100 Torr, in the direct monitoring cell (as described in section 2.9). Appreciable [^{36}Cl]–chlorine surface counts were recorded on the samples examined (Table 6.4). It is important to consider the effect of supported layers on these vapour-solid interactions. The fact that the radiochemical technique is based on detection of weak β^- decay of the [^{36}Cl]–chlorine radioisotope (Equation 2.3), may result in [^{36}Cl]–chlorine within the organic layer remaining undetected by the Geiger Müller tubes.

The effect of the 'quasi-liquid' organic phase on the vapour-solid interactions and the detection of the [^{36}Cl]–chlorine labelled *t*-butyl chloride is examined in section 6.3.10. A fundamental understanding of the role of the supported layer in the vapour-solid interactions is necessary before interpreting the [^{36}Cl]–chlorine radiochemical data.

Table 6.4 : Exposure of [^{36}Cl]–Chlorine Labelled *t*-Butyl Chloride to Oxide Supported Organic Layer Catalyst Derived from Chlorinated γ-Alumina

Experiment	Surface+Gas Count	Gas Count	Surface Count
1*	18505 ± 441	11508 ± 472	6997 ± 150
2$^{\Delta}$	14377 ± 704	11640 ± 629	2745 ± 153

* Data from 5 readings of 32min count duration, standard deviation of mean quoted.
$^{\Delta}$ Data from 12 readings of 4min count duration, standard deviation of mean quoted.

6.3.4 Uptake of [^{36}Cl]–Chlorine Labelled *t*-Butyl Chloride on SF_4 Fluorinated γ-Alumina and β-AlF_3

This section is concerned with the vapour-solid interactions between SF_4 fluorinated γ-alumina and β-AlF_3 with [^{36}Cl]–chlorine labelled *t*-butyl chloride. Solid samples of SF_4 fluorinated γ-alumina and β-AlF_3 were prepared via the procedures outlined in sections 2.3.3 and 2.3.6 respectively. The solids are active halogen exchange catalysts and were of interest as potential Friedel-Crafts catalysts (76,77,138,139). Interaction of the probe molecule [^{36}Cl]–chlorine labelled *t*-butyl chloride and the solids was examined via direct monitoring Geiger Müller technique

(discussed in section 2.9). Catalytic evaluation of the solids in model Friedel-Crafts reactions was reviewed in Chapter 4.

The SF_4 Fluorinated γ-alumina (0.5g) was loaded into the direct monitoring cell (Figure 2.10) and an aliquot of [^{36}Cl]–chlorine labelled *t*-butyl chloride (100 Torr : 1.2 mmol), introduced via a calibrated manifold. The counts from the two Geiger Müller tubes were recorded at specific time intervals, to minimise the counting error due to the random nature of the decay process. Count duration was set depending on the activity of the [^{36}Cl]–chlorine labelled *t*-butyl chloride in use.

Initial exposure of the fluorinated solid to [^{36}Cl]–chlorine labelled *t*-butyl chloride resulted in a distinctive yellow deposit appearing on the surface of the solid. Within the next 30 to 60 min the deposit turned purple and was very similar in appearance to the layer formation observed on oxide supported organic layer catalysts (75-77). Interestingly, on examination of the [^{36}Cl]–chlorine radiochemical data, the removal of [^{36}Cl]–chlorine from the vapour phase did not result in an appreciable [^{36}Cl]-chlorine surface count on the solid. Analysis of the [^{36}Cl]–chlorine radiochemical data indicated that the [^{36}Cl]–chlorine surface count on the SF_4 fluorinated γ-alumina was in fact negligible.

The [^{36}Cl]–chlorine count for the gas phase and the gas and solid count for two different samples of SF_4 fluorinated γ-alumina on exposure to [^{36}Cl]–chlorine labelled

t-butyl chloride are shown in Figures 6.4 and 6.5. Count duration was set at 1900 and 240 seconds for [^{36}Cl]–chlorine labelled *t*-butyl chloride samples with specific count rates of 8 and 47 count s^{-1} per 100 Torr respectively.

Both the SF_4 fluorinated γ-alumina samples examined showed an initial drop in the [^{36}Cl]–chlorine gas phase count over the solids, followed by a slow continual removal of the [^{36}Cl]–chlorine labelled *t*-butyl chloride from the vapour phase. Comparison of the [^{36}Cl]–chlorine gas phase count with the gas and solid count indicated there was no appreciable [^{36}Cl]–chlorine surface count on the SF_4 fluorinated γ-alumina samples. This behaviour is in contrast to that observed for exposure of [^{36}Cl]–chlorine labelled *t*-butyl chloride to CCl_4 chlorinated γ-alumina (Figure 6.3), where appreciable [^{36}Cl]–chlorine was detected on the CCl_4 chlorinated surface. Interestingly, chlorinated γ-alumina samples exhibited high catalytic activity in model Friedel-Crafts reactions studied earlier while SF_4 fluorinated γ-alumina was catalytically inactive (chapter 4).

Vapour-solid interactions between [^{36}Cl]–chlorine labelled *t*-butyl chloride and β-AlF_3 was studied via the direct monitoring technique. Exposure of the β-AlF_3 to the [^{36}Cl]–chlorine labelled *t*-butyl chloride probe molecule did not result in a significant change in the [^{36}Cl]–chlorine gas phase count (Figure 6.6). The [^{36}Cl]–chlorine gas phase count decreased slowly over time, without any visible change in the appearance of the β-AlF_3 surface. Comparison of the [^{36}Cl]–chlorine gas phase

Figure 6.4 : Exposure of SF_4 Fluorinated γ-Alumina to [^{36}Cl]–Chlorine Labelled *t*-Butyl Chloride (Sample 1)

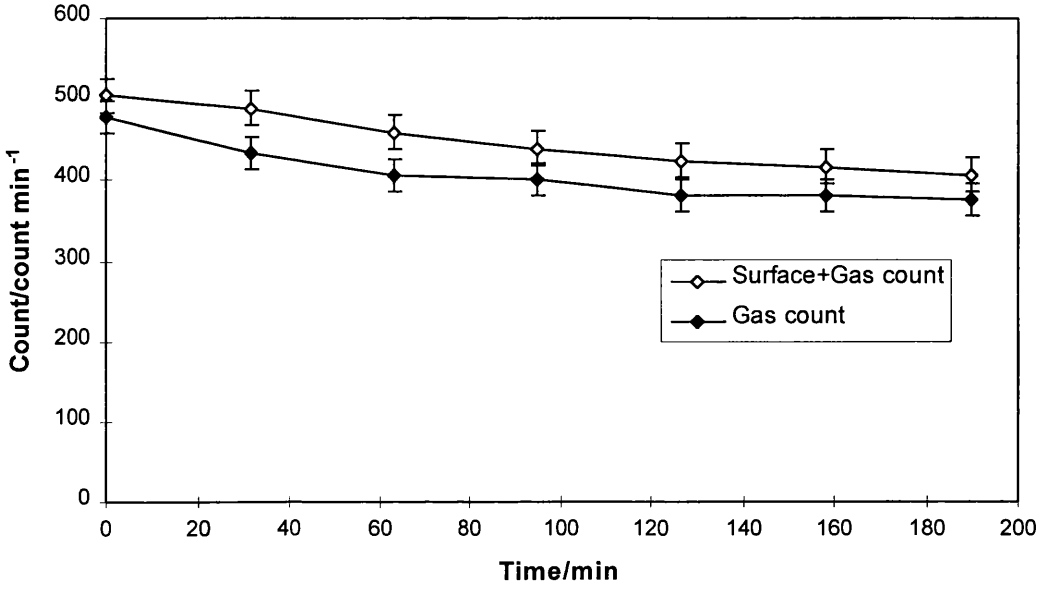

Figure 6.5 : Exposure of SF_4 Fluorinated γ-Alumina to [^{36}Cl]–Chlorine Labelled *t*-Butyl Chloride (Sample 2)

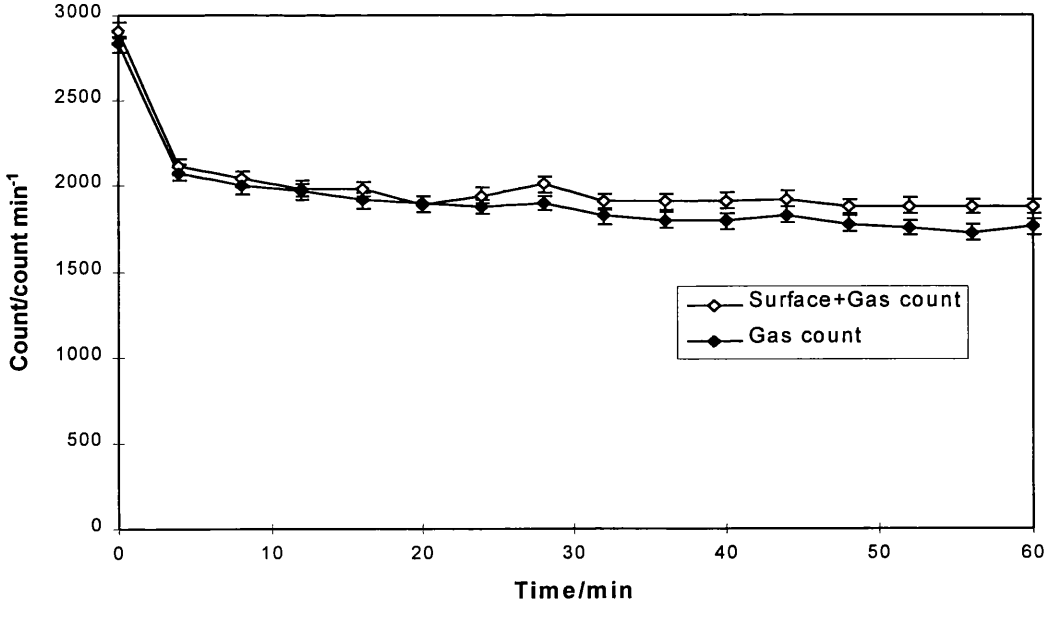

count with the gas and solid count indicated that there was no appreciable [^{36}Cl]–chlorine associated with the surface of the β-AlF_3.

Figure 6.6 : Exposure of β-AlF_3 to [^{36}Cl]–Chlorine Labelled *t*-Butyl Chloride

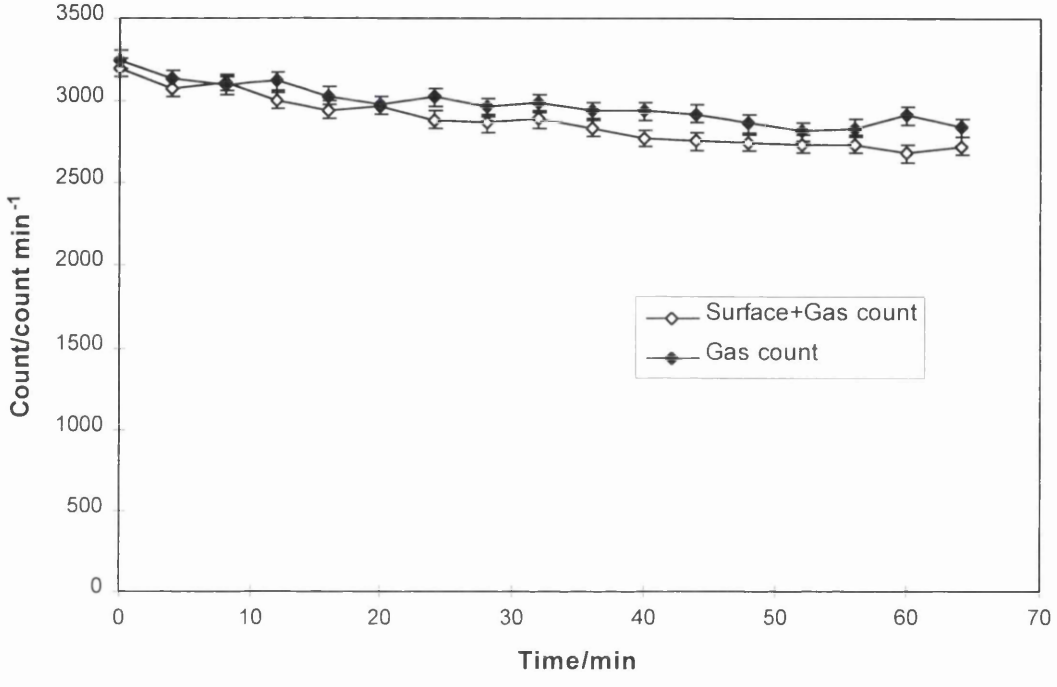

The β-AlF_3 system appears to show a reduced affinity for the [^{36}Cl]–chlorine labelled *t*-butyl chloride compared with SF_4 fluorinated γ-alumina. Deposition of a highly coloured layer on the surface of the solid, on exposure to the [^{36}Cl]–chlorine labelled *t*-butyl chloride, appears to be unique to SF_4 fluorinated γ-alumina. It is worth noting that β-AlF_3 showed limited catalytic activity in the model Friedel-Crafts reactions studied while SF_4 fluorinated γ-alumina was catalytically inactive (see

Chapter 4). The behaviour of the [^{36}Cl]–chlorine labelled *t*-butyl chloride probe molecule on β-AlF_3 and SF_4 fluorinated γ-alumina is discussed in conjunction with findings from the model Friedel-Crafts reactions studied (Chapter 7).

6.3.5 Uptake of [^{36}Cl]-Chlorine Labelled *t*-Butyl Chloride on Oxide Supported Organic Layer Catalyst Derived from SF_4 Fluorinated γ-Alumina

This section is concerned with the vapour-solid interaction between [^{36}Cl]–chlorine labelled *t*-butyl chloride and supported layer catalysts derived from exposure of SF_4 fluorinated γ-alumina to 1,1,1-trichloroethane. The catalytic activity of the supported layer catalysts in halogen exchange reactions, was reviewed in Section 1.9, led to interest in their potential application as Friedel-Crafts catalysts (76,77,130). These catalysts are referred to as oxide supported organic layer catalysts and were prepared as outlined in Section 2.3.

A sample of the oxide supported organic layer catalyst (0.5g) was exposed to [^{36}Cl]–chlorine labelled *t*-butyl chloride (100 Torr : 1.2 mmol), with a specific count rate of 47 counts s^{-1} per 100 Torr, in the direct monitoring cell (as described in section 2.9). The experimental procedure was identical to that adopted for the previous radiochemical studies. The presence of a supported organic layer on the solid surface may affect the nature of the vapour-solid interaction with [^{36}Cl]–chlorine labelled *t*-butyl chloride. Another important consideration is the fact that β^- decay of [^{36}Cl]–chlorine (Equation 2.3) is a weak phenomena and therefore material in the layer may

not be detected by the Geiger Müller counters. The presence of the highly coloured organic layer on the surface of the oxide prevents observation of coloured deposit formation, should it occur on exposure to the [^{36}Cl]–chlorine labelled *t*-butyl chloride probe molecule.

Initial exposure of the oxide supported organic layer catalyst to [^{36}Cl]–chlorine labelled *t*-butyl chloride resulted in a drop in the [^{36}Cl]–chlorine gas phase count (Figure 6.7). Thereafter the gas phase count continued to decrease slowly, indicating volatile material was being removed from the gas phase and deposited on the solid. Comparison of the [^{36}Cl]–chlorine gas count with the gas and solid count, however, indicated that there was no appreciable [^{36}Cl]–chlorine solid surface count.

The presence of the supported organic layer on the surface of the SF_4 fluorinated γ-alumina probably alters the nature of the vapour-solid interactions that occur on exposure to the [^{36}Cl]–chlorine labelled *t*-butyl chloride probe molecule. Interestingly, examination of the oxide supported organic layer catalysts derived from chlorinated γ-alumina (discussed in section 6.3.3), showed appreciable [^{36}Cl]–chlorine associated with the solid. The behaviour of the supported layer on halogenated γ-aluminas is examined in more detail in section 6.3.10.

Figure 6.7 : Exposure of Layer Catalyst Derived from SF_4 Fluorinated γ-Alumina to [^{36}Cl]–Chlorine Labelled *t*-Butyl Chloride

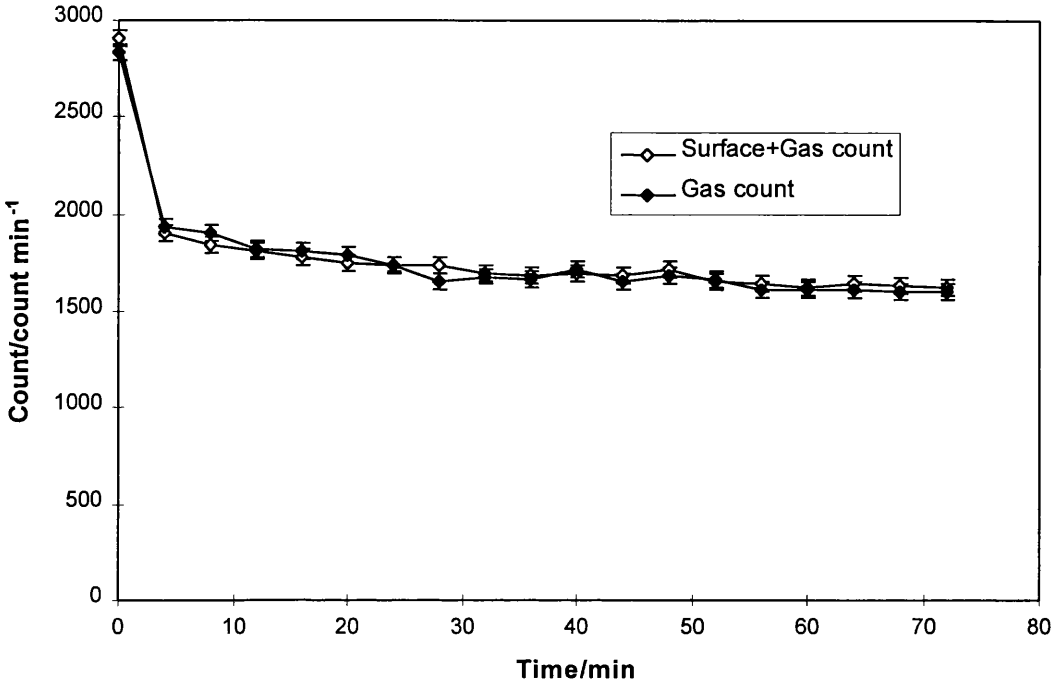

6.3.6 Uptake of [^{36}Cl]–Chlorine Labelled 2-Chloropropane on Solid Surfaces

This section is concerned with the nature of the interaction between [^{36}Cl-chlorine labelled 2-chloropropane and the solid materials discussed in section 6.1. The [^{36}Cl]–chlorine labelled 2-chloropropane was not studied in as much detail as the *t*-butyl chloride probe molecule. Primarily, the study was designed to establish whether behaviour of a secondary alkyl halide with the solids was similar to that observed for tertiary alkyl halide, *t*-butyl chloride. Development of a procedure for preparing [^{36}Cl]–chlorine labelled 2-chloropropane and the procedure adopted for this

work are described in sections 3.5 and 2.2.8 respectively.

Interaction of the [^{36}Cl]–chlorine labelled 2-chloropropane with the solid materials of interest was studied via the direct monitoring Geiger Müller technique (as in section 2.9). The principles of the direct monitoring technique and the generation of a [^{36}Cl]–chlorine gas phase count and gas/solid count have been extensively discussed in sections 6.1 to 6.3.5 for [^{36}Cl]–chlorine labelled *t*-butyl chloride.

On exposure of $AlCl_3$ (0.5 g) to [^{36}Cl]–chlorine labelled 2-chloropropane (100 Torr : 1.2 mmol) a pale yellow deposit was observed forming on the surface of the solid. The interaction was less vigorous that that observed for exposure of $AlCl_3$ to [^{36}Cl]–chlorine labelled *t*-butyl chloride (discussed in section 6.3.1). A plot of the [^{36}Cl]–chlorine surface count and gas phase count as a function of time shows a continual decrease in the volatile [^{36}Cl]–chlorine labelled 2-chloropropane and an increase in the [^{36}Cl]–chlorine solid surface count. (Figure 6.8). Comparison of the interaction of [^{36}Cl]–chlorine labelled *t*-butyl chloride with that of 2-chloropropane on $AlCl_3$ will be discussed in chapter 7.

The main objective of the [^{36}Cl]–chlorine labelled 2-chloropropane studies was to compare the behaviour of the chlorinated and fluorinated solid surfaces. In the [^{36}Cl]–chlorine labelled *t*-butyl chloride radiochemical experiments (sections 6.3.1 to

6.3.3) the chlorinated surfaces showed an affinity for the probe molecule resulting in appreciable [^{36}Cl]–chlorine surface counts, whereas the fluorinated materials showed no appreciable [^{36}Cl]–chlorine associated with the solid surfaces (Figure 6.3.4 and 6.3.5). Notably, however, removal of [^{36}Cl]–chlorine from the gas phase was observed for the fluorinated materials.

Solid samples (0.5g) were exposed to [^{36}Cl]–chlorine labelled 2-chloropropane (100 Torr : 1.2 mmol), with a specific count rate of 19 count s^{-1} per 100 Torr, in the direct monitoring counting cell. The radiochemical data is summarised in Table 6.5.

Figure 6.8 : Exposure of Solid $AlCl_3$ to [^{36}Cl]–Chlorine Labelled 2-Chloropropane

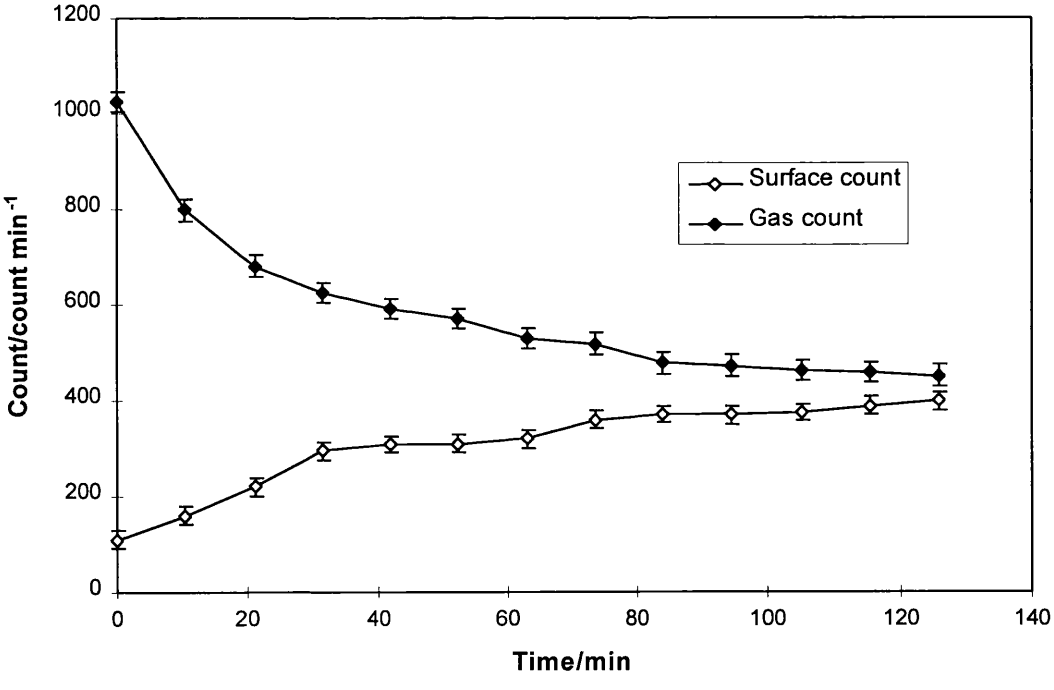

Table 6.5 : Uptake of [^{36}Cl]–Chlorine Labelled 2-Chloropropane on Solid Surfaces

Solid	Surface+Gas Count	Gas Count	Surface Count*
Calcined γ-alumina	13237 ± 156	8648 ± 178	4589 ± 143
CCl_4 Chlorinated γ-alumina	13673 ± 366	8968 ± 406	4705 ± 77
Oxide Supported Organic Layer Catalyst Derived from CCl_4 Chlorinated γ-alumina, 1,1,1-Trichloroethane	12285 ± 262	10626 ± 200	1659 ± 87
SF_4 Fluorinated γ-alumina	8420 ± 421	8156 ± 270	Negligible
β-AlF_3	7118 ± 192	6794 ± 184	Negligible
Oxide Supported Organic Layer Catalyst Derived from SF_4 Fluorinated γ-alumina, 1,1,1-Trichloroethane	7689 ± 212	7360 ± 159	Negligible

* Data in all experiments is based on between 6-10 readings, of 10.5min count duration, standard deviation of mean quoted.

Uptakes of [^{36}Cl]–chlorine labelled 2-chloropropane on the halogenated surfaces are similar to those observed for the [^{36}Cl]–chlorine labelled *t*-butyl chloride probe molecule. Calcined γ-alumina, chlorinated γ-alumina and the oxide supported organic layer catalyst derived from chlorinated γ-alumina, showed appreciable [^{36}Cl]–chlorine solid surface counts. In contrast β-AlF_3, fluorinated γ-alumina and the oxide supported organic layer catalyst derived from fluorinated γ-alumina, had negligible [^{36}Cl]–chlorine surface counts. Notably removal of the [^{36}Cl]–chlorine labelled 2-chloropropane from the vapour phase over fluorinated γ-alumina was observed but did not result in an appreciable [^{36}Cl]–chlorine solid surface count. This apparently

contradictory behaviour for the [^{36}Cl]–chlorine labelled 2-chloropropane was also observed for the *t*-butyl chloride / SF_4 fluorinated γ-alumina system (Figures 6.4 and 6.5) and is discussed in chapter 7.

6.3.7 Uptake of [^{36}Cl]–Chlorine Labelled Acetyl Chloride on $AlCl_3$ and CCl_4 Chlorinated γ-Alumina

This section is concerned with the vapour-solid interactions of [^{36}Cl]–chlorine labelled acetyl chloride with $AlCl_3$ and CCl_4 chlorinated γ-alumina respectively. The process for labelling acetyl chloride was realised successfully late in the project, and therefore only a brief investigation of the material in vapour-solid interactions was possible. Interest in acetyl chloride arises from the important role which Friedel-Crafts acylation reactions play in industrial-synthesis (i.e. ibuprofen synthesis shown in scheme 1.4) (36).

The solid $AlCl_3$ is well established as the standard industrial Friedel-Crafts catalyst of industry (discussed in Chapter 1) and hence interaction of [^{36}Cl]–chlorine labelled acetyl chloride with $AlCl_3$ was investigated. Solid CCl_4 chlorinated γ-alumina had shown the greatest catalytic activity of the solids examined in the model Friedel-Crafts alkylation reactions, without showing activity in a more demanding benzoylation reactions (Chapter 4). The interaction of [^{36}Cl]-chlorine labelled acetyl chloride with CCl_4 chlorinated γ-alumina was studied for comparison with $AlCl_3$.

The solids $AlCl_3$ and CCl_4 chlorinated γ-alumina were prepared as outlined in sections 2.3.5 and 2.3.2 respectively. Development of the procedure for preparing [^{36}Cl]–chlorine labelled acetyl chloride and the procedure adopted for this work are described in sections 3.6 and 2.2.10 respectively. Interaction of the [^{36}Cl]–chlorine labelled acetyl chloride with the solid materials was studied via the direct monitoring Geiger Müller technique (detailed in section 2.9). Solid samples (0.5g) were exposed to [^{36}Cl]–chlorine labelled acetyl chloride (100 Torr : 1.2 mmol), with a specific count rate of 63 count s^{-1} per 100 Torr, in the direct monitoring counting cell. The counts from both Geiger Müller tubes were recorded at a specific time intervals. The count duration was set to minimise the counting error due to the random nature of the decay process.

Interestingly, exposure of [^{36}Cl]–chlorine labelled acetyl chloride to $AlCl_3$ did not result in any visible change in the appearance of the solid surface. This is in contrast to the vigorous reaction and yellow colouration observed when $AlCl_3$ was exposed to [^{36}Cl]–chlorine labelled *t*-butyl chloride (discussed in section 6.3.1). The [^{36}Cl]–chlorine count for the vapour phase showed a continual reduction in the [^{36}Cl]–chlorine labelled acetyl chloride in the gas phase with time (Figure 6.9). Notably, removal of the [^{36}Cl]–chlorine labelled acetyl chloride did not result in an increase in the [^{36}Cl]–chlorine surface count on the solid. This apparent lack of detection of the [^{36}Cl]–chlorine deposited on the surface of the solid is possibly associated with self

absorption of the weak β^- decay of the [^{36}Cl]–chlorine radioisotope and will be discussed later.

Figure 6.9 : Exposure of Solid $AlCl_3$ to [^{36}Cl]–Chlorine Labelled Acetyl Chloride

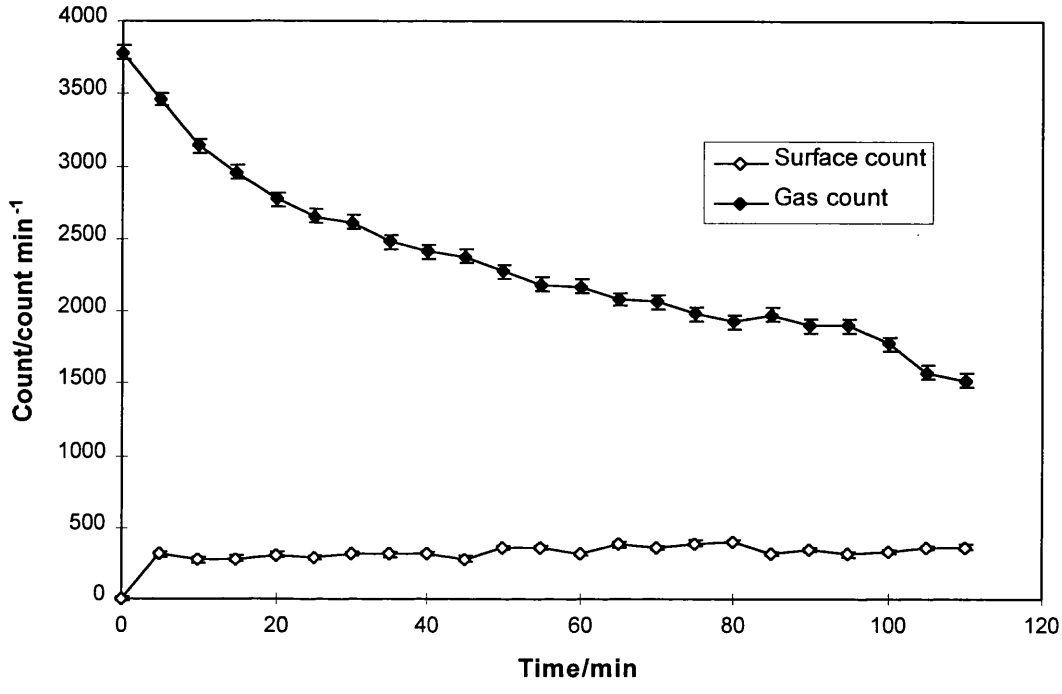

Chlorinated γ-alumina was exposed to [^{36}Cl]–chlorine labelled acetyl chloride in the same manner as $AlCl_3$. The [^{36}Cl]–chlorine radiochemical data produced on exposure of the [^{36}Cl]–chlorine labelled acetyl chloride probe molecule to chlorinated γ-alumina are shown in Figure 6.10. Interaction of the [^{36}Cl]–chlorine labelled acetyl chloride with CCl_4 chlorinated γ-alumina, appears to be very similar to that observed for $AlCl_3$ (Figure 6.9). Removal of [^{36}Cl]–chlorine labelled acetyl chloride from the

vapour phase after initial increase in the [^{36}Cl]–chlorine surface count on the solid, did not result in an increase in the [^{36}Cl]–chlorine surface count on the solid. The affinity of the chlorinated γ-alumina for the [^{36}Cl]–chlorine labelled acetyl chloride is evident from removal of the probe molecule from the vapour phase.

Figure 6.10 : Exposure of CCl_4 Chlorinated γ-Alumina to [^{36}Cl]–Chlorine Labelled Acetyl Chloride

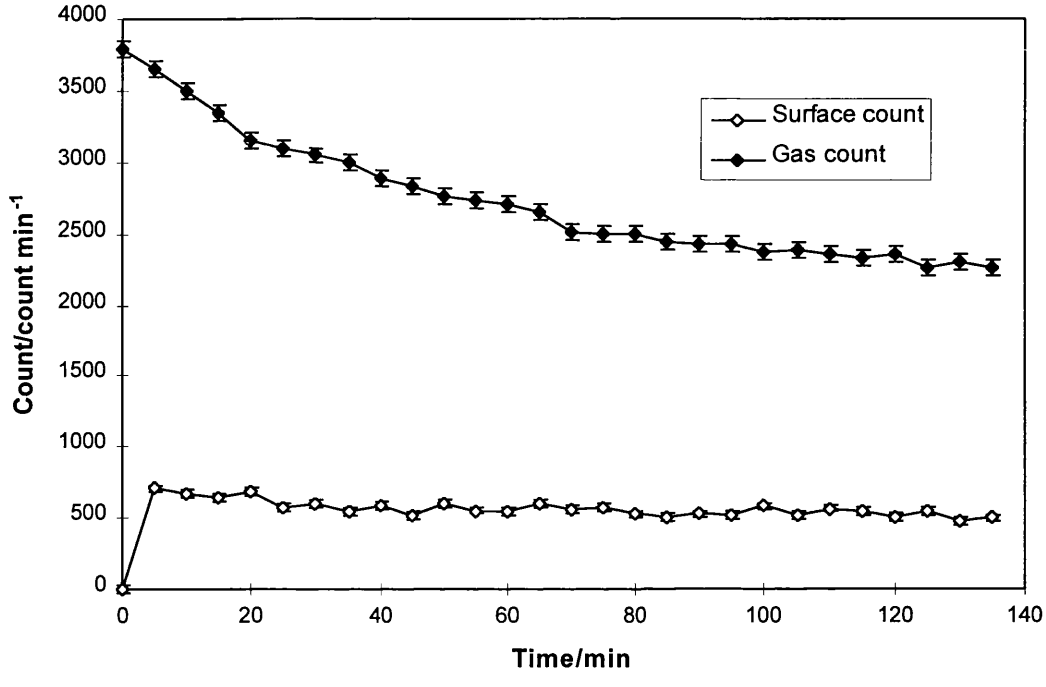

The probe molecule [^{36}Cl]–chlorine labelled acetyl chloride, on the basis of the reduction of [^{36}Cl]–chlorine in the vapour phase, appears to behave similarly on $AlCl_3$ and CCl_4 chlorinated γ-alumina. An important consideration is the lability of the [^{36}Cl]–chlorine species on the solid surfaces following interaction. Interaction of

the acyl halide with the solids examined is a function of the availability and strength of the active sites on the solid surface. Studying the lability of the [^{36}Cl]–chlorine species on the solid surfaces will indicate the affinity of the [^{36}Cl]–chlorine for the surface sites and give an impression of the relative strength of surfaces acidic sites on the two solids.

6.3.8 Lability of [^{36}Cl]–Chlorine Labelled *t*-Butyl Chloride and 2-Chloropropane on $AlCl_3$ and CCl_4 Chlorinated γ-Alumina

This section is concerned with the removal/displacement of [^{36}Cl]–chlorine species from the $AlCl_3$ and CCl_4 chlorinated γ-alumina surfaces. Chlorinated γ-alumina was of particular interest as it exhibits Friedel-Crafts catalytic activity comparable with $AlCl_3$ in model alkylation reactions (Chapter 4). Vapour-solid interactions of $AlCl_3$ and chlorinated γ-alumina with the probe molecules [^{36}Cl]–chlorine labelled *t*-butyl chloride, 2-chloropropane and acetyl chloride are detailed in sections 6.3.1 /6.3.2, 6.3.6 and 6.3.7 respectively.

Lability of [^{36}Cl]–chlorine associated with the solid surfaces was examined in order to develop a fundamental understanding of the nature of the reagent-solid interactions (i.e. ability to remove surface adsorbed species from solid surfaces indicates the relative strength of reagent-solid interaction). Studying the lability of [^{36}Cl]–chlorine on $AlCl_3$ and CCl_4 chlorinated γ-alumina, allowed comparison of the archetypal Lewis acid catalyst with a new heterogeneous catalyst. The basis of

the lability studies involved monitoring changes in [^{36}Cl]–chlorine surface count on solid surfaces after exposure to a dynamic vacuum and exposure to unlabelled HCl.

All operations were performed in the direct monitoring cell (Figure 2.10) with changes in the [^{36}Cl]–chlorine surface count on the solids monitored via the direct monitoring Geiger Müller counting technique (discussed in section 6.2.2). After exposure of the solids to the [^{36}Cl]–chlorine labelled probe molecules, the [^{36}Cl]–chlorine surface count on the solid was recorded. The system was pumped under dynamic vacuum, to remove volatile material and weakly absorbed species, before recounting the [^{36}Cl]–chlorine surface count on the solid (i.e. post pumping). A percentage retention of [^{36}Cl]–chlorine on the solid surface was calculated based on the [^{36}Cl]–chlorine solid surface counts pre and post pumping. Thereafter successive aliquots of unlabelled HCl (100 Torr : 1.2 mmol) were introduced and removed from the counting cell until the [^{36}Cl]–chlorine surface count on the solid remained constant. Percentage [^{36}Cl]-chlorine displacement was calculated based on the [^{36}Cl]-chlorine surface count pre and post HCl addition.

The technique for investigation of the lability of surface adsorbed species is based on monitoring changes in the [^{36}Cl]–chlorine solid surface count. It is important to note that materials, such as SF_4 fluorinated γ-alumina and β-AlF_3, which showed no appreciable [^{36}Cl]–chlorine solid surface count, are not suitable for lability studies of surface adsorbed species.

Samples of $AlCl_3$ and CCl_4 chlorinated γ-alumina labelled with [^{36}Cl]–chlorine, following exposure to [^{36}Cl]–chlorine labelled *t*-butyl chloride, were exposed to a dynamic vacuum before recording the [^{36}Cl]–chlorine solid surface count. The [^{36}Cl]–chlorine surface count on $AlCl_3$ was of the same order of magnitude as the initial surface count prior to exposure to the dynamic vacuum (Table 6.6). Interestingly, chlorinated γ-alumina samples behave very differently, with a decrease of approximately 28% in the [^{36}Cl]–chlorine solid surface count (i.e. ~72% retention). The initial removal of [^{36}Cl]–chlorine from the solid surface, indicates that [^{36}Cl]–chlorine is less strongly bound to the CCl_4 chlorinated γ-alumina surface than to the $AlCl_3$ surface.

Table 6.6 : [^{36}Cl]–Chlorine Labelled *t*-Butyl Chloride on $AlCl_3$ and CCl_4 Chlorinated γ-Alumina

Solid	Surface Count	Surface Count (Post Pumping)	% Retention
$AlCl_3$*	29769 ± 1589	33079 ± 1379	**100**
CCl_4 Chlorinated γ-alumina$^{\Delta}$	11204 ± 518	8115 ± 326	**72**
CCl_4 Chlorinated γ-alumina$^{\bullet}$	13334 ± 664	9598 ± 379	**72**

* Data from 14 readings of 4min count duration, standard deviation of mean quoted.
$^{\Delta}$ Data from 4 readings of 32min count duration, standard deviation of mean quoted.
$^{\bullet}$ Data from 5 readings of 14min count duration, standard deviation of mean quoted.

The solid surfaces labelled with [^{36}Cl]–chlorine, following treatment with [^{36}Cl]–chlorine labelled *t*-butyl chloride and exposure to dynamic vacuum, were treated with unlabelled HCl. Successive aliquots of unlabelled HCl (100 Torr : 1.2 mmol) were introduced to the labelled solids for approximately 1h before removing and recounting the solid. This process was continued until no further drop in the [^{36}Cl]–chlorine solid surface count was observed. The radiochemical data highlighted significant differences in the lability of the [^{36}Cl]–chlorine associated with $AlCl_3$ and CCl_4 chlorinated γ-alumina surfaces (Table 6.7). The [^{36}Cl]–chlorine associated with the $AlCl_3$ surface was not appreciably displaced/removed by the unlabelled HCl (i.e. only ~10% displacement). In contrast, the [^{36}Cl]–chlorine surface count on the CCl_4 chlorinated γ-alumina was significantly reduced on exposure to unabelled HCl (i.e. ~62% displacement).

Table 6.7 : Exchange of HCl with [^{36}Cl]-Chlorine Labelled *t*-Butyl Chloride on $AlCl_3$ and CCl_4 Chlorinated γ-Alumina.

Solid	**Surface Count**	**Surface Count (Post HCl Addition)**	**% Displacement**
$AlCl_3$*	33079 ± 1379	29904 ± 1678	**10**
CCl_4 Chlorinated γ-alumina$^{\Delta}$	9598 ± 379	3608 ± 201	**62**

* Data from 5 readings of 4min count duration, standard deviation of mean quoted.
$^{\Delta}$ Data from 4 readings of 14min count duration, standard deviation of mean quoted.

The lability of [^{36}Cl]–chlorine species associated with $AlCl_3$ and CCl_4 chlorinated γ-alumina following exposure to [^{36}Cl]–chlorine labelled 2-chloropropane was investigated. Retention of the [^{36}Cl]–chlorine associated with the solid surfaces after exposure to a dynamic vacuum and following displacement by addition of unlabelled HCl, are shown in Tables 6.8 and 6.9 respectively. Behaviour of the [^{36}Cl]–chlorine surface count for the respective solids was similar to that observed for the [^{36}Cl]–chlorine labelled *t*-butyl chloride (Table 6.6 and 6.7).

Pumping the solids under dynamic vacuum again showed the strong affinity of the $AlCl_3$ for the [^{36}Cl]–chlorine species, with no apparent decrease in the [^{36}Cl]–chlorine surface count observed (i.e. ~100% retention) (Table 6.8). The CCl_4 chlorinated γ-alumina showed a small decrease in the [^{36}Cl]–chlorine solid surface count when the solid was exposed to a dynamic vacuum (i.e. ~91% retention).

Table 6.8 : [^{36}Cl]–Chlorine Labelled 2-Chloropropane on Solid $AlCl_3$ and CCl_4 Chlorinated γ-Alumina

Solid	Surface Count	Surface Count (Post Pumping)	% Retention
$AlCl_3$*	4001 ± 118	4264 ± 137	**100**
CCl_4 Chlorinated γ-alumina$^{\Delta}$	4705 ± 77	4302 ± 192	**91**

* Data from 5 readings of 10.5min count duration, standard deviation of mean quoted.
$^{\Delta}$ Data from 5 readings of 10.5min count duration, standard deviation of mean quoted.

Significant differences in lability of the [^{36}Cl]–chlorine adsorbed on the solids $AlCl_3$ and CCl_4 chlorinated γ-alumina were observed when unlabelled HCl was introduced to the respective systems (Table 6.9). The [^{36}Cl]–chlorine surface count on $AlCl_3$ was essentially unchanged (i.e. only ~7% displacement), indicating a strong association of the [^{36}Cl]–chlorine labelled 2-chloropropane with the solid surface. In contrast the [^{36}Cl]–chlorine associated with the CCl_4 chlorinated γ-alumina surface was reduced, following exposure to unlabelled HCl (ie ~79% displacement).

Table 6.9 : Exchange of HCl with [^{36}Cl]-Chlorine Labelled 2-Chloropropane on $AlCl_3$ and CCl_4 Chlorinated γ-Alumina.

Solid	**Surface Count**	**Surface Count (Post HCl Addition)**	**% Displacement**
$AlCl_3$*	4264 ± 137	3963 ± 62	**7**
CCl_4 Chlorinated γ-alumina$^{\Delta}$	4302 ± 192	915 ± 138	**79**

* Data from 4 readings of 10.5min count duration, standard deviation of mean quoted.
$^{\Delta}$ Data from 4 readings of 10.5min count duration, standard deviation of mean quoted.

The [^{36}Cl]–chlorine radiochemical data from the [^{36}Cl]–chlorine labelled *t*-butyl chloride and 2-chloropropane studies, implies that the solid $AlCl_3$ surface has a stronger affinity for the alkyl halides molecules than CCl_4 chlorinated γ-alumina. Findings from the radiochemical studies are discussed in conjunction with the findings from the Friedel-Crafts studies, in chapter 7.

6.3. 9 Lability of [^{36}Cl]–Chlorine Labelled Acetyl Chloride on $AlCl_3$ and CCl_4 Chlorinated γ-Alumina

Friedel-Crafts reactions are often problematic, with reagents and products becoming strong bound to the catalyst surface (36). This is particularly true for acylation reactions due to the strong interaction between the lone pairs of electrons of the acyl oxygen and the Lewis acid sites on solid catalysts, such as $AlCl_3$ (discussed in section 1.3). Separation of the reactants and products from the $AlCl_3$ catalyst, performed by hydrolysis, results in the production of considerable quantities of waste. The section is concerned with the lability of the acyl halide species following interaction of [^{36}Cl]–chlorine labelled acetyl chloride with $AlCl_3$ and CCl_4 chlorinated γ-alumina.

Radiochemical data from exposure of $AlCl_3$ and CCl_4 chlorinated γ-alumina to [^{36}Cl]–chlorine labelled acetyl chloride were reviewed in section 6.3.7. Lability of the [^{36}Cl]–chlorine species associated with the surface of the solids was investigated via the direct monitoring Geiger Müller technique (discussed in section 6.2.2).

The [^{36}Cl]–chlorine species associated with the $AlCl_3$ solid were strongly bound to the $AlCl_3$ surface, with exposure to a dynamic vacuum not reducing the [^{36}Cl]–chlorine solid surface count to any appreciable extent (Table 6.10). High retention of the [^{36}Cl]–chlorine on the $AlCl_3$ solid surface (i.e. ~100% retention), was not observed on CCl_4 chlorinated γ-alumina solid surfaces. Exposure of the [^{36}Cl]–

chlorine labelled chlorinated γ-alumina to a dynamic vacuum resulted in an approximately 34% decrease in the [^{36}Cl]–chlorine surface count (i.e. ~67% retention). The retention data indicated that $AlCl_3$ exhibits a stronger affinity for the [^{36}Cl]–chlorine labelled acetyl chloride than CCl_4 chlorinated γ-alumina.

Table 6.10 : [^{36}Cl]–Chlorine Labelled Acetyl Chloride on Solid $AlCl_3$ and CCl_4 Chlorinated γ-Alumina

Solid	Surface Count	Surface Count (Post Pumping)	% Retention
$AlCl_3$*	1652 ± 76	2172 ± 83	**100**
CCl_4 Chlorinated γ-alumina$^{\Delta}$	2969 ± 72	1958 ± 141	**66**

* Data from 22 readings of 5min count duration, standard deviation of mean quoted.
$^{\Delta}$ Data from 27 readings of 5min count duration, standard deviation of mean quoted.

Introduction of unlabelled HCl to the [^{36}Cl]–chlorine labelled surfaces highlighted significant differences in the lability of the [^{36}Cl]–chlorine labelled acetyl chloride on the different solids (Table 6.11). Exposing $AlCl_3$ to unlabelled HCl resulted in a small decrease in the [^{36}Cl]–chlorine surface count on the solid, with most of the [^{36}Cl]–chlorine labelled species being retained on the surface (i.e. only ~17% displacement). The [^{36}Cl]–chlorine labelled acetyl chloride, was more labile on CCl_4 chlorinated γ-alumina, with exposure to unlabelled HCl resulting in

approximately 74% of the [^{36}Cl]–chlorine being displaced from the solid surface. The turnover of reactant molecules on the CCl_4 chlorinated γ-alumina is discussed section 6.3.10.

Table 6.11 : Exchange of HCl with [^{36}Cl]-Chlorine Labelled Acetyl Chloride on $AlCl_3$ and CCl_4 Chlorinated γ-Alumina.

Solid	Surface Count	Surface Count (Post HCl Addition)	% Displacement
$AlCl_3$*	2172 ± 83	1860 ± 51	**14**
CCl_4 Chlorinated γ-alumina$^{\Delta}$	1958 ± 141	502 ± 50	**74**

* Data from 6 readings of 5min count duration, standard deviation of mean quoted.
$^{\Delta}$ Data from 6 readings of 5min count duration, standard deviation of mean quoted.

6.3.10 Behaviour of [^{36}Cl]–Chlorine Labelled *t*-Butyl Chloride and Benzene on an Oxide Supported Organic Layer Catalyst

Interaction between the Friedel-Crafts reactants, [^{36}Cl]–chlorine labelled *t*-butyl chloride and benzene, with the oxide supported organic layer catalysts was investigated via the direct monitoring Geiger Müller counting technique (discussed in section 2.9). The objective was to study the nature of the interaction of the Friedel-Crafts reagents with CCl_4 chlorinated γ-alumina and the oxide supported organic layer catalyst, derived from dehydrochlorination/oligomerisation of 1,1,1-trichloroethane on CCl_4 chlorinated γ-alumina. Solid samples of the CCl_4 chlorinated γ-alumina and the layer catalyst were prepared as outlined in sections 2.3.2 and 2.3.4 respectively.

Exposure of CCl_4 chlorinated γ-alumina (0.5g) to [^{36}Cl]–chlorine labelled *t*-butyl chloride (100 Torr : 1.2 mmol) resulted in an uptake of the [^{36}Cl]–chlorine labelled species on the surface of the solid (Figure 6.11). The [^{36}Cl]–chlorine surface count was seen to decrease marginally when the system was pumped under dynamic vacuum to remove volatile material or weakly absorbed species. Subsequent addition of benzene vapour to the [^{36}Cl]–chlorine labelled solid surface, did not alter the [^{36}Cl]–chlorine surface count to any measurable extent. In a second experiment, exposing CCl_4 chlorinated γ-alumina to benzene vapour prior to [^{36}Cl]–chlorine labelled *t*-butyl chloride, showed a similar [^{36}Cl]–chlorine surface count (Figure 6.12).

Figure 6.11 : [^{36}Cl]–Chlorine Surface Count Rate from CCl_4 Chlorinated γ-Alumina After Exposure to [^{36}Cl]–Chlorine Labelled *t*-Butyl Chloride

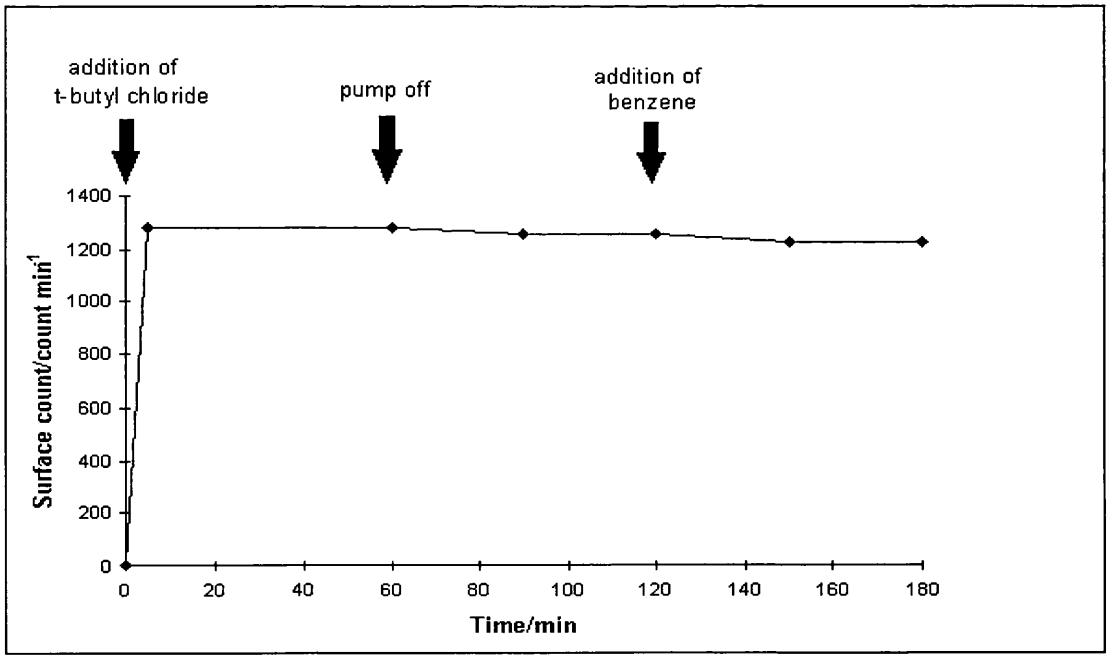

Figure 6.12 : [^{36}Cl]–Chlorine Surface Count Rate from CCl_4 Chlorinated γ-Alumina Exposed to Benzene Prior to [^{36}Cl]–Chlorine Labelled *t*-Butyl Chloride

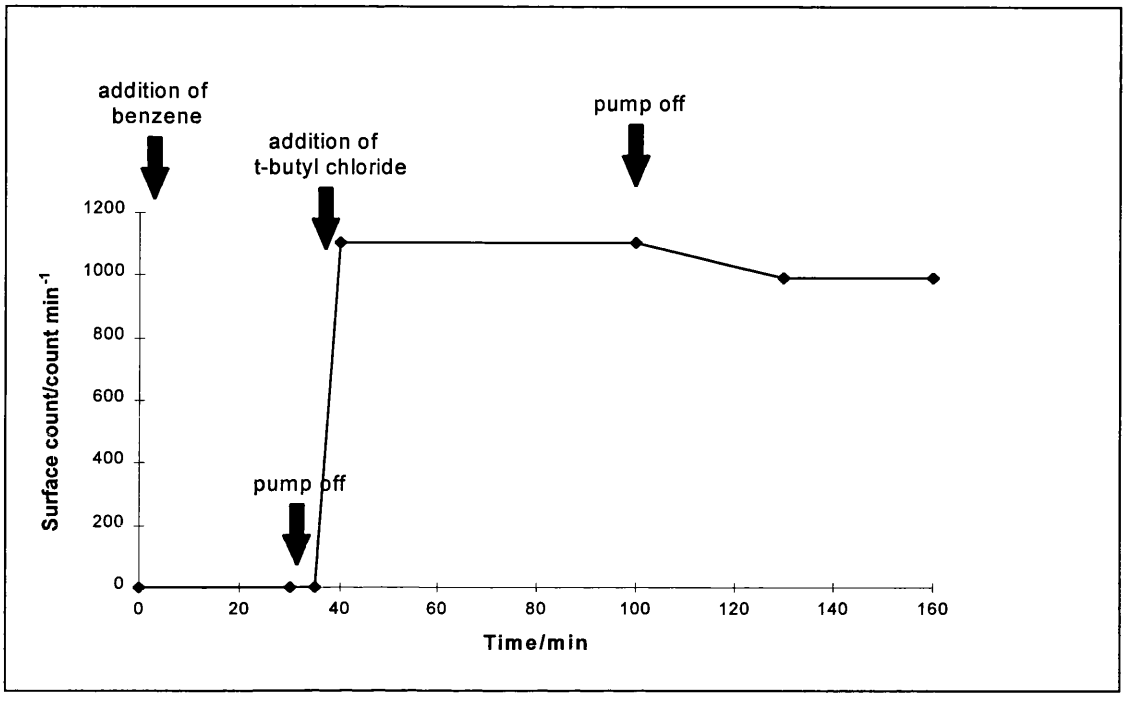

The same experimental procedure was adopted to study the interaction of [^{36}Cl]–chlorine labelled *t*-butyl chloride and benzene on the oxide supported organic layer catalyst. It is important to note that the [^{36}Cl]–chlorine surface count from the solid may represent radioactivity present at the organic surface, within the layer or at the inorganic-organic interface. Significant differences in the behaviour of the [^{36}Cl]–chlorine was observed depending on the order of addition of the Friedel-Crafts reagents to the oxide supported organic layer catalyst (Figure 6.13 and 6.14). Interestingly, when the supported organic layer catalyst, treated with benzene prior to [^{36}Cl]–chlorine labelled *t*-butyl chloride, was exposed to a dynamic vacuum the

[^{36}Cl]–chlorine solid surface count was seen to rise (Figure 6.14). This strongly implies that the Friedel-Crafts reagents, benzene and *t*-butyl chloride, are held within the supported organic layer and are displaced from the layer on pumping under dynamic vacuum. The fact that [^{36}Cl]–chlorine within the supported organic layer is not observed by the Geiger Muller counters, is particularly important, and must be considered when examining radiochemical data from supported layer materials.

Figure 6.13 : [^{36}Cl]–Chlorine Surface Count Rate from an Oxide Supported Organic Layer Catalyst After Exposure to to [^{36}Cl]–Chlorine Labelled *t*-Butyl Chloride

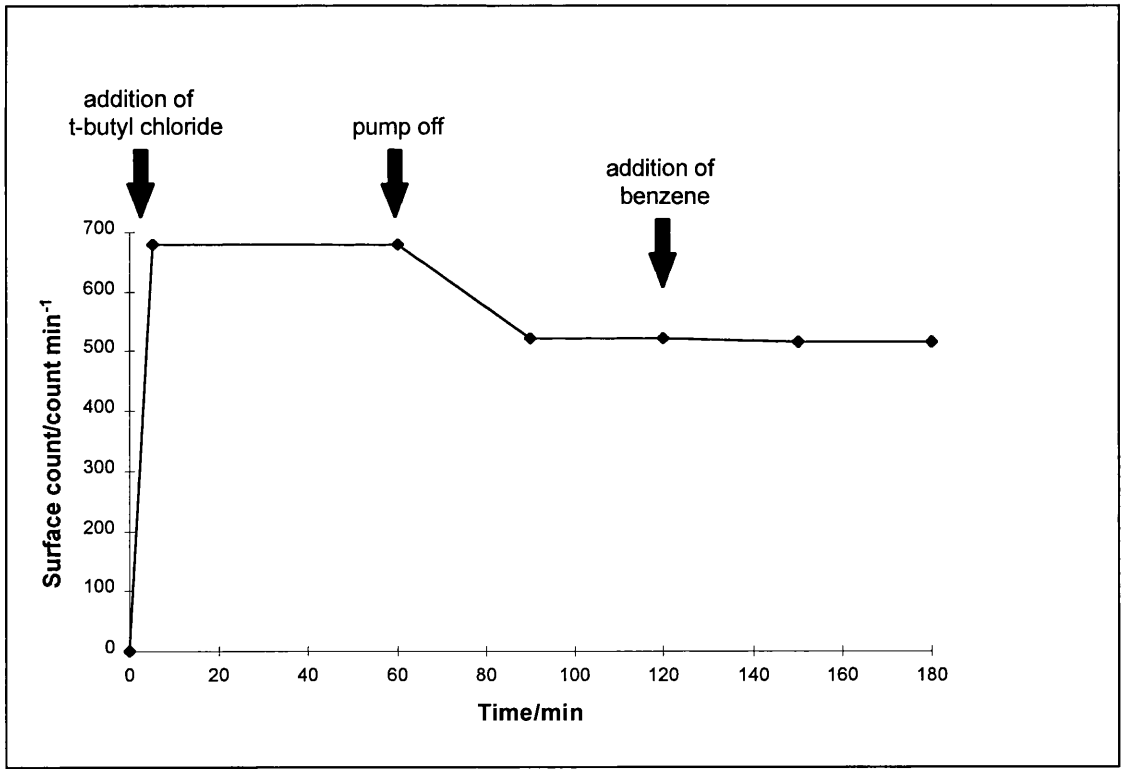

Figure 6.14 : [^{36}Cl]–Chlorine Surface Count Rate from an Oxide Supported Organic Layer Catalyst Exposed to Benzene Prior to [^{36}Cl]–Chlorine Labelled *t*-Butyl Chloride

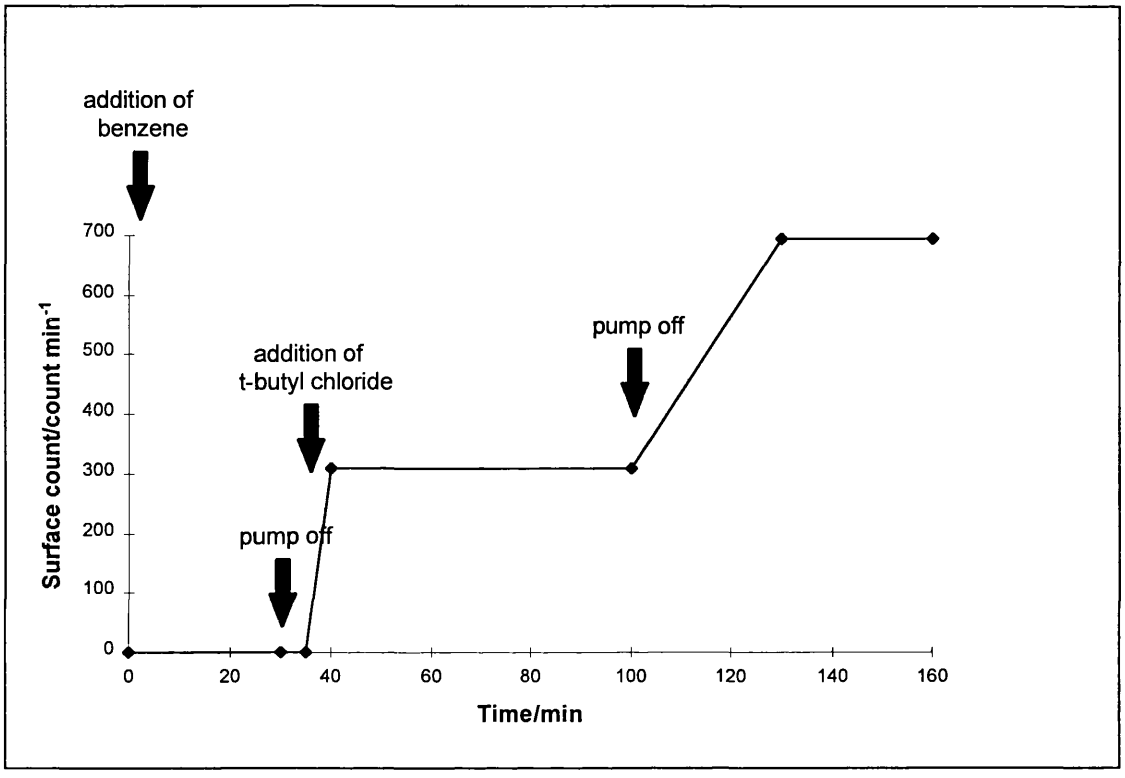

CHAPTER 7

DISCUSSION AND CONCLUSIONS

Chapters 3-6 have described the results from Friedel-Crafts catalysis, synthesis of reagents, [^{36}Cl]-chlorine radiochemical studies and *in-situ* infrared experiments. In this chapter the key findings are discussed and a general overview given, relating this work to conventional Friedel-Crafts catalysis. Chlorinated and fluorinated γ-alumina, oxide supported organic layer catalysts and β-AlF_3 were examined in two key model Friedel-Crafts systems (i) *t*-butyl chloride/toluene and (ii) *t*-butyl chloride/benzene: with the catalytic performance compared to the archetypal Lewis acid catalyst $AlCl_3$ (reviewed in Chapter 4). The nature of the vapour-solid interactions between the Friedel-Crafts reagents and the solid surfaces was probed by exposing the solid surfaces to [^{36}Cl]-chlorine radiolabelled alkyl and acyl halide species. In addition, the interactions between the reagents and the solid surfaces were monitored via *in-situ* infrared experiments (Chapter 5). Findings from the different studies are combined within this chapter in an attempt to gain a fundamental understanding of the respective Friedel-Crafts catalytic activity observed on the solid surfaces.

7.1 Summary of Key Findings

The most surprising finding from this work was the difference in Friedel-Crafts catalytic performance between the solids, CCl_4 chlorinated γ-alumina and SF_4 fluorinated γ-alumina, in the model Friedel-Crafts alkylation reactions studied

(Sections 4.4.1 and 4.4.2). GC data showed a high level of conversion (i.e. 100%) of *t*-butyl chloride to Friedel-Crafts products in the alkylation of toluene and benzene in the presence of the CCl_4 chlorinated γ-alumina, comparable with the behaviour of $AlCl_3$ in these reactions. In contrast, SF_4 fluorinated γ-alumina was catalytically inactive and did not produce any Friedel-Crafts products when examined in the same systems. Interestingly, the deposition of a highly coloured layer on the surface of the SF_4 fluorinated γ-alumina was observed when the solid was exposed to the Friedel-Crafts reactants.

Investigation of the vapour-solid interactions of *t*-butyl chloride with CCl_4 chlorinated γ-alumina and SF_4 fluorinated γ-alumina respectively showed very different behaviour. Exposure of the CCl_4 chlorinated γ-alumina solid surfaces to [^{36}Cl]-chlorine labelled *t*-butyl chloride resulted in an appreciable [^{36}Cl]-chlorine solid surface count, whereas the SF_4 fluorinated γ-alumina solid had a negligible [^{36}Cl]-chlorine surface count (Sections 6.3.2 and 6.3.4). Monitoring of the vapour-solid interactions via *in-situ* infrared studies showed that *t*-butyl chloride was removed from the vapour phase over both solid surfaces, notably with the production of HCl in the vapour phase over CCl_4 chlorinated γ-alumina (Section 5.3). Volatile material was not observed over the solid SF_4 fluorinated γ-alumina solid.

Treatment of γ-alumina chlorinated with CCl_4, with 1,1,1-trichloroethane to form a supported organic layer on the solid surface, modified the Friedel-Crafts

catalytic performance of the halogenated solid. The layer catalyst was moderately catalytic in the alkylation of toluene with *t*-butyl chloride (i.e. ~45-50% conversion) but inactive in the more demanding alkylation of benzene (Table 4.1 and 4.2). Exposure of the supported layer catalyst to [^{36}Cl]-chlorine labelled *t*-butyl chloride indicated that the alkyl halide species is absorbed within the supported organic layer.

Fluorination of γ-alumina with an SOF_2/SF_4 mixture resulted in a solid with greater catalytic activity than the inactive SF_4 fluorinated γ-alumina (i.e. 36% and 8% conversion of *t*-butyl chloride to Friedel-Crafts products in the alkylation of toluene and benzene respectively). Similar catalytic performance was observed for β-AlF_3, with 46% and 5% conversion of *t*-butyl chloride to Friedel-Crafts products in the alkylation of toluene and benzene respectively (Table 4.2 and 4.3). Interestingly, exposure of γ-alumina fluorinated with an SOF_2/SF_4 mixture and β-AlF_3 to [^{36}Cl]-chlorine labelled *t*-butyl chloride, resulted in negligible [^{36}Cl]-chlorine solid surface counts on both solids. The Friedel-Crafts catalytic activity of the solids examined as potential Friedel-Crafts catalysts are discussed throughout this chapter.

7.2 Behaviour of CCl_4 Chlorinated γ-Alumina in Model Friedel-Crafts Reactions

Solid γ-Alumina chlorinated with CCl_4 is the most promising Friedel-Crafts catalyst of the solids examined during this work. In the alkylation of toluene with *t*-butyl chloride it performed similarly to the archetypal Lewis acid catalyst, $AlCl_3$,

with complete conversion of *t*-butyl chloride to the Friedel-Crafts products, 4-*t*-butyltoluene and 3-*t*-butyltoluene (63 : 35) in approximately 60 min (Figure 7.1). Substitution of the *t*-butyl chloride species at the para and meta positions on the aromatic ring system is consistent with the electronic and steric effects of the $-CH_3$ substituent on the ring and the bulky alkyl halide species (154).

Figure 7.1 : Reaction of *t*-Butyl Chloride and Toluene (1:10) in the Presence of Solid CCl_4 Chlorinated γ-Alumina

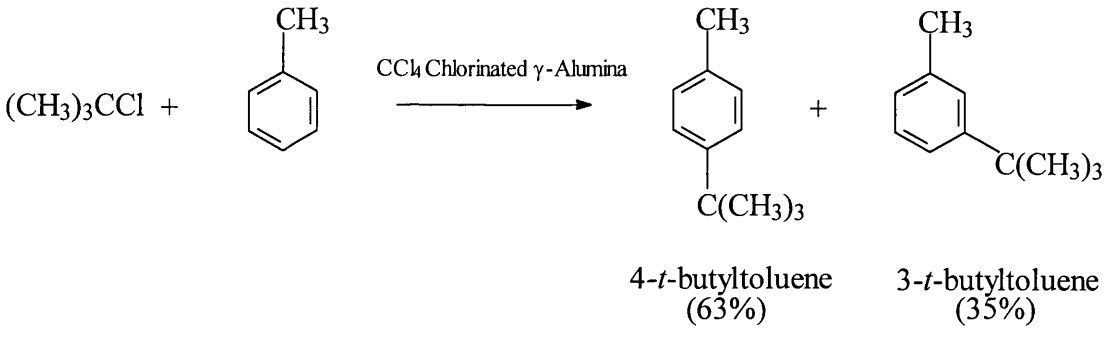

In the more demanding alkylation of benzene, the solid CCl_4 chlorinated γ-alumina catalysed complete conversion of *t*-butyl chloride to the Friedel-Crafts products, *t*-butylbenzene and di-*t*-butylbenzene. Although CCl_4 chlorinated γ-alumina gave a similar level of conversion of *t*-butyl chloride to Friedel-Crafts products as $AlCl_3$, the rate of conversion was somewhat slower taking ~6 h for complete conversion vs. ~2 h for $AlCl_3$ (Figure 4.4). The relative ratio of the two Friedel-Crafts products appeared to vary depending on the batch of CCl_4 chlorinated γ-alumina used (i.e. *t*-butylbenzene 61-92% : di-*t*-butylbenzene 8-39%). This is

assumed to be the result of variations in the level of chlorination from batch to batch, due to the nature of the chlorination process (75). It important to note that reaction selectivity was not extensively examined in this work, as the principal objective was to develop an understanding of the Friedel-Crafts chemistry on the solid surfaces via *in-situ* infrared analysis and [^{36}Cl]-chlorine radiotracer studies.

Examination of the vapour-solid interaction between solid CCl_4 chlorinated γ-alumina and the Friedel-Crafts reactants *t*-butyl chloride, 2-chloropropane and acetyl chloride were studied via the direct monitoring Geiger Müller counting technique and *in-situ* infrared studies (reviewed in chapters 5 and 6). [^{36}Cl]-chlorine labelled *t*-butyl chloride was the key probe molecule, as it enabled comparisons to be made with the findings from the model Friedel-Crafts alkylation reactions studied (Chapter 4). The direct monitoring Geiger Müller counting technique involved exposing the solid surfaces to volatile [^{36}Cl]-chlorine radiolabelled species, in a counting vessel, while recording the [^{36}Cl]-chlorine gas and solid surface counts (79,80). The [^{36}Cl]-chlorine surface counts on the solid reflect the degree of interaction of the alkyl or acyl halide with the solid surface.

Samples of the solid CCl_4 chlorinated γ-alumina exposed to [^{36}Cl]-chlorine labelled *t*-butyl chloride showed significant [^{36}Cl]-chlorine uptake on the solid surface (Table 6.3). The drop in pressure of [^{36}Cl]-chlorine labelled *t*-butyl chloride in the vapour phase, over solid CCl_4 chlorinated γ-alumina, coincided with an

increase in the [^{36}Cl]-chlorine detected on the solid surface (Figure 6.3). Interestingly, the same type of behaviour was observed for solid $AlCl_3$ exposed to [^{36}Cl]-chlorine labelled *t*-butyl chloride, resulting in an appreciable [^{36}Cl]-chlorine solid surface count (Table 6.1). It would appear that both CCl_4 chlorinated γ-alumina and the archetypal Lewis acid, $AlCl_3$, possess active surface sites which have an affinity for Lewis basic reagents such as *t*-butyl chloride.

Lability of the [^{36}Cl]-chlorine species associated with the CCl_4 chlorinated γ-alumina and $AlCl_3$ solid surfaces, following exposure to [^{36}Cl]-chlorine labelled *t*-butyl chloride, was examined in order to determine the relative strength of the vapour-solid interactions. The potential to remove the surface adsorbed [^{36}Cl]-chlorine from the solid surfaces was examined by exposing the [^{36}Cl]-chlorine labelled solids to (i) a dynamic vacuum, and (ii) unlabelled HCl; while monitoring any changes in the [^{36}Cl]-chlorine solid surface count. The two solids which had shown very similar catalytic activity in the model Friedel-Crafts alkylation reactions studied (Chapter 4), showed very different behaviour with respect to the lability of the surface adsorbed [^{36}Cl]-chlorine species.

Pumping the [^{36}Cl]-chlorine labelled CCl_4 chlorinated γ-alumina solid under dynamic vacuum resulted in a measurable decrease in the [^{36}Cl]-chlorine associated with the solid surface (i.e. ~28% drop in the [^{36}Cl]-chlorine surface count). In the case of $AlCl_3$, however, no measurable change was observed in the [^{36}Cl]-chlorine

solid surface count (Table 6.6). Subsequent exhaustive treatment of the [^{36}Cl]-chlorine labelled CCl_4 chlorinated γ-alumina and $AlCl_3$ solids with unlabelled HCl vapour, resulted in displacement/removal of ~62% and ~10% of the [^{36}Cl]-chlorine associated with the solid surfaces respectively (Table 6.7). The observed differences in the displacement/removal of the [^{36}Cl]-chlorine species associated with the solid surfaces, may indicate that the alkyl halide is less strongly bound to the CCl_4 chlorinated γ-alumina solid than the $AlCl_3$ solid.

It is likely that the Friedel-Crafts catalytic activity of CCl_4 chlorinated γ-alumina is the result of activation of the Friedel-Crafts reactant molecules on interaction with surface sites on the solid. Previous studies of the CCl_4 chlorination process in which γ-alumina was treated with [^{36}Cl]-chlorine and [^{14}C]-carbon labelled CCl_4, led to a model surface structure of chlorinated γ-alumina being proposed (75). The radiochemical data indicated that the CCl_4 chlorination process resulted in two distinct types of surface chlorine (i.e. ~70% facile to exchange with unlabelled HCl and ~30% inert to exchange). It was proposed that the chlorine which exchanged readily, was associated with Brønsted acid sites on the solid surface (Figure 1.8) and the inert chlorine species, was associated with Lewis acid sites on the solid surface (Figure 1.9).

Significantly, the percentage of [^{36}Cl]-chlorine removed/displaced from the solid CCl_4 chlorinated γ-alumina surface on introduction of unlabelled HCl (i.e.

~62%) is fairly comparable with the ratio of Brønsted acid sites : Lewis acid sites, proposed by earlier workers (i.e. 65 : 35) (75). The similarity in the proposed ratio of active sites and the % displacement/removal of [^{36}Cl]-chlorine associated with the solid, led to us adopting the model structure they proposed. The model surface of the CCl_4 chlorinated γ-alumina proposes surface Lewis acid sites consisting of an octahedral Al^{3+}, two tetrahedral Al^{3+} and four chlorine atoms, with the coordinatively unsaturated Al^{3+} bound to two chlorine atoms each acting as a bridge to the neighbouring tetrahedral Al^{3+} and the Al^{3+} beneath the plane (Figure 1.9). The Brønsted acid site was believed to be a terminal Al-Cl associated with a neighbouring surface hydroxyl group (Figure 1.8).

It is very difficult to determine the exact nature of the surface sites on the CCl_4 chlorinated γ-alumina solid. The vapour-solid interaction of the *t*-butyl chloride with the proposed model surface of solid CCl_4 chlorinated γ-alumina may be envisaged as taking place at two possible sites:

(i) Interaction of the alkyl halide at Lewis acid sites on the surface of the solid CCl_4 chlorinated γ-alumina (Figure 7.2).

(ii) Interaction of the alkyl halide at Brønsted acid sites on the surface of the solid CCl_4 chlorinated γ-alumina (Figure 7.3).

Figure 7.2 : Interaction of *t*-Butyl Chloride at the Proposed Lewis Acid Site on CCl_4 Chlorinated γ-Alumina

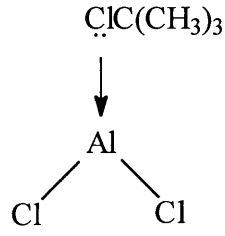

Figure 7.3 : Interaction of *t*-Butyl Chloride at the Proposed Brønsted Acid Site on CCl_4 Chlorinated γ-Alumina

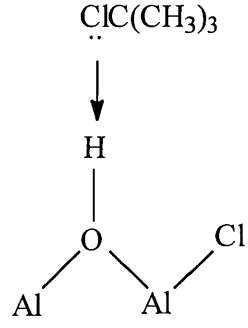

It is interesting to note that addition of unlabelled HCl to the [^{36}Cl]-chlorine labelled CCl_4 chlorinated γ-alumina solid surface, resulted in an increase in the [^{36}Cl]-chlorine gas phase count. This observation is consistent with previous studies by other workers on solid CCl_4 chlorinated γ-alumina treated with R[^{36}Cl] in which [^{36}Cl]-chlorine displaced/removed from the solid surface was believed to have been associated with surface Brønsted acid sites on the solid (75).

Interactions of the alkyl halide, *t*-butyl chloride, with the solid surfaces was also investigation by *in-situ* infrared analysis (Chapter 5). Exposure of solid CCl_4 chlorinated γ-alumina to *t*-butyl chloride vapour resulted in complete removal of the *t*-butyl chloride from the vapour phase, with the evolution of HCl(g) (Section 5.3). Monitoring of the system over time showed a growth of HCl(g) in the vapour phase without any change in the appearance of the CCl_4 chlorinated γ-alumina solid.

Production of HCl in the vapour phase following deposition of *t*-butyl chloride on the solid CCl_4 chlorinated γ-alumina surface could be due to several different processes. If the interaction involves a straight forward dehydrochlorination of the alkyl halide it might have been expected that either $H^{36}Cl(g)$ would be produced in the vapour phase or that $H^{36}Cl$ species would be adsorbed on the surface of the solid in the radiochemical studies (Figure 7.4). The presence of an appreciable [^{36}Cl]-chlorine solid surface count on the chlorinated γ-alumina (Table 6.3), and the decrease in the [^{36}Cl]-chlorine gas phase count (Figure 6.3), may indicate that the $H^{36}Cl$ is adsorbed on the surface of the solid.

It is also possible that the *t*-butyl chloride did not undergo a reaction on the CCl_4 chlorinated γ-alumina, instead becoming complexed to the active surface sites on the solid (Figure 7.5). Generation of HCl(g) observed in the vapour phase in *in-situ* infrared analysis could be an artefact of the chlorination process rather than reaction of the alkyl halide (i.e. via dehydrochlorination).

Figure 7.4 : Dehydrochlorination of [^{36}Cl]-Chlorine Labelled *t*-Butyl Chloride on CCl_4 Chlorinated γ-Alumina

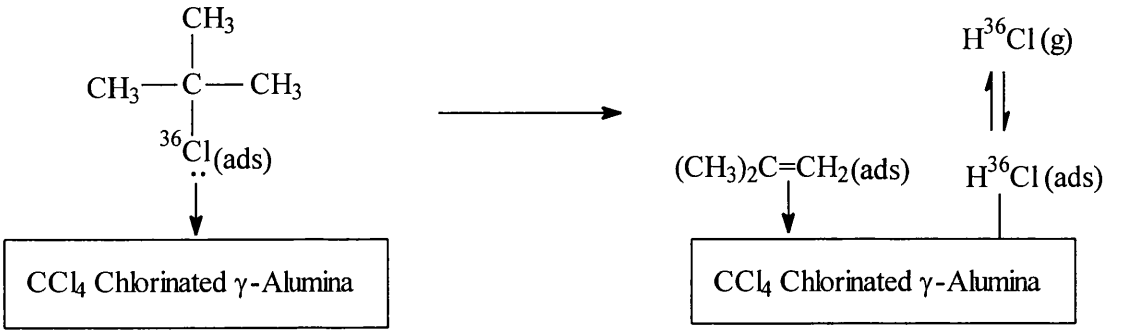

Figure 7.5 : Adsorption of [^{36}Cl]-Chlorine Labelled *t*-Butyl Chloride on CCl_4 Chlorinated γ-Alumina

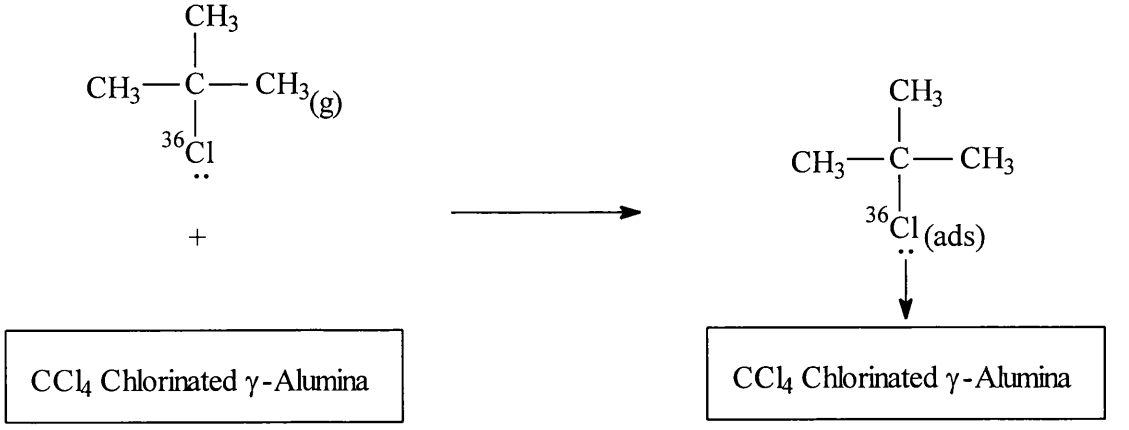

Catalytic activity of the solid CCl_4 chlorinated γ-alumina in the model Friedel-Crafts alkylation reactions studied will be the result of activation of the alkyl halide via interaction with acidic sites on the surface of the solid. The nature of the surface sites, has been discussed (75), concluding that the reactant molecules may interact with both Lewis and Brønsted acid sites on the solid surface. As discussed earlier, it is not possible to define exactly how the *t*-butyl chloride interacts with the surface sites and therefore activation of the alkyl halide to form a transient carbenium ion may be the result of two processes (Figure 7.6):

(i) Adsorption of the *t*-butyl chloride on the surface of the CCl_4 chlorinated γ-alumina to form a transient carbenium ion complex (Figure 7.6(i)).

(ii) Equilibrium involving dehydrochlorination of *t*-butyl chloride on the surface of the CCl_4 chlorinated γ-alumina and protonation via surface Brønsted acidity to form a transient carbenium ion (Figure 7.6 (ii)).

Formation of the carbenium ion promotes Friedel-Crafts reactions via electrophilic aromatic substitution of the electron rich toluene or benzene starting materials. It has been shown in this work that solid CCl_4 chlorinated γ-alumina is an active Friedel-Crafts alkylation catalyst, comparable with the archetypal Lewis acid catalyst $AlCl_3$. Attempts to reuse the solid catalyst for subsequent Friedel-Crafts

alkylation reactions proved unsuccessful (section 4.4.3). This may be the result of reactant molecules binding strongly to active sites on the solid, effectively deactivating the catalytic activity, analogous to the behaviour of $AlCl_3$. In addition, the hygroscopic nature of the chlorinated γ-alumina solid makes it susceptible to loss of surface acidity via coordination of water molecules, when residual moisture is present in the system.

Figure 7.6 : Proposed Interactions of *t*-Butyl Chloride with CCl_4 Chlorinated γ-Alumina to Form Transient Carbenium Ions for Friedel-Crafts Reactions

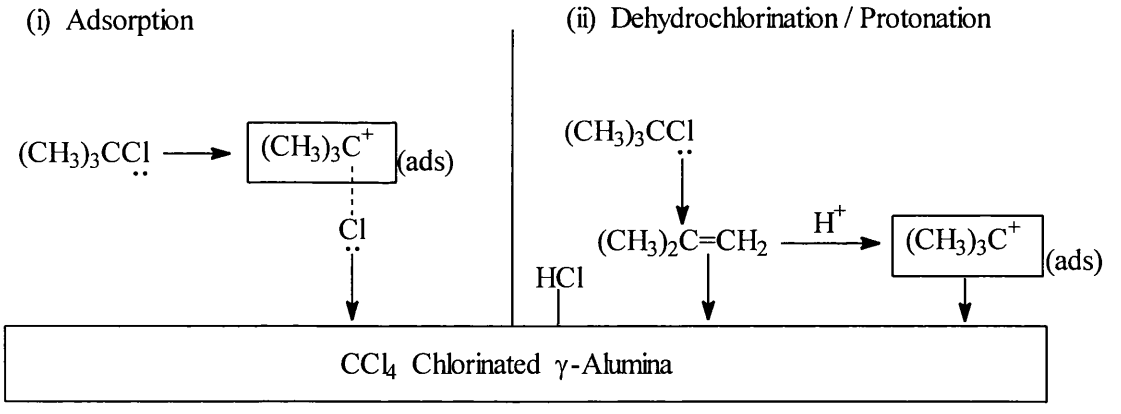

The high catalytic activity of the solid CCl_4 chlorinated γ-alumina in the model Friedel-Crafts alkylation systems studied led to interest in the potential use of the solid as a catalyst in Friedel-Crafts acylation reactions. Acylation reactions are

known to be particularly problematic with complexation of the Lewis basic reagents on catalyst surfaces, such as $AlCl_3$, effectively rendering the solid inactive (36). A good example of this problem is shown in the synthesis of the ibuprofen intermediate 4-isobutylacetophenone via $AlCl_3$ catalysis (Section 1.3).

A preliminary study was made to determine whether solid CCl_4 chlorinated γ-alumina was an active catalyst in the reaction of benzoyl chloride and benzene (Section 4.4.5). Initial attempts to prepare benzophenone by stirring benzoyl chloride and benzene (1:10 molar ratio) at room temperature were unsuccessful. The success of previous workers who employed higher temperature conditions, led to the adoption of a reaction system in which the solid CCl_4 chlorinated γ-alumina was suspended in benzoyl chloride at 438 K and dry benzene added slowly, while maintaining the temperature (155). GCMS analysis of the reaction mixtures consistently showed the presence of two broad features of molecular mass 122 a.m.u. and 226 a.m.u., some unreacted starting materials and the absence of any benzophenone product. It has been concluded that the two broad features observed are the result of hydrolysis of the benzoyl chloride starting material to give benzoic acid (122 a.m.u.) and benzoic anhydride (226 a.m.u.) (Figure 7.7).

Uptake of [^{36}Cl]-chlorine labelled acetyl chloride was examined on solid CCl_4 chlorinated γ-alumina and the archetypal Lewis acid catalyst, $AlCl_3$, via the direct monitoring Geiger Müller counting technique (Section 6.3.7) (79,80). The two solids

behaved very similarly, with initial removal of [^{36}Cl]-chlorine from the vapour phase resulting in an increase in the [^{36}Cl]-chlorine surface count on the solid, i.e. first five minutes of interaction (Figures 6.9 and 6.10). Thereafter the [^{36}Cl]-chlorine gas phase counts continued to decrease over both solids without any increase in the [^{36}Cl]-chlorine solid surface counts. This apparent contradiction between removal of [^{36}Cl]-chlorine from the gas phase and no increase in the [^{36}Cl]-chlorine solid surface count, is believed to be due to [^{36}Cl]-chlorine species being undetected by the Geiger Müller counters due to self absorption of the [^{36}Cl]-chlorine weak β^- decay.

Figure 7.7 : Hydrolysis of Benzoyl Chloride Producing Benzoic Acid and Benzoic Anhydride

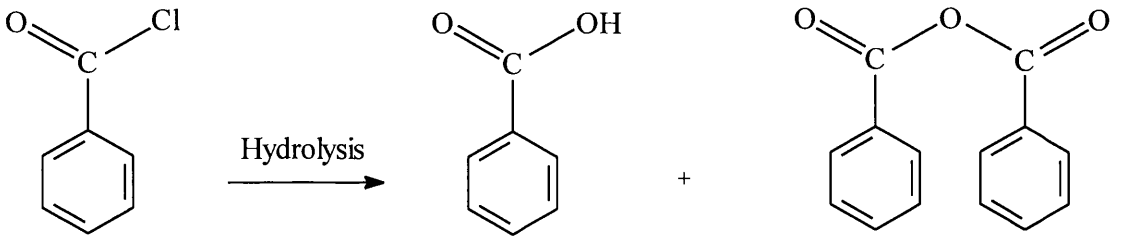

Benzoic Acid
(122 a.m.u.)

Benzoic Anhydride
(226 a.m.u.)

When the [^{36}Cl]-chlorine labelled solid surfaces were pumped under dynamic vacuum and unlabelled HCl introduced, the surface adsorbed [^{36}Cl]-chlorine species on the two solids behaved very differently. The surface adsorbed [^{36}Cl]-chlorine

species were strongly retained on the $AlCl_3$ solid, while the material associated with the CCl_4 chlorinated γ-alumina solid was apparently removed/displaced by dynamic vacuum (i.e. 34% of the surface [^{36}Cl]-chlorine removed) and on introduction of HCl (i.e. 74% of the surface [^{36}Cl]-chlorine displaced). Interestingly, these findings are similar to the observations made for interaction of the solids with [^{36}Cl]-chlorine labelled *t*-butyl chloride and 2-chloropropane, possibly indicating that the alkyl and acyl halides are more strongly bound to $AlCl_3$ than the CCl_4 chlorinated γ-alumina solid. We propose that the inactivity of the CCl_4 chlorinated γ-alumina solid in the Friedel-Crafts acylation reaction studied is due to a reduced surface acidity of the solid vs. the archetypal Lewis acid catalyst, $AlCl_3$.

7.3 Behaviour of Oxide Supported Organic Layer Catalysts Derived from CCl_4 Chlorinated γ-Alumina in Model Friedel-Crafts Reactions

Treatment of the CCl_4 chlorinated γ-alumina with 1,1,1-trichloroethane or 1,1,1-trichloroethene to form a supported organic layer catalyst (75), altered the Friedel-Crafts catalytic activity of the halogenated solid. In the Friedel-Crafts alkylation reaction of *t*-butyl chloride and toluene the conversion of *t*-butyl chloride to Friedel-Crafts products dropped from 100% to ~45-50% conversion, when a supported organic layer was present on the CCl_4 chlorinated γ-alumina solid (Table 4.1). Examination of the layer catalyst in the more demanding alkylation of benzene, showed that the presence of the supported layer rendered the solid catalytically inactive (Table 4.4).

Interaction between the oxide supported organic layer catalyst derived from CCl_4 chlorinated γ-alumina and the Friedel-Crafts reactants, [^{36}Cl]-chlorine labelled *t*-butyl chloride and benzene, was investigated via the direct monitoring Geiger Müller radiochemical counting technique (Section 6.3.10). Significant differences in the [^{36}Cl]-chlorine surface counts were observed depending on the order of addition of the two reactants (Figure 6.13 and 6.14). Addition of benzene prior to the [^{36}Cl]-chlorine labelled *t*-butyl chloride resulted in an increase in the [^{36}Cl]-chlorine surface count, when the system was pumped under dynamic vacuum (Figure 6.14). This behaviour strongly implies that the [^{36}Cl]-chlorine labelled *t*-butyl chloride species was held within the supported organic layer, where it was undetected by the Geiger Müller counters.

The lack of detection of the [^{36}Cl]-chlorine in the supported layer is attributed to self-absorption of the [^{36}Cl]-chlorine weak β^- radiation, screening decay events which occur within the layer. It would appear that [^{36}Cl]-chlorine surface counts recorded for the supported organic layer catalyst, reflect events occurring at the surface of the organic layer, not within the layer or at the inorganic-organic interface.

In-situ infrared analysis confirmed that most of the *t*-butyl chloride over the oxide supported organic layer catalyst, was removed from the vapour phase and deposited on the solid (Figure 5.3). It was not possible from the infrared studies to determine whether the alkyl halide was adsorbed on or within the organic layer.

Deposition of the chlorocarbon organic layer on CCl_4 chlorinated γ-alumina solid resulted in a decrease in Friedel-Crafts catalytic activity vs. the halogenated precursor. The possibility to turnover reactant molecules within the supported layer, however, suggests that there is potential for use of the layer catalyst under flow conditions. In such a system the supported organic layer could be envisaged as acting as a 'quasi-liquid' phase into which reactant molecules can be absorbed prior to reaction.

7.4 Behaviour of β-AlF_3 in Model Friedel-Crafts Reactions

The activity of β-AlF_3 as an active halogen exchange catalyst in the dismutation of $CHClF_2$ to CHF_3 (78,133), led to interest in the potential of the solid as a Friedel-Crafts catalyst. In the Friedel-Crafts alkylation reactions of toluene and benzene with *t*-butyl chloride, the use of β-AlF_3, resulted in the conversion of 46% and 8% of the *t*-butyl chloride respectively to Friedel-Crafts products (Chapter 4). Interestingly, the β-AlF_3 solid was a considerably more active Friedel-Crafts alkylation catalyst than the non-catalytic SF_4 fluorinated γ-alumina solid (Table 4.2 and 4.3). The catalytic performance of β-AlF_3 was not extensively studied in this work, due to the relatively low levels of conversion achieved compared with the solid CCl_4 chlorinated γ-alumina. The nature of interaction between the alkyl halide, *t*-butyl chloride, and the solid was investigated via *in-situ* infrared and [^{36}Cl]-chlorine radiotracer studies.

The conversion of the *t*-butyl chloride to Friedel-Crafts products in the presence of β-AlF_3 was noticeably different from that observed for the other catalytically active solids examined. GC data from the alkylation of toluene shows an initial rapid conversion of *t*-butyl chloride to Friedel-Crafts products, in the first five minutes of the reaction, followed by a period in which no further Friedel-Crafts products were formed (Figure 4.3). Monitoring the disappearance of *t*-butyl chloride from the reaction medium, during the alkylation of benzene, showed a very similar type of behaviour i.e. an initial rapid drop in the *t*-butyl chloride was followed by a sustained period in which no further *t*-butyl chloride was consumed (Figure 4.5). It is interesting to note that the initial rate of conversion of *t*-butyl chloride in the alkylation of toluene, by β-AlF_3 is comparable to the highly active Friedel-Crafts alkylation catalyst CCl_4 chlorinated γ-alumina. No physical change in the appearance of the solid β-AlF_3 was observed during these reactions.

Exposure of β-AlF_3 to [^{36}Cl]-chlorine labelled *t*-butyl chloride, via the direct monitoring Geiger Müller counting technique, did not result in any significant change in the [^{36}Cl]-chlorine gas phase count (Section 6.3.4). Comparison of the [^{36}Cl]-chlorine gas phase count with the gas and solid phase counts, indicated that there was no appreciable [^{36}Cl]-chlorine associated with the surface of the solid β-AlF_3 (Figure 6.6). Similarly exposure of β-AlF_3 to [^{36}Cl]-chlorine labelled 2-chloropropane resulted in a negligible [^{36}Cl]-chlorine surface count. This apparent lack of interaction of the [^{36}Cl]-chlorine labelled alkyl halide species with the β-AlF_3

solid, seems surprising considering that the solid shows some catalytic activity in the model Friedel-Crafts alkylation reactions studied. In order to develop a model which explains the apparently very low interaction of the β-AlF_3 solid with *t*-butyl chloride, and the moderate catalytic activity, we will discuss the structure of β-AlF_3 and its potential to activate the Friedel-Crafts reagents.

Kemnitz investigated the nature of the active sites on the β-AlF_3 via FTIR photoacoustic spectroscopic studies of chemisorbed pyridine (134). The metastable β-AlF_3 solid phase is closely related to the hexagonal tungsten bronze structure and has a pseudo hexagonal crystal habit (137). The network is built up from very regular AlF_6 octahedra, rotated by 7.2° from the ideal HTB structure, with hexagonal hollow channels or cavities in the solid structure. The Al-F mean bond distance is very close to the sum of the Al^{3+} and F^- ionic radii, resulting in hexagonal hollow channels with a 350pm diameter (Figure 7.8). A cavity diameter of this size is sufficiently large for water and nitrogen molecules to enter but C_1 hydrocarbons are too large to penetrate the channels. BET surface area measurements of the β-AlF_3 solid have shown it to have a surface area of ~30m^2/g (138).

Infrared analysis of chemisorbed pyridine on the β-AlF_3 solid showed only pyridine adsorption, with no pyridinium ion being detected. The β-AlF_3 surface structure was therefore characterised as consisting exclusively of Lewis acid sites (134). Exposure of the β-AlF_3 solid to *t*-butyl chloride vapour via *in-situ* infrared

studies (Section 5.3), showed that *t*-butyl chloride is removed from the vapour phase and deposited on the solid (Figure 5.2). This behaviour clearly shows the affinity of the solid for the alkyl halide and is not necessarily contradictory to the [^{36}Cl]-chlorine radiochemical data, as it is generated at considerably lower concentration of alkyl halide (i.e. 20 Torr vs 100 Torr).

Figure 7.8 : Linking of the AlF_6 Octahedra in HTB structure of β-AlF_3 [001] face

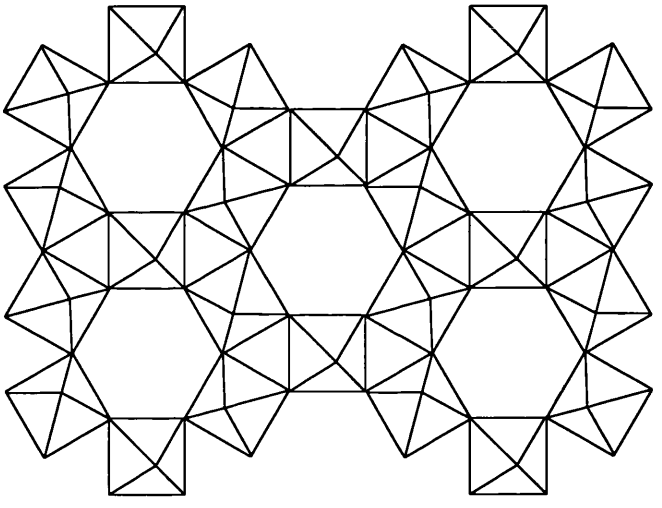

It was concluded that the activity of the β-AlF_3 solid, in the model Friedel-Crafts alkylation reactions studied, is the result of activation of the alkyl halide species via interaction with Lewis acid sites on the solid. From the diameter of the channels (i.e. 350pm), it is more likely that interaction of the alkyl halide is with Lewis acid sites on the surface of the β-AlF_3 solid (134), and not within the bulk.

Rapid initial conversion of reactants to products, apparently deactivating the solid towards further catalysis, may indicate that the Lewis acid active sites are effectively deactivated by coordination of the Lewis basic reagent, *t*-butyl chloride.

7.5 Behaviour of SF_4 Fluorinated γ-Alumina in Model Friedel-Crafts Reactions

Examination of the catalytic activity of fluorinated γ-alumina solids in model Friedel-Crafts alkylation reactions showed that the activity was dependent on the nature of the fluorinating species (Chapter 4). Solid γ-alumina fluorinated with SF_4 was catalytically inactive in the alkylation of toluene and benzene, whereas γ-alumina fluorinated with an SOF_2/SF_4 mixture resulted in conversion of *t*-butyl chloride to the Friedel-Crafts products (i.e. 36% and 8% conversion of *t*-butyl chloride in the alkylation of toluene and benzene respectively, Tables 4.2 and 4.3).

Interestingly, although not a catalyst for the Friedel-Crafts reactions studied, the SF_4 fluorinated γ-alumina interacted with the reactants forming a bright orange deposit on the surface of the solid. In addition, the GC data showed a significant reduction in the level of *t*-butyl chloride in the reaction medium, on exposure to the SF_4 fluorinated γ-alumina (Figure 4.2). Analysis of the vapour-solid interaction by *in-situ* infrared indicated, that *t*-butyl chloride was removed from the vapour phase and deposited on the SF_4 fluorinated γ-alumina (section 5.3). Deposition of the *t*-butyl chloride on the solid surface resulted in a yellow coloured layer forming on

the solid, without volatile material being detected thereafter in the vapour phase. This behaviour is very different from that observed over the CCl_4 chlorinated γ-alumina, in which no coloured deposit was formed and HCl(g) was released from the solid surface into the vapour phase (section 5.3).

The most surprising finding from this work was the very different catalytic performance of the CCl_4 chlorinated γ-alumina and SF_4 fluorinated γ-alumina solids, in the model Friedel-Crafts reactions studied (Chapter 4). The high catalytic performance of the CCl_4 chlorinated γ-alumina solid was comparable with the archetypal Lewis acid catalyst, $AlCl_3$, while the SF_4 fluorinated γ-alumina solid was catalytically inactive. On the basis of simple electronegativity, we may have predicted that the fluorinated γ-alumina would be more active than the chlorinated analogue. In order to develop a rationale to explain the observed differences in behaviour, model surface structures of the halogenated γ-aluminas and the nature of the interaction of these surfaces with the Friedel-Crafts reagents were considered.

Previous workers proposed a model surface structure for γ-alumina chlorinated with CCl_4 and $COCl_2$ in order to explain the nature of the Lewis and Brønsted acid sites present on the solid (Figures 1.8 and 1.9) (75). Fluorination of γ-alumina with SF_4 was believed to result in analogous surface sites (144). The model surface consists of bridging fluorine Al-F-Al (Lewis acid site), and terminal

fluorine species Al-F associated with hydroxyl groups (Brønsted acid site), as shown in Figure 7.9.

The vapour-solid interaction between [^{36}Cl]-chlorine labelled *t*-butyl chloride and the SF_4 fluorinated γ-alumina was investigated via the direct monitoring Geiger Müller counting technique (section 6.3.4). Initial interaction of the vapour and the solid resulted in the formation of a pale yellow layer on the surface of the solid, which turned purple within 30-60 minutes. The layer formation observed on the solid was very similar in appearance to the supported organic layer catalysts prepared via treatment of SF_4 fluorinated γ-alumina with 1,1,1-trichloroethane (76,77).

Interestingly, the [^{36}Cl]-chlorine radiochemical data showed a reduction in the [^{36}Cl]-chlorine gas phase count without an appreciable [^{36}Cl]-chlorine surface count being recorded on the solid (Figure 6.4 and 6.5). This apparent contradiction between removal of the [^{36}Cl]-chlorine from the vapour phase and the absence of a [^{36}Cl]-chlorine surface count on the SF_4 fluorinated γ-alumina, implies that the [^{36}Cl]-chlorine species is deposited on the solid surface but is undetected by the Geiger Müller counters. In contrast, exposure of [^{36}Cl]-chlorine labelled *t*-butyl chloride to the CCl_4 chlorinated γ-alumina resulted in a decrease in the [^{36}Cl]-chlorine gas phase count and a corresponding increase in the [^{36}Cl]-chlorine surface count on the solid (Figure 6.3).

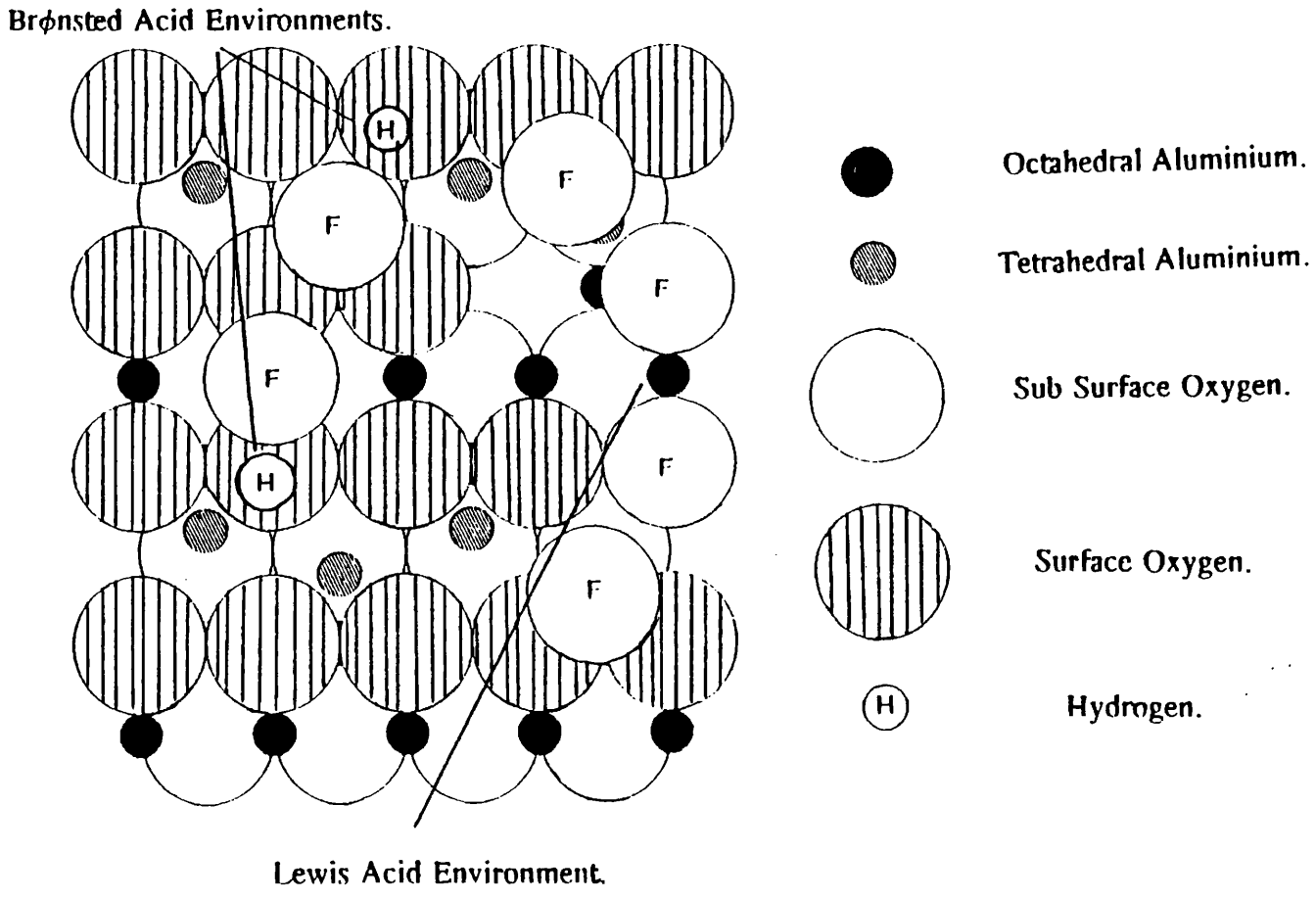

Figure 7.9 : Possible Brønsted and Lewis Acid Sites on SF_4 Fluorinated γ-Alumina

Formation of the highly coloured layer deposit on the surface of the SF_4 fluorinated γ-alumina on interaction with the *t*-butyl chloride, suggests that there is a strong interaction between the Lewis basic reagent and the solid. *In-situ* infrared studies have shown that layer formation occurs without releasing volatile material into the vapour phase (note - HCl(g) observed over CCl_4 chlorinated γ-alumina). On the basis of the model surface structure adopted, interaction of *t*-butyl chloride with the solid SF_4 fluorinated γ-alumina can occur at two possible sites:

(i) Interaction of the chlorine lone pair of the *t*-butyl chloride at a coordinatively unsaturated Al^{3+} site on SF_4 fluorinated γ-alumina, i.e. Lewis Acid Site (Figure 7.10).

(ii) Interaction of the chlorine lone pair of the *t*-butyl chloride at a hydroxyl group on SF_4 fluorinated γ-alumina, i.e. Brønsted Acid Site (Figure 7.11).

Figure 7.10 : Interaction of *t*-Butyl Chloride at the Proposed Lewis Acid Site on SF_4 Fluorinated γ-Alumina

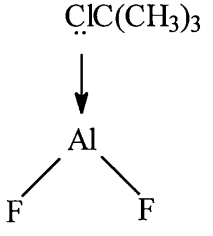

Figure 7.11 : Interaction of *t*-Butyl Chloride at the Proposed Brønsted Acid Site on SF_4 Fluorinated γ-Alumina

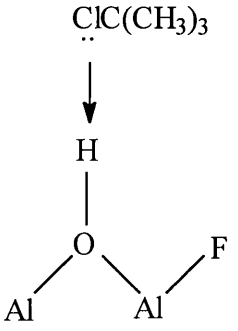

Determining the exact composition of the coloured layer deposited on the surface of the SF_4 fluorinated γ-alumina solid was difficult, as the layer degraded on exposure to air and moisture. GCMS analysis of the Friedel-Crafts reaction mixture, following exposure of the SF_4 fluorinated γ-alumina to *t*-butyl chloride, gave a fragmentation pattern, believed to be an artefact of the supported organic layer (section 4.4.2). The smallest unit or 'building block' was a C_4 hydrocarbon unit, consistent with the $(CH_3)_3CCl$ dehydrochlorination product $(CH_3)_2C{=}CH_2$. It was concluded that formation of the supported organic layer on the solid SF_4 fluorinated γ-alumina was the result of dehydrochlorination and oligomerisation of the C_4 hydrochlorocarbon starting material $(CH_3)_3CCl$ (Figure 7.12). Analogous layer formation has been documented for the liquid phase fluorination of 1,1,1-trichloroethane with $SbCl_5.4HF$ (156-158) and, more relevant to this work, in the treatment of SF_4 fluorinated γ-alumina with 1,1,1-trichloroethane (144).

Figure 7.12 : Proposed Mechanism for Formation of a Supported Organic Layer on SF_4 Fluorinated γ-Alumina

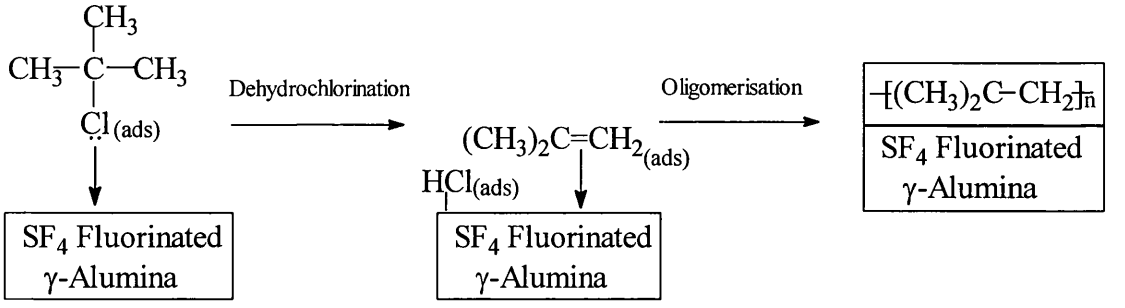

We concluded that the inactivity of the SF_4 fluorinated γ-alumina in the Friedel-Crafts alkylation reactions studied, was the result of a competitive reaction of *t*-butyl chloride with the solid surface, via dehydrochlorination and oligomerisation, producing a highly coloured supported organic layer. If this hypothesis is correct then deposition of the [^{36}Cl]-chlorine labelled *t*-butyl chloride on the SF_4 fluorinated γ-alumina solid would have been expected to result in either:

(i) $H^{36}Cl(g)$ produced in the vapour phase and therefore no significant change in the [^{36}Cl]-chlorine gas phase count.

(ii) $H^{36}Cl$ adsorbed on the surface of the solid producing an increase in the [^{36}Cl]-chlorine surface count on the SF_4 fluorinated γ-alumina.

As discussed earlier, the [^{36}Cl]-chlorine gas phase count decreased on addition of R^{36}Cl and no appreciable [^{36}Cl]-chlorine count was detected on the solid (section 6.3.4). It is believed that the SF_4 fluorinated γ-alumina is sufficiently acidic that it adsorbs the H^{36}Cl on the solid surface, within the supported organic layer at the inorganic-organic interface between the SF_4 fluorinated γ-alumina solid and the supported organic layer. The [^{36}Cl]-chlorine adsorbed within the layer is not detected by the Geiger Müller counters due to self absorption of the [^{36}Cl]-chlorine β^- decay, within the supported layer. Interestingly, exposure of SF_4 fluorinated γ-alumina treated with 1,1,1-trichloroethane to [^{36}Cl]-chlorine labelled *t*-butyl chloride, resulted in removal of the [^{36}Cl]-chlorine from the vapour phase but no appreciable [^{36}Cl]-chlorine surface count on the solid (Figure 6.7). Absorption of the alkyl halide into the supported organic layer implies that the surface active sites are unaffected by the presence of the layer.

It is concluded therefore that the inactivity of the SF_4 fluorinated γ-alumina in the Friedel-Crafts alkylation of benzene with *t*-butyl chloride, is the result of preferential formation of a supported organic layer on the solid surface (Figure 7.13).

Figure 7.13 : Proposed Interaction of SF_4 Fluorinated γ-Alumina in the Friedel-Crafts Reaction of *t*-Butyl Chloride and Benzene

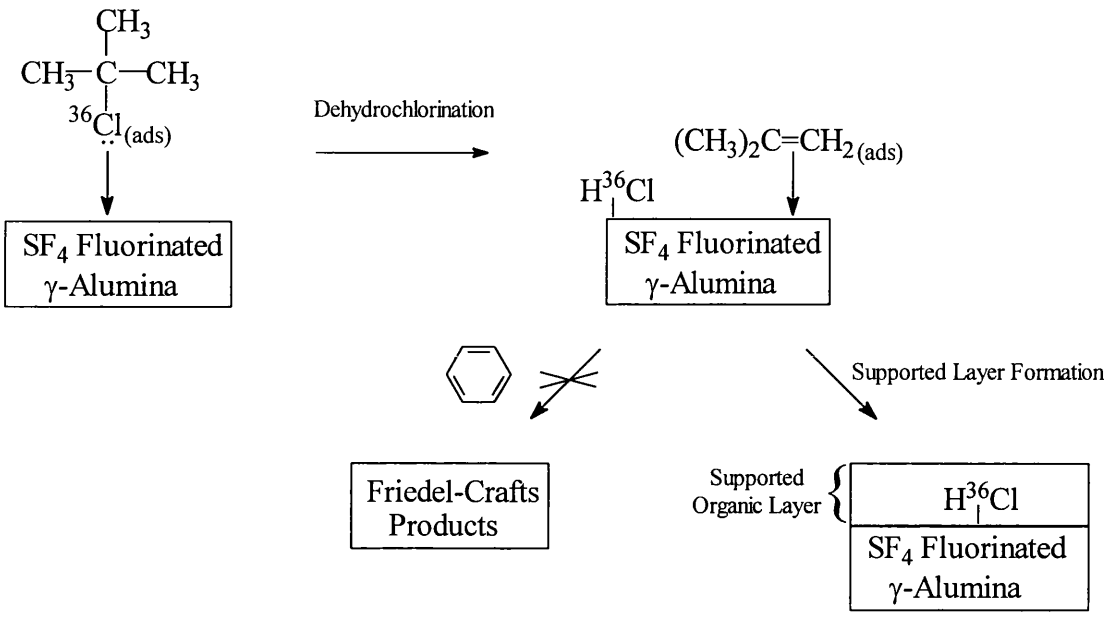

A key objective of this work was to understand why the various solid surfaces exhibited very different catalytic activities in the model Friedel-Crafts alkylation reactions studied (Chapter 4). The CCl_4 chlorinated γ-alumina was highly active, whereas γ-alumina fluorinated with SF_4 and an SOF_2/SF_4 mixture were catalytically inactive and moderately active respectively. The model surface structures of the fluorinated and chlorinated γ-aluminas are analogous (Figure 1.8/1.9 and 7.9).

Previous studies have shown that chlorination and bromination of γ-alumina results in only surface chlorine and bromine species, as the halogenating species are too large to be incorporated in the bulk without disruption of the crystal lattice (75,159). The smaller fluorine atom, however, has been shown to fluorinate both the bulk and surface of the solid (144). The greater degree of halogenation and the enhanced electronegativity of the fluorine vs. chlorine atoms, is believed to result in strong Lewis acid sites on the solid. The presence of electronegative fluorine atoms make the Lewis acid sites on the SF_4 fluorinated γ-alumina stronger than the Lewis acid sites on the analogous chlorinated surface, resulting in a solid capable of dehydrochlorination of the Friedel-Crafts starting material, *t*-butyl chloride, and formation of a supported organic layer. The catalytic activity observed on γ-alumina fluorinated with an SOF_2/SF_4 mixture is assumed to be due to a reduction in the degree of fluorination of the solid, by the weaker fluorinating agent, SOF_2.

7.6 Conclusions

This work has established that CCl_4 chlorinated γ-alumina is an active Friedel-Crafts alkylation catalyst, comparable in the reactions studied with the archetypal Lewis acid catalyst, $AlCl_3$. Treatment of the γ-alumina with CCl_4 results in surface chlorine species, Al-Cl terminal chlorine species, associated with Brønsted acid sites and readily exchangeable, and Al-Cl-Al bridging chlorine species, associated with Lewis acid sites and inert to exchange (75). The Friedel-Crafts activity of the chlorinated solid is believed to be the result of activation of the alkyl

halide species via interaction with the solid surface, to form a transient carbenium ion. It is difficult to determine the exact nature of the interaction between the Lewis basic reagent and solid surface as it may involve simple adsorption of the alkyl halide at Brønsted acid sites or a more complex equilibrium involving dehydrochlorination of the alkyl halide at the Lewis acid sites and protonation of the resultant alkene via surface Brønsted acidity.

Solid γ-alumina fluorinated with SF_4 was not an active Friedel-Crafts alkylation catalyst, due to interaction of the alkyl halide starting material with the solid surface preferentially forming a highly coloured supported organic layer. Formation of the supported organic layer is analogous to the dehydrochlorination and oligomerisation observed in the formation of the oxide supported organic layer catalysts, via treatment of SF_4 fluorinated γ-alumina with 1,1,1-trichloroethane (144). The character of the surface fluorine species on the solid is believed to be analogous to the surface species on chlorinated γ-alumina, although the smaller fluorine atoms promote bulk and surface fluorination.

Layer formation is attributed to the high surface acidity of the SF_4 fluorinated γ-alumina, produced by the greater degree of halogenation and the enhanced electronegativity of the fluorine atom relative to the chlorine atom. Failure of the CCl_4 chlorinated γ-alumina to form a supported organic layer, implies that the SF_4 fluorinated γ-alumina has stronger Lewis acid sites than the CCl_4 chlorinated

γ-alumina. It was concluded that formation of the supported organic layer is the result of dehydrochlorination and oligomerisation of the alkyl halide species at the Al-F-Al fluorine bridging Lewis acid sites on the SF_4 fluorinated γ-alumina.

Fluorination of γ-alumina with an SOF_2/SF_4 mixture resulted in a solid with greater catalytic activity in the model Friedel-Crafts alkylation reactions than SF_4 fluorinated γ-alumina, but not as active as CCl_4 chlorinated γ-alumina. The nature of the surface fluorine species are believed to be anologous to the SF_4 fluorinated γ-alumina, however, SOF_2 is a weaker fluorinating agent and is therefore unlikely to fluorinate as efficiently as SF_4. The reduced level of fluorination proposed, results in a solid of intermediate Lewis acidity, not capable of promoting formation of a supported layer, instead activating the alkyl halide starting material towards Friedel-Crafts reactions.

Catalytic performance of CCl_4 chlorinated and SF_4 fluorinated γ-alumina, treated with 1,1,1-trichloroethane, were examined in the model Friedel-Crafts alkylation reactions, to determine the effect of the supported organic layer. Deposition of the organic layer on CCl_4 chlorinated γ-alumina showed reduced catalytic activity vs. the halogenated precursor. The nature of the surface sites on the solid are believed to be analogous to the chlorinated γ-alumina, however, absorption of the reactant molecules onto and within the supported organic layer modify the catalytic activity. Why the supported organic layer modifies the catalytic potential of

the CCl_4 chlorinated γ-alumina is not completely understood. The supported organic layer on SF_4 fluorinated γ-alumina, like its halogenated precursor, was catalytically inactive in the Friedel-Crafts reactions studied. Enhanced acidity of the Lewis acid sites on the SF_4 fluorinated γ-alumina (i.e. Al-F-Al), result in adsorption of the alkyl halide species within the supported organic layer at the inorganic-organic interface.

In addition to the fluorinated γ-aluminas, β-AlF_3 was examined in the model Friedel-Crafts alkylation reactions and showed moderate catalytic activity, comparable with SOF_2 fluorinated γ-alumina. The catalytic activity is the result of interaction of the alkyl halide starting material, *t*-butyl chloride, with the Lewis acid sites on the surface of the β–AlF_3 (134). Rapid conversion of the alkyl halide starting material to Friedel-Crafts products, followed by no further conversion after the first five minutes of the reaction, implies that the Lewis acid sites on the solid surface are deactivated on contact with the Friedel-Crafts reagents. It was concluded that deactivation was due to coordination of the Lewis basic alkyl halide species with the Lewis acid sites on the surface of the solid, with the reactant molecules too large to enter the channels in the porous structure.

REFERENCES

1. C. Friedel and J.M. Crafts, Bull. Soc. Chim. France, 29 (1878) 2.
2. T. Zincke, Ber. Dsch. Chem. Ges., 2 (1869) 737.
3. S. Grucarevic and V. Merz, Ber. Dsch. Chem. Ges., 6 (1873) 60.
4. C. Friedel and J.M. Crafts, Bull. Soc. Chim. France, 2 (1878) 146.
5. G.A. Olah, 'Friedel-Crafts Chemistry and Related Reactions', J. Wiley, New York, (1973) 28.
6. N.O. Galloway, J. Am. Chem. Soc., 59 (1937) 1474.
7. L.I. Smith and F.J. Dobrovolny, J. Am. Chem. Soc., 48 (1926) 1413.
8. G.A. Olah, 'Friedel-Crafts Chemistry and Related Reactions', J. Wiley, New York, (1973).
9. G.A. Olah, W.S. Tolgyesi, S.J. Kuhn, M.E. Moffat, I.J. Bastein and E.B. Baker, J. Am. Chem. Soc., 85 (1963).
10. H. Meerwin, Ann, 455 (1927) 227.
11. P. Pfeiffer, Organische Molekulverbindugen, Ferdinand Enke, Stuggart, (1927).
12. B.P. Susz and J.J. Wuhrmann, Helv. Chim. Acta., 40 (1957) 971.
13. J. Wilinski and R.J. Kurland, J. Am. Chem. Soc., 100 (1978) 2233.
14. F. Bigi, G. Casnati, G. Sartori and G. Predieri, J. Chem. Soc., Perk. Trans. 2 (1991) 1319.
15. M.J.S. Dewar, 'Electronic Theory of Organic Chemistry', Oxford Press, New York, (1949).

16. H.C. Brown and J.D. Brady, J. Am. Chem. Soc., 74 (1952) 3580

17. G.A. Olah and S.J. Kuhn, J. Am. Chem. Soc., 80 (1958) 6535.

18. G.A. Olah and S.J. Kuhn, J. Am. Chem. Soc., 80 (1958) 6541.

19. G.A. Olah, S. Kobayashi and J. Nishimura, J. Am. Chem. Soc., 95 (1973) 564.

20. G.A. Olah and S. Kobayashi, J. Am. Chem. Soc., 93 (1971) 6964.

21. F.A. Cotton and G. Wilkinson, 'Advanced Inorganic Chemistry' 4th Edn. J. Wiley, New York, (1980).

22. I.R. Beattie, J. Chem. Soc., Dalton Trans., 666 (1976).

23. I.R. Beattie, J. Chem. Phys. 64 (1976) 1909.

24. J.S. Shirk and A.E. Shirk, J. Chem. Phys. 64 (1976) 910.

25. K. Pauling, J. Palmer and N. Elliot, J. Am. Chem. Soc., 60 (1938) 1852.

26. J.A.A. Ketelaar, C.H. MacGillavry and P.A. Renes, Rec. Trans. Chim., 66 (1974) 501.

27. W. Blitz and W. Wien, Z. Anorg. Allg. Chem. 121 (1922) 257.

28. W. Blitz and W. Klemn, Z. Anorg. Allg. Chem. 152 (1926) 267.

29. W. Blitz and A. Voigt, Z. Anorg. Allg. Chem. 39 (1923) 126.

30. R.F. Porter and E.E. Zeller, J. Chem. Phys. 33 (1960) 858.

31. H. Staudinger and H.A. Brown, Ann, 110 (1926) 447.

32. O. Grummit, E.E. Seusel, W.R. Smith, R.E. Burr and H.P. Laurelma, J. Am. Chem. Soc., 67 (1945) 910.

33. E.R. Kline, B.N. Campbell and E.C. Spaeth, J. Org. Chem., 214 (1959) 1781.

34. D.G. Walker, J. Phys. Chem., 64 (1960) 939.

35. D.G. Walker, J. Phys. Chem., 65 (1961) 1367.

36. J.H. Clark (Ed.), 'Chemistry of Waste Minimisation', Chapman and Hall, Glasgow, 2 (1995).

37. A. Krzywicki and M. Marczewski, J. Chem. Soc., Faraday Trans., 1 (1980) 1311.

38. R.S. Drago and E.E. Getty, J. Am. Chem. Soc., 110 (1988) 3311.

39. R.S. Drago, S.C. Petrosius and C.W. Chronister, Inorg. Chem., 33 (1994) 367.

40. R.S. Drago and E.E. Getty, Inorg. Chem., 29 (1990) 1186.

41. R.S. Drago, S.C. Petrosius and P.B. Kaufman, J. Mol. Catal., 89 (1994) 317.

42. J.H. Clark, K. Martin, A.J. Teasdale and S.J. Barlow, J. Chem. Soc., Chem. Commun., (1995) 2037.

43. J.H. Clark, A.P. Kybett, D.J. Macquarrie, S.J. Barlow and P. Landon, J. Chem. Soc., Chem. Commun., (1989) 1353.

44. S.J. Barlow, J.H. Clark, M.R. Darby, A.P. Kybett, P. Landon and K. Martin, J. Chem. Research (5), (1991) 74.

45. A. Cornelis, C. Dony, P. Laszlo and K.M. Nsuda, Tetrahedron Lett., 32 (1991) 1423.

46. A. Cornelis, P. Laszlo and S. Wang, Tettrahedron Lett., 34 (1993) 3489.

47. V. Quaschning, J. Deutsch, P. Druska, H.J. Niclas and E. Kemnitz, J. Catal., 177.2 (1998) 164.

48. G.A. Olah, D. Meidar, R. Malhotra, J.A. Olah and S.C. Narang, J. Catal., 61 (1980) 96.

49. J.H. Clark and in part S.R. Cullen, S.J. Barlow and T.W. Bastock, J. Chem. Soc., Perkin Trans., 2 (1994) 1117.

50. 'Envirocats Supported Reagents', Contract Chemicals, Merseyside.

51. K. Martin, Ph.D. Thesis, U.C.W. University of Aberystwyth, (1987).

52. B. Chiche, A. Finiels, C. Gauthier, P. Geneste, J. Graille and D. Pioch, J. Org. Chem. 51 (1986) 2128.

53. C. Gauthier, B. Chiche, A. Finiels and P. Geneste, J. Mol. Catal., 50 (1989) 219.

54. A. Corma, M.J. Climent, H. Garcia and J. Primo, Appl. Catal, 49 (1989) 109.

55. K. Gaare and D. Akporiaye, J. Mol. Catal. A, 109 (1996) 177.

56. J.S. Beck, J.C. Vartuli, W.J. Roth, M.E. Leonavics, C.T. Kresge, K.D. Schmitt, C.T.W. Chu, D.H. Olsen, E.W. Sheppard, S.B. McCullen, J.B. Higgins and J.L. Schlenker, J. Am. Chem. Soc., 114 (1992) 10834.

57. E.A. Gunwegh, S.S. Gopie and H.V. Bekkuns, J. Mol. Catal. A, 106 (1996) 151.

58. Y. Izumi, K. Matsuo and K. Urabe, J. Mol. Catal., 18 (1983) 299.

59. Y. Izumi, R. Hasebe and K. Urabe, J. Catal., 84 (1983) 402.

60. Y. Izumi and K. Urabe, Structures in Surface Science and Catalysis, 90 (1994) 1.

61. Y. Izumi, N. Nafsume, H. Takamine, I. Tamaoki and K. Urabe, Bull. Chem. Soc. Jpn., 62 (1989) 2159.

62. Y. Izumi, M. Ono, M. Kitagawa, M. Yoshida and K. Urabe, Microporous Materials, 5 (1995) 255.

63. T. Nishimura, T. Okahura and M. Misono, Applied Catalysis, 73 (1991) L7.

64. Y. Izumi, M. Ogawa and K. Urabe, Applied Catalysis A : General, 132 (1995) 127.

65. F. Arena, R. Dario and A. Parmaliana, Applied Catalysis A : General, 170 (1998) 127.

66. A. Kawada, S. Mitamura and S. Kobayashi, J. Chem. Soc., Chem. Commun., (1993) 1157.

67. A. Kawada, S. Mitamura and S. Kobayashi, Synlett., (1994) 545.

68. T. Mukaiyama, K. Suzuki, S.J. Han and S. Kobayashi, Chem. Lett., (1992) 435.

69. I. Hachiya, M. Moriwaki and S. Kobayashi, Bull. Chem. Soc. Jpn., 68 (1995) 2053.

70. A. Kawada, S. Mitamura and S. Kobayashi, J. Chem. Soc., Chem. Commun., (1996) 183.

71. 'Cleanline 7', EPSRC, (1996).

72. K.R. Seddon, J. Chem. Technology and Biotechnology, 68.4 (1997) 351.

73. M.G. Hitzler, F.R. Smail, S.K. Ross and M. Poliakoff, J. Chem. Soc., Chem. Commun., 3 (1998) 359.

74. D.G. McBeth, J.M. Winfield, B.W. Cook and N. Winterton, J. Chem. Soc., Dalton Trans., (1990) 671.

75. J. Thomson, G. Webb and J.M. Winfield, J. Mol. Catal., 67 (1991) 117; 68 (1991) 347.

76 J. Thomson, G. Webb and J.M. Winfield, J. Chem. Soc., Chem. Commun., (1991) 323.

77. J. Thomson, G. Webb, J.M. Winfield, D. Bonniface, C. Shortman and N. Winterton, Appl. Catal. A : General, 97 (1993) 67.

78. A. Hess, E. Kemnitz, A. Lippitz, W.E.S. Unger and D.H. Menz, J. Catal., 148 (1994) 270.

79. A.S. Al-Ammar and G. Webb, J. Chem. Soc., Faraday Trans., 74 (1978) 195.

80. G.A. Kolta, G. Webb and J.M. Winfield, Appl. Catal., 2 (1982) 257.

81. J.J. Kipling and D.B. Peakall, J. Chem. Soc., (1957) 834.

82. K.B. Day and V.J. Hill, J. Phys. Chem. 57 (1953) 946.

83. J.F. Brown, D. Clark and W. Elliot, J. Chem. Soc., (1953) 84.

84. J. Thomson, Ph.D. Thesis, University of Glasgow, (1988).

85. W.A. England, J. Chem. Soc., Chem. Commun., (1976) 895.

86. L.L. VanReigen, Ph.D. Thesis, Technical University of Eindhoven, (1964).

87. S. Soled, J. Catal., 81 (1983) 252.

88. G. Weatherbee and C.H. Bartholmew, J. Catal., 87 (1984) 55.

89. G.C. Chinchen, K.C. Waugh and D.A. Whan, Appl. Catal., 25 (1986) 101.

90. T.Y. Chou, C.H. Leu and C.T. Yeh, Catal. Today, 26 (1995) 53.

91. B.C. Gates, 'Catalytic Chemistry', J. Wiley, New York, (1992).

92. A.F. Wells, 'Structural Inorganic Chemistry', 5th Edn., Oxford Uni. Press, London (1984) 553.

93. B.C. Lippens, Ph.D. Thesis, Technical University of Delft, (1961).

94. J.B. Peri and R.B. Hannan, J. Phys. Chem., 64 (1960) 1526.

95. J.B. Peri, J. Phys. Chem., 69 (1965) 211.

96. J.B. Peri, J. Phys. Chem., 69 (1965) 220.

97. T.R. Hughes, H.M. White and R.J. White, J. Catal., 13 (1969) 58.

98. F.E. Kiviat and L. Petrakis, J. Phys. Chem., 77 (1973) 1232.

99. S.M. Riseman, F.E. Massoth, G. Murahli-Dhar and E.M. Eyring, J. Phys. Chem., 86 (1982) 1760.

100. G.M. Schwab and U. Heyde, Zeits. F. Physik. Chemie B8 (1930) 147.

101. R.N. Peace and G.F. Walz, J. Am. Chem. Soc., 53 (1931) 3730.

102. H.A. Taylor and W.E. Hanson, J. Chem. Phys., 7 (1939) 418.

103. S. Patai (Ed.), 'The Chemistry of Carbon-Halogen Bond', J. Wiley, U.K., (1973) Part 1.

104. T.G. Carver and L. Andrews, J. Chem. Phys., 50 (1969) 4223; 50 (1969) 4235.

105. A.G. Noble and P. A. Lawrence, Proc. 3rd Int. Congr. Catal., Amsterdam, (1964) 320.

106. O. Ruff and C. Thiel, Ber., 38 (1905) 549.

107. A. Bendada, Ph.D. Thesis, University of Glasgow (1990).

108. F.S. Fawcett and C.W. Tullock, Inorg. Synth., 7 (1963) 119.

109. R.E. Dodd, L.A. Woodward and H.L. Roberts, J. Chem. Soc., Faraday Trans., 52 (1956) 1052.

110. F.A. Cotton, J.W. George and J.S. Vaughn, J. Chem. Phys., 28 (1958) 994; E.L. Muetterties and W.D. Philips, J. Am. Chem. Soc., 81 (1959) 1084.

111. W.M. Tolles and W.D. Gwinn, J. Chem. Phys. 36 (1962) 119.

112. F. Seel and O. Deemter, Z. Anorg. Allg. Chem., 301 (1959) 113.

113. C. Smith, Angew. Chem. Int. Ed. Engl. 1 (1962) 467.

114. C.W. Tullock, D.D. Coffman and E.L. Muetterties, J. Am. Chem. Soc., 86 (1964) 357.

115. G.M. Begun, W.H. Fletcher and D.F. Smith, J. Chem. Phys., 42 (1965) 2236.

116. P. Camboulives, Compt. Rend., 150 (1910) 175.

117. M. Tanaka and S. Ogasawara, J. Catal., 16 (1970) 157.

118. R.L. Richardson and S.W. Benson, J. Am. Chem. Soc., 73 (1951) 5096.

119. A. Corma and V. Fornes, Appl. Catal., 61 (1990) 175.

120. G.B. McVicker, C.J. Kim and J.J. Eggert, J. Catal., 80 (1983) 315.

121. A. Bendada, G. Webb and J.M. Winfield, Eur. J. Solid State Inorg. Chem., 33 (1996) 907.

122. R.I. Hedge and M.A. Barteau, J. Catal., 120 (1989) 387.

123. J.M. Saniger, N.A. Sanchez and J.O. Flones, J. Fluorine Chem., 88 (1998) 117.

124. A. Corma, V. Fornes and E. Ortega, J. Catal., 92 (1985) 284.

125. J.R. Schlup and R.W. Vaughan, J. Catal., 99 (1986) 304.

126. V.M. Allenger, D.D. McLean and M. Tenman, J. Catal., 131 (1991) 305.

127. T.H. Ballinger and J.T. Yates Jr., J. Phys. Chem., 96 (1992) 1417.

128. E. Garbowski, J.P. Candy and M. Primet, J. Chem. Soc., Faraday Trans.I, 79 (1983) 835.

129. E. Garbowski and M. Primet, J. Chem. Soc., Faraday Trans.I, 81 (1985) 497.

130. A. Bendada, D. Bonniface, F. McMonagle, R. Marshall, C. Shortman, R.R. Spence, J. Thomson, G. Webb, J.M. Winfield and N. Winterton, J. Chem. Soc., Chem. Commun., (1996) 1947.

131. S. Brunet, B. Requierne, E. Matouba, J. Barrault and M. Blanchard, J. Catal., 152 (1995) 70.

132. A. Hess and E. Kemnitz, J. Fluorine Chem., 74 (1995) 27.

133. E. Kemnitz and A. Hess, J. Prakt. Chem., 334 (1992) 591.

134. A. Hess and E. Kemnitz, J. Catal., 149 (1994) 449.

135. C.H. Kline and J.J. Turkevich, J. Chem. Phys. 12 (1944) 300.

136. C. Morterra, G. Magnacca, G. Cerrato, N. Del Favero, F. Filippi and C.V. Folonari, J. Chem. Soc., Faraday Trans.I, 89 (1993) 135.

137. A. LeBail, C. Jacobini, M. Leblanc, R. DePape, H. Duroy and J.L. Fourquet, J. Solid State Chem. 77 (1988) 96.

138. E. Kemnitz, A. Hess, G. Rother and S. Troyanov, J. Catal., 159 (1996) 332.

139. I. Grohmann, A. Hess, E. Kemnitz, W. Fentrup, W.E.S. Unger, J. Wong, M. Rowen, T. Tanaka and M. Froba, J. Mater. Chem., 8 (1998) 1453

140. A.J. Vogel, 'Textbook of Practical Inorganic Chemistry', Longmans, London, (1962) 179.

141. F. Amar, D.R. Dalton, G. Eisman and M.J. Haugh, Tetrahedron Lett. 35 (1974) 3033.

142. A.J. Vogel, 'Textbook of Practical Organic Chemistry', Longmans, London, (1989).

143. W.J. Neill and M. Kahn, J. Am. Chem. Soc., 80.2 (1958) 2111.

144. F. McMonagle, Ph.D. Thesis, University of Glasgow, (1995).

145. D.G. McBeth, Ph.D. Thesis, University of Glasgow, (1987).

146. D.J. Malcolme-Lawes, 'Introduction to Radiochemistry', MacMillan Press Ltd., London, (1979).

147. G. Friedlander, J.W. Kennedy, E.S. Macias and J.M. Miller, 'Nuclear and Radiochemistry', J. Wiley, New York, (1981).

148. W.D.S. Scott, Ph.D. Thesis, University of Glasgow, (1997).

149. K.A. Brownlee, 'Statistical Theory and Methodology in Science and Engineering', J. Wiley, New York, (1960).

150. C.A. Bennet and N.L. Franklin, 'Statistical Analysis in Chemistry', J. Wiley, New York, (1954).

151. D.H. Williams and I. Fleming, 'Spectroscopic Methods in Organic Chemistry', 4th Edn., McGraw-Hill, London, (1987).

152. 'Infrared Characteristic Group Frequencies', J. Wiley, New York, (1994).

153. 'The Aldrich Library of ^{13}C and ^{1}H FT NMR Spectra', 1st Edn., 1 (1993).

154. M.J. Schlatter and R.D. Clark, J. Am. Chem. Soc., 75 (1953) 361.

155. P. Landon, Ph.D. Thesis, University of York, (1993).

156. M. Blanchard and S. Brunet, J. Mol. Catal., 62 (1990) L33.

157. S. Brunet, C. Batiot, J. Barrault and M. Blanchard, J. Fluorine Chem., 59 (1992) 33.

158. S. Brunet, C. Batiot, J. Barrault and M. Blanchard and J. M. Coustard, J. Fluorine Chem., 63 (1993) 227.